The development and applications of a micro-gap perforated electrode flow through cell

A thesis submitted in fulfilment

of the requirements for the degree of

Doctor of Philosophy

in

Chemistry and Engineering

at

The University of Waikato

by

Hilary Nath

THE UNIVERSITY OF
WAIKATO
Te Whare Wānanga o Waikato

December 2011

Abstract

Electrochemical techniques provide convenient and environmentally compatible ways of bringing about chemical transformations. However they generally lose their economic viability when used with low conducting electrolyte systems. This has limited their usefulness in the treatment of water and wastewater. Increasing the electrolyte concentration of these systems is not an option as it is with industrial processes such as the chlor-alkali process. Cell resistance is the major limiting factor. Cell resistance can be reduced by reducing the inter-electrode gap. A novel micro gap perforated electrode flow through (PEFT) cell has been developed for efficient and cost effective treatment of aqueous systems of low ionic strength.

The PEFT cell is an undivided flow through design which encompasses both parallel plate and porous electrode features. It consists of plate electrodes and flow is both through the electrodes and parallel to the surfaces of the two electrodes. The perforations in the electrodes and the short flow distance between the electrodes allow the inter-electrode gap to be reduced to 50 microns and less without causing excessive resistance to hydraulic flow. With reduced electrical resistance, effective electrochemical treatment of natural water and other low electrolyte systems is possible.

The PEFT cell was first applied to overcome a local water supply problem; the Waikato region's iron and manganese contaminated bore waters. These waters form stable colloidal suspensions during slow air oxidation. The problem can be overcome by rapid electrochemical oxidation using the PEFT cell. Electrochemical oxidation was found to be more effective and efficient than chemical oxidation allowing removal of iron and manganese to meet drinking water standards with minimal formation of disinfection by-products (DBP).

Electrochemical oxidation of water and wastewater systems is brought about principally by chlorine mediated indirect oxidation processes. A 240 μm gap PEFT cell, with a graphite anode was used for chlorine generation. It produced chlorine at current efficiencies above 60% with an energy consumption of 4.83 kWh/kg of chlorine from a 0.5 mol/L NaCl solution. This result compares well with industrial hypochlorite production using an undivided cell.

Chlorine mediated electro-oxidation of effluents was successfully demonstrated by the degradation of textile dyes in water. Complete single pass electrochemical decolourisation of indigo carmine (IC) dye effluent containing 0.35 mol/L NaCl was achieved using a graphite anode PEFT cell. Energy consumption was 0.8 kWh/m^3 or 8.3 kWh/kg of dye. This is an order of magnitude less than the energy consumption reported for colour removal using graphite anodes. It is comparable or lower than most colour removal work carried out using metal oxide coated dimensionally stable anodes (DSAs) and boron doped diamond (BDD) anodes. Reduction of pH from 7 to 3 reduced the energy consumption for decolourisation of IC dye by 50% and also increased the TOC removal by 20%. When $NaSO_4$ was used as the electrolyte rather than sodium chloride, colour removal was much less effective.

A single pass through a 50 μm gap PEFT cell with a stainless steel cathode and a graphite anode operated at 5.5 V achieved a 6 log inactivation of *Escherichia coli* bacteria in a water sample containing only 1.7 mmol/L of chloride ions. The power consumption was 0.5 kWh/m^3 of water. The narrow inter-electrode gap allows high electric fields to be produced from low applied voltages. When the cell was operated at above 5.0 volts, a synergistic electric field effect was observed. Specific lethality of the chlorine was increased to at least 50 L/(mg min), approximately two orders of magnitude higher than in the absence of the field. Increased specific lethality means that disinfection can be achieved at much lower free available chlorine levels than previously possible. This reduces the risk of DBP formation.

Improved current efficiencies and reduced energy consumption for electrolysis at low electrolyte concentrations were achieved by partial insulation of the active

anode surface of a 50 μm gap PEFT cell. This electro-catalytic effect was consistent with enhanced transport of the electroactive species to the active part of the electrode, reducing concentration and resistance overpotentials. In the electrochemical production of chlorine from 0.85 mmol/L NaCl at a current density of 2 mA/cm^2, current efficiency was tripled and power consumption was reduced by a factor of two, relative to the cell without the anode modification.

The reduction in the inter-electrode gap to 50 μm and less has allowed the production of electric field strengths greater than 10 kV/cm from applied voltages of less than a 100V. Field strengths between 1and 10 kV/cm are known to cause reversible electroporation whereas irreversible electroporation occurs above 10 kV/cm. Evidence for irreversible electroporation was provided by the 6 log inactivation of *Escherichia coli* (in the absence of chlorine) at an applied electric field of 22.5 kV/cm generated in a 40 μm gap PEFT cell by a 90 V DC supply. The energy consumption was 430 J/mL and without cooling, the temperature remained below 42^oC. Inactivation was achieved by 20 hydrodynamically generated DC pulses. The low applied voltage, the elimination of the need for pulsed electric fields, avoidance of external cooling and the simplicity of the experiment bring commercial non thermal electro-pasteurisation one step closer.

Acknowledgements

I am deeply indebted to my supervisor Assoc. Prof. Alan Langdon for his guidance, never ending encouragement and enthusiasm. I am grateful for your extraordinary kindness, patience, support and above all for imparting knowledge. You were more than a supervisor right from the very beginning. I could not have wished for a better supervisor.

I would also like to thank Dr. Rob Torrens my second supervisor for his support and encouragement during the research.

I would like to express my sincere thanks to technical officers John Little, Wendy Jackson, Pat Gread, Amu Uperti, Jenny Stockdill, Jannine Rhodes and Annie Barker at the Department of Chemistry, for their support from the very beginning of the research.

The Department of Engineering technical staff Stewart Finlay, Lisa Li, Indar Singh, Brett Nichol, Yuanji Zhang and Engineering Workshop team for helping me with instruments, tools and fabrications.

A special thanks to Lynne Parker, at the Department of Biology for training me on microbiological analysis, which led to important results, also to Dr. Barry O'Brien for introducing me to Lynne.

The help from technical staff on special instruments Steve Cameron, Helen Turner and Anjana Rajendram and also Stephen Hardy and Peter Jarman of instrument supports team are greatly acknowledged.

I would like to thank my colleagues, Prakash Sirinivasan for the TOC analysis and Jacob Jaine for TEM micrographs.

Prof. Deliang Zhang for providing me with titanium electrode material, Prof. Alistair Wilkins for helping me with the GCMS work and Dr. Johan Verbeek and Talia Hicks for providing and demonstrating me the SPME technique for THM analysis.

I would also like to thank the Science Librarian, Cheryl Ward who has been very helpful in finding specific literature from other sources and in compiling my thesis.

Education New Zealand is acknowledged for granting me the New Zealand International Doctoral Research Scholarship (NZIDRS) and the extension provided by the University of Waikato Doctoral Scholarship.

My sincere thanks go out to my friend, Dr. Peter Sun at the School of Management for all his support and guidance in settling down comfortably with my family in New Zealand.

Finally to my mother, siblings and in-laws, thank you for your love, support and prayers throughout the years. To my dearest children Andreana and Jerome, thank you for your big smiles and words of affection that kept me cheerful throughout this work and my wife Nilakshi, you always stood beside me with love and respect that have led me to where I am.

Table of Contents

List of Figures

List of Tables

List of symbols and abbreviations

A	Area (of electrode)
AC	Alternating current
AOP	Advanced oxidation processes
BDD	Boron doped diamond
BTEX	Benzene, Toluene, Ethtylbenzene, Xylene
CE	Current Efficiency
CFU	Colony forming units
cm	centimetre
DC	Direct current
DES	Department of Environmental Services
DO	Dissolved oxygen
DSA	Dimensionally Stable Anode
EAOP	Electrochemical advanced oxidation processes
EC	Energy Consumption
EDAX	Energy Dispersive Analysis through X-ray spectroscopy
E_e^A	Equilibrium potential at the anode reaction
E_e^C	Equilibrium potential at the cathode reaction
EU	European Union
F	Faraday constant
G	Conductance
GCMS	Gas Chromatography Mass Spectroscopy
h	Hours
h	Hydraulic head
HS	Headspace
i	Hydraulic gradient
IC	Indigo Carmine dye
IR_{CELL}	Voltage drop due to cell resistance
$IR_{CIRCUIT}$	Voltage drop due to circuit resistance
K	Cell constant
k	Kilo

L	Inter-electrode gap
L	Litres
M	Molecular weight
MAV	Maximum available value
MCL	Maximum Contaminant Level
mm	millimetre
mol	Moles
η_A	Anodic overpotential
η_C	Cathodic overpotential
NTU	Nephelometric Turbidity Units
ø	Current efficiency
PAH	Polycyclic aromatic hydrocarbons
PC	Power Consumption
PCB	Polychlorinated biphenols
PEF	Pulsed electric field
PEFT	Perforated electrode flow through
PU	Polyurethane
PVC	Poly Vinyl chloride
Q	Volumetric flow rate
RB2	Reactive Blue 2 dye
RB4	Reactive Blue 4 dye
RO	Reverse osmosis
SDWA	Safe drinking water act
SEM	Scanning electron microscope
SHE	Standard hydrogen potential
SPME	Solid Phase Microextraction
TEM	Transition electron microscope
THMs	Trihalomethanes
TOC	Total Organic Carbon
UF	Ultra filtration
US EPA	United States Environmental Protection Agency
UV	Ultra violet
V	Voltage
VIS	Visible

W	Watt
WHO	World Health Organisation
θ	Material yield
ρ	Density of fluid
ΔG	Free energy change
μ	Microns
σ	Charge density
δ	Thickness of the hydrodynamic boundary layer
Re	Reynolds number
ϵ_0	Permittivity of free space
κ	Dielectric constant

Chapter 1: Introduction and literature review

1.1 General introduction

Access to safe drinking water is an essential aspect of modern urban living. Clean water is also needed for agriculture and for industry. Water use associated with population growth and economic development has placed increasing demands on water resources. It has been estimated that by 2025, 1.8 billion people will live in regions of severe water scarcity (W.H.O., 2006). Likely future shortages of water make it imperative to maximise the use and reuse of existing resources and minimise water degradation through pollution. Water treatment technologies have evolved over the last century and can, at a cost, deal with most water quality problems. Challenges for the future will be to develop technologies that will allow good quality water to be produced affordably from more marginal sources. An example of such a marginal source is the iron and manganese containing bore water drawn from peat soils of the Waikato region. Electrochemical technologies are likely to play a role in meeting the challenges posed by such water sources.

Dealing with the mixtures of organic and inorganic compounds in natural and industrial waters presents a diverse range of problems for which there is no universal strategy. Oxidation is a widely used tool. Degradable pollutants can be removed cost effectively by biological oxidation. More refractory compounds require physical-chemical methods (filtration, coagulation, adsorption, and flocculation), chemical oxidation (use of chlorine, hydrogen peroxide and per sulphates) and advanced oxidation processes (AOP) (Fenton's reaction, ozone and UV radiation). However, all these techniques have some major disadvantages. For example, filtration and adsorption are not always sufficient to achieve the discharge limits; coagulation and flotation generate large amounts of sludge; chemical oxidations have low capacity rates and need transportation and storage of dangerous reactants; and advanced oxidation processes require high investment costs (Panizza & Cerisola, 2009). In this context, oxidative electrochemical

technologies offer an alternative solution to the water treatment industry, because electrons provide efficient, cost-effective, easily automated and clean reagents (Rajeshwar & Ibanez, 1997).

In electro-oxidation, contaminants can be removed by direct electrolysis, where pollutants exchange electrons directly with the anode surface without involvement of other substances, or indirect electrolysis, where contaminants do not exchange electrons directly with the anode surface but through the mediation of electro-generated oxidative intermediate species, which shuttle the electrons between the electrode and the contaminants. Indirect oxidation is the most common mechanism operating in electrolytic water purification. The most commonly used electro-generated oxidizing intermediate is active chlorine produced by the anodic oxidation of chloride ions. Up until now the electrochemical reactor designs have not been able to economically produce sufficient chlorine to cause complete oxidation of contaminants in low chloride containing low conducting systems. Common practice has been the production of chlorine using the chlor-alkali process where a saturated brine solution is electrolysed to produce chlorine which is subsequently dosed into the water as the oxidant. Extensive research and development has improved the electrochemical chlorine production reaction by developing electro-catalytic coatings on anode surfaces (metal oxide coated dimensionally stable anodes (DSA) which reduce the reaction overpotentials. Electrochemical reactions take place at the interface of an electronic conductor, the electrode, and an ion conductor, the electrolyte and are of heterogeneous nature. Though catalytic coatings improve the electron transfer process at the anode, reaction efficiencies are poor at low electrolyte (chloride) concentrations due to mass transfer limitations. Improving the mass transport is the key to increasing the efficiency at low electrolyte concentrations such as found in natural water and wastewater systems. One approach to improve the mass transfer has been to increase the electrode area by using flow through systems of porous and porous media bed electrodes. These electrode systems suffer problems of current and potential distribution and also of cell resistance due to the accumulation of gas bubbles in the porous medium.

An obvious way of reducing cell resistance is to reduce the inter-electrode gap. However in conventional parallel plate electrochemical cells, where flow is between the electrodes, hydrodynamic considerations limit reduction of electrode separation to millimetre dimensions; even at millimetre dimensions these systems require high pressures to deliver adequate flow rates. The development of a parallel plate cell where each electrode has a regular array of drilled perforations such that the flow path through the cell can be reduced to a few millimetres offers a way of further reducing the inter-electrode gap without causing excessive resistance to hydrodynamic flow.

1.2 Literature review

1.2.1 Evolution of electrochemical technology

Electrochemistry is the branch of chemistry concerned with the interrelation of electrical and chemical effects (Bard & Faulkner, 2001). A large part of this field deals with the study of chemical changes caused by the passage of an electric current and the production of electrical energy by chemical reaction. The field of electrochemistry encompasses a wide array of different phenomena, devices and technologies. Electrochemical engineering can be considered as a daughter of chemical engineering, whose origin was in the 19th century but which developed significantly during World War II (Lapicque, 2004). Up to the mid 20th century the primary disciplines, for example physics, chemistry, biology, physical chemistry and electrochemistry, were the basis of the main scientific discoveries, whereas the development of processes was carried out by engineers having a high expertise in mechanics and technology. Chemical engineering gradually became a discipline in the middle of the twentieth century, and two important, complementary tools fed this development: (i) transport and transfer phenomena resulting from investigations in physics made by Nernst, Einstein, Navier, Stokes, Planck and Maxwell, and (ii) a conceptual approach in designing reactors and processes (Lapicque, 2004).

In its early years, electrochemical engineering was an engineering discipline in a setting of booming industry in the developed countries. With the development of new investigative techniques, new theories for more efficient processes were successfully applied to large-scale electrochemical processes such as aluminium production, chlor–alkali electrolysis, deposition of metals and metal protection. Subsequently electrochemical technology had to adapt to the global economic and business environments caused by energy issues, progressive competition from other technologies, shortages of particular raw materials and environmental issues. When energy became scarcer and more expensive due to the successive oil shocks of the 1970s and the early 1980s emphasis on the reduction of energy consumption became a priority in all industrial processing including electrochemical processing.

More recently the focus of developments in electrochemical technologies has been towards environmental protection. Using electricity to treat water was first proposed in UK in 1889 (Guohua, 2004). The application of electrolysis in mineral beneficiation was patented by Elmore in 1904. Electro-coagulation with aluminium and iron electrodes was patented in the US in 1909. The electro-coagulation of drinking water was first applied on a large scale in the US in 1946 (Guohua, 2004). However, due to the relatively large capital costs and the expensive electricity supply, electrochemical water and wastewater technologies have not found widespread application. With the ever increasing standards for drinking water supplies and stringent environmental regulations regarding wastewater discharge, electrochemical technologies have gained renewed importance during the past two decades.

Electrochemical technology plays an important role in the modern industrial and commercial world. The applications are diverse and ever increasing and intersect many disciplines. An overall perspective of the scope of industrial electrochemistry can be outlined as follows (Scott, 1992):

- Inorganic electro synthesis
- Extraction and production of metals
- Organic electro synthesis
- Metal finishing and processing

- Water purification and effluent treatment
- Energy generation
- Corrosion
- Sensors and monitors

Today, electrochemical technologies have been developed to a state that they are not only comparable with other technologies in terms of cost but are also more efficient and more compact. For some processes electrochemical technologies are indispensable, for example the chlor-alkali process for chlorine production and the treatment of wastewaters containing difficult pollutants. Electrochemical techniques have become competitive with chemical, catalytic and biochemical processes, due to their many advantages, (Scott, 1992):

- Mild conditions in processes, e.g. low temperature and pressure
- Improved selectivity of existing reactions
- Availability of novel chemical transformations
- Reduction in the number of synthesis steps
- Improved management of potential pollutants
- Avoidance of hostile and hazardous reagents
- Use of unconventional feed stocks
- Treatment of small to large volumes from micro litres up to millions of litres
- Phase separations
- Amenability to automation

Environmental aspects have become key issues in the development of industrial processes to meet the requirements of sustainable development (Juttner, 2007). In the context of sustainable development, electrochemistry offers promising approaches due to the use of the electron as a ‘‘clean reagent’’(Rajeshwar, Ibanez, & Swain, 1994; Trasatti, 1995). There is common agreement among workers in the field that electrochemically based processes will be increasingly used in the future to meet the economic and social challenges resulting from utilisation of low-grade raw materials, requirement for energy savings and the need to protect the environment.

1.2.2 Problems associated with electrochemical technology

Electrochemical techniques generally become less effective when they have to deal with low conducting electrolyte solutions, especially those of natural and environmental systems. While electrochemical techniques offer attractive possibilities for a variety of treatments of water and wastewater, including electro-chlorination, electro-oxidation and recovery of metals by electrolytic stripping, they are generally too inefficient to be economically viable (Guohua, 2004; Martinez-Huitle & Brillas, 2008; Martınez-Huitle & Brillas, 2009). The inefficiency arises from:

- High cell resistance resulting from low electrolyte concentrations and constraints on the reduction of the inter-electrode gap
- Polarization effects (gas bubble accumulation)
- Mass transport characteristics (ineffective mixing)
- Selection of electrode material

Another critical point is the stability of cell components in contact with aggressive media, in particular, the durability and long-term stability of the electrodes and electro-catalysts. Optimisation of the above parameters is the key in developing optimum cell design. One opportunity for improved cell design is the development of a flow through cell using perforated electrodes (see Section 1.1).

1.2.3 Engineering for electrochemical reactions

Electrochemical reaction engineering deals with design, development and prediction of production rates of electrochemical processes for industrial processes. As in chemical engineering, it focuses on the right choice of the electrochemical reactor, its size and geometry, mode of operation, and the operation conditions. This includes calculation of performance parameters, such as space-time yield, current efficiency, selectivity, degree of conversion, and energy efficiency for a given reaction in a specified reactor. Electrochemical thermodynamics deals with driving forces and the energies of the electrochemical reaction. Forecasts of how fast the reactions may occur are answered by

electrochemical kinetics. Kinetic predictions need input from fundamental investigations of the reaction mechanism and the micro-kinetics at the molecular scale (Juttner, 2007; Pletcher, 1984b; Rajeshwar, et al., 1994). While micro-kinetics describes charge transfer under idealized conditions at the laboratory scale, macro-kinetics deals with the kinetics of the large-scale process for a certain cell design, taking into account the various transport phenomena. The micro-kinetics combined with calculations of the spatial distribution of the potential and current density at the electrodes leads to the macro-kinetic description of an electrochemical reactor (Juttner, 2007; Lapicque, 2004; Scott, 1992). The relation between micro- and macro-kinetics is shown schematically in Figure 1.1.

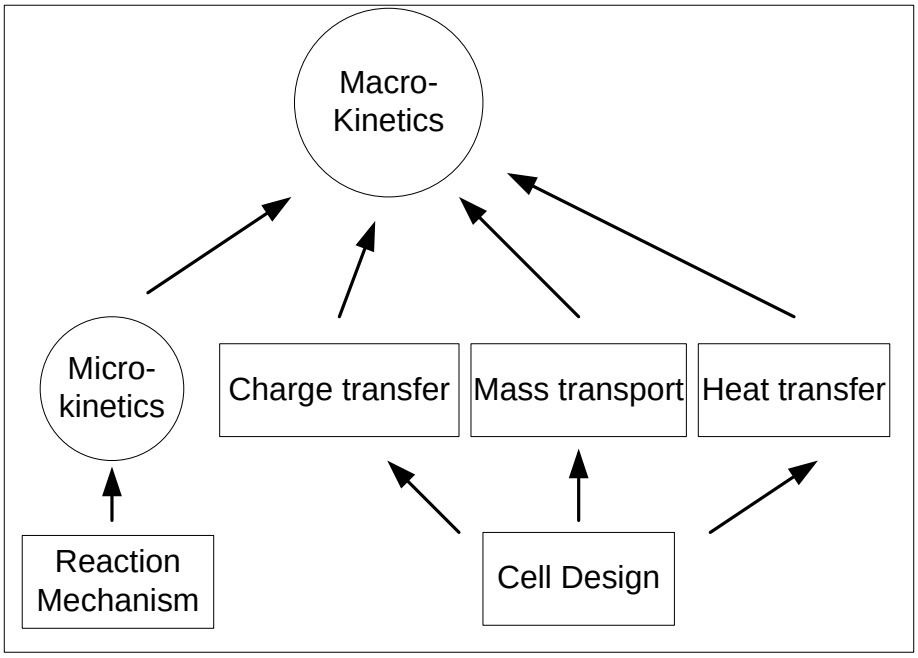

Figure 1.1 - Concept of micro-kinetics and macro-kineticsfor electrochemical reactions, adapted from Juttner,2007.

The phenomenon of charge transport, which is unique to all electrochemical processes, must be considered along with mass, heat, and momentum transport. The charge transport determines the current distribution in an electrochemical cell, and has far-reaching implications on the current efficiency, space-time yield, specific energy consumption and the scale-up of electrochemical reactors.

1.2.4 Figures of merit

From an industrial perspective the percentage return on investment is the final criterion for success or otherwise of a process. An indication of economic viability can be obtained from the so called "figures of merit" for the process, in the diverse applications of electrochemistry; figures of merit allow comparisons to be made. It is commonly not possible to optimise all the figures of merit; change in one cell design or electrolysis parameter to improve one figure of merit will be unfavourable to another. Often a trade off the importance of the figures of merit is necessary to find the overall economic optimum. The principle figures of merits are defined below

The ***material yield,* θ,** is defined by

$$\theta = \frac{\textit{moles of starting material converted to product}}{\textit{moles of starting material consumed}} X\ 100 \qquad \textit{(Eq. 1-1)}$$

It determines the consumption of raw material for the desired tonnage of product. Material yield (θ) will be almost always less than 100% due to impure starting materials. Material yield is sometimes discussed in terms of ***selectivity*** where

$$\textit{Selectivity} = \frac{\textit{moles of desired product}}{\Sigma\ \textit{moles of all product}} \qquad \textit{(Eq. 1-2)}$$

The ***current efficiency, ø,*** is the yield based on the charge passed during electrolysis. It is defined as:

$$\emptyset = \frac{\textit{charge used in forming the product}}{\textit{total charge consumed}} X\ 100 \qquad \textit{(Eq. 1-3)}$$

where the charge used in forming the product is calculated using Faraday's law. A value of **ø** below 100% indicates side reactions and the formation of by-products. These reactions arise from electrolysis of solvent or other solution species rather than the starting material e.g. production of oxygen during chlor-alkali process from oxidation of water.

The ***percentage conversion per pass*** is the percentage of starting material consumed on each pass through the reactor. Since electrolysis is a heterogeneous process, the percentage conversion per pass depends on the ratio of the active electrode area to the cell volume and to the flow rate of the electrolyte. A high conversion per pass is advantageous if, for example, the starting material is not to be recycled (e.g. effluent treatment) or the product must be extracted during each cycle. This is obtainable with most existing cell designs only when a slow flow rate is used and leads to long residence times and poor mass transport conditions. Hence a cell with a high conversion per pass at a high flow rate is often a desirable goal and indeed provides a driving force for designing cells with a high surface area per unit volume.

The ***energy consumption*** is the electrical energy required (or power dissipated) to make a unit weight of the product and it is normally quoted in kilowatt-hours per kilogram (kWh/kg). It is a function of both the electrolysis conditions and the cell design. The energy consumption (kWh/kg) is given in the equation

$$Energy\ consumption = \frac{nFV}{3.6 \times 10^4 \, ø \, M} \qquad (Eq.\ 1\text{-}4)$$

Where ***M*** is the molecular weight in kilograms, ***n*** is number of electrons involved in the reaction of interest and ***F*** is the Faraday constant. It can be seen that the energy consumption does not depend directly on current density but really only on the cell voltage and the current efficiency. Hence the energy consumption can be minimized only by selecting the electrolysis conditions so that the current is used solely for the reaction of interest and by making the cell voltage as low as is

practicable. The cell voltage is a complex quantity made up of a number of terms and is given by the equation;

$$V = E_e^C - E_e^A - |\eta_A| - |\eta_C| - IR_{CELL} - IR_{CIRCUIT} \qquad (Eq.\ 1\text{-}5)$$

E_e^A and E_e^C are the equilibrium potentials for the anode and cathode reactions respectively, η_A and η_C terms are the anodic and Cathodic overpotentials, and IR_{CELL} and $IR_{CIRCUIT}$ are the voltage drops due to the resistance of the cell and the circuit respectively. The $(E_e^C - E_e^A)$ may be calculated from the free energy change for the overall cell reaction by:

$$\Delta G = -nF\ (E_e^C - E_e^A) \qquad (Eq.\ 1\text{-}6)$$

In electrolytic processes the overpotentials and *IR* terms represent energy inefficiencies and hence will require a larger cell voltage for a given current. In general the overpotential can contain a contribution from the electron transfer process and from mass transport. Industrial cells are designed to operate under conditions where the contribution from the mass transport is minimised. For a simple electron transfer reaction, the overpotential is given by

$$|\eta| = \frac{2.3\,RT}{\alpha nF}(\log I - \log I_0) \qquad (Eq.\ 1\text{-}7)$$

Where I and I_0 are the observed and exchange current densities and α is the transfer coefficient. The electron transfer overpotential term will depend on the transfer coefficient and on the exchange current density and it is the measured Tafel slope rather than $2.3RT/\alpha nF$ which is important. Depending on the Tafel slope, this overpotential will increase by 30-250 mV for each decade increase in current. The electron transfer overpotential is related to the kinetics of the electron transfer process (Pletcher, 1984b). Electron transfer will depend upon the electrolysis conditions such as electrolyte, pH, temperature and particularly the

electrode material. The electrode material is critical where it must selectively catalyse the reaction of interest.

The cell resistance R_{CELL} can be decreased by making the inter-electrode gap smaller and using concentrated electrolyte solutions. The final term $IR_{CIRCUIT}$ is the potential drop across the wires, various connectors and other parts of the electrical circuit.

The ***space time yield*** is a measure of the rate of production per unit volume of reactor and is normally quoted in units such as mol/Lh. The space time yield is proportional to the effective current density, current efficiency and the active surface area of electrode per unit volume.

1.2.5 Electrochemical cell designs

The design of the cell will affect all the figures of merit for an electrochemical process. The principal factors in a cell design that influence its performance are (Pletcher, 1984b):

- Presence and absence of a separator and its type
- Mass transport regime
- Arrangement of electrodes
- Inter-electrode gap
- Potential distribution at both electrodes
- Electrode materials

The factors above are accommodated differently in cell designs according to its application. Despite the differences, there are some common conventions in cell design;

- Minimal inter-electrode gap
- Uniform potential distribution over the electrode surface
- Construction materials compatible with electrolyte and electrolysis products
- Maximised mixing to allow mass transfer
- Direct integration of the cell into a process

- Avoidance of electrode separators if possible
- Simplest and cheapest process requirements

One of the most important issues in cell design is to maintain high mass transfer rates as the main reactions take place at the electrode surfaces. To improve mass transfer at the surface of the electrode, common methods such as gas sparging, high fluid velocity, use of baffles and incorporation of various types of turbulence promoters are employed. Sono-electrochemical processes have also been tested to enhance mass transfer (Guohua, 2004). In addition to procuring a high mass transfer rate, cell construction should account for easy access to and exchange of cell components (Anglada, Urtiaga, & Ortiz, 2009). A recent overview of the various available types of electrochemical cell/reactor designs are shown in Figure 1.2.

Two main types of electrodes exist, two-dimensional and three-dimensional constructions. The latter guarantee a high value of electrode surface to cell volume ratio. As given in Figure 1.2 both types of electrodes can be used as static or moving electrodes. The use of moving electrodes leads to increased values of the mass-transport coefficient due to turbulence promotion. Among the two-dimensional electrodes, static parallel and cylindrical electrode cells are used in most reactor designs especially in electrochemical oxidation of waste-waters.

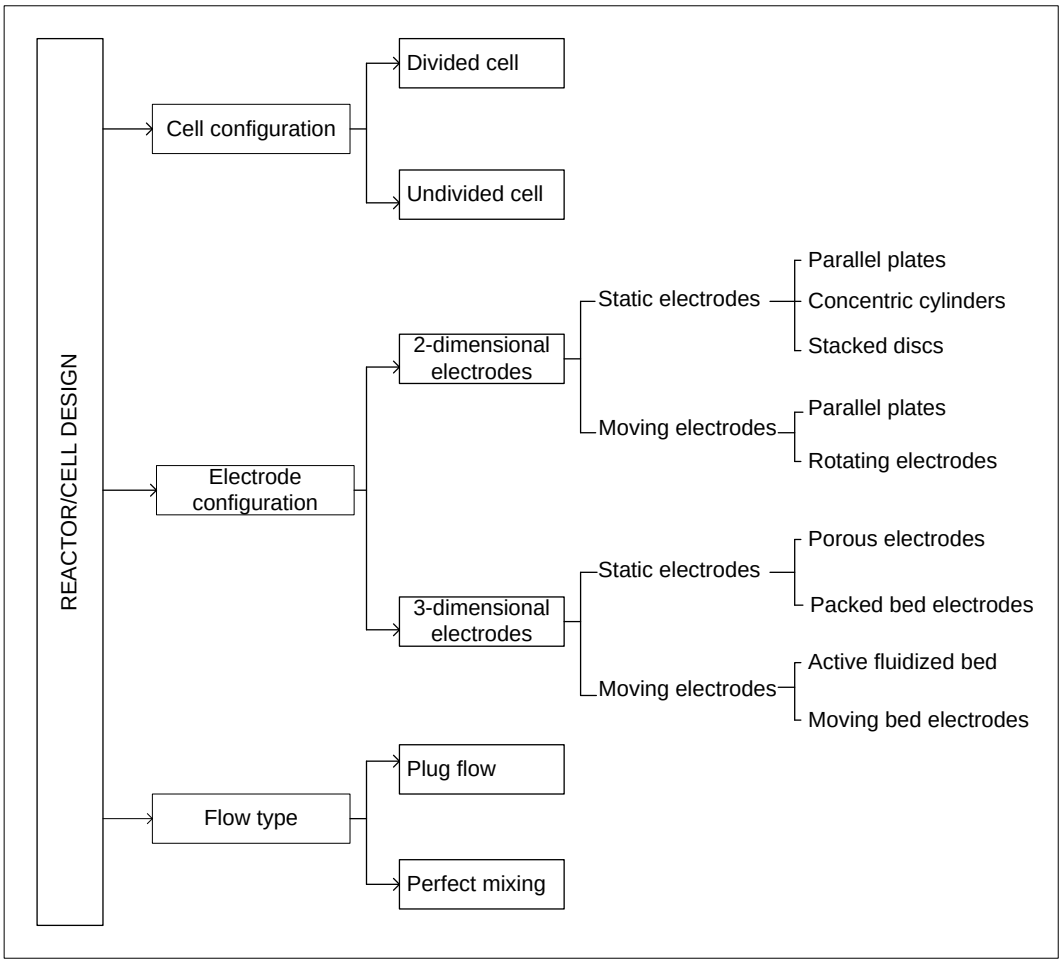

Figure1.2 - Classification of electrochemical reactors in terms of cell configuration, electrode geometry and flow type, adapted from (Anglada, et al., 2009).

Cell designs using the parallel plate geometry in a filter press arrangement are widely installed due to the ease of scale-up to a larger electrode area, by incorporation of more electrode pairs or an increased number of cell stacks (Rajeshwar & Ibanez, 1997).

Besides the electrode geometry, the configuration of the cell, divided or undivided has to be considered in the reactor design. In divided cells, the anolyte and catholyte are separated by a porous diaphragm or an ion conducting membrane. For divided cells the choice of the separating diaphragm or membrane is as important as the choice of electrode materials for the proper functioning of the electrolytic process. Overall, the use of divided cells should be avoided whenever possible because separators are costly, increase the inter-electrode gap and cause

mechanical and corrosion problems (Anglada, et al., 2009). In the case of flow characteristics within a reactor, two types of limiting hydrodynamic behaviour may be considered, namely, plug flow and perfect mixing.

Most undivided electrochemical systems use solid parallel plate electrodes and a flow by configuration. The flow by configuration places a lower limit on the reduction of the inter-electrode gap. An alternative flow regime where the flow passes through the electrodes and travels a minimal distance between them offers the possibility of reducing the inter-electrode gap without excessively increasing resistance to flow. Some work with porous electrodes using a flow through configuration has been reported (Ateya, Al-Kharafi, Abdallah, & Al-Azab, 2005; B. G. Ateya, Arafat, & Kafafi, 1977; Bae, Chakrabarti, & Roberts, 2008; Menini, Henuset, & Fournier, 2005; You, Zhang, & Chen, 2009). Most of this work was designed to improve efficiency by increasing electrode surface area. The porous electrode flow through cell systems suffer from non uniform current and potential distribution and also accumulation of hydrogen gas bubbles in the porous media increasing the cell resistance and in the case of porous media bed, expansion of the media bed at high cathodic voltages (Nava, Oropeza, Ponce de León, González-García, & Frías-Ferrer, 2008; Newman & Tobias, 1962; Saleh, 2004). The possibility of achieving better hydrodynamics by a flow through configuration, using electrodes with a regular array of drilled perforations, rather than porous electrodes, does not seem to have been reported.

1.2.6 Electro-oxidation

Electrochemical oxidation of contaminants in water can occur through direct oxidation or indirect oxidation (Anglada, et al., 2009). Direct oxidation involves two steps: (1) diffusion of pollutants from the bulk solution to the anode surface and (2) oxidation of pollutants at the anode surface. During indirect electrochemical oxidation, a strong oxidizing agent is electrochemically generated at the anode surface and this oxidizes the contaminants (see Figure 1.3). The indirect oxidation mechanism is more favourable in contaminant removal processes and is used frequently in the water treatment applications (Chiangi, Changi, & Wen, 1995; Deng & Englehardt, 2007; Murphy, Hitchens, Kaba, & Verostko, 1992; Yang & James, 2007).

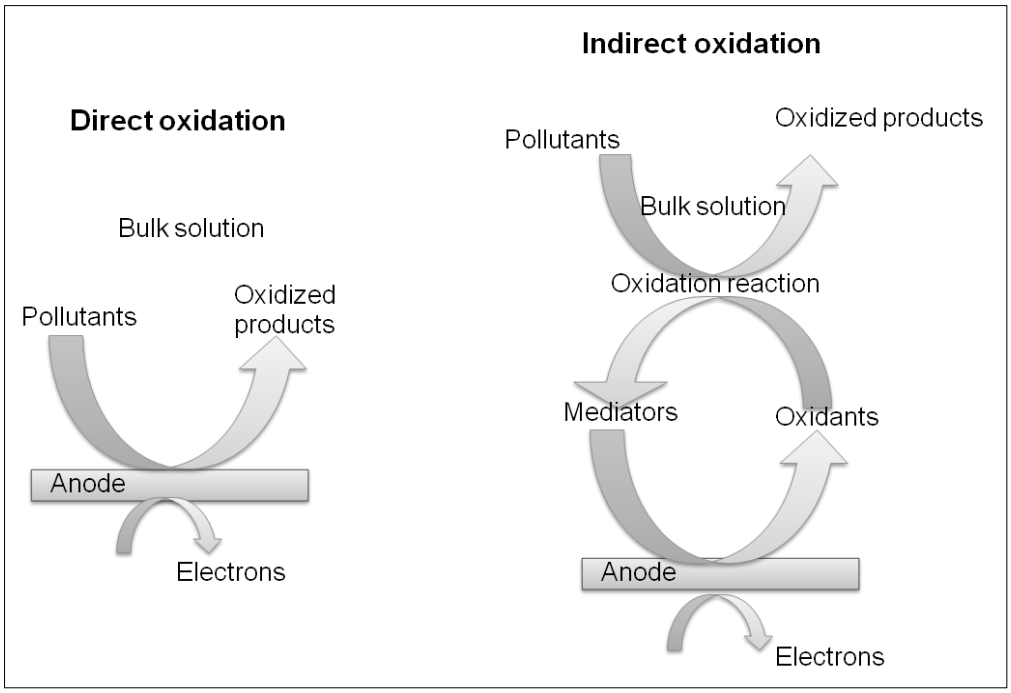

Figure 1.3 - Pollutant removal pathways in electrochemical oxidation - direct and indirect oxidation adapted from Chiangi et al. 1995.

The production of chlorine as the mediator oxidizing species has been shown to be very effective (Deng & Englehardt, 2007; Marcos, Santos, Josealdo, & Carmem, 2006; Una, Altay, Koparal, & Ogutveren, 2008).

1.2.7 Oxidation of iron and manganese in groundwater

Groundwater comprises about 95 per cent of the planet's freshwater not locked up in the polar ice caps. Two billion people depend directly upon aquifers for drinking water, and 40% of the world's food is produced by irrigated agriculture that relies largely on groundwater (United Nations Environmental Program, 2003). In the future, aquifer development will continue to be the basis of economic development and reliable water supplies will be needed for domestic, industrial and irrigation purposes. Aquifers are very convenient sources of water, which is relatively easily and cheaply extracted and often used without further treatment. In some regions of the planet however, natural contamination make these water resources unusable.

Iron and manganese occur naturally in water, especially groundwater. Water containing excessive amounts of iron and manganese can stain clothes, discolour plumbing fixtures, and add a "rusty" taste and appearance to water. The taste of beverages, such as tea and coffee, may also be affected by iron and manganese contaminants. Manganese is known to affect neurological and muscle function in humans. The US Environmental Protection Agency and the Safe Drinking Water Act (SDWA) has established a secondary (aesthetic) standard, a Maximum Contaminant Level (MCL) for iron in drinking water as 0.3 mg/L and for manganese it is 0.05 mg/L. While at present, health standards for either iron or manganese in drinking water have not been set, a health based standard for manganese is possible. The US Department of Environmental Services (DES) Health Risk Assessment Program has adopted an interim health based standard for manganese of 0.84 mg/L.

The type and concentration of iron and manganese present in water determines the best procedure and treatment process to be used for removal. Iron and manganese can be present in water in one of three forms: dissolved, particulate and colloidal. The predominance of one form over another is dependent on the water's pH. The two most common treatment methods used are removal by oxidation/filtration and adsorption onto ion exchange media. Oxidation involves the introduction of an

oxidising agent which chemically reacts with the iron or manganese to form insoluble hydrous oxides which can be filtered out.

Oxidation can be carried out in one of the following methods:

- aeration - blowing/spraying air through the water
- addition of dissolved chemical oxidants - chlorine, calcium hypochlorite, chlorine dioxide and potassium permanganate
- adsorption onto reactive greensand media

The process of oxidation followed by filtration is often the treatment of choice when concentrations are above 10 mg/L. The use of ion exchange resins for the removal of iron and manganese has limited application due to the requirement that the contaminants be in dissolved form and at levels less than 10 mg/L. This is due to the tendency of oxygen to react with the iron and manganese thereby increasing the potential for clogging and build-up on the resin surface. Iron fouling can also be caused by iron bacteria. The iron bio-fouling problem is both complex and widespread. It attacks wells and water systems around the world in varied aquifer environments, both contaminated and pristine. In some places, it causes great damage; in others, it is considered a minor nuisance. Iron bacteria can be controlled by periodic well chlorination or by chlorination, retention, and filtration of extracted water. Activated carbon is usually used as the filter material so the excess chlorine can also be removed.

1.2.8 Groundwaters of New Zealand

New Zealand groundwaters are known to have high levels of iron and manganese, naturally derived from water-rock interactions (Rosen, 2001). Iron and manganese will be present in groundwater if dissolved oxygen levels are very low because the reduced forms of iron and manganese are much more soluble than the oxidized forms. High iron and manganese containing aquifers are commonly associated with peat layers, slow moving waters and consequent oxygen depletion. Groundwater makes up to 90 percent of Waikato Region’s freshwater supplies and is used for drinking water, industrial, agricultural and horticultural supplies. About 400 bore wells are drilled annually (Hadfield, 2001). Groundwater in the

region is often naturally contaminated with iron and manganese of the order of 20.0 mg/L iron and 0.9 mg/L manganese. A problem associated with the removal of this iron and manganese is that oxidation by forced aeration often forms highly stable brownish colloidal suspensions which do not settle on standing and are also difficult to filter. Currently, bores with this problem groundwater are often abandoned because treatment requires both expensive addition of chemicals and filtration. These problem waters have also been found to contain high levels of dissolved organic carbon (140 mg/L) and silica (32 - 40 mg/L) derived from the peat layers and the volcanic subsoil and which are believed to be implicated in the formation of the stable colloidal suspensions. It has been found that rapid chemical oxidation with calcium hypochlorite favours the formation of aggregated flocs which facilitates the removal of the contaminant metal ions (Carlson & Schwertmann, 1987).

1.2.9 Formation of trihalomethanes (THMs) during groundwater treatment

When free available chlorine is present in water there is the possibility of reaction with natural organic matter, mostly humic acid and fulvic acid, to form trihalomethanes (THMs) (Ivancev-Tumbas, Bozo, Tamas, & Karlovic, 1999). The most significant THMs formed based on occurrence and toxicity are chloroform ($CHCl_3$), dichlorobromomethane ($CHCl_2Br$), chlorodibromomethane ($CHClBr_2$), and bromoform ($CHBr_3$) (Choa, Kongb, & Ohb, 2003). In the 1970s these THM molecules were identified in water as disinfection by-products (DBPs) formed during chlorination of surface water (Hsu, Jeng, Chang, Chien, & Han, 2000). All these molecules are considered as being possible carcinogens and therefore human exposure to such compounds should be minimised (Bull et al., 1995; Chang, Chao, Chiang, & Lee, 1996; Choa, et al., 2003). The US Environmental Protection Agency and European Union (EU) have set the maximum total THM concentration in drinking water at 80 and 100 µg/L respectively. WHO on the other hand provide guidelines for each THM compound (W.H.O, 2004). The New Zealand guideline for drinking water quality stipulates maximum allowable values (MAVs) for each of the four THMs as chloroform 0.2 mg/L, dichlorobromomethane 0.06 mg/L, chlorodibromomethane 0.15 mg/L, and

bromoform 0.1 mg/L (Ministry of Health, 2005). The factors influencing THM formation are total organic carbon (TOC), structure of the organic matter, free chlorine concentration, the contact time with the free chlorine, TOC to chlorine ratio, pH and temperature (Ivancev-Tumbas, et al., 1999). It is important to know the levels of THM formation during groundwater treatment especially when chlorine mediated oxidation is involved.

1.2.10 Electro-chlorine generation

The electrolytic generation of chlorine oxidants has many advantages in water treatment, the principal one being that onsite generation of the chlorine eliminates the transport, handling and the storage of dangerous chlorine gas or hazardous concentrated hypochlorite (Khelifa, Moulay, Hannane, Benslimene, & Hecini, 2004; Martinez-Huitle & Brillas, 2008). The electro-generation of chlorine process is safe, environmentally friendly, easily operated and known to inactivate a wide range of micro-organisms ranging from bacteria to viruses and algae, the primary function of a disinfectant (Kerwick, Reddy, Chamberlain, & Holt, 2005; Martinez-Huitle & Brillas, 2008).

Chlorine electro-generators are of two types: undivided cell and divided cell. Undivided chlorine electro generators produce hypochlorite solutions (along with a gaseous mixture of oxygen and hydrogen) whereas divided cell electro-generators produce separate chlorine and hydrogen gas streams. Undivided cells can be used in two ways: as producers of bulk hypochlorite which is dosed into water and inline generators which produce a mixture of oxidizing species such as free chlorine and hypochlorite formed from the chloride dosed into a parallel side stream of the main flow.

The active chlorine species are generated at the anode by the following reaction

$$2Cl^- \leftrightarrow Cl_{2(aq)} + 2e^- \qquad E^o = 1.36V \qquad \text{(Eq. 1-7)}$$

The chlorine formed, depending upon the pH, then reacts with water to form HOCl, OCl^- and Cl^- according to the equilibria (at 298 K) (Nazaroff & Alvarez-Cohen, 2001):

$$Cl_{2(g)} \leftrightarrow Cl_{2(aq)} \qquad K_H = 0.062\ mol\ L^{-1}\ atm^{-1} \quad (Eq.\ 1\text{-}8)$$

$$Cl_{2(aq)} + H_2O \leftrightarrow HOCl + Cl^- + H^+ \qquad K_1 = 5 \times 10^{-4}\ mol^2L^{-2} \quad (Eq.\ 1\text{-}9)$$

$$HOCl \leftrightarrow H^+ + OCl^- \qquad K_2 = 2.6 \times 10^{-8}\ mol\ L^{-1} \quad (Eq.\ 1\text{-}10)$$

Competing anode reactions are the electrolysis of water to produce oxygen, reactive oxidation products and oxidation of the electrode. Cost effectiveness of undivided cell electro-chlorinators are limited by cell resistance which results in low current and power efficiencies and the high capital costs associated with the expensive electrode materials designed to minimize oxygen production and anode oxidation (Guohua, 2004). The most commonly used anode materials in commercial hypochlorite production are dimensionally stabilized anodes (DSA) of titanium coated with either oxides of ruthenium and iridium or platinum metal (Jeong, Kim, & Yoon, 2009; Khamtorn, Shin, Jeong , & Chung, 2009 ; Khelifa, et al., 2004; Martinez-Huitle & Brillas, 2008; Rajkumar & Kim, 2006). In addition to chlorine production, these electrodes have been reported to produce higher oxides of chlorine by chemical and electrochemical reactions *(Eqs. 1-11 and 1-12)* at increasing hypochlorite concentrations (Onofrio, Serena, Alessandro, & Giuseppe, 2009):

$$3OCl^- \leftrightarrow ClO_3^- + 2Cl^- \qquad (Eq.1\text{-}11)$$

$$6OCl^- + 3H_2O \leftrightarrow 2ClO_3^- + 4Cl^- + 6H^+ + 1.5O_2 + 6e^- \qquad (Eq.1\text{-}12)$$

Polcaro et al. (Polcaro, Vacca, Mascia, & Ferrara, 2008) report that hydroxyl radicals generated by water oxidation also produce compounds such as hydrogen peroxide, ozone and eventually chlorites and chlorates at DSAs. Recently interest has been shown in the use of boron doped diamond (BDD) anodes to improve chlorine production but this material increases the formation of the undesired

oxidised chlorine products (Bergmann & Rollin, 2007; Bergmann, Rollin, & Lourtchouk, 2009).

Graphite, while suffering from low chlorine production current efficiencies, offers the advantages of low cost, drinking water compatibility and a lesser likelihood of the formation of more toxic highly oxidised chlorine products. Perhaps improved cell design can compensate for lower current efficiency.

1.2.11 Electrochemical treatment of wastewater: textile effluents

Chlorine mediated electrochemical oxidation provides one strategy for the reduction in organic content such as BOD and colour of industrial wastewaters. For example the rapidly growing textile industry consumes a considerable amount of water producing effluents with very strong colour, high loading of COD, suspended solids, dissolved solids, high temperatures and with a wide variation of pH (Körbahtia & Tanyolac, 2009; Mohan, Balasubramanian, & Ahmed Basha, 2007). A textile dyeing process generally consists of desizing, scouring, bleaching, dyeing, finishing and drying operations. Each operation is combined with many rinsing steps which discharge large volumes of coloured effluents. The textile industry consumes a large variety of dye stuffs depending on the fabric type, finish required and depth of colour. Textile effluents are high in colour due to the unfixed dyes. The extent of dye fixation to a fabric depends on the fibre, method of application, depth of shade and the type of dye. In general 10-50% of unfixed dyes can get into the wastewater stream (Chatzisymeon, Xekoukoulotakis, Coz, Kalogerakis, & Mantzavinos, 2006; Flox, Ammar, Arias, Brillas, Vargas-Zavala, & Abdelhedi, 2006). The dye concentration in the textile effluent is usually lower than the concentrations of other auxiliary chemicals used, but the strong colour makes it visible causing aesthetic problems in wastewater discharges. The treatment of the textile dyes in wastewater is further complicated by high concentrations of surfactants, fixation agents and finishing agents. Dye and auxiliary chemical manufacturers are under continuing pressure to make the products perform better especially to be resistant to environmental influences, colour fastness and colour intensity, all of which contribute to the problem of their

removal from wastewaters. This is why the conventional physiochemical and biological treatment processes are often not effective in treating coloured textile effluents. While biological treatment processes have been efficient and economical in decontaminating textile effluents in the past, because effluents are now more recalcitrant to biodegradation, the situation is changing and increasingly they do not meet the discharge standards. Also biological and physiochemical treatment processes require long residence times, large areas for processing and generate large volumes of hazardous sludge which require further treatment. In addition environmental regulations are becoming more and more stringent forcing the industry to look for better alternatives such as electro-chlorine mediated oxidation.

Electro-chlorine mediated oxidation involves strongly oxidising chlorine and chlorine–oxygen species such as HClO and ClO^- (Rajeshwar & Ibanez, 1997). It can be applied as an inline *in-situ* technique if the effluents contain sufficient levels of chloride ions. The electrolysis of aqueous chloride solutions in an undivided cell involves the direct oxidation of chloride ions at the anode to yield soluble chlorine *(Eq. 1-7)* and the reduction of water at the cathode giving hydroxide ion and hydrogen gas. If the local concentration of dissolved chlorine exceeds its solubility, then super-saturation drives the formation of bubbles of chlorine gas. As electro-generated chlorine diffuses away from the anode, it rapidly disproportionate to hypochlorous acid and chloride ion *(Eq. 1-9)*. The hypochlorous acid is in equilibrium with hypochlorite ion as given in *Eq. 1-10*. Figure 1.5 shows the calculated speciation diagram for active chlorine species (Cl_2(aq), Cl^{-3}, HClO and ClO^-) formed by 20% electrolytic conversion of 0.1 mol/L NaCl. The mediated oxidation of dyes with these species is expected to be faster in acidic than in alkaline media because of the higher standard reduction potentials of the $Cl_{2(aq)}$ (E^o = 1.36 V vs. SHE) and HClO (E^o = 1.49 V vs. SHE) relative to ClO^- (E^o = 0.89 V vs. SHE).

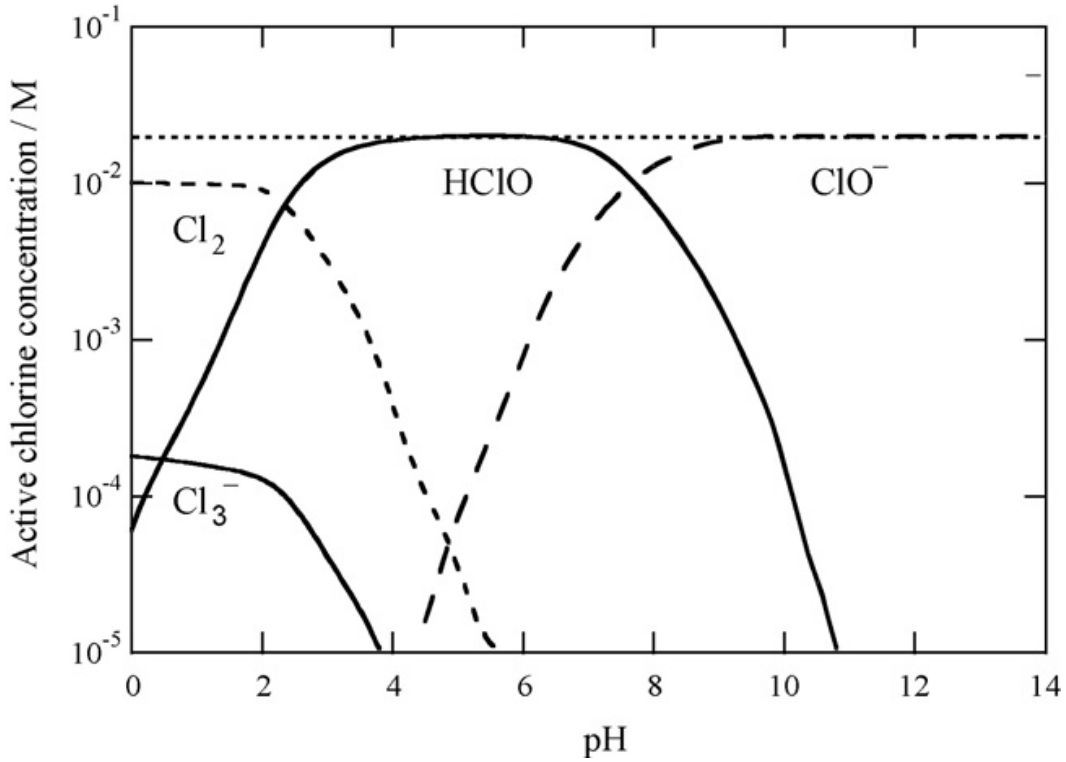

Figure 1.4 - Speciation diagram for the chlorine–water system calculated for the electrolysis of 0.1 mol/L chloride ion at 25°C in an undivided cell with a conversion of 0.2. Taken from Martınez-Huitle & Brillas, (2009).

As the chlorine produced in undivided cells used in decolourisation would be in alkaline and further the dye solutions are generally alkaline, the active chlorine species is the less than optimum ClO^-. It reacts as follows (Raghu & Ahmed Basha, 2007):

$$Dye + ClO^- \rightarrow CO_2 + H_2O + Cl^- \qquad \textit{(Eq. 1-13)}$$

The effectiveness of the electro-generated chlorine could be further reduced by:
(i) The anodic oxidation of chlorite ion from reaction *(Eq. 1-14)* to chlorate and perchlorations from reactions *Eq. 1-15* and *Eq. 1-16*, respectively (Kim & Rajkumar, 2006; Rajkumar & Palanivelu, 2004):

$$ClO^- + H_2O \rightarrow ClO_2^- + 2H^+ + 2e^- \qquad \textit{(Eq. 1-14)}$$

$$ClO_2^- + H_2O \rightarrow ClO_3^- + 2H^+ + 2e^- \qquad \textit{(Eq. 1-15)}$$

$$ClO_3^- + H_2O \rightarrow ClO_4^- + 2H^+ + 2e^- \qquad \textit{(Eq. 1-16)}$$

(ii) The loss of ClO^- by reduction to chloride ion at the cathode:

$$ClO^- + H_2O + 2e^- \rightarrow Cl^- + 2OH^- \quad \textit{(Eq. 1-17)}$$

and (iii) Reactions in the bulk solution such as:

$$2HClO + ClO^- \rightarrow ClO_3^- + 2Cl^- + 2H^+ \quad \textit{(Eq. 1-18)}$$

$$2ClO^- \rightarrow 2Cl^- + O_2 \quad \textit{(Eq. 1-19)}$$

$$ClO^- + H_2 \rightarrow Cl^- + H_2O \quad \textit{(Eq. 1-20)}$$

The rates of electrode reactions *Eq. 1-7* and *Eq. 1-14* to *1-17* are a function of the electrocatalytic activity of the anode, chloride concentration, stirring or flow rate, temperature and current density.

1.2.12 Electro-disinfection

The lack of clean drinking water causes millions of deaths each year and 43% of water-related deaths are due to diarrhea which can be eliminated by providing efficient affordable drinking water disinfection treatment systems (W.H.O., 2006). Chlorination remains the most commonly used method of disinfection due to its strong primary function of microbial inactivation and secondary residual disinfection. The undesirable taste, odour and formation of potentially toxic chlorinated by-products have been identified as the major negatives to the chlorine disinfection process. Recent studies have revealed that electro-chlorination can achieve disinfection at lower chlorine concentrations than chemical chlorination (Diao, Li, Guc, Shi, & Xie, 2004 ; Helme, Ismail, Scarano, & Yang, 2010). This has been attributed to non-chlorine oxidizing agents such as short lived reactive oxygen species formed during electrolysis of water. Reduced chlorine concentrations reduce the problems of chlorine taste and odour and the possibility of formation of chlorinated by-products (Jeong, et al., 2009; Li, Zhu, & Ni, 2010). The role played by reactive oxygen species (ROSs) remains controversial. In chloride free systems ROSs cannot achieve the microbial

inactivation required for drinking water disinfection and do not provide residual disinfection (Kerwick, et al., 2005).

Most electrochemical methods for disinfection rely on externally produced chlorine (Chlor Generators Ltd, 2004; Cumberland Electrochemical Limited, 2004; Khelifa, et al., 2004) and the development of the electrochemical cells have been focused on electro-chlorination rather than electro-disinfection. More recently there has been attention to the development of inline disinfection systems (Drees, Abbaszadegan, & Maiera, 2003; Jeong, et al., 2009; Palmas, Polcaro, Vacca, Mascia, & Ferrara, 2007). Generally these systems require added chloride to produce sufficient chlorine to achieve the disinfection. Raising the chloride ion concentration has water quality implications. Ideally an electrochemical disinfection device should be capable of producing sufficient chlorine with the naturally available chlorides.

A possible advantage of *in-situ* electro-disinfection devices is the greater effectiveness of chlorine when produced *in-situ* (Diao, et al., 2004 ; Jeong, Kim, & Yoon, 2006; Li et al., 2004). While this increased effectiveness has been attributed to ROSs, Saran et al. (1999) have suggested that reactive chlorine species (chlorine radicals) may also be contributing.

Another possible advantage of *in-situ* electro-disinfection using a cell with reduced inter-electrode gap is the possibility of synergistic effects caused by the electric field (Feng et al. 2004). Abderrahmane et al. (2008) described experiments in which they attempted to discriminate between chlorine effects, ROS effects and field effects. While Na_2SO_4 was used as the electrolyte and they used a sterile distilled water system to suspend their bacteria, they make no mention of rigorously excluding chloride from their microbial growth medium. It is possible that the effects they observed were due to the chlorides introduced into the system from the growth medium. They claim that field effects were identified but their field strengths of less than 1 V/cm were much lower than those for which disruption of cell membranes i.e. electroporation effects can be expected.

1.2.13 Electro-disinfection by electroporation

Microbial inactivation by irreversible electroporation provides an opportunity for chlorine free disinfection. While there is no literature on the application of electroporation to water disinfection, non thermal electro-pasteurisation has received much attention from the food industry because it offers the possibility of a rapid process for providing microbiologically safe, minimally processed, fresh-like food products (Barsotti, Merle, & Cheftel, 1999; Morales-de la Pen, Salvia-Trujillo, Rojas-Grau, & Martın-Belloso, 2010; Soliva-Fortunya, Balasab, Dietrich Knorr, & Olga Martın-Belloso, 2009). Typically a high electric field, high frequency bipolar pulsed electric fields (PEF) are applied while maintaining ambient temperatures. Commercial applications remains problematic because of high applied voltages (of the order of kV), high capital costs, high energy consumption, inability to process continuously and the need for cooling (Huang & Wang, 2009; Meneses, Jaeger, Moritz, & Knorr, 2010). The development of a flow through electrochemical system with much reduced inter-electrode gaps provides an opportunity to utilise electroporation effects at much lower applied voltages and consequently lower energy consumption.

The accepted theory for the microbial inactivation by high electric field continues to be the dielectric rupture of the cell membrane caused by Maxwell stress. The charge separation that results when an electric field of a strength such that the transmembrane potential exceeds approximately 1 V causes cell wall rupture and leakage of cell contents (Machado, Pereira, Martins, Teixeira, & Vicente, 2010; Wesierska & Trziszka, 2007; Zhang, Barbosa-Canovas, & Swanson, 1995; Zimmermann, Pilwat, & Riemann, 1974). While the effect of pulse width and pulse frequency at high pulse frequencies has been investigated (Buckow, Schroeder, Berres, Baumann, & Knoerzer, 2010; Picart, Dumay, & Cheftel, 2002; Putri, Syamsiana, & Hawa, 2010) the effectiveness of low frequency pulses or continuous field treatments have received less attention. Recent reports (Wang, Bhunia, & Lua, 2006) have noted that high continuous DC fields cause cell lysis and subsequent microbial inactivation. The use of DC fields, if effective, or

hydrodynamically pulsed DC fields, would simplify treatment systems and reduce cost.

1.2.14 Electrocatalytic effects

One of the major barriers to greater uptake of electrochemical technologies in water treatment is cost. Where treatment relies on electrochemical production of active species such as chlorine, there is a strong incentive to find ways of catalysing the electrode reactions so that the electroactive species can be produced more efficiently. There is continuing interest in developing electrocatalysts to achieve this. The most accepted definition of electrocatalysis is the "effect of electrode material on the electrode reaction rate" (Guerrini & Trasatti, 2006) and it is the general understanding that catalysis lowers the activation energy and/or reaction mechanism to achieve enhanced rates. Example, elecrocatalytic systems used in chlorine production include dimensionally stable anodes (DSAs) where titanium electrodes are coated with ruthenium oxide and iridium oxide and boron doped diamonds (BDDs). According to Guerrini and Trasatti the effect of an electrode material can be "real" or "apparent" and depends on whether the electron transfer process is affected. If the electron transfer is affected it is called "real" electrocatalysis whereas if the effect results from increased electrode area or transport effects it is called "apparent" electrocatalysis. Real electrocatalysts lower electrode reaction overpotentials and improve selectivity (Pletcher, 1984a).

1.2.15 Previous work at the University of Waikato

In previous work at the University of Waikato, Wang (Wang, 2005) used porous titanium electrodes in a membrane cell to produce chlorine for disinfection in a divided cell where the chlorine contacted the solution to be treated by diffusing through the porous anode. Matheison (Mathieson, 2006) in studies of electro-flotation and electro-flocculation of municipal and tannery wastewaters used an anode bed of aluminium shavings separated from a stainless steel cathode by a fine non-conducting nylon mesh. In this way the distance between the corroding

anode and the inert cathode was reduced to ~ 100 μm (Mathieson, Langdon, & Jamieson, 2004; Mathieson, 2006). The basic unit of the Wang cell and the nylon mesh spacer of the Matheison cell formed the basis of the development of a perforated electrode flow through (PEFT) cell which is the topic of this thesis.

1.3 Aims and objectives of the present study

A central aim of the present research project was to design, develop and apply electrochemical cell systems that were efficient and cost effective for the treatment of water and wastewater of low ionic strength.

The work was motivated by the challenge of finding a solution to a water supply problem. Many bore waters from the peat soils of the Waikato region are naturally contaminated with iron and manganese. A key objective was to determine whether electrochemical oxidation could be used instead of chemical oxidation in the treatment of those problem iron waters that otherwise form stable colloidal suspensions when oxidised by air.

It is well known that electrochemical oxidation of water and wastewater systems is indirect and mediated by electrochemically produced chlorine. Therefore another key objective was to optimise the efficiency of chlorine production from the levels of chloride ions naturally present.

Cost effective chlorine production would allow useful studies of the electrochemical treatment of effluents (for example degradation of dye effluents) and electro-disinfection of water.

In the development of the PEFT cell system it was envisaged that the gap between electrodes would be minimised to improve cell efficiency. It was realised that significant electric fields would be produced. These fields may be capable of reversible and irreversible electroporation effects. A final objective was to investigate this possibility.

1.4 Thesis outline

Chapter 1 defines the area of study with a general introduction, and examines the literature on the evolution of electrochemical technology, important parameters in electrolytic cell design and development and applications of electrochemical techniques in line with the PEFT cell applications carried out in this research and summarises specific objectives of the work.

General materials and methods are described in Chapter 2.

Chapter 3 describes the evolution of the PEFT cell with the inter-electrode gap being reduced from 240 µm to 40 µm and how it was optimised to produce chlorine at minimum cost and with useful flow rates.

Metal ion removal from naturally contaminated groundwater was undertaken as the first application where the 240 µm gap PEFT cell was employed as an electro-oxidation device is given in Chapter 4. This chapter also investigates the colloidal iron formation during natural air oxidation and the formation of trihalomethanes during electrochemical oxidation of Waikato's problematic iron contaminated groundwater.

Demonstration that the cell could produce chlorine cost effectively in Chapter 5 led to studies of its application as a dye degradation technology in Chapter 6 and as electro-disinfection technology in Chapter 7. During the disinfection studies the synergistic effect of field induced electroporation on chlorine lethality was identified.

As part of the electroporation studies the unexpected result, that a partially insulated anode gave rise to significantly improved chlorine current efficiency was observed. Details of this electro-catalytic effect are described in Chapter 8.

Further development of partially insulated anode systems for producing fields above 10 kV/cm allowed investigation of irreversible electroporation and the

possibility of non thermal electro-pasteurisation. This work is described in Chapter 9.

Chapter 10 is the general discussion describing further applications of the PEFT cell.

Chapter 11 contains a summary of the main conclusions and recommendations for future research.

Chapter 2: Materials and methods

During the work five cells were developed. They were a cylindrical flow through cell and four perforated electrode flow through (PEFT) cells. The PVC housing material used for the PEFT cell assembly, electrical components and hydraulic components remained the same.

2.1 Materials used in cell construction

The electrode materials were chosen to be compatible with water treatment, to be cost effective and corrosion resistant. The anode, cathode and the spacing material (inter-electrode gap) used in the construction of the various PEFT cells are summarised in Table 2.1.

Table 2.1- Electrode materials, spacers and hydraulic flow gap in the developed cells

Cell	**Anode**	**Cathode**	**Spacer – electrode gap**	**Flow gap**
Cylindrical cell	Carbon fibre felt	Stainless steel mesh	Nylon mesh – 240 µm	240 µm
240µm gap PEFT	Graphite[a]	Stainless steel mesh	Nylon mesh – 240 µm	240 µm
50 µm gap PEFT	Graphite[b]	Stainless steel plate	Cello tape – 50 µm	50 µm
50 µm gap (insulated anode) PEFT	Stainless steel[c]	Stainless steel plate	Polyurethane – 50 µm ± 2µm	1-2 µm
40 µm gap (anodized Ti anode) PEFT	Titanium/TiO_2	Stainless steel plate	Duraseal – 40 µm	40 µm

a. No hole pattern, hole (perforation) density 10 holes/cm^2

b. Hexagonal pattern, hole density 6 holes/cm^2
c. Surface facing the cathode coated with Polyurethane varnish

2.1.1 Anode materials and their surface modifications

The initial cylindrical cell design with an anode of carbon fibre felt was abandoned when it was found that the anode deteriorated rapidly. The PEFT cell design subsequently adopted used a 2.0 mm thick graphite sheet drilled with 1 mm diameter perforations. The graphite sheet was sourced from Graphite Australia, No. 11, 161-163 Gympie Terrace, Noosaville, 4566, Queensland, Australia. The specifications of the graphite material are given in Table 2.2.

Table 2.2- Specifications of the graphite anode material

Physical parameter	Value
Bulk Density	>1.72 g/cm^3
Maximum particle size	0.8 mm
Specific Resistance	<8.0 μΩ m
Thermal Conductivity	150.2 W/m-°C
Compressive Strength	>30MPa
Flexural Strength	13.5 MPa

This material was chosen because of its good electrical and robust mechanical properties, resistance to oxidation, and compatibility with drinking water supplies.

For the 240 μm gap PEFT cell, the anode was perforated by drilling 1 mm diameter holes at a hole density of 10 holes/cm^2 on a rectangular grid leaving an exposed planar anode area of 48.3 cm^2 (Nath, Wang, Torrens, & Langdon, 2011).

The 50 μm gap PEFT cell used a graphite anode with 1 mm diameter perforations drilled in a hexagonal pattern with a hole density of 6 holes/cm^2.

The 50 μm gap (insulated SS anode) PEFT cell used a stainless steel anode (316 grade plate with a thickness of 0.5 mm) perforated by programmed mechanical

drilling of 1 mm diameter holes in a hexagonal array at a hole density of 6 holes/cm^2. A 50 µm ± 2 µm polyurethane film, polyurethane gloss clear varnish (Wattyl, Estapol) thinned by adding mineral turpentine (10% by volume) was applied by manual brushing and after overnight drying in a 40°C oven well defined perforations through the film were made by careful hand drilling to ensure that the metal surfaces of the perforations were cleanly exposed (Nath & Langdon, 2010).

The 40 µm gap (anodized titanium anode) PEFT used a 1 mm thick titanium anode perforated by programmed mechanical drilling of 1 mm diameter holes in a hexagonal array at a hole density of 6 holes/cm^2 (Nath & Langdon, 2011). The anode was coated with a self organised TiO_2 nano film generated *in-situ* by anodizing in 1mol/L $(NH_4)H_2PO_4$ (fluoride free) as described in detail by Ghicov et al. (Ghicov, Tsuchiya, Macak, & Schmuki, 2005). The one molar solution was prepared by dissolving the salt of ammonium dihydrogen phosphate ($(NH_4)H_2PO_4$) laboratory reagent (Assay 98%>) in double distilled water. The conductivity and pH of the solution was 42.5 mS/cm and 5.1 respectively. Anodizing was carried out in the PEFT cell with a stainless steel cathode at a constant 20 V DC applied across the electrodes. The formation of the film was monitored by measuring the current and anodizing was stopped after two hours when no further decrease in current was observed (see Figure A.1 in Appendix A)

The Figure 2.1 shows that anodizing formed a dispersed particle coating.

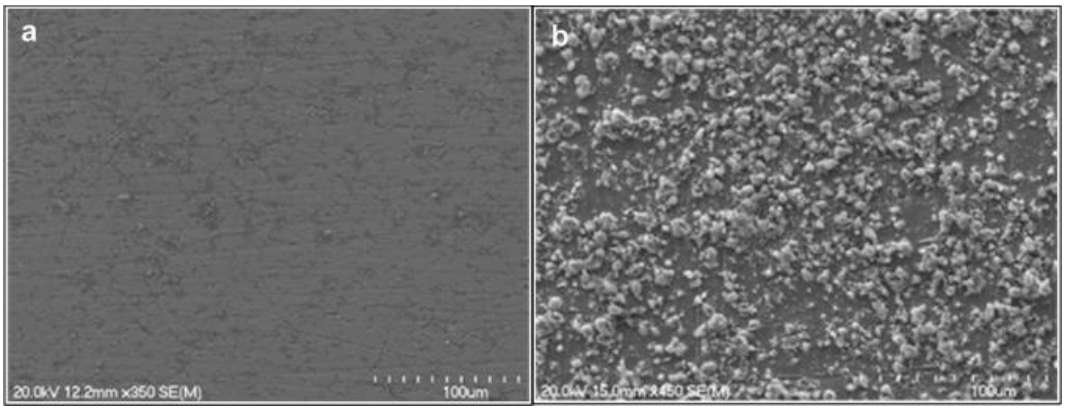

Figure 2.1 – Surface of the titanium plate. (a) before anodizing, (b) after anodizing

The elemental composition of the titanium plate before and after anodizing obtained using Scanning Electron Microscope Energy Dispersive Analysis (SEM – EDAX). Figure 2.2 and Table 2.3 give the spectrum and composition of the Ti anode before anodizing.

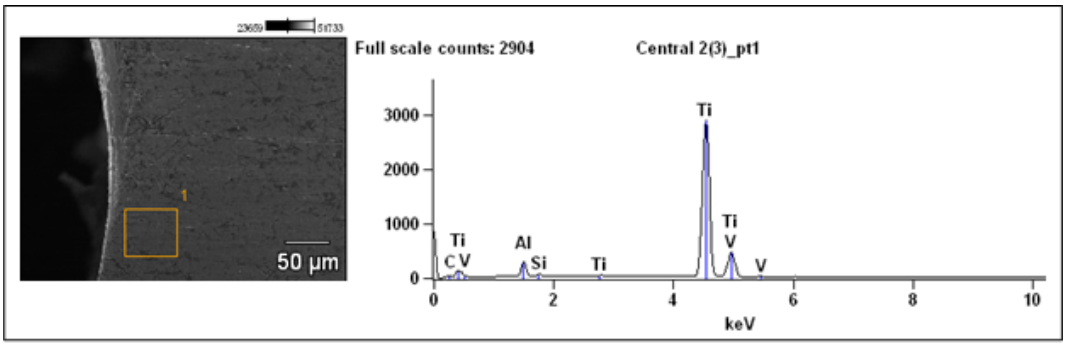

Figure 2.2 – Elemental composition of the titanium plate surface before oxide layer formation; SEM - EDAX report.

Table 2.3 - Elemental composition of the electrode surface before anodizing

	point	*C-K*	*Al-K*	*Si-K*	*Ti-K*	*V-K*
Weight%	*Central 2(3)_pt1*	2.75	4.39	0.61	88.01	4.24
% Error	*Central 2(3)_pt1*	±0.33	±0.09	±0.06	±0.65	±0.41

The elemental composition of the particles and the smooth electrode surface after anodizing is given in Figure 2.3. Figure 2.3 (a) indicates the surface features analysed, Figure 2.3 (b) gives the composition of planar surface and Figure 2.3 (c) and Table 2.4 gives the composition of the particles. The presence of oxygen on the planar surface is evidence of the formation of a thin oxide layer on the titanium metal.

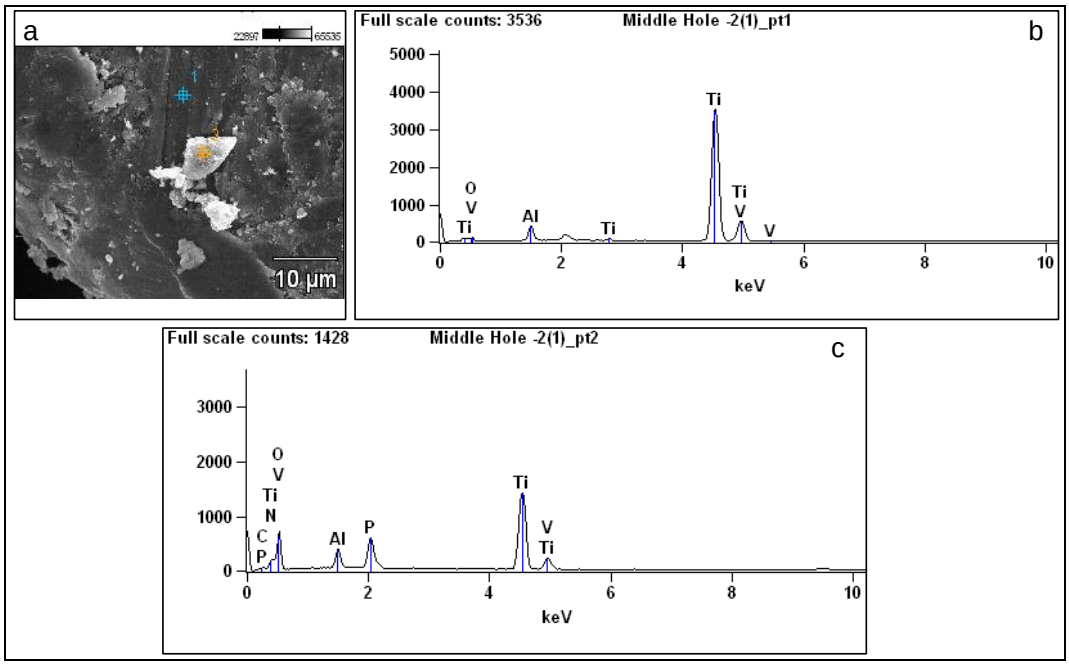

Figure 2.3 – SEM-EDAX data after anodizing the titanium plate: (a) image of point 1(planar region) and point 2 (particle) analysed ;(b) elemental spectrum for planar region showing the presence of oxygen; (c) elemental spectrum of oxide particle.

Table 2.4 – Elemental composition of the electrode surface after anodizing point 1(pt1):planar region, point2 (pt2) on a particle

	Point	*C-K*	*N-K*	*O-K*	*Al-K*	*P-K*	*Ti-K*	*V-K*
Weight%	*Middle Hole -2(1)_pt1*			10.62	4.60		80.83	3.94
Error%	*Middle Hole -2(1)_pt1*			±1.52	±0.08		±0.55	±0.34
Weight%	*Middle Hole -2(1)_pt2*	1.59	0.00	52.81	3.83	5.99	34.56	1.23
Error%	*Middle Hole -2(1)_pt2*	±0.42	±0.00	±0.76	±0.08	±0.14	±0.36	±0.15

Elemental mapping data given in Appendix A.2 provides further evidence of a uniform thin oxide layer coated with randomly distributed oxide particles.

2.1.2 Cathode materials

The material used as the cathode was 316 stainless steel throughout the cell development process. A stainless steel mesh material with 0.25mm sieve size and wire diameter 0.10 mm was used in the initial work carried out with the cylindrical cell, which was wrapped around the ceramic core. The same stainless

steel mesh material was cut into a disk in the 240 μm gap PEFT cell. In later work the mesh was replaced by a 0.5 mm thick 316 stainless steel plate, perforated by programmed mechanical drilling similar to the preparation of the anode. The use of polished stainless steel allowed the inter-electrode gap to be reduced from 240 to 50 μm.

This particular stainless steel composition was selected because of its high corrosion resistant properties.

2.1.3 Spacer materials

A twin ply nylon mesh having a 1.0 mm sieve size and 0.12 mm fibre diameter was used as an electrode separator for 240 μm gap PEFT cell. It was replaced by a 50 μm strip of inert cellulose (3M Scotch^{TM} tape 375, USA) in the 50 μm gap PEFT cell. Further reduction in the inter-electrode gap to 40 μm was achieved by using a spacer of polypropylene (Duraseal) adhesive tape lamination.

2.2 Electrochemical experimental arrangement

The electrochemical experiment arrangement is shown in Figure 2.4. The PEFT cell was connected to a direct current source with a maximum of 5 A and 30 V through an ammeter and a voltmeter to measure the current and voltage. A flow regulated peristaltic pump (Watson Marlow 504S, with regulated DC power supply connected with 6.4 mm silicon tubing with a maximum flow rate of 1500 mL/min at 15 psi (~ 1bar) pressure) was used to circulate water through the cell.

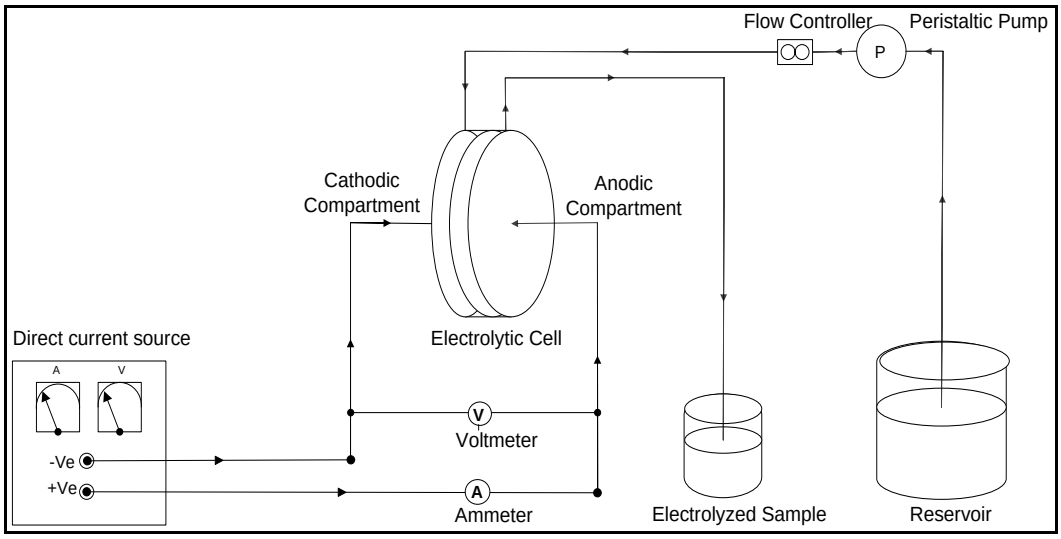

Figure 2.4- Diagram of the experimental set up of the PEFT cell

When the experiment required multiple passes through the PEFT cell, the collected sample was recycled through the cell. Details of current, voltage and flow rate were recorded manually.

2.3 Iron water

Problem iron waters that form stable colloids on air oxidation were collected from a groundwater bore (bore A) located at 956TuhikarameaRoad, Hamilton, New Zealand. A map locating the position of the bore well *A* is given in Appendix A.3. Samples were collected after thorough flushing of the system and the container, tightly capped without an air space and used within 30 minutes of sampling.

All other synthetic iron water samples were prepared using deionised Millipore system water (pH in the range of 4.2 - 4.5 and conductivity less than 2 µS/cm at 20°C).

2.4 Analytical methods

2.4.1 Residual chlorine analysis

The iodometric titration method described in Vogel (Vogel, 1997) was used. All the sodium chloride solutions were prepared by dissolvingNaCl (BDH analar reagent) in de-ionized water (conductivity < 2 mS/cm). Sodium iodide 10% solution (BDH analar reagent), sodium thiosulfate (BDH analar reagent) made up to concentrations of 0.1, 0.25, and 0.5mol/L, glacial acetic acid (Merck Laboratory Reagent), and starch indicator (BDH analar reagent) were used as required. To avoid the escape of chlorine, the electrolyzed solution was collected into a known volume of 10% sodium iodide. The samples were immediately titrated against the standardized thiosulfate. During the electrolyte recycling experiment, the samples were collected after successive cycles through the cell.

2.4.2 Analysis of ferrous content

The ferrous ion concentration of samples was measured using the 1,10 Phenanthrolein spectrophotometric method (Vogel, 1997). A dilution series of known ferrous ion ($FeSO_4.7H_2O$, MW 278.02, BDH analar reagent) solutions (0.2 - 4.0 mg/L) were used to prepare a calibration curve, absorbance versus ferrous ion concentration (Appendix A.4). A volume of 10 mL oxidized water sample was taken to a 50 mL falcon tube, added 5.0 mL of 0.2 mol/L sodium acetate (UNILAB Ajax, analar reagent) 4.0 mL of 0.25% 1, 10 phenanthrolein (SERVA, Fein Biochemica, Heidelberg, analar reagent) and made up to the 50 mL mark with distilled water, mixed well, allowed to remain for 10 minutes for the colour to develop and the absorbance was measured at 515 nm by a CARY 100 Scan UV-VIS spectrophotometer.

2.4.3 Residual metal ions and silica concentrations

Residual metal ion concentrations (iron and manganese) and silica in water were analysed by an Inductively Coupled Plasma – Mass Spectroscopy (ICP-MS) (ICP-MS PerkinElmer SCIEX ELAN DRC II).

2.4.4 Chloride ion concentration

The chloride ions in water was analysed by the mercury(II) thiocyanate spectrophotometric method (Vogel, 1997). A 20 mL sample of the chloride solution was placed in a 50 mL falcon tube, 2.0 mL of 0.25 mol/L ammonium iron (III) sulphate (BDH analar reagent) in 9 mol/L nitric acid (UNIVAR, 70% v/v, AR) added, followed by 2.0 mL of saturated solution of mercury (II) thiocyanate (BDH analar reagent) in ethanol. Allowed to stand for 10 minutes and measured the absorbance of the sample at 460 nm by a CARY 100 Scan UV-VIS spectrophotometer. Calibration curve is given in Appendix A.5. Commonly used NaCl concentrations and unit conversions are given in Table A.1 in Appendix A.5.

2.4.5 Turbidity measurements

The turbidity of the treated groundwater samples were measured using a HACH 2100P Turbidimeter, in Nephelometric Turbidity Units (NTU).

2.4.6 pH & conductivity

The pH was measured using a BA350 series 3 EDT Instruments pH meter, and the conductivity was measured using a CyberScan100 Con Eutech instrument.

2.4.7 Particle size and charge measurements

A Malvern Zetasizer instrument (Zetasizer 3000HS/IHPL, Malvern Instruments Ltd, UK) was used to measure the particle size and charge distributions in naturally occurring colloidal systems in ground water.

2.4.8 Cell conductance

A conductance cell and bridge (University of Auckland) was used to measure the conductance of the PEFT cell at different electrolyte concentrations and to calculate the cell constant. The instrument had a conductance range 0.1 – 10^5 µS.

2.4.9 Temperature

When the temperature of the water samples measured a mercury bulb thermometer -10 to 110°C ± 0.5°C was used.

2.4.10 Colour removal

The spectra of the two dyes Indigo Carmine and Reactive Blue 2 were obtained using the Cary 1000 spectrophotometer and the maximum absorbance wavelengths were identified at 611 nm and 617 nm respectively. Solutions with known concentrations of the two dye effluents were quantitatively diluted to form two series of dye solutions and the absorbance was measured to generate the calibration curves obeying the Beer-Lambert Law (Vogel, 1997). An aliquot of 10 mL was drawn after each cycle of treatment through the PEFT cell, absorbance was measured using a Cary 1000 spectrophotometer and converted to dye concentration using the calibration curves. Absorbance of the untreated water sample was used to obtain the original concentration of the dye solution to calculate the percentage colour removal. The spectra and the calibration curves for the two dyes are given in Appendix D.1.

2.4.11 Total Organic Carbon (TOC)

The TOC levels in groundwater were analysed using a TOC analysis instrument (TOC Analyser, TruSpec CN – LECO Carbon/Nitrogen determinator).During the electro-decolourisation experiments the TOC in the treated dye water samples were analysed with a IL550 TOC-TN Analyzer (Lachat Instruments) loaded with OmniToc 4.05 software.

2.4.12 Head space solid phase microextration gas chromatography mass spectroscopy (HS SPME GC MS)

The head space solid phase microextraction (HS SPME) coupled with gas chromatography mass spectrometry (GC MS) was employed to determine trihalomethane (THMs) formation during groundwater treatment. The technique is well established and approved by the US EPA (Stack, Fitzgerald, O'Connell, & James, 2000).

Solid phase microextraction was performed using a Supelco No. 5-7300 manual SPME fibre assembly fitted with a 100 µm polydimethylsiloxane (PDMS) fibre (see Appendix A.6 for more details and diagrams). The fibre was conditioned at 250°C for 1 hour prior to use and blank desorption was performed. Samples of 4 mL were transferred to SPME vials (10 mL, Supelco) which contained 250 µL of saturated sodium chloride (BDH analar reagent) solution and a magnetic bar. The samples were sealed using a screw cap, containing a PTFE- faced rubber septum. The vials were clamped in place on a magnetic stirring plate and the SPME assembly was secured above the vial cap. The syringe unit with the fibre was lowered into the vial with the fibre suspended in the head space above the liquid layer of the samples at ambient temperature (20°C) with a stirring rate 250 rpm. An extraction time of 10 minutes was selected and the fibre was immediately retracted back into the needle and transferred without delay (<1 minute) to the injection port of the gas chromatograph (GC). A desorption time of 2 minutes and a desorption temperature was 220°C was selected (Appendix A.6 – Figure A.8). The actual depth of the SPME needle in the injection port liner can be controlled. A position of 2.5 on the needle scale was determined experimentally to position the fibre in the hottest part of the GC liner.

Chromatographic analysis was performed using a Hewlett Packard (HP) 6890 series gas chromatograph coupled to HP 5973 mass selective detector. The

GC/MS interface temperature was set at 280°C, with a source temperature 180°C. The initial oven temperature was set at 40°C for 4 minutes, ramped at 15°C/min to 220°C and held for 1 minute. The analytical column was Zebron ZB-5, 5% phenyl polysiloxane and 95% dimethylpolysiloxane semi-polar (30 m x 0.25 mm, 0.25 µm film thickness). The carrier gas was helium at head a space pressure of 15 psi, used in splitless mode. Chloroform was the THM studied in this work; therefore the quantification was performed in the selective ion monitoring (SIM) mode. The ions used were m/z 83, 85 and 87 with dwell time of 100 ms.

High purity GC grade chloroform (Merck, GC grade, 99.9% purity) was used to prepare a series of standard dilutions in the range 10 – 125 µg/L to generate the calibration curve (see Appendix A.7).

2.4.13 Microbiological analysis

The prepared electrolyte solutions and all glassware used were autoclaved at 121 °C for 15 minutes. The bacteria *Escherichia coli,* was a teaching strain used at the University of Waikato Microbiology Department and derived from K12 strain, were spiked at an initial concentration of 4×10^6 CFU/mL (Colony Forming Units). The *E. coli* was cultivated overnight on a shaker in a water bath using a nutrient broth (meat extract 1.0 g/L, yeast extract 2.0 g/L, peptone 5.0 g/L, sodium chloride 5.0 g/L) culture medium at 37 °C; and the pH was 7.4. When a culture medium with no chlorides was required the SK culture medium (KH_2PO_4 - 0.78 g, K_2HPO_4 - 2.3 g, $(NH_4)_2SO_4$ - 1.0 g, $MgSO_4.7H_2O$ - 0.1 g, sodium citrate dihydrate - 0.6 g, glucose - 2.0 g, water 1 L, at 37 °C, pH 7.3) was used to make sure no chloride ions were present in the system and eliminating the possibility of chlorine generation during the treatment process. Each mL of bacterial suspension contained 2×10^9 CFU. The plate count technique was used to detect the survival cell counts after treatment (Stainer, Ingraham, Wheelis, & Painter, 1986). Appropriate dilutions of the bacterial cells were used to inoculate nutrient agar (Lab M) plates. Inoculated plates then incubated at 35°C for 24 h. The survival number of cells after the treatment was determined by counting the number of colonies developed after incubation and multiplying it with the dilution factor.

The log values of the ratio of number of cells survived after treatment and initially inoculated to the sample is reported as the log survival fraction.

2.4.14 Scanning Electron microscope (SEM)

SEM studies performed using SEM EDAX (Hitachi S-4700) were used to analyse the composition of sludge formed during different groundwater treatment processes. Colloidal constituents were studied by nebulising groundwater samples on to aluminium stubs, freeze drying overnight, platinising and examining the platinised sample.

2.4.15 Transmission Electron Microscope (TEM)

TEM was used (Phillips CM-30) to examine the nature of the colloidal species formed during oxidation of problem iron waters. Samples were nebulised onto a TEM copper grid and air dried overnight in a desiccator.

2.4.16 Light microscope

An Olympus multi level optical zoom light microscope was used to inspect the titanium electrode surface before and after anodizing.

2.4.17 Particle size distribution

The particle size distribution in the naturally oxidising problem groundwater sample was carried out using a membrane filtration technique where MilliPore™ membrane filters (47.0 mm diameter membrane filters and single use cartridge type) with pore size range 5.0 µm to 0.025 µm were used.

2.4.18 Hydraulic conductivity measurements

The flow through nature of the cell required a study of the hydraulic conductivity of the cell. The constant head technique was used to calculate the hydraulic conductivity using Darcy's law. An experiment was set up (Figure 2.6) to provide the parameters static hydraulic head and volumetric flow rate. The path length and cross-sectional area was taken from the cell design. The procedure allowed water to move through the cell under a steady state head condition while the volume of water flowing through the cell was measured over a period of time. Knowing the quantity Q of water (250 mL), path length L (0.35 cm) of the electrodes, cross-sectional area A of the cell, time t required for the quantity of water Q to be discharged, and hydraulic head h (1.0 m), allowed the hydraulic conductivity to be calculated.

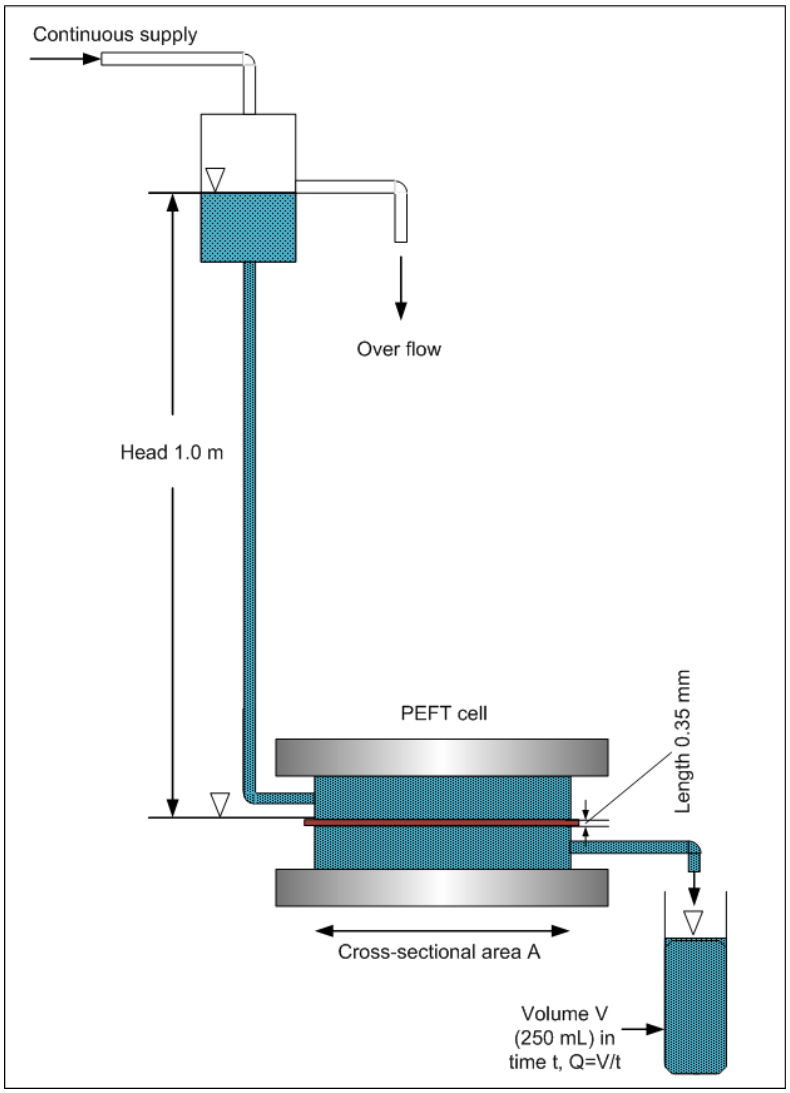

Figure 2.5 – Schematic diagram of the constant head experimental set up used to measure hydraulic conductivity of the PEFT cell

In order to investigate Q/H relationships, the experimental arrangement shown in Figure 2.7 was used. The inlet to the PEFT cell was connected to the main water supply and just before the cell a T joint connected with a capillary tube standing vertically to allow the water to rise according to the pressure experienced by the fluid due to the electrode system of the cell; the water was allowed to flow freely out of the cell at the same level (horizontally). The volumetric flow rate was measured using a measuring cylinder and stopwatch. The hydraulic head, *h*, created in the capillary tube was representing the pressure build up due to the cell and was calculated using the equation $P = h\rho g$.

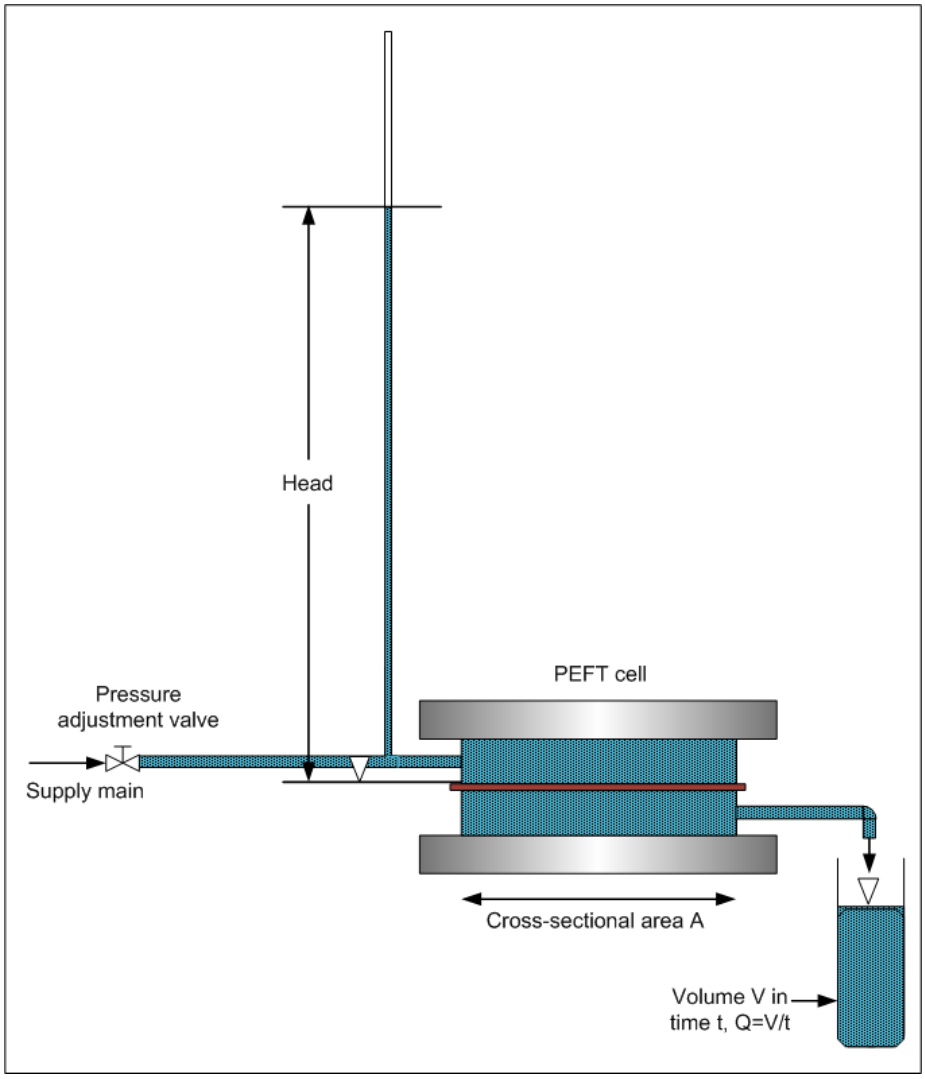

Figure 2.6 – Schematic drawing of the experimental setup used for the hydraulic pressure and flow rate measurements (not to scale)

2.4 Electrical equipment

2.4.1 Power supply

The PEFT cell was powered by a single direct current source Dick-Smith Electronics, 0 – 30 V, 0 - 5A regulated DC power with variable current and voltage limit, input 230–240 V AC 50 Hz. Most experiments used only this power supply but for the electro-pasteurisation work, a second power source Topward 6303A, 0 – 60V, 0 - 3A was coupled in series to achieve higher voltages up to 90 V.

2.4.2 Current and voltage measurements

The DC power source and the PEFT cell were connected through an ammeter (Fluke 73 III Multimeter) and a voltmeter (Fluke 77 Series II Multimeter) to measure the current and voltage. The minimum reading of the ammeter was ± 0.01 mA and in the voltmeter it was ± 0.001 mV

Chapter 3: Design, development and optimization of the PEFT cell

The overall performance of an electrolytic cell is determined by a complex interaction of parameters such as cell design, electrode potential, electrode materials, concentration of electro active species, electrolysis medium, temperature, pressure and mass transport regimes (Pletcher, 1984b). The cell design is the key parameter which affects all the figures of merit for an electrolytic process. Another important factor in designing an electrolytic cell is the divided or undivided nature of electrodes, with the presence or absence of a separator (membrane). These parameters and factors were considered during the design and development process of the PEFT cell.

3.1 Initial design and development

The design and development work started from previous work carried out in the department by Grant Mathieson (Mathieson, 2006) on electrolytic purification of water, specially looking at a corroding anode, flow through, treatment system employed as an electro-flocculation device; and Xijin Wang's work on the development of an electrochemical cell for the production of chlorine in dilute aqueous solutions using a divided membrane cell (Wang, 2005). The major drawback in Mathieson's work was the potential and electric current distribution problems in the corroding anode leading to very high power consumption and difficulties in controlling the electrolytic parameters necessary to quantify treatment efficiencies. The short coming of Wang's work was the large inter-electrode gap with porous titanium electrodes in a divided membrane cell where the electrical efficiencies were very low. Even the latest work using an undivided cell without a membrane experienced low current efficiencies due to large inter-electrode gaps (Bae, et al., 2008). These problems were addressed in the PEFT cell development process.

3.1.1 Initial thinking – cylindrical cell design

As was pointed out in the introduction, designing an electrochemical cell with minimum resistance is the challenge for any electrochemical engineer. In much of the previous work this goal has been achieved by using high electrolyte concentrations. High concentrations are not compatible with the environmental systems of the present work. Another approach to minimise cell resistance is by reducing the inter-electrode gap. This approach was successfully used by Mathieson and is also the basis of the Zappi cell (Zappi & Weinberg, 2001). In this work the inter-electrode gap was reduced to a few millimetres using an insulating nylon mesh to prevent short circuiting. In order to be able to install the device inline and further to be able to increase electrode area a cylindrical device was initially designed. A cylindrical cell will also allow increases in electrode area to be easily achieved by increasing cell length. The electrode materials were chosen to be compatible with drinking water requirements; carbon fibre felt for the anode and stainless steel for the cathode. The felt was wrapped tightly around a porous ceramic cylindrical former, a nylon mesh was tightly wrapped around the felt and finally stainless mesh was wrapped around the nylon. The whole assembly was mounted inside a PVC casing with electrodes connected as shown in Figure 3.1 and 3.2. A flow direction (piping) diagram and an image of the setup are given in the Appendix B.1.

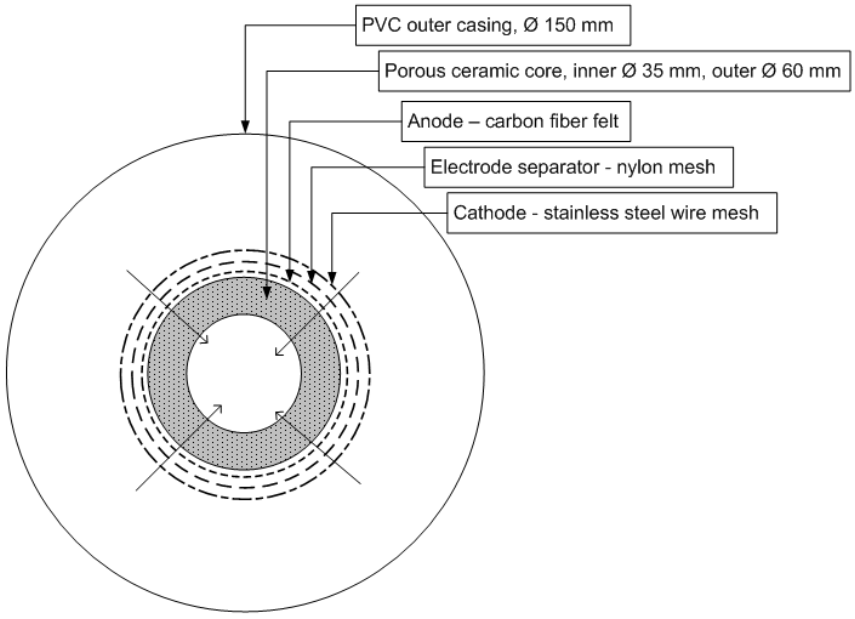

Figure 3.1 - Cross section of the cylindrical cell design

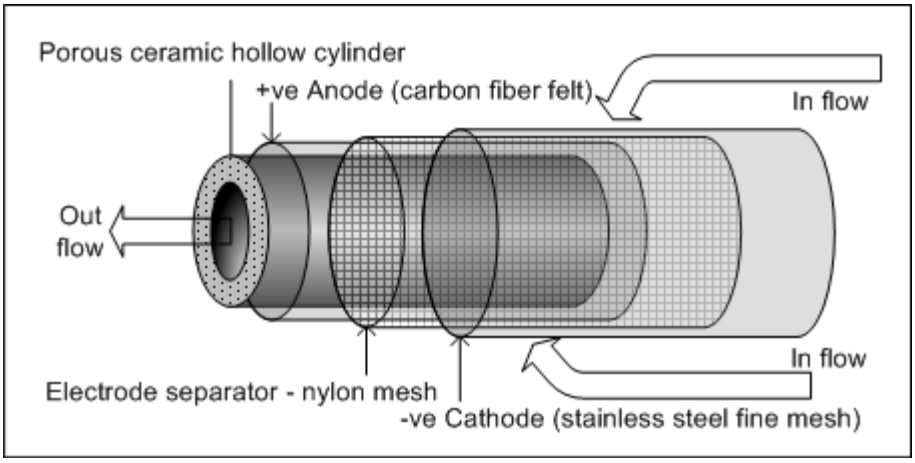

Figure 3.2 - The core of the cylindrical cell design

There were practical problems associated with this design. The major problem was that the highly fibrous nature of the felt resulted in carbon fibres penetrating the nylon mesh and short circuiting the cell. It was also likely that both flocculated materials and gas bubbles would accumulate in the porous ceramic core and the carbon fibre felt anode. Another problem with the carbon fibre felt anode was the electrical contact, achieved by winding titanium wire around felt at one end of the tubular assembly. Rapid burning of the felt at the point contact was observed.

3.1.2 Hydraulic considerations

One of the consequences of reducing the gap between electrodes is the increased resistance to hydraulic flow past the electrodes when operated as a conventional electrochemical cell where flow is forced between the electrodes. A major advantage of the flow through configuration is the better hydrodynamics that can be achieved. With the electrode flow through configuration individual flow paths through the gap are minimised.

3.1.3 Porous versus perforated electrodes

In related work Menini *et al*. (2005) used porous electrodes made with spongy titanium. While these electrodes offer a higher surface to volume ratio (Menini, Henuset, & Fournier, 2005), they and others have found that these porous electrodes had current and potential distribution problems (Ateya, et al., 1977). For example non uniform distribution of current density caused non homogenous oxidation reduction reactions and high power consumptions. Also porous electrode material accumulated fine gas bubbles inside the pores of the electrode increasing the internal resistance of the cell hence decreasing the electrical efficiencies and increasing energy consumption (Mahmoud, 1999).

The desired result of flow through configuration without using fine porous electrodes can be achieved by using electrodes made pervious by drilling a series of perforations. This led to the perforated electrode flow through (PEFT) cell design.

3.1.4 New thinking – perforated electrode flow through cell (PEFT)

Given that it was desired to use a carbon anode (to be compatible with drinking water) and the only material available was planar (120 × 120 × 2 mm) graphite sheets, this material was used for the anode and perforations in the form of 1 mm holes were drilled according to a predetermined drilling pattern. The perforated graphite anode, the stainless steel mesh cathode and the nylon mesh were assembled with the nylon mesh maintaining a minimum inter-electrode gap. This configuration allowed good flow characteristics including continual exposure of the electrodes to fresh solution and flushing of electrolysis products from the inter-electrode gap. Perpendicular flow through the cell was maintained by appropriately drilled PVC discs placed behind the electrodes in the cathodic and anodic chambers respectively. The flow direction was maintained from cathode to anode. The Figure 3.3 illustrates the schematics of PEFT cell assembly (see image in Appendix B.2).

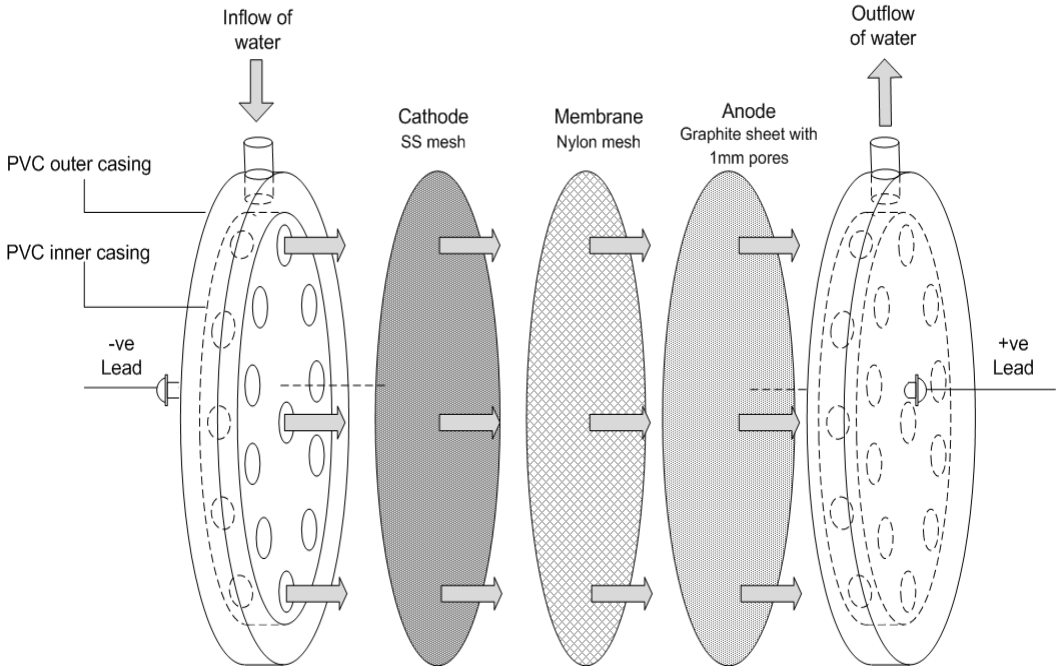

Figure 3.3 -Schematic diagram of an expanded view of the perforated electrode flow through cell assembly

The specifications of the materials used are given in Section 2.1. This design allowed reduction of the inter-electrode gap to the thickness of the separating membrane employed. During the initial stages of the work when a stainless steel mesh was used as the cathode, two layers of nylon mesh, giving a 240 µm inter-electrode gap, were required to avoid short circuiting. The improved chlorine generation efficiency achieved with this system suggested that further improvement could be achieved by further reducing the inter-electrode gap. When the stainless steel mesh cathode was replaced by a perforated stainless steel plate, a single thickness of the nylon mesh was sufficient to avoid short circuiting. Further reduction in the gap was achieved by replacing the nylon mesh by a circular strip of cello tape (thickness 50 microns) placed around the perimeter of the cathode. This modification allowed a fivefold reduction in the inter-electrode gap and a corresponding reduction in the internal resistance (Figure 3.4).

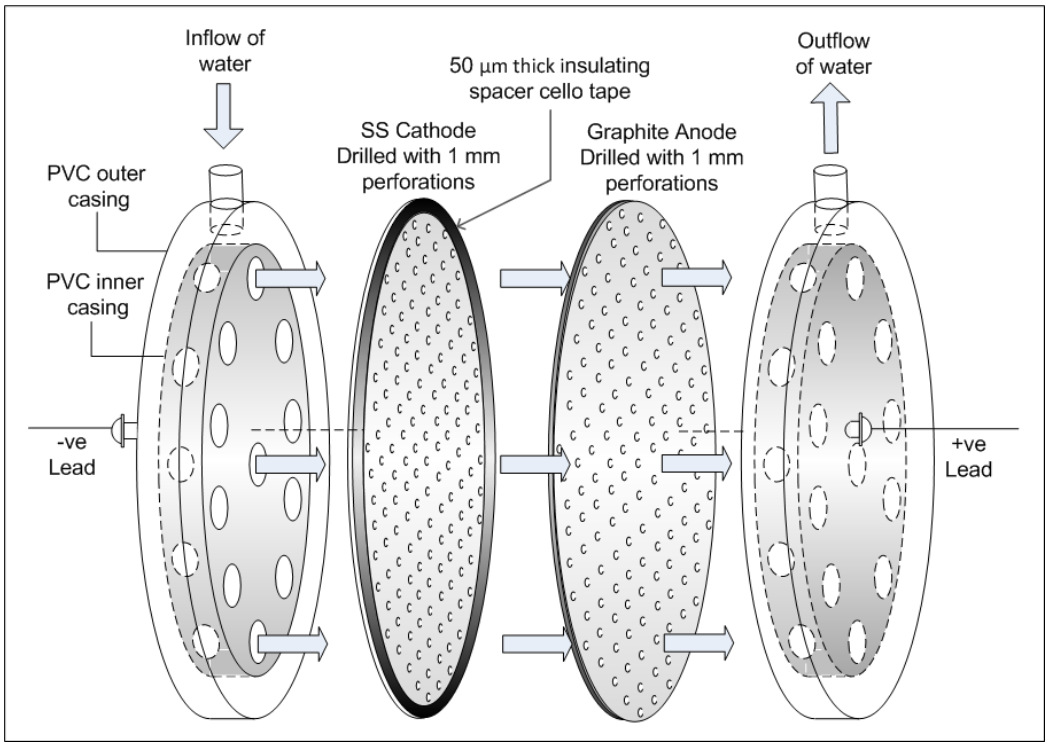

Figure 3.4 - Schematic of the perforated electrode flow through cell with a 50 µm inter-electrode gap

Further optimisation of the PEFT cell performance was achieved by considering the pattern of holes, flow direction, hole density, alignment of holes between anode and cathode, inter-electrode gap and hole diameter. The Section 3.2 addresses each parameter and its effect on the cell performance.

3.2 Optimization of the PEFT cell design

3.2.2 The hole pattern

There are two main choices for the hole pattern; a square pattern and a hexagonal pattern. The hexagonal arrangement allows the possibility of closest packing, the maximum possible hole density (Figure 3.5a), whereas the square pattern allowed uniform flow paths if the holes of the cathode and anode are arranged in a staggered configuration (Figure 3.5c). The effect of staggering the holes for both drilling patterns increases the flow paths across the electrodes surface and hence the contact time (see Figure 3.5a). However, staggering the holes in hexagonal

pattern leaves potentially stagnant regions on the electrode surfaces. To achieve uniform flow patterns with the hexagonal hole arrangement a modified hexagonal drilling pattern is required in which if the hole to hole site distance of the first electrode is ***a*** and the hole to hole distance of the second electrode is taken to be ***1.75a*** and the sites are drilled so that in a staggered configuration the central site of the lower density distribution faces the undrilled hole of the central site of higher site density distribution this is represented by the Figure 3.5b where flow is from low density to the high density. It is clear from Figure 3.5b that this gives the most uniform flow distribution over the electrodes with minimal stagnant regions.

Because a simple hexagonal arrangement allowed the possibility of greater hole densities this arrangement was adopted. For the present work hexagonal hole densities of 3 and 6 holes/cm^2 were employed.

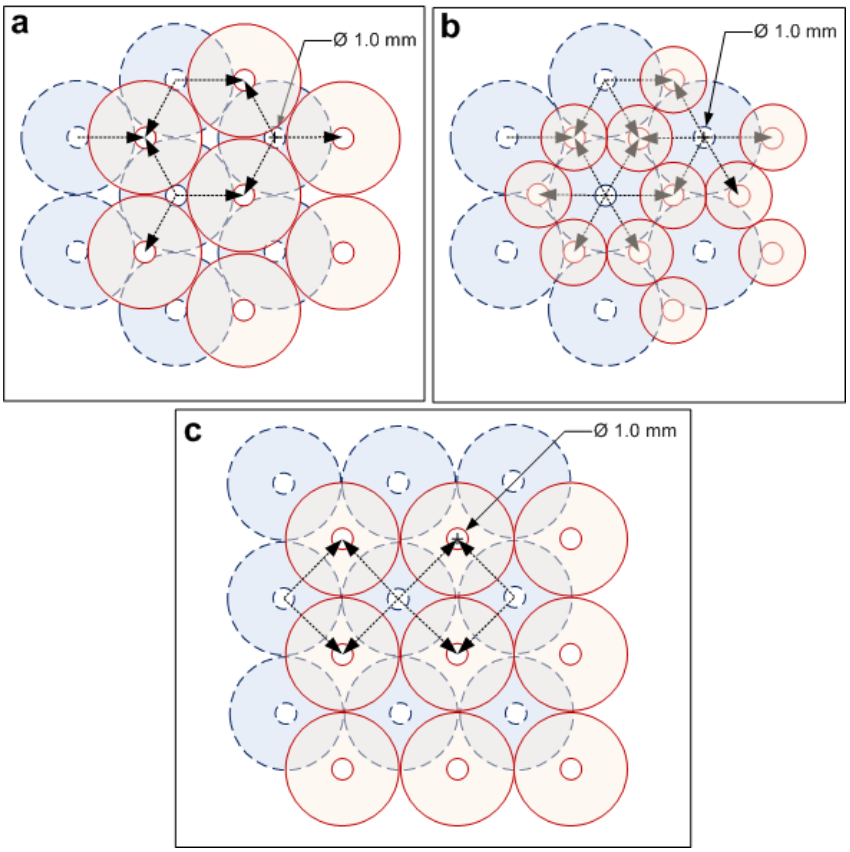

Figure 3.5 -Hole patterns drilled on electrodes, (a) Hexagonal hole pattern with equal density of holes on both electrodes fully staggered; (b) Hexagonal hole pattern with high density of holes on the anode and low density of holes on the cathode fully staggered; (c) Square hole pattern with equal hole density on both electrodes fully staggered.

In order to test the effect of key parameters on cell performance, studies of chlorine generation at a given chloride ion concentration of 0.1 mol/L NaCl, maintained at consistent pH 5.5 and conductivity of 6.2 mS/cm at 20°C were performed.

3.2.2 The effect of flow direction

In order to test whether there would be an effect of flow direction on the electro oxidation of chloride ions, an experiment was performed in which flows were from cathode to anode and anode to cathode. The results are given in Figure 3.6.

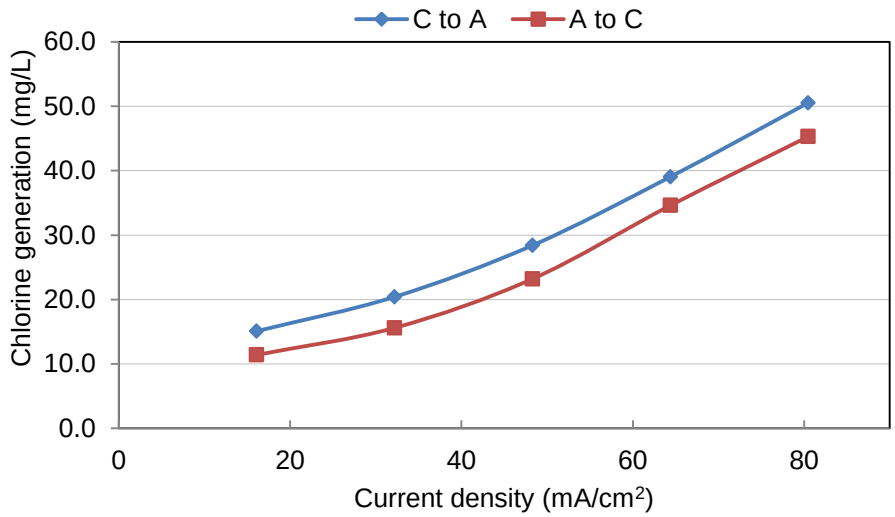

Figure 3.6 - The effect of flow direction on chlorine generation at increasing current densities (flow rate 190 mL/min, holes aligned, 3 holes/cm^2, 1 mm holes)

The results show that flow direction clearly has an important effect on chlorine generation efficiency. More chlorine was produced when the flow was from cathode to anode. The average current efficiency (CE) for the cathode to anode flow direction was 9% which was 2% higher than the average anode to cathode flow. The average energy consumption (EC) for cathode to anode flow direction was 40 kWh/kg of chlorine compared to the average EC for anode to cathode flow was 50 kWh/kg of chlorine. The proportional increase in current efficiency is matched by a corresponding decrease in energy consumption.

This effect can be understood by the likelihood of chlorine reduction if the flow direction is such that the oxidised chlorine flows pass the cathode where reduction back to chloride ions could occur. If the electrochemical reaction involved was a reduction process, then by similar reasoning the expected optimum flow direction would be from anode to cathode.

3.3 Optimisation of the PEFT cell electrodes

3.3.1 The effect of hole density: aligned configuration

In order to test the effect of hole density, two electrode systems with 3 and 6 holes/cm^2 in the hexagonal hole pattern were assembled in an aligned configuration in the PEFT cell (the arrangement of hexagonal hole pattern on the 90 mm diameter electrode surfaces are given in Appendix B.3). The chlorine generation was measured as a function of current density and the results are given in Figure 3.7.

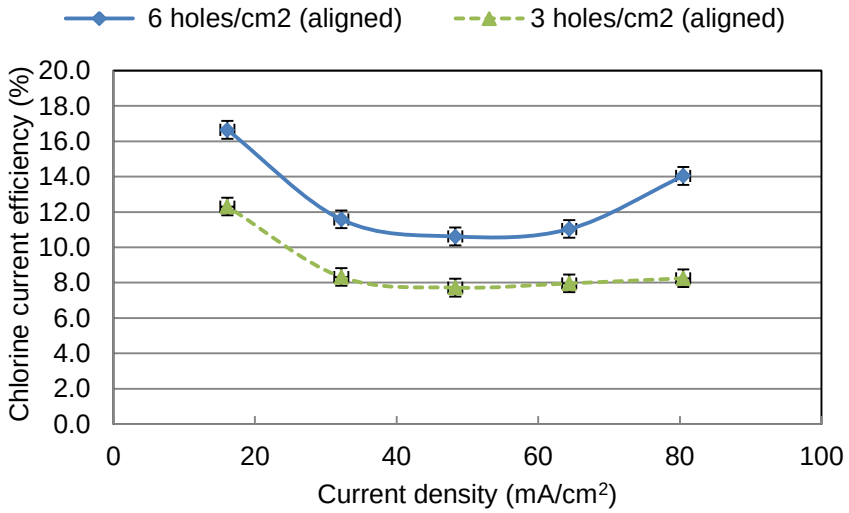

Figure 3.7 - The effect of hole density on chlorine current efficiency with increasing current density (flow rate 190 mL/min, holes aligned configuration, 0.1 mol/L NaCl).

The results show that the higher hole density 6 holes/cm^2 produced more chlorine than the lower hole density and with increasing current density the difference in the rate of production increased. Apparently the increased electrode area provided

by the internal surfaces of the perforations more than compensated for the planner electrode area lost when the holes were drilled. The effect of hole size and hole density on the total active electrode area are summarised in Appendix B.5. The average current efficiency for the higher hole density was 13% which was 4% higher than the lower hole density. The corresponding energy consumptions (EC) for the higher and lower hole densities were 29 and 42 kWh/kg of chlorine respectively, a difference in EC of approximately 30%.

The effect of hole density was also studied at increasing flow rates at constant current density. The results given in Figure 3.8 show that higher density of holes generated more chlorine and the difference in the yield was most significant at low flow rates. This result could be largely due to the reduction in the retention time in the cell at increased flow rates.

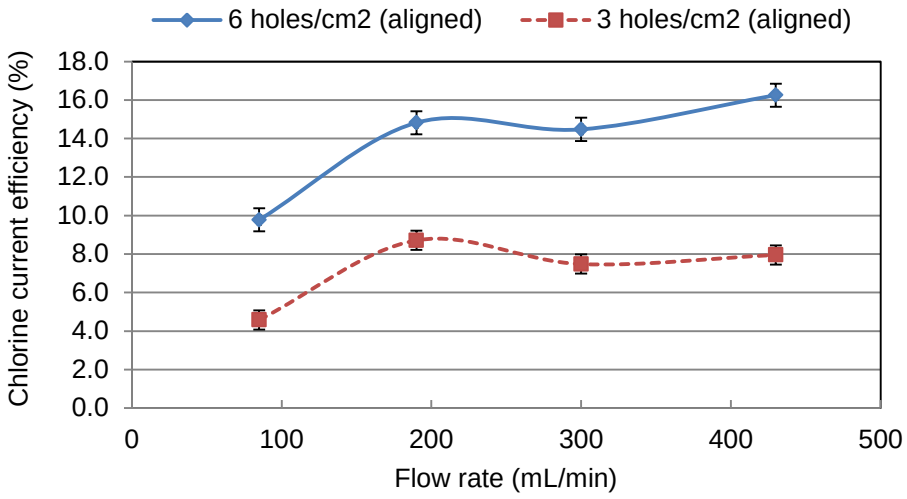

Figure3.8 - The effect of hole density on chlorine current efficiency with increasing flow rate (current density 80mA/cm^2, holes aligned configuration, 0.1 mol/L NaCl)

The hole density is an important parameter in a PEFT cell design. There will be a physical threshold value on the hole density depending on the area of the electrode and the diameter of the perforations.

3.3.2 The effect of staggering holes

In the aligned configuration, the centres of the perforations of the electrodes faced each other and the electrolyte moved through the cell with minimum deviation of flow path. In the staggered configuration, the centres of the perforations of one electrode were displaced to face the midpoint of the triangular array defined by the hexagonal hole pattern (see Figure 3.5A). Flow was now forced to sweep across the electrode surface.

The same two hole densities were employed to study the effect of the staggering. The results for the variation of chlorine generation with current density at constant flow rate are given in Figure 3.9. The data for the aligned configuration is also shown for comparison.

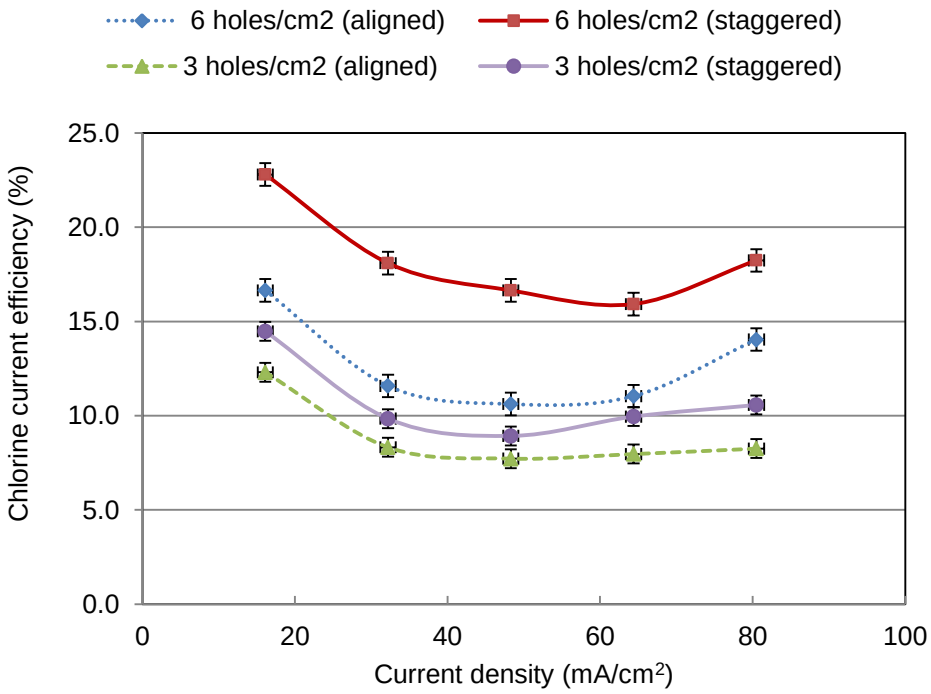

Figure 3.9 - The effect of hole configuration on chlorine current efficiency with increasing current density (flow rate 190 mL/min, 0.1 mol/L NaCl)

Initially for both hole densities and both hole configurations, the current efficiency decreased with current density. However the decrease was less for the

staggered configuration. This effect can be understood by the hydrodynamic effects. In the aligned configuration the solution between the electrodes will remain largely stagnant and become depleted of chloride so that electrolysis of water predominates. In the staggered configuration the solution between the electrodes is continually replenished the hydrodynamic boundary layer is minimised. Higher current efficiency at higher hole density can be explained in geometric terms. The effective electrode surface area is increased by the walls of the perforations so that the actual current density at the electrode surfaces is lower than the average current density based upon cell cross-section.

The effect of hole configuration with flow rate is illustrated in Figure 3.10. For a given hole density the yield doubled when the holes were staggered. Comparing aligned configuration at low hole density with staggered at the higher hole density, it shows a fourfold increment in chlorine generation.

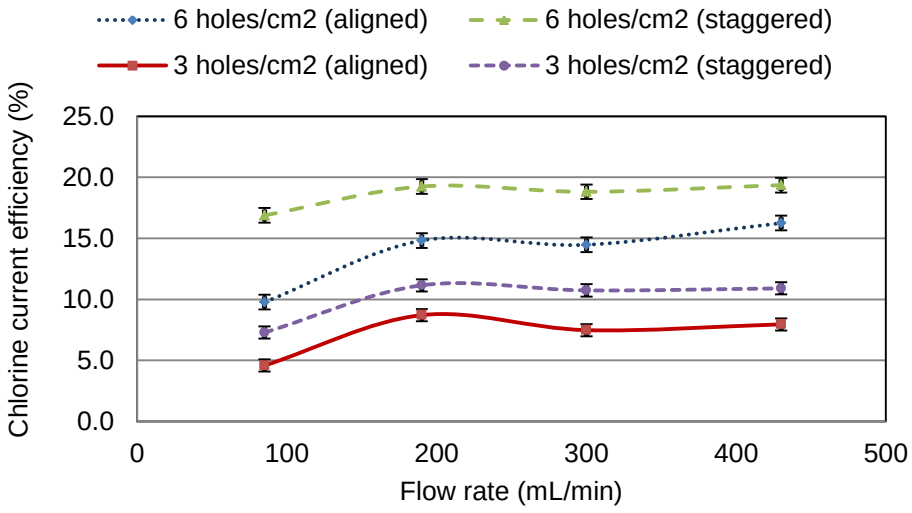

Figure 3.10 - The effect of hole configuration on chlorine current efficiency with increasing flow rate (0.1 mol/L NaCl , current density 80 mA/cm^2)

The average current efficiency (CE) at the higher hole density for the staggered configuration was 18 % and for the aligned configuration it was 13 %, the percentage increment in the current efficiencies was 44 %. Comparing the energy consumptions corresponding to the above CE conditions the staggered configuration consumed 30 % less energy per kilogram of chlorine generated. In all future work the staggered configuration was adopted.

3.3.3 The effect of inter- electrode gap

As discussed in Section 1.1.2 the inter- electrode gap is a major contributor to the PEFT cell efficiency. Cells of inter-electrode gaps of 0.3, 0.1 and 0.05 mm were set up as explained in Section 2.1. The current efficiency for chlorine generation at constant chloride concentration and flow rate was studied as a function of current density and the results are given in Figure 3.11.

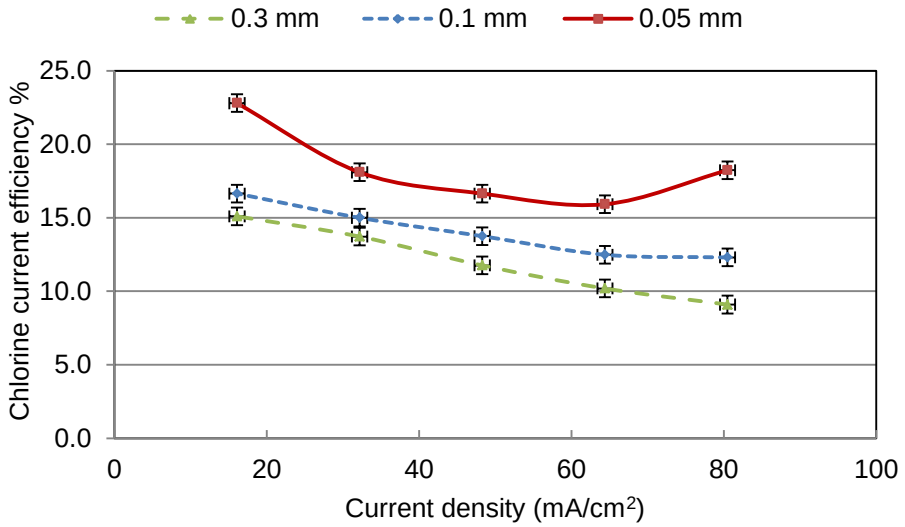

Figure 3.11 -The effect of inter-electrode gap on chlorine current efficiency with increasing current densities (flow rate 190 mL/min, 6 holes/cm^2, staggered configuration, 0.1 mol/L NaCl)

It is evident that current efficiency increased with reduced inter-electrode gap. Current efficiencies are generally higher at the low current densities. The increase in current efficiency for the 0.05 mm gap at the highest current density is contrary to the general trend and may be due to artefacts caused by water electrolysis.

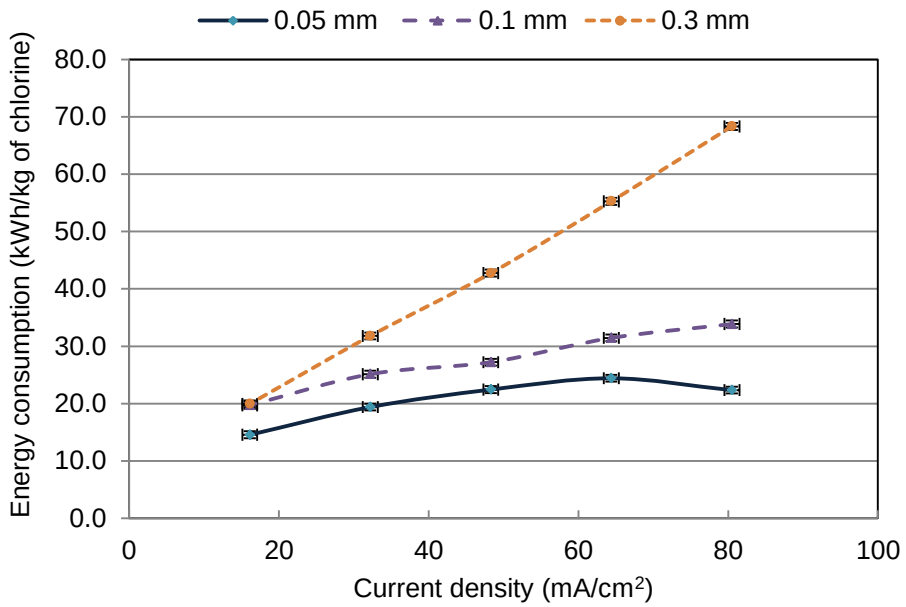

Figure 3.12 -The effect of inter-electrode gap on energy consumption with increasing current densities (flow rate 190 mL/min, 6 holes/cm^2, staggered configuration, 0.1 mol/L NaCl)

The effect of improved current efficiency is reflected in the energy consumption given in Figure 3.12. The reduction of the gap from 0.3 to 0.05 mm has reduced energy consumption at the highest current densities from approximately 70 to just above 20 kWh/kg of chlorine.

The effect of the inter-electrode gap was studied with increasing flow rates at 0.1 mm and 0.05 mm gaps which is given in the Figure 3.13.

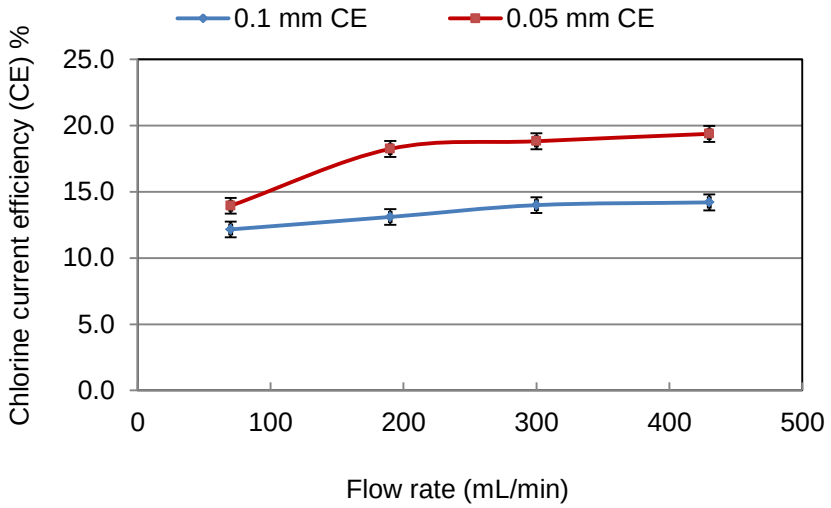

Figure 3.13 - The effect of inter-electrode gap on chlorine current efficiency with increasing flow rates (current density 80 mA/cm^2, 6 holes/cm^2, staggered configuration, 0.1 mol/L NaCl)

The reduced inter-electrode gap increased the chlorine current efficiency. Increased flow rate gradually increased the current efficiencies for both inter-electrode gaps studied.

Increase in chlorine current efficiencies at low inter-electrode gap can be directly attributed to the reduced internal resistance. The reduction in inter-electrode gap could change the hydrodynamic flow pattern between the electrodes moving from uniform to more turbulent flow which reduces the thickness of the electrical double layer allowing more chloride ions to oxidize at the anode surface. The important feature of the PEFT cell design is the ability to increase the flow rate through the cell without sacrificing the current efficiencies and hence improving the energy consumptions.

3.3.4 The effect of hole diameters

The effect of hole diameter was studied using a hole density of 3 holes/cm^{2}and hole diameters of 1 mm to 2 mm and 3 mm. The results of chlorine current efficiency with current density at constant flow rate are given in the Figure 3.14.

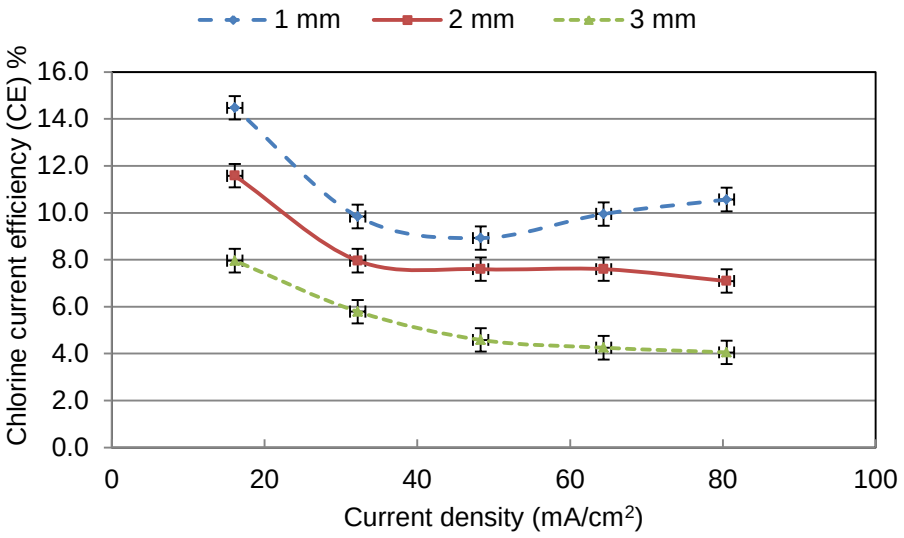

Figure 3.14 - The effect of increase in hole diameter on the chlorine current efficiency with increasing current densities (hole density 3 holes/cm^2, staggered configuration, flow rate 190 mL/min, 0.1 mol/L NaCl)

It is clear that chlorine generation was most efficient with the smallest hole size. Decreasing the hole diameter resulted in progressive improvement in the current efficiency giving and an approximately 50% improvement in CE going from 3 mm to 1 mm. The downward trend of current efficiency with current density for the 2 and 3 mm hole diameters is consistent with normal trends, the upward trend associated with the high current densities obtained for the 1 mm holes may be an effect resulting from water electrolysis.

A likely explanation for the improvement in current efficiency with reduced hole size is the differing contribution of the hole wall area to the overall electrode area. The area of the surface lost is given by $\boldsymbol{\pi r^2}$ whereas area of wall gained by a hole is circumference multiplied by the depth of hole ($\boldsymbol{2\pi r}$ x $\boldsymbol{d}$). For a given active depth of a hole area lost by drilling small holes is more than compensated by the wall area gained so that effective electrode area is increased and effective current density decreased so that current efficiency is improved.

The effect on current efficiency of increasing hole diameters at different flow rates is shown in Figure 3.15.

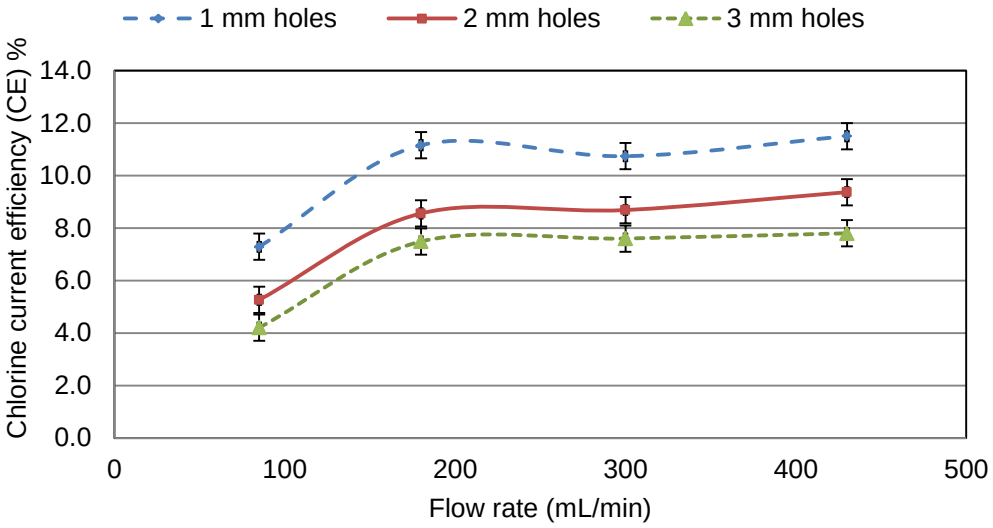

Figure 3.15 - The effect of increase in hole diameter on the chlorine current efficiency with increasing flow rates (hole density 3 holes/cm^2, 0.1 mol/L NaCl, staggered configuration, current density 80 mA/cm^2)

Two trends are apparent. Current efficiency increased as hole size decreased and also increased with flow rate up to a flow rate of 200 mL/min. Above this flow rate current efficiency remained essentially constant. The former effect is consistent with the effect of current density on current efficiency described above which was attributed to the compensation of area lost by drilling small holes by the wall area gained. The effect of flow rate is consistent with a reduction in the hydrodynamic boundary layer of the planner electrode surface as flow changes from laminar flow to turbulent flow above 200 mL/min.

3.3.5 The effect of anode hole diameter

Drilling different size holes provides a means of varying the active electrode area. The reaction of interest occurred at the anode so effect of anode hole diameter was investigated using the hole density of 6 holes/cm^2 and hole sizes ranging from 0.5 to 3.0 mm diameters. The results are given in Figure 3.16.

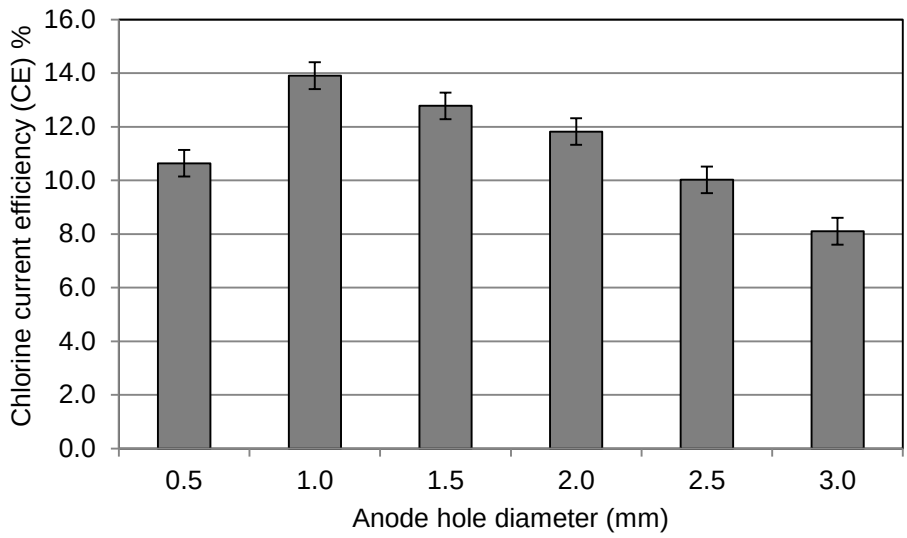

Figure 3.16 - The effect of anode hole diameter on chlorine current efficiency (current density 80 mA/cm^2,hole density 6 holes/cm^2, flow rate 70 mL/min, staggered configuration, 0.1 mol/L NaCl)

The results show that current efficiency improved as hole size decreased consistent with the greater effective electrode area. This trend was reversed for hole sizes below 1 mm. A likely explanation for this reversal is polarization effects caused by less efficient sweeping of gas bubble accumulations on the planar regions of the anode surface. Such an accumulation of gas bubbles should lead to an increase in cell resistance. In order to test this possibility the resistance of the cell was measured as a function of hole size. The results are summarised in Figure 3.17.

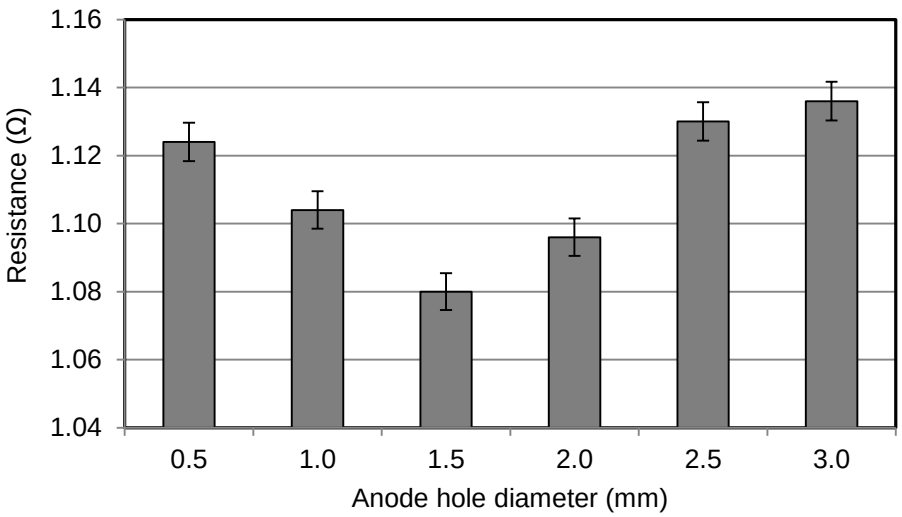

Figure 3.17 - The effect of increasing anode hole diameter on the cell resistance at constant current density of 80 mA/cm^2 (flow rate 190 mL/min, staggered configuration, hole density 6 holes/cm^2, electrolyte concentration 0.1 mol/L NaCl)

The results indicate that the lowest resistance was at 1.5 mm anode hole diameter. The increase in resistance below 1.5 mm hole diameter supports the argument that at low anode hole diameters the narrow flow paths across the planar area of the electrodes resulted in less efficient sweeping of gas bubble accumulation.

3.3.6 The cell constant

The cell constant is defined by the equation:

$$k = l/A \qquad \textit{(Eq. 4-1)}$$

it can be obtained by measuring the conductance of the cell (G) when filled with a solution of known conductivity (κ) using the equation:

$$k = \kappa_{\times} G \qquad \textit{(Eq. 4-2)}$$

Alternatively the cell constant can be estimated geometrically from the equation

$$k = l/A \qquad \textit{(Eq. 4-3)}$$

The experimentally determined cell constants along with the calculated cell constants for a fixed inter-electrode gap of 0.05 mm and (1) the planar surface area of the electrodes and (2) the planar surface area of the electrode plus the perforation rim areas for varying hole sizes are summarised in Figure 3.18.

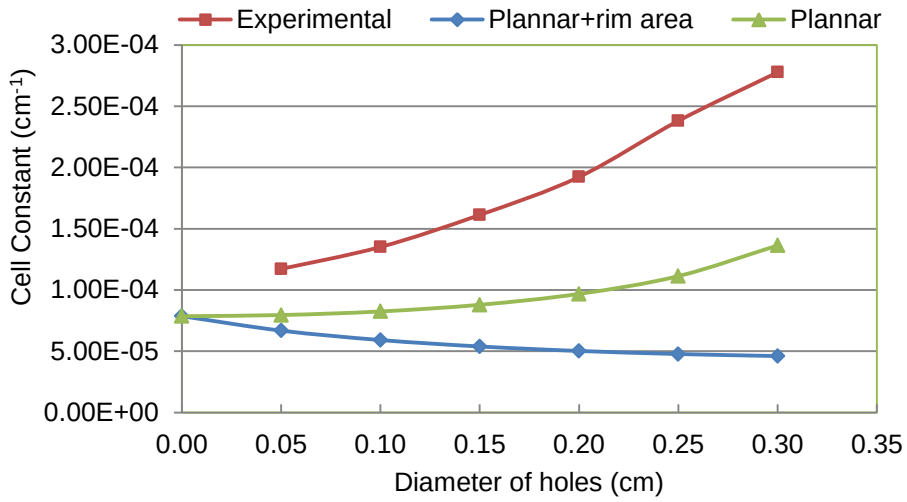

Figure 3.18 - Effect of hole diameter on the cell constant (flow rate 190 mL/min, electrolyte 0.1 mol/L NaCl, holes staggered, 6 holes/cm^2)

The calculated results which considered the wall area represent a lower limit of the geometrically defined cell constant. In practice only the wall area close to the electrode surface will make a significant contribution to the cell constant.

The large discrepancy between the measured cell constant and the calculated values indicate that the effective resistance of the cell under the conditions of measurement was much higher than anticipated from the conductivity of the solution used. Apparently there was a reactive contribution to the overall impedance of the system and this is reflected by the higher values of the cell constant. The reactive contribution could come from the capacitance resulting from the large electrode area and the narrow inter-electrode gap.

3.3.7 PEFT cell hydraulics

One of the consequences of reducing the space/gap between electrodes is the increased resistance to hydraulic flow when operated as a conventional electrochemical cell where flow is forced between the electrodes. For example to achieve a flow of 200 mL/min, through a 50 micron gap between two 64 cm^2 electrodes would require a pressure of approximately 8.6 kPa. One of the major advantages of the perforated electrode flow through configuration is that

individual flow paths from the perforations through the gap are never more than a few millimetres. For example to achieve a 200 mL/min through a PEFT cell with 381 holes of an area of 64 cm^2 would be 1 kPa.

The flow through the system of holes and channels of the PEFT cell is quite similar to flow through a porous medium which is described by Darcy's law.
The measure was originally used to know how water passes through a geologic material and was introduced by the French Engineer Henry Darcy (Nazaroff & Alvarez-Cohen, 2001). Hydraulic conductivity is expressed as a measure of length versus time, in this instance it is millimetres per second. The constant head method was used to obtain the parameters required to calculate the hydraulic conductivity and is given in Section 2.5.5. The hydraulic conductivity *K* was obtained by using the equations:

$$Q = A\,v \qquad \textit{(Eq. 4-4)}$$

Where *Q* is volumetric flow rate, *v* is the flow velocity and *A* is area
Using Darcy's Law

$$V = K\,i \qquad \textit{(Eq. 4-5)}$$

and expressing the hydraulic gradient *i* as:

$$i = h/L \qquad \textit{(Eq. 4-6)}$$

Where *h* is the difference of hydraulic head over distance *L*, yields:

$$Q = AKh/L \qquad \textit{(Eq. 4-7)}$$

Solving for *K* gives:

$$K = QL/Ah \qquad \textit{(Eq. 4-8)}$$

The hydraulic conductivity calculated for the hole density 6 holes/cm^2 assembled in staggered configuration with increasing anode hole diameters and hydraulic conductivity for the hole density 3 holes/cm^2 in staggered configuration with increasing hole diameters on both electrodes are given in Figure 3.19.

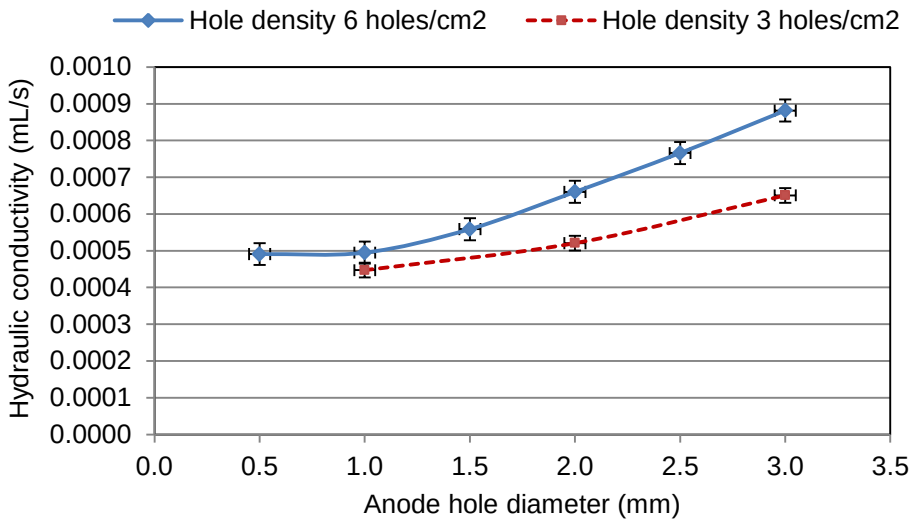

Figure 3.19 -Effect of anode hole diameter on the hydraulic conductivity (cathode hole diameter 1 mm, constant hydraulic head of 1.0 m, staggered hole configuration)

The results indicate that hydraulic conductivity increased with hole diameter and with hole density. When the hole diameter is increased the width of the flow path through the gap between the electrodes is also increased and so the resistance to flow is reduced. Increasing the hole diameter will have the effect of reducing the path length between the holes for a given hole density.

3.3.8 Pressure versus flow rate

The appropriateness of using Darcy's Law to describe the hydrodynamics of the PEFT cell was confirmed by investigating flow as a function of hydrostatic head. Two inter-electrode gaps (50 µm and ~ 2 µm) were used in PEFT cell having 1 mm hole with a hole density of 6 holes/cm^2. The results are summarised in Figure 3.20.

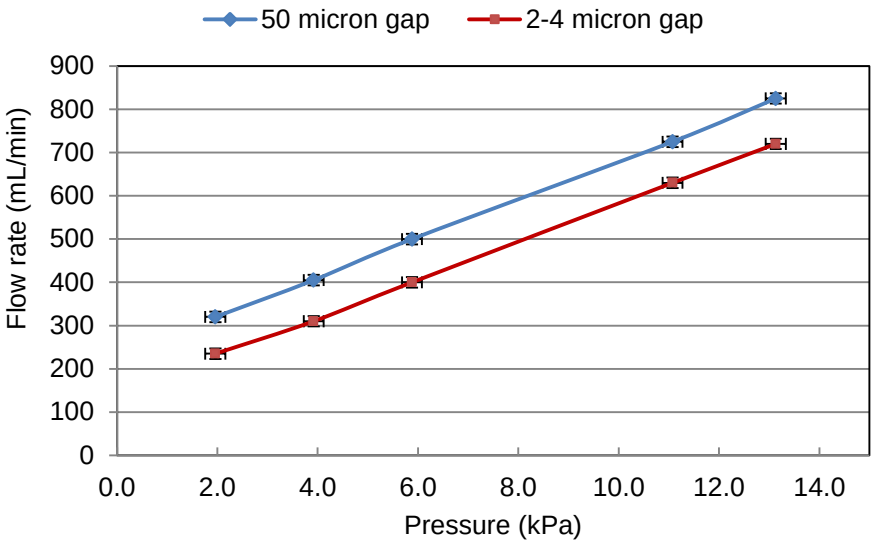

Figure 3.20 -Increase in hydraulic pressure with flow rate (1 mm hole diameter in both electrodes, holes staggered configuration, hole density 6 holes/cm^2)

The linear increase in flow rate with pressure is consistent with Darcy's law. Reducing the inter-electrode gap from 50 microns to 2-4 microns reduced the overall hydraulic conductivity by approximately 100 mL/min, at a given pressure. Interestingly, hydraulic conductivity is not reduced in proportion to the reduction in gap width. As the flow path across the electrodes surfaces is not constrained, it will broaden as the gap becomes smaller so there will be less overall resistance to flow.

3.4 Evolution of the PEFT cell

In the initial PEFT cell the electrodes were a drilled graphite anode and a stainless steel mesh cathode. The deformation of the mesh required a 300 micron separation achieved by a two layers of nylon mesh to avoid short circuiting. When a non deformable drilled stainless electrode was used the inter-electrode gap could be reduced to 50 microns without short circuiting problems. The gap was maintained by a circular rim of cello tape leaving flow over the active part of the electrodes unrestricted. When this cell was used for disinfection studies (Section 7.3.6) enhanced inactivation over and above that expected for the chlorine produced indicated the possibility of an electric field effect. In an attempt to exploit the field effect in the absence of chlorine production, a polyurethane film

was applied to the anode. However the application of the PU film did not achieve perfect insulation and exposed electrode surfaces in the holes allowed current to flow. The measurement of chlorine produced indicated significantly higher current efficiencies at low chloride ion concentrations, an effect that has been described as an electro-catalytic effect (Chapter 8). When the PU film was applied in a way to ensure perfect insulation no current flowed and no electrolytic microbial inactivation was observed. It was realised that to generate a field in the inter-electrode gap electrical contact had to be maintained even if most of the electrode surface was insulated to minimise current. An anodic system of titanium covered with an anodized layer of TiO_2 provided a partially insulated electrode that allowed fields up to 20 kV/cm to be achieved from an applied voltage of 90 V. A 6 log microbial inactivation confirmed that field effects i.e. irreversible electroporation could be achieved at applied voltages much lower than previously reported (Chapter 9). These developments are summarised in Table 3.1.

Table 3.1 – The evolution of the PEFT cell with respect to inter-electrode gap

	Anode	Cathode	electrode gap	Spacer	Application
1	graphite plate *t-2.5mm, d-1.0mm*	Stainless steel*t-2.5mm, d-1.0mm*	240 µm	Nylon mesh *Twin ply*	Electro-chlorination Electro-oxidation
2	graphite plate *t-2.5mm, d-1.0mm*	Stainless steel*t-2.5mm, d-1.0mm*	50 µm	Cello tape	Optimization PEFT Electro-decolourization Electro-disinfection
3	Ti/TiO_2 layer *t-2.5mm, d-1.0mm*	Stainless steel*t-2.5mm, d-1.0mm*	40 µm	Duraseal tape *pp*	Electro-pasteurisation
4	Stainless steel coated with *PU* *t-2.5mm, d-1.0mm*	Stainless steel*t-2.5mm, d-1.0mm*	1-2 µm		Electro-catalytic effect

t - thickness of the plate, *d*- diameter of perforations, *pp*-polypropylene clear adhesive tape , *PU*- polyurethane 50µm thickness coating

3.5 Conclusions

This chapter has investigated the effect on cell performance of major PEFT cell design variables and has pointed the direction for optimisation.

- The flow direction should be such that the electrolytic product species of interest should be formed at the exit electrode.
- Geometric considerations led to the conclusion that a modified staggered hexagonal hole pattern would allow the highest hole density and provide the most uniform flow patterns. In the present work however, a simple hexagonal hole pattern was used.
- A staggered hole configuration gives approximately 40% increase CE relative to an aligned configuration.
- Current efficiency increases as the inter-electrode gap decreases.
- The hydrodynamics of the PEFT cell are superior to conventional parallel plate electrode systems.

Chapter 4: Investigation of iron and manganese removal from groundwater

This chapter will consider the application of PEFT electrochemical system for the removal of iron and manganese from problem groundwaters. Chemical and electrochemical oxidation will be compared. Aspects of the colloid chemistry will be investigated with view of gaining a better understanding of the mechanisms involved and some consideration will be given to the formation of trihalomethanes.

4.1 Rapid chemical oxidation of problem Waikato iron water

When slow air oxidation of iron containing groundwaters form stable colloidal suspensions they are called problem iron waters. It is generally accepted in the water industry that rapid oxidation using chemical oxidants is sufficient to achieve satisfactory removal of iron from these problem waters (Munter, Ojaste, & Sutt, 2005; Nath & Langdon, 2010a, 2010b). In order to provide baseline data with which to evaluate electrochemical oxidation, initial studies were carried out by dosing with chemical oxidizing agents (potassium persulfate, calcium hypochlorite and sodium hypochlorite). These results were then compared with results obtained by electrochemical oxidation using a graphite/stainless steel mesh 240 micron gap PEFT cell (see Section 2.1) at NaCl concentration of 1g/L and using a constant current density 78.6 mA/cm^2, flow rate of 190 ml/min, and a single pass through the cell. The control experiment was always the equivalent experiment where only air oxidation was involved.

Data for iron, manganese and turbidity removal using a six fold excess of chemical reagents and electrochemical treatment in the presence of 1 g/L of NaCl are given in Figures 4.1, 4.2 and 4.3. The full sets of data for different chemical dosages are in the Appendix C.

Figure 4.1 shows that of the chemical oxidants, satisfactory removal was achieved only with hypochlorites. The electrochemical method proved to be more efficient than even a large excess of chemical oxidants. Total removal of iron occurred within four hours of standing.

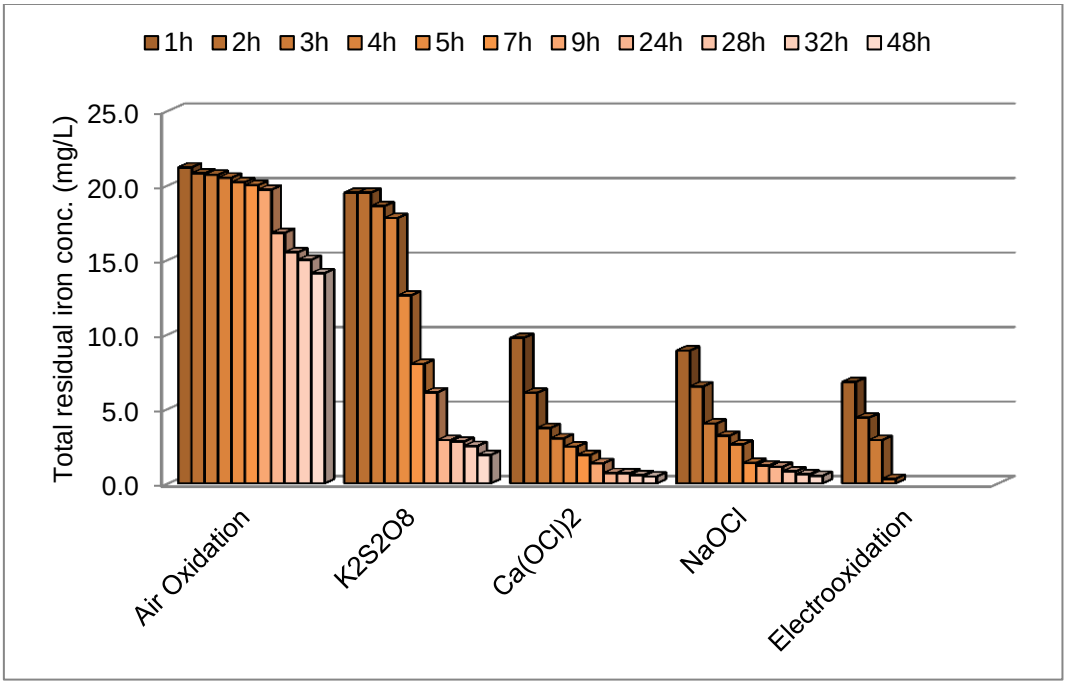

Figure 4.1 - Residual iron concentration in groundwater during air oxidation compared with rapid oxidation processes using chemical and electrochemical methods (pH 6.7, temperature 20°C)

The data for manganese removal (Figure 4.2) show similar trends to those observed for iron removal. However when chemical oxidants were used residual manganese levels were greater than the maximum allowable value (MAV) threshold of 0.04 mg/L. In contrast, when electrochemical oxidation was used the initial removal rate was slower but after 48 hours a residual concentration of 0.01 mg/L, within the MAV threshold, was obtained.

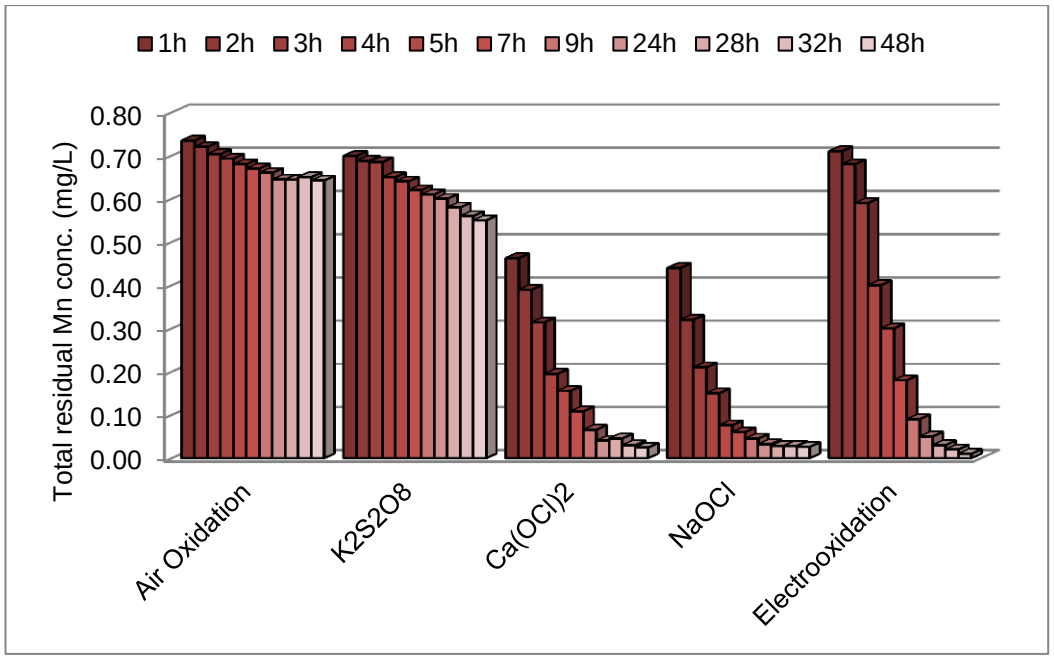

Figure 4.2 - Residual manganese concentration in groundwater during air oxidation compared with rapid oxidation processes using chemical and electrochemical methods (pH 6.7, temperature 20°C).

Turbidity data (Figure 4.3) further supported the effectiveness of the electrochemical treatment. Electro-oxidation gave the best results in removing the turbidity, within 10 hours of post electrolysis time to below 1.0 NTU.

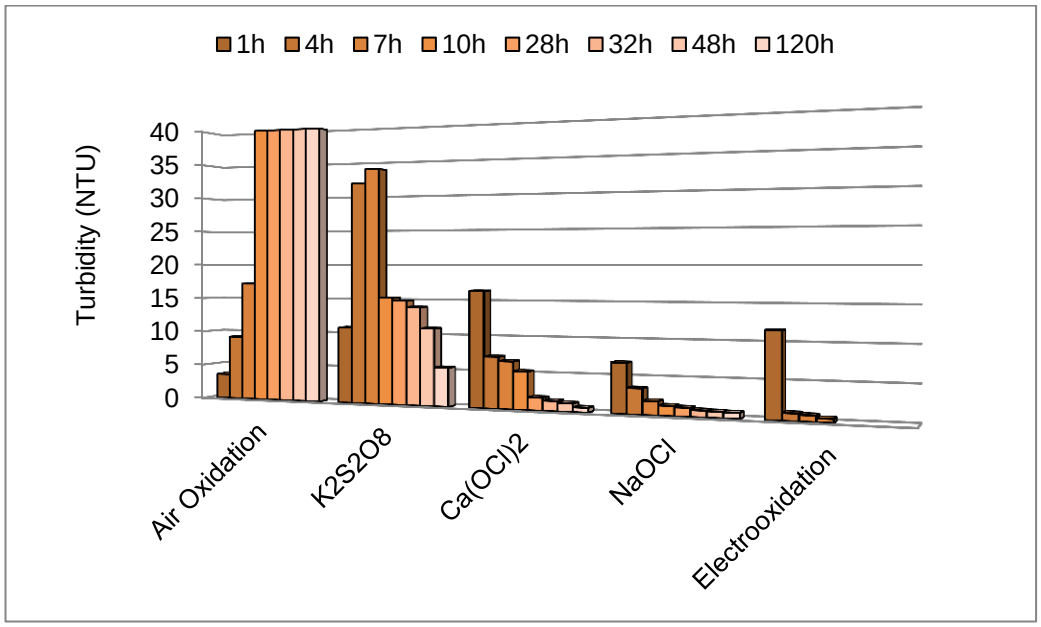

Figure 4.3 - Turbidity in bore water during air oxidation compared with rapid oxidation processes using chemical and electrochemical methods (pH 6.7, temperature 20°C)

Out of the three chemical oxidizing agents, sodium hypochlorite generally performed better than calcium hypochlorite. Potassium persulfate, although a strong oxidizing agent, was relatively ineffective as an oxidant for the removal of iron and manganese from the problem water

Overall electro-oxidation performed better than chemical oxidation processes both in terms of the reduced amounts of chlorine required and the settle ability of the flocs that resulted.

4.2 Factors contributing to the effectiveness of electro-oxidation of Fe(II) solutions

Some factors that may contribute to the greater effectiveness of chlorine produced electrochemically relative to the chlorine released from hypochlorite could be the presence of other chemical species including other oxidizing agents formed electrolytically. These species include molecular oxygen, ROSs and pH affects caused by the imbalance of hydroxyl production at the cathode and the protons produced at the anode (see Section 1.2).

An experiment was designed to determine the relative roles of the oxygen and ROSs in the absence of chloride relative to the same experiment when 1 g/L of chloride added to water. A simulated water sample containing approximately 20 mg/L of iron in double distilled water was purged with nitrogen gas to remove the dissolved oxygen and ferrous sulphate was added while nitrogen continued to purge the solution. The pH was adjusted to 7.2 and passed through the PEFT cell without electrolysis and allowed to oxidize in air. A second sample at the same pH was passed through the PEFT cell with electrolysis. The two runs were compared with a third experiment where the iron was oxidized with the presence of 1 g/L of NaCl. In each case the electrolysis was carried out at constant current density 78.6 mA/cm^2. Data is shown in Figure 4.4.

In the case of the purged system approximately 40% oxidation of the iron occurred during the passage through the cell and continued oxidation on standing

resulted in approximately 85% oxidation after 100 minutes. When the solution was electrolysed instantaneous oxidation increased to 70% and further oxidation occurred on standing. In the air oxidation without electrolysis the pH was observed to drop whereas when electrolysed pH rose to 7.8. When chloride ions were present and the solution was electrolysed instantaneous 100% oxidation occurred during the passage through the cell and the pH fell to 5.5.

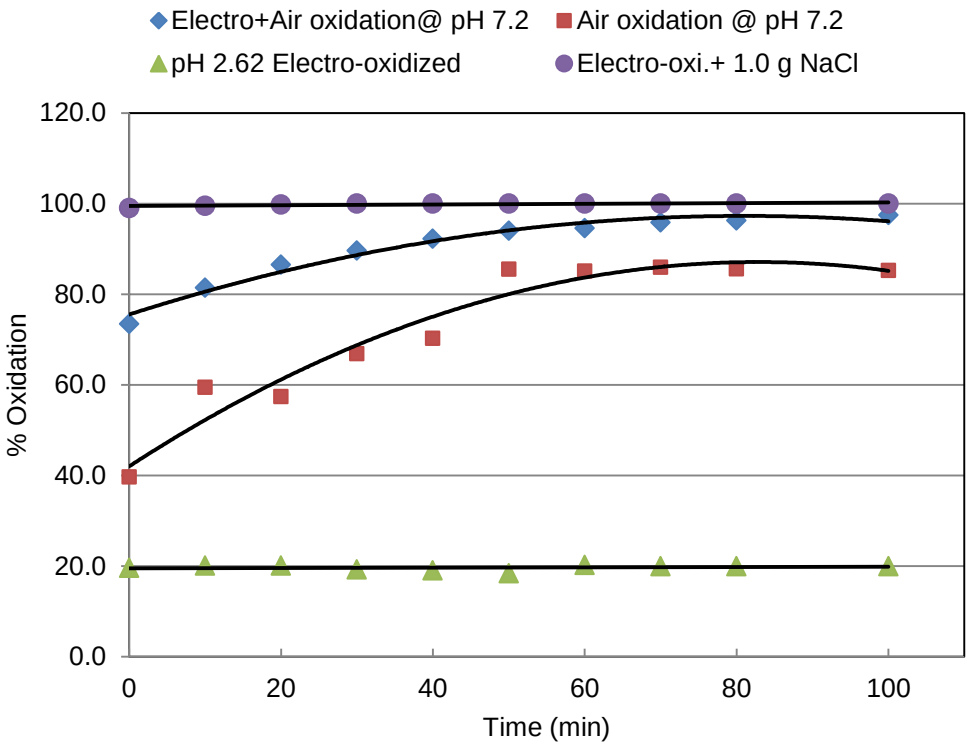

Figure 4.4 - Comparing oxidation of iron in water post electro-oxidation with natural air oxidation at pH 7.2 and post electro-oxidation of iron water sample at pH 2.62 undergoing air oxidation.

The instantaneous oxidation in the absence of electrolysis indicated how readily Fe(II) oxidized at neutral pH. The additional instantaneous oxidation when electrolysed is evidence for the oxidizing contribution of the molecular oxygen and ROSs formed during electrolysis. The continued oxidation upon standing will have been due to air oxidation.

The data for iron oxidation in the presence of the chloride ions is a clear confirmation of the critical role of electrolytically produced chlorine acting as mediator in an indirect oxidation process.

The experiment was repeated at pH 2.62 to avoid the possibility of air oxidation. Fe(II) solutions are stable at this pH. Upon electrolysis 20% oxidation occurred indicating the likely role of ROSs because molecular oxygen is unlikely to be an effective oxidizing species at this pH.

4.3 Electro-oxidation of iron and manganese in groundwater

Electrochemical oxidation of groundwater was carried out to remove the naturally contaminant metal ions, iron and manganese. The PEFT cell configuration used, materials and the electrochemical experimental methods are given in Section 2.1 and 2.2.

4.3.1 The role of the nature and concentration of anions present

In preliminary experiments on electro-oxidation of natural groundwater (groundwater from bore well *A*, conductivity of 266 µS/cm 10 to 12 mg/L NaCl) achieved only 47% immediate iron oxidation at 5 A and 24.7 V. Addition of sodium chloride to the groundwater increased instantaneous oxidation efficiency. Oxidation efficiency was studied at constant current density (78.6 mA/cm^2) and with increasing additions of sodium chloride, shown in Figure 4.5. At a level of 3.0 g/L of added salt and at electrolytic conditions of 5 A, 6.1 V, conductivity 3.9 mS/cm and a flow rate of 190 mL/min, instantaneous oxidation of 99% of the iron was achieved (Figure 4.5). In contrast, the addition of 3.0 g/L sodium sulphate immediately oxidized only 58% of the iron present in the groundwater. Also shown on Figure 4.5 is data for natural and forced air oxidation. While forced air oxidation is much more rapid than natural air oxidation, neither air oxidation curves indicate significant instantaneous oxidation.

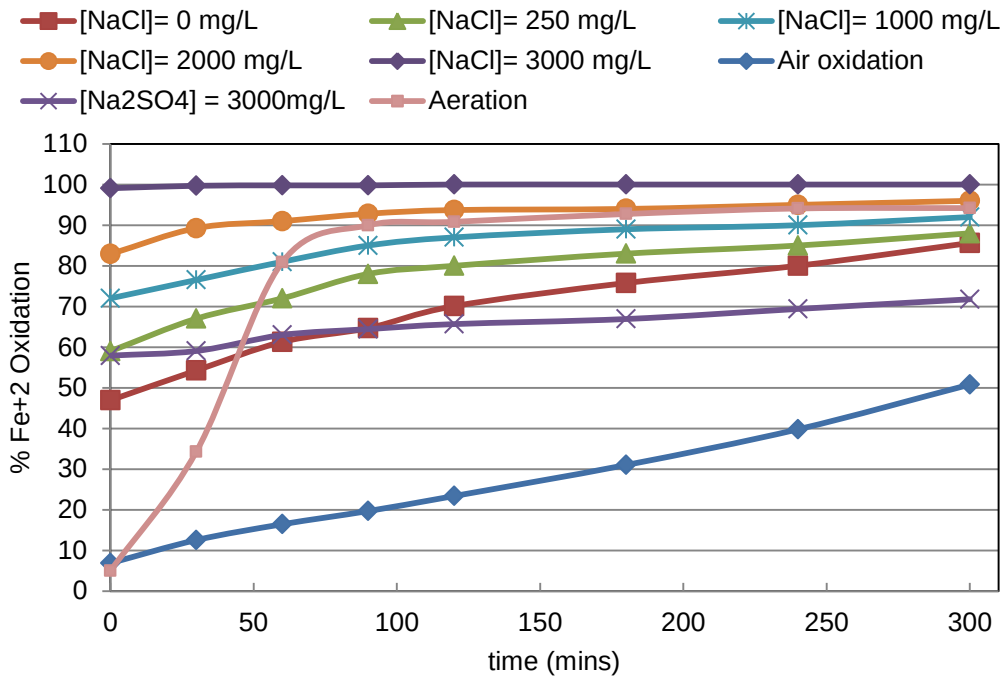

Figure 4.5 - Electro-oxidation of iron in groundwater at constant current density 78.6 mA/cm^2 and flow rate of 190 mL/min, single pass through the cell.

4.3.2 Oxidation and turbidity

The turbidity of the 100% oxidized groundwater sample with the 3 g/L of NaCl added settled rapidly and lowered metal ion concentrations to levels well below drinking water standards within 5 hours (Figure 4.6). Under these conditions the ferric ions hydrate, hydrolyse and precipitate as ferric hydroxide. Rapid aggregation and settling is probably facilitated by the relatively high ionic strength (Gregory, 2006). At 2 g/L added NaCl, results are similar but do not achieve the same levels of oxidation or clarification, presumably because of the lower levels of chlorine generated. At 1 g/L added NaCl, lower initial oxidation meant that oxidation continued after exiting from the cell and turbidity also increased in sharp contrast to the higher chloride concentrations where turbidity decreased immediately after the water exited the cell.

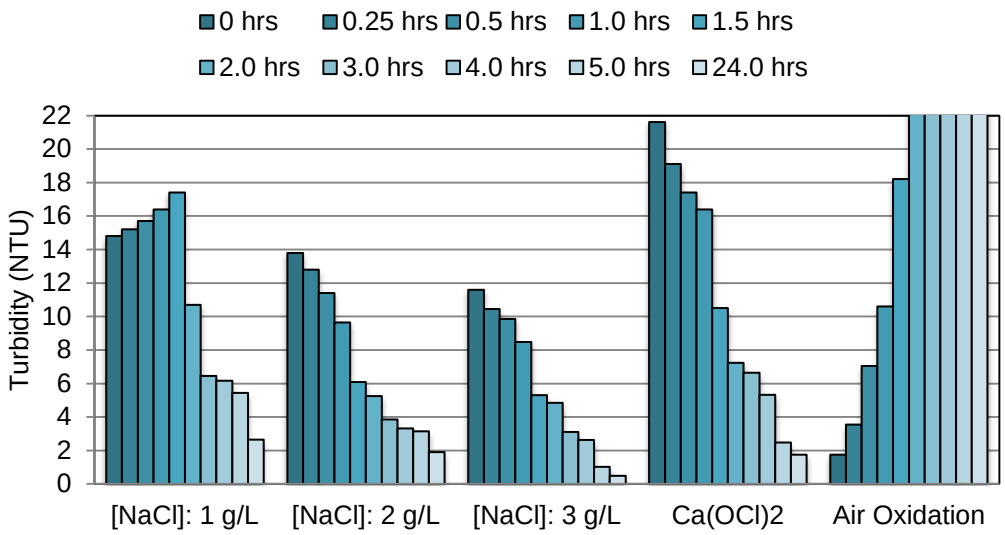

Figure 4.6 - The turbidity measurements of the electro-oxidized bore water with time.

4.3.3 Metal ion removal: Single pass treatment

Data for metal ions remaining after filtration for a single pass through the cell at three NaCl concentrations using three current densities are shown in Figure 4.7. Data for Na_2SO_4 at a concentration equal to the highest NaCl concentration and at the highest current density, along with data for air oxidation, are also included for comparison. The treated water was allowed to stand for 3 hours and then filtered through 0.45 μm filters and the filtrate analysed for soluble (non-oxidized) iron and manganese. Also included on Figure 4.7 above each data bar are the amounts of chlorine that were produced in an analogous experiment with solutions made up to contain the same electrolyte concentrations but no iron or manganese.

Increasing the chloride concentration reduced the concentration of remaining non-oxidized iron consistent with the greater production of chlorine. The oxidation and removal of manganese was much less than that of iron presumably because the reduction potential of manganese is much higher. Even at the highest concentration of sodium chloride and highest current density iron and manganese concentrations (0.3 and 0.5 mg/L respectively) were higher than the New Zealand drinking water standard levels (0.2 mg/L and 0.04 mg/L respectively) The result obtained when sodium sulfate electrolyte was used, when compared with the

result for air oxidation alone, indicated a level of electro-oxidation where chlorine species were absent. This could be due to three contributing factors; transient reactive oxygen species (ROS) reported to be formed during the electrolysis of water (Fiessinger, Richard, Hontiel, & Husquere, 1981; Kerwick, et al., 2005; Panizza & Cerisola, 2005; Polcaro et al., 2007); the result of direct oxidation of the metal species at the electrodes (Anglada, et al., 2009; Chiangi, et al., 1995; Deng & Englehardt, 2007); or the effect of the higher oxygen concentrations produced as a result of water electrolysis

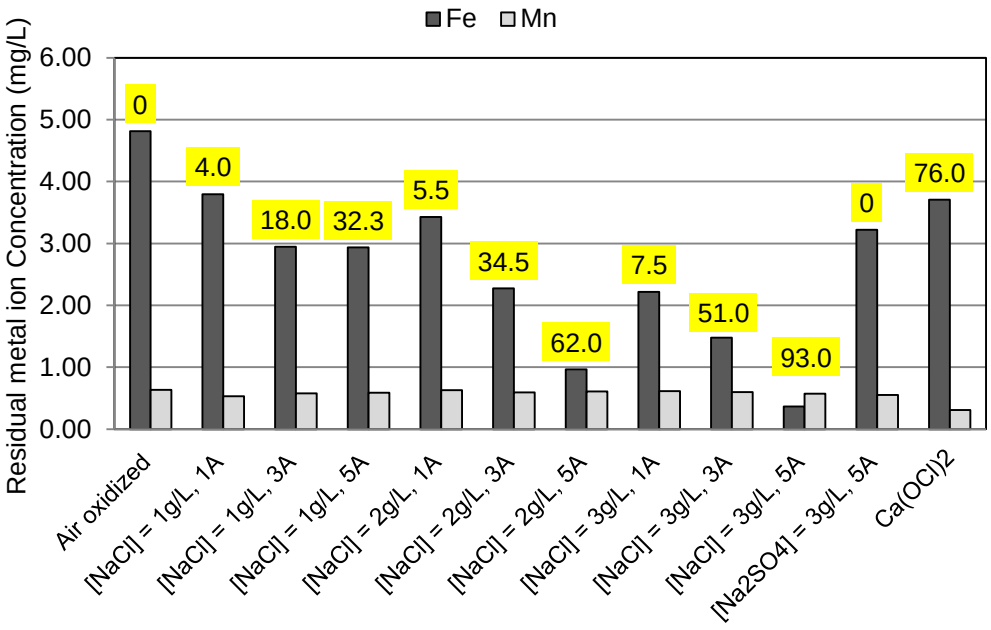

Figure 4.7 - Soluble iron and manganese content in water after 3 hrs post single pass electro-oxidation at a flow rate 190 mL/min. Total chlorine production in mg/L is given on top of each data bar.

The problem of the high metal residuals shown in Figure 4.7, and also the high chloride added, was addressed by a multiple pass experiment.

4.3.4 Multiple pass treatment

An acceptable chloride level in drinking water is 250 mg/L (Ministry of Health, 2005). The problem to be solved was how to use the electrochemical device to achieve adequate metal removal at this salt concentration. The approach adopted was to use multiple passes through the cell. Data for successive treatment cycles

at 250 mg/L NaCl are shown in Figure 4.8. Total oxidation of the iron was achieved after 4 cycles.

Data above each bar on the chart are the amounts of chlorine calculated from the total charge passed and current efficiency under the same electrolysis conditions. According to this calculation the total chlorine produced after four passes was 36 mg/L which compares favorably with the 93 mg/L chlorine necessary in the 3 g/L experiment to produce a similar level of oxidation. The reduced chlorine requirement is an important factor in treating groundwater because it reduces the possibility of forming chlorinated organics (Bull, et al., 1995; Chang, et al., 1996; Hsu, et al., 2000; Kool & Van, 1984; Yang, 2004).

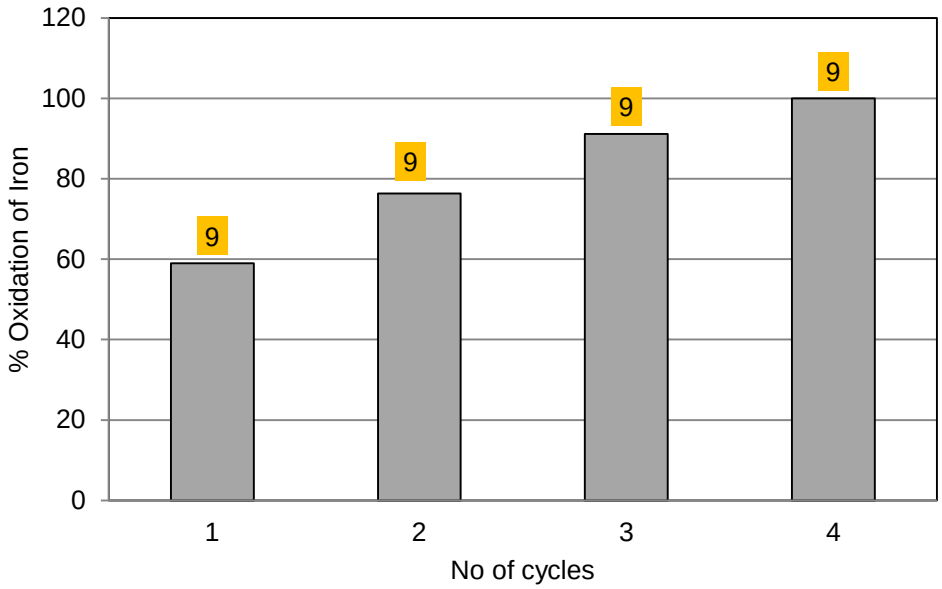

Figure 4.8 - Percentage of iron oxidized in groundwater at each cycle in the multiple pass system, flow rate: 190 mL/min, [NaCl]: 250 mg/L, current density: 78.6 mA/cm^2. (value on top of each bar indicates the estimated chlorine generated (mg/L) during each cycle)

The reduced chorine requirement could be a result of increased contact time, oxygen and ROSs. Data for metal ions remaining after filtration of the treated water is summarized in Figure 4.9.

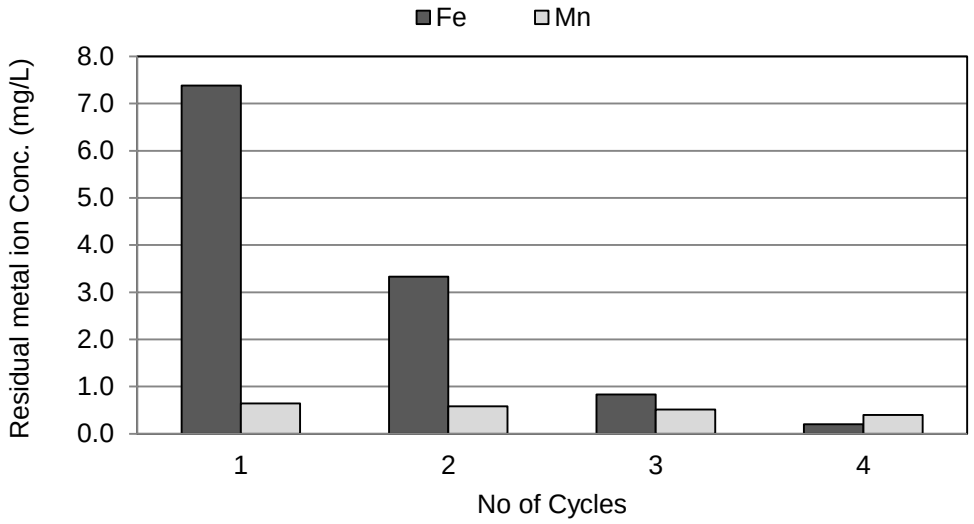

Figure 4.9 - Residual after filtration concentration of iron and manganese in groundwater after each cycle through the PEFT cell, measured one hour post electro-oxidation, flow rate: 190 mL/min, [NaCl] : 250 mg/L, current density: 78.6 mA/cm^2.

It is clear that the four cycles that are required for complete oxidation of the iron allow its almost complete removal upon filtration. The poor removal of manganese, even when harsh oxidizing conditions are employed is consistent with the greater magnitude of the manganese reduction potential (E^0:Fe^{3+}/Fe^{2+} = + 0.77V, MnO_2/Mn^{2+} = +1.23V) (Rosen, 2001; Vogel, 1997). Evidence for this is provided in Figure 4.9 which shows that most of the iron is removed before there is significant manganese decrease.

4.3.5 Power consumption

While the multiple pass experiment achieves 100% oxidation at a lower level of chlorine production than the single pass experiment at 3 g/L, the multiple pass experiment requires almost six times more power (multiple pass: 18.4 kWh/m^3 and single pass 3g/L: 2.7 kWh/m^3) to achieve the same level of metal removal. This is mainly due the low current efficiency of chlorine production at the low concentration (2.0%) but increased cell resistance is also a factor in the multiple pass experiment (conductivity of 250 mg/L of NaCl: 595 µS/cm, conductivity of 3

g/L NaCl: 3.9 mS/cm). In addition the recycled solution contained fine bubbles that could have adhered to the electrodes increasing resistance.

4.4 Aspects of the colloid chemistry of problem groundwater

The importance of rapid oxidation in the treatment of iron and manganese containing groundwaters is not fully understood. Under natural air oxidation conditions, the slowly oxidized metal ions undergo hydrolysis to form sub units of hydrous oxides which react with other water constituents (silica and/or organic material) to form stable colloidal suspensions (Stumm & Morgan, 1981).

$$Fe^{+2} \rightarrow Fe^{+3} + e^{-} \qquad \textit{(Eq. 4.1)}$$

$$Fe^{+3} + 3H_2O = Fe(OH)_{3(s)} + 3H^{+} \qquad \textit{(Eq. 4.2)}$$

The usual explanation for the formation of colloidal suspensions is that the metal hydroxides in the presence of negatively charged silica particles or humic macromolecules become coated and acquire a net negative charge. This negative charge effectively stabilises the oxide particles against further aggregation(Kohn & Roberts, 2006). Supporting this explanation are reports that high concentration of anionic inorganic species such as phosphates and silica cause iron oxides to be negatively charged and to form stabilised colloids in water (Mayer & Jarrell, 1996) and the adsorption of dissolved silica results in electrostatic stabilisation of colloidal iron oxides (Cameron & Liss, 1984).

In order to better understand the nature of colloids from Waikato problem groundwater and their stabilisation, TEM, SEM, light scattering, electrophoresis and pH studies of air oxidized iron water taken from bore A were undertaken.

4.4.1 TEM studies

A sample of bore well *A* water was withdrawn and allowed to undergo slow air oxidation for 24 hours. A sample was nebulised onto TEM copper grits and TEM

images were taken (Figure 4.10). The image shows dark particles consistent with the more dense iron particles surrounded by lighter particles consistent with less dense silica (Yuan, TAO, Yan, Tan, & Qiu, 2010)(see Appendix C). While the images indicate some degree of iron particle association, the resulting aggregates are generally less than 1 micron and thus are unlikely to settle out. The smaller silica particles also appear to have aggregated to form small clumps some of which have become attached to the iron particles. It is not clear whether these particles were formed from gelatinous silicic acid during TEM slide preparation or whether they existed as particles in the natural water.

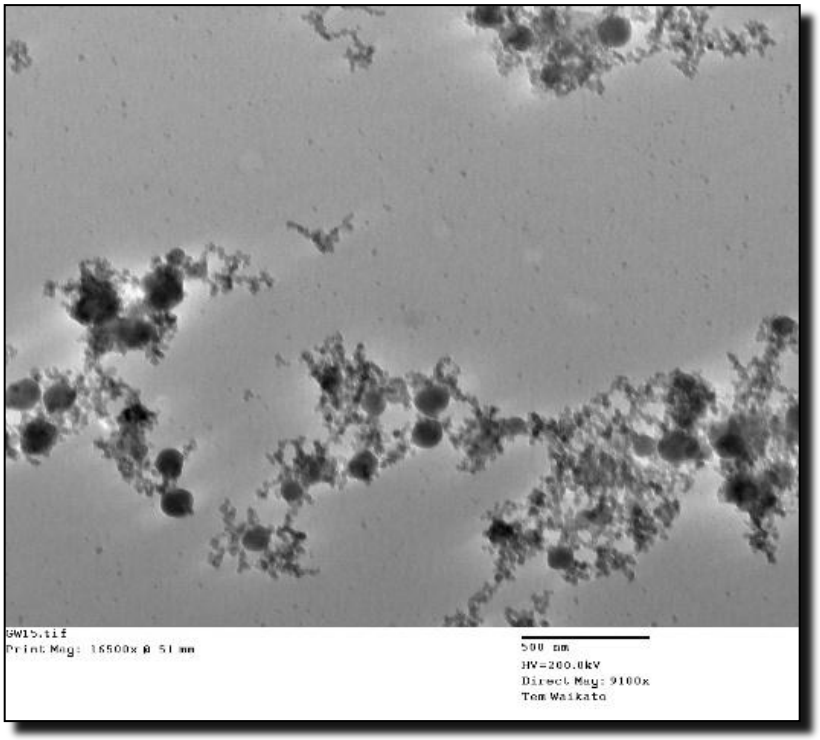

Figure 4.10 - TEM image: groundwater undergoing slow oxidation

4.4.2 SEM studies

Further evidence of association of iron and silica was obtained by Scanning Electron Microscope Energy Dispersive Analysis through X-ray spectroscopy (SEM–EDAX). The technique of elemental mapping was performed on a sample of the iron-silica complex. Results are given in Figure 4.11. The elemental mapping shows that silica and iron distributions overlap confirming that silica is associated with the iron in the aggregates.

The percentage elemental composition in the aggregates represents approximate ratios of silica, iron and manganese in the groundwater samples that were used in the experiments.

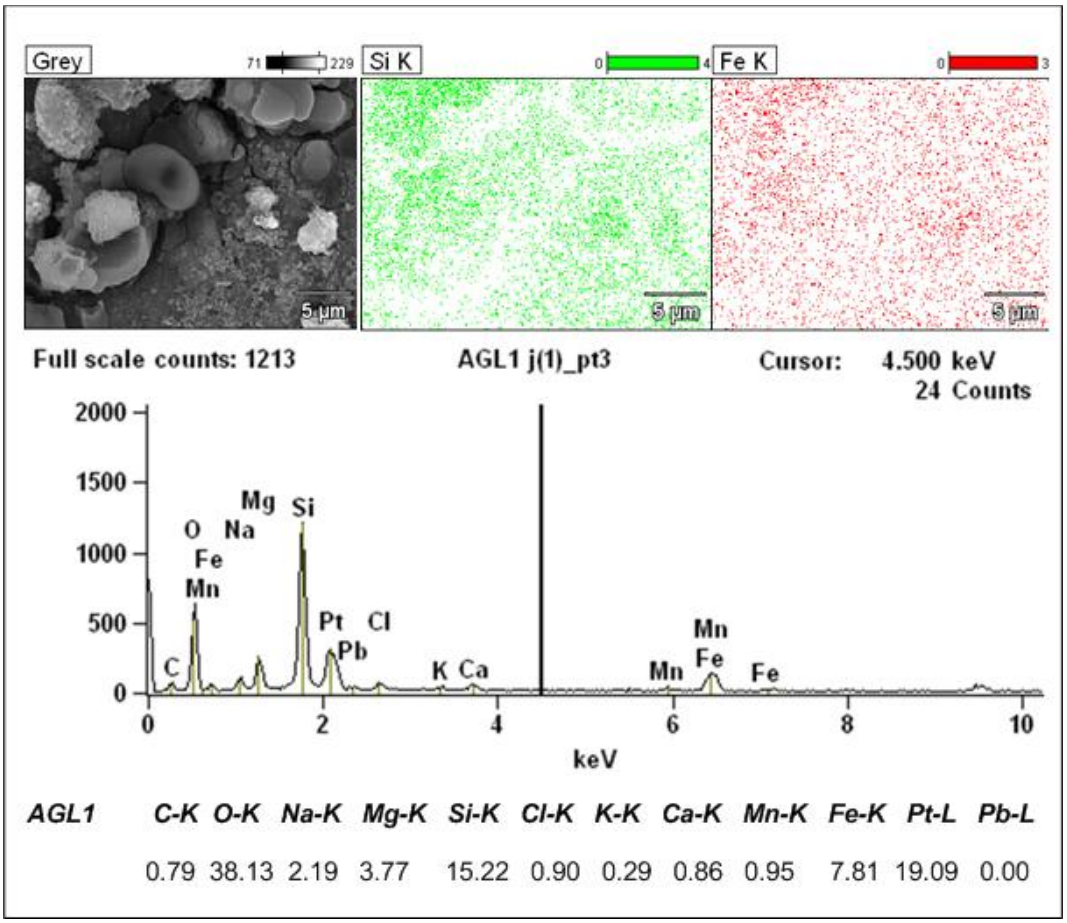

Figure 4.11– SEM –EDAX report and elemental mapping of a sludge sample taken from an air oxidized groundwater sample taken from bore A

4.4.3 Elemental composition of iron water colloids

The elemental composition of the iron water colloids and its dependence on particle size was investigated by membrane filtration and ICP-MS analysis. The results are given in Figure 4.12. Most of the silica particles were found in the smallest particle size range less than 25 nm confirming the assignment of the smaller particles observed in the TEM studies. Manganese was also found in the small size ranges but iron particles occurred in two broad distributions centred on

3 microns and 0.8 microns respectively. Given that the upper limit of colloidal stability is generally taken as 1µm (Gregory, 2006), the presence of the larger iron particles is consistent with the observation that some of the oxidised iron settles on standing while the smaller iron manganese and silica particles showed little tendency to settle.

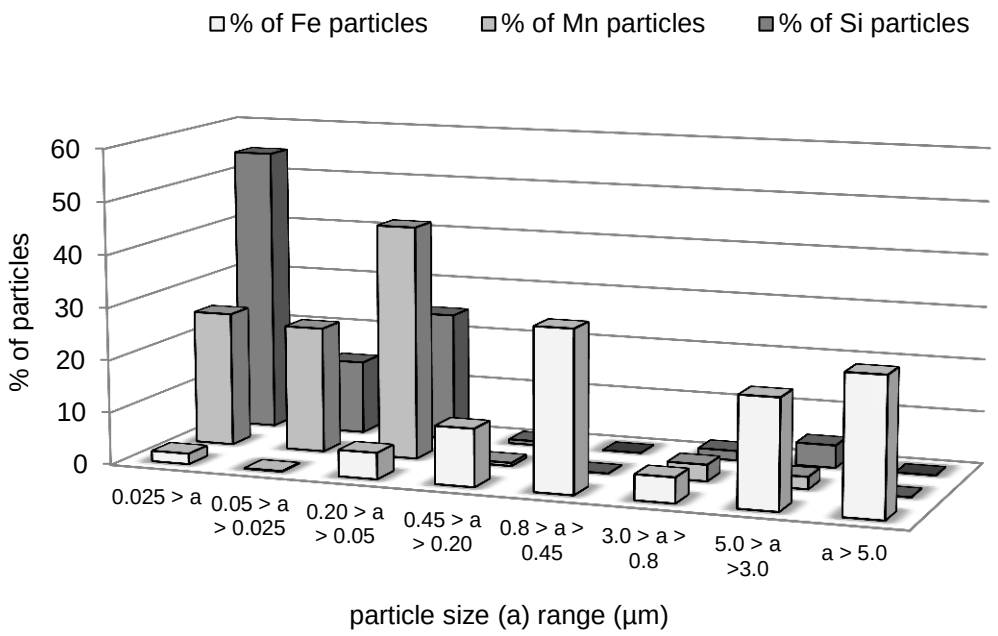

Figure 4.12 - Soluble iron and manganese content in water after 3 hrs post single pass electro-oxidation at a flow rate 190 mL/min.

4.4.4 Particle size distribution with time

The variation of the particle size distribution with time in an air oxidized groundwater sample was followed using the Zetasizer instrument. The results, Figure 4.13, show initial size distributions one hour after extraction of groundwater and again after 48 hours. Two types of particle were observed. A small particle size distribution (25-50 nm) consistent with the TEM results attributed to silica and a larger particle distribution (200 – 450 nm) consistent with the iron silica aggregates also observed in the TEM studies. While both types of

particle increased in size over 48 hours even the aggregates were still well below 1 micron and showed little tendency to settle.

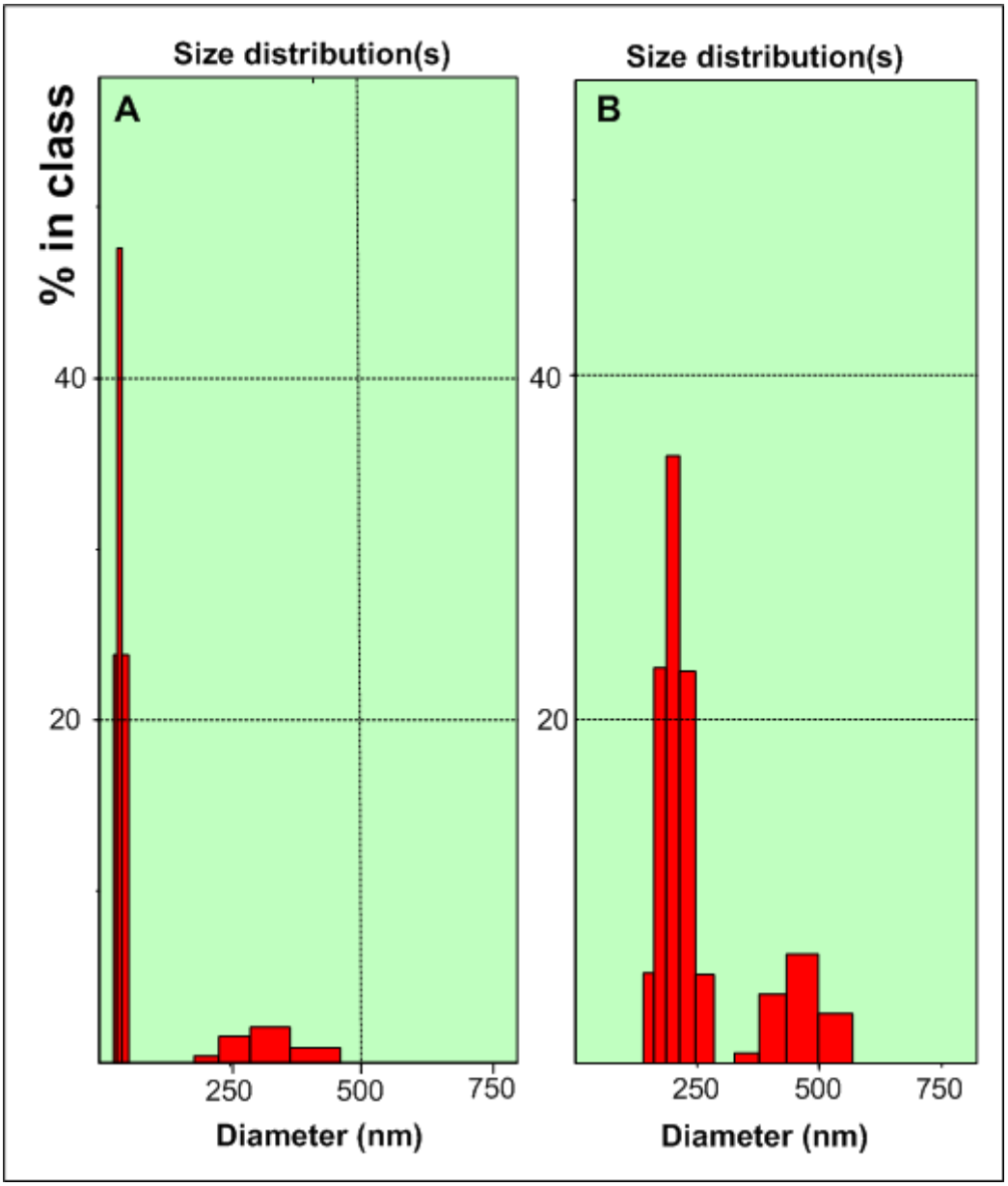

Figure 4.13 - Particle size distribution in air oxidized groundwater A: after 1 hour B: after 48 hrs (Malvern Zetasizer measurements)

4.4.5 Variation of particle charge with time

The Malvern Zetasizer instrument was used to follow changes in particle charge over time. Data taken after one hour of groundwater extraction and exposure to air is given in Figure 4.14 A. It is evident that there were two distinct particle types,

one negatively charged and the other positively charged. At the pH of the experiment (6.5-6.8), the silica particles would be expected to be negatively charged and the iron particles would be expected to be positive. The results are consistent with this expectation indicating small negatively charged silica particles and larger positively charged iron particles.

Reinvestigation of the same water sample after a month (Figure 4.14 B) indicated that the particles with zeta potentials of – 100 mV and + 100 mV respectively were absent and had been replaced by modified particles with a zeta potential of approximately – 25 mV. The pH was observed to have risen from 6.8 to 8. These changes provide evidence for the aggregation of the initial positive and negative particles to form composite particles with a net negative charge. This result is consistent with the TEM data which was interpreted as the coating of the positive iron particles with the negative silica particles. A similar result was reported by Carlson and Schwertmann (1987) for iron and manganese contaminated Finnish groundwater.

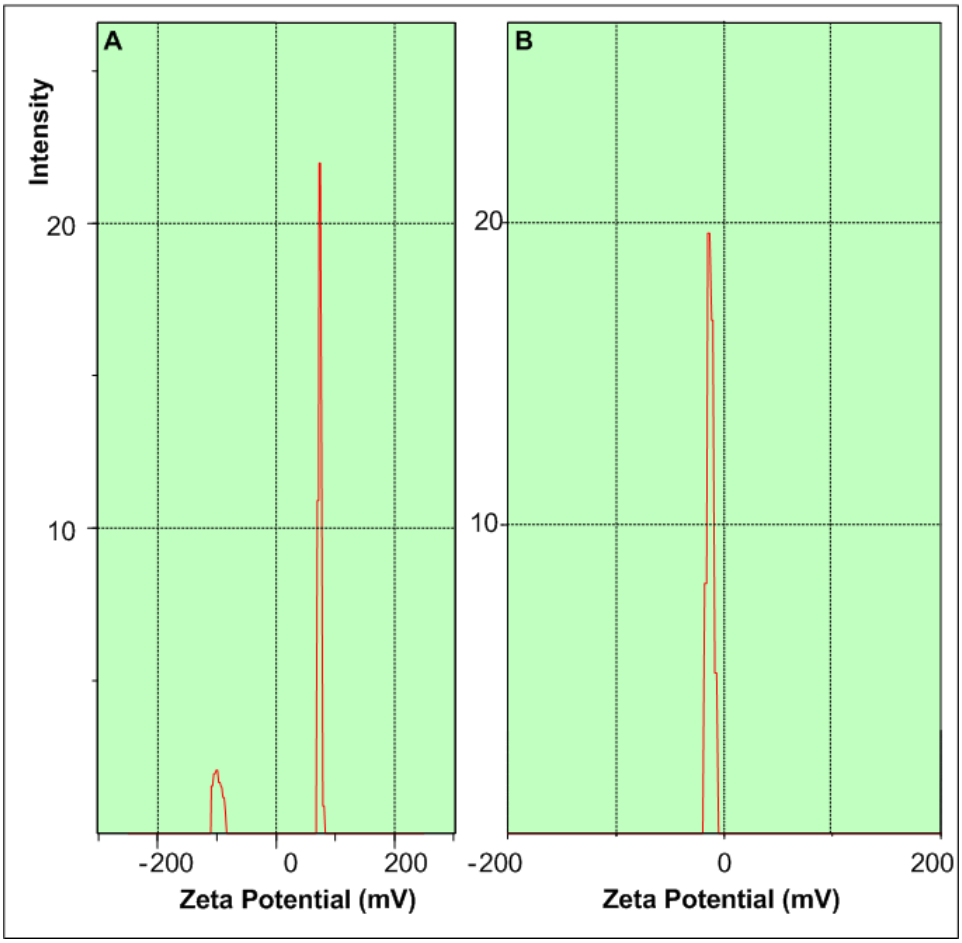

Figure 4.14 - Zeta potentials of the particles in groundwater undergoing air oxidation,A: after 1 hr B: after 1 month

The rise in the pH indicates that this association is accompanied by chemical effects. A simple explanation for this effect is provided by Carlson and Schwertmann (1981) where Fe(OH) group of the iron oxide reacts with the Si(OH) group of the silica forming a Si-O-Fe linkage and releasing a hydroxyl ion.

4.4.6 Rapid oxidation

In contrast to the stable colloidal suspensions formed during slow oxidation, when iron water is oxidised rapidly using a strong chemical oxidising agent (eg. $Ca(OCl)_2$), rapid aggregation and settling of the iron is observed.

A sample of Waikato iron water oxidised with $Ca(OCl)_2$, was air dried and TEM images were taken (Figure 4.15).

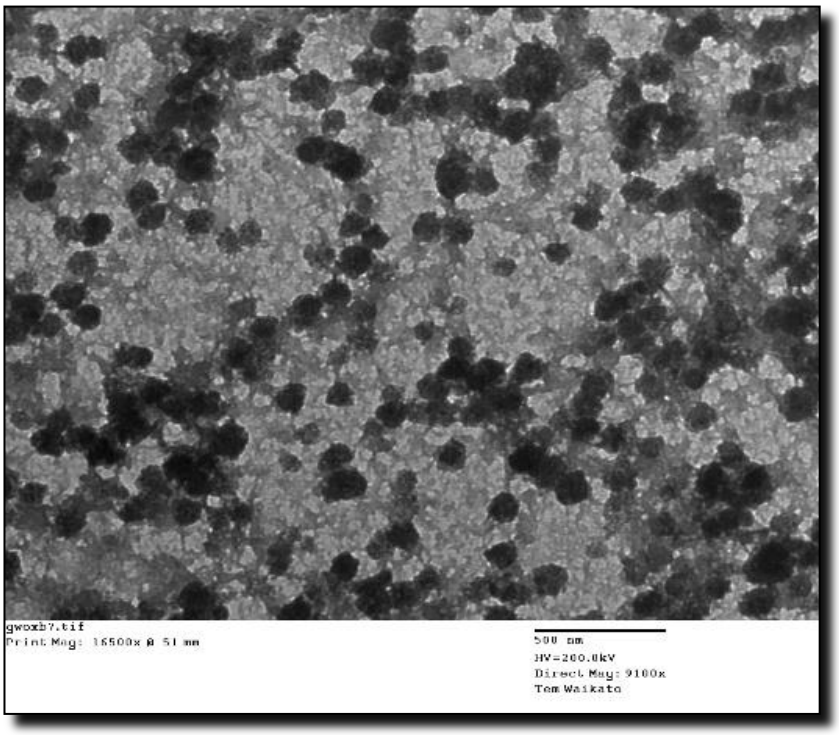

Figure 4.15 - TEM image of groundwater undergoing rapid oxidation

In strong contrast to the result for slow oxidation (Figure 4.10), the image shows a large aggregate of clustered dark iron particles dispersed through a mass of the smaller silica particles. The size of the aggregate is such that rapid settling can be anticipated.

4.4.7 Discussion of colloid formation mechanism

The most commonly used explanation for the stability of colloidal suspensions formed during slow oxidation is that under these conditions, the metal ions undergo hydrolysis to form sub units of hydrous oxide. In the presence of negatively charged silica particles or humic macromolecules, these particles have time to become coated with negatively charged silica or organic species resulting in their acquiring a net negative charge. This charge effectively stabilizes them against further aggregation. If the oxidation takes place rapidly, high concentrations of the primary hydrous oxide particles are formed in close

proximity and aggregate before their surfaces become coated with the negative particles. Thus flocs are formed and the oxidized metal settles.

4.5 Formation of trihalomethanes (THMs) during groundwater treatment

4.5.1 Formation of chloroform: post chemical treatment

The formation of chloroform or THMs during ground water treatment was studied with the addition of chemical oxidizing agent calcium hypochlorite. Estimated stoichiometric equivalents of 10 fold (126.0 mg/L) and 4 fold (54.3 mg/L) concentrations of calcium hypochlorite required to react with 20 mg/L of iron present in the groundwater was added to two water samples and the chloroform formation was monitored up to 5 hours using the SPME HS GC MS see Section 2.4.12. The results are given in Figure 4.16.

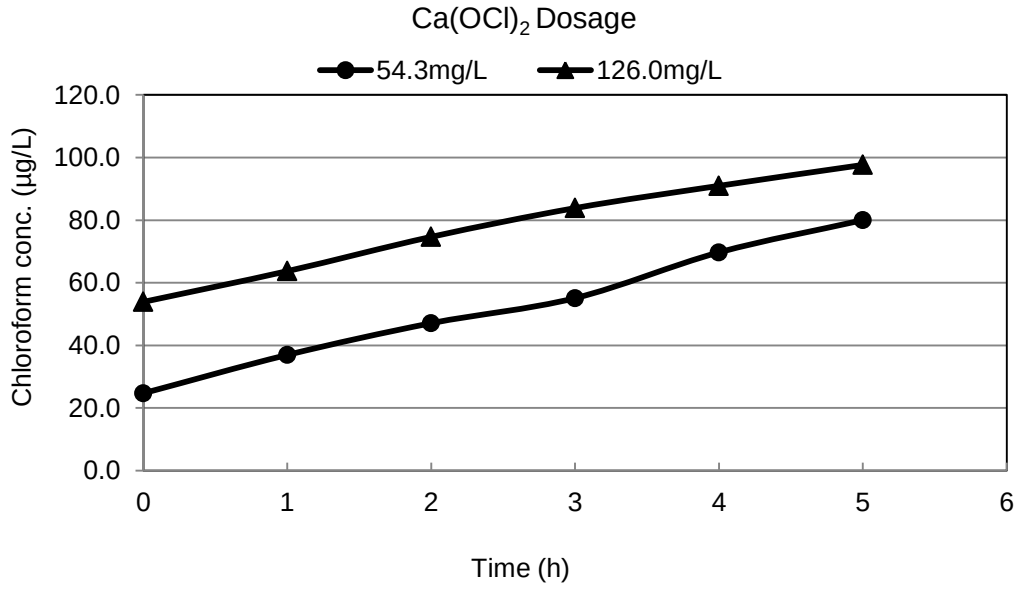

Figure 4.16 – Formation of chloroform in groundwater post chemical treatment (pH 7.0, temperature 18°C)

The dissolved organic matter (DOC) content in the groundwater samples was 130 mg/L. Higher concentration of hypochlorite showed a higher formation of chloroform (THMs). Most of the research on THM formation during water treatment processes gives similar results (El-Dib & Ali, 1995; Hsu, et al., 2000). The concentration of chloroform formed in water increased with time reflecting the prolonged lifetime of free chlorine in aqueous systems.

4.5.2 Formation of chloroform: Electrochemical vs. chemical oxidation

The formation of THMs during electrochemical and chemical oxidation of groundwater was compared by analysing the levels of chloroform in water after equivalent dosages of oxidizing agents applied to oxidise the iron and manganese. Firstly the groundwater sample was electrochemically oxidized (1.5 g/L [NaCl], 5.0 A, pH 6.5, temp. 18°C) where the free chlorine produced was determined and equivalent dosage of calcium hypochlorite was added to the second water sample. The chloroform (THM) formed during the two oxidation processes were analysed and given in Figure 4.17.

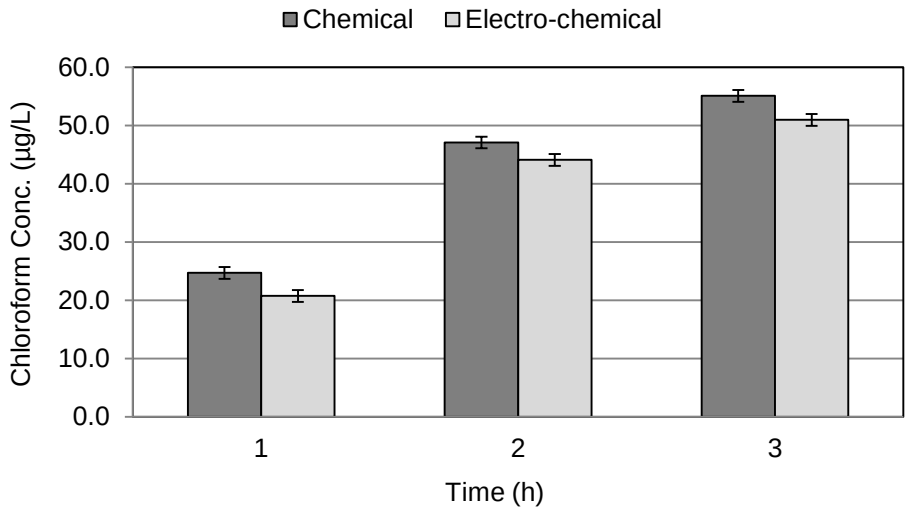

Figure 4.17 – Comparing chloroform formation in groundwater post chemical and electrochemical treatment (electrochemical treatment: 1.5 g/L [NaCl], 78.6 mA/cm^2,190 mL/min flow, rate single pass chemical treatment: 32.8 mg/L, pH 6.5 and temp. 18°C).

During chemical treatment pH was observed to fall from 6.8 to 6.2 whereas in electrochemical oxidation the pH rose from 6.8 to 8.0. The lower pH favours the concentration of molecular chlorine; the chlorinating agent and hence higher chloroform concentration were observed in the chemical oxidation.

4.5.3 Chloroform formation: single and multiple pass electrochemical treatment

The two electrochemical systems that completely removed iron from groundwater, a single pass with 3.0 g/L of NaCl and four passes with 250 mg/L NaCl in groundwater were re-produced to find out which system generated less THMs during metal ion removal. The results are given in Figure 4.18.

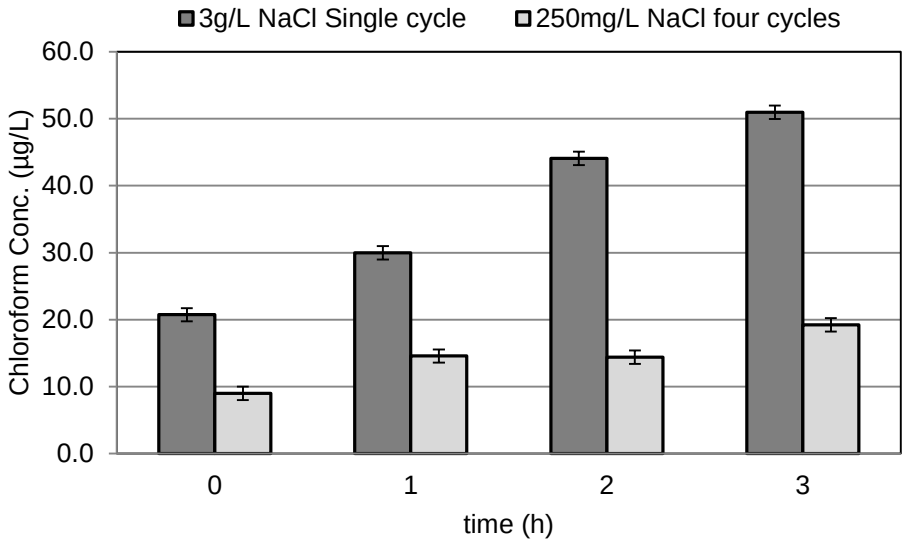

Figure 4.18 - Formation of chloroform in groundwater - post electrochemical oxidation, single pass treatment versus multiple pass treatment.

Figure 4.18 shows approximately 50% increase in chloroform formation post single pass treatment at the higher concentration compared to the multiple pass system at 250 mg/L. Groundwater treated for the purpose of human consumption would have chloride concentrations closer to this lower level and the multiple pass system would give low levels of THMs.

4.5.4 Formation of chloroform: retention of groundwater with and without sludge

Retention of the treated groundwater with and without ferric hydroxide sludge separation made a difference in the formation of chloroform (THMs) and the results are given in Figure 4.19. There was approximately 20% less chloroform (THMs) formed in the water samples where the settling metal ion sludge was removed. This difference was observed in both electrochemical and chemical treatment systems. When the sludge was removed from the water, a large fraction of the organic matter gets eliminated along with it. Typically the sludge is removed from drinking water supplies as part of clarification and filtration processes before it is stored.

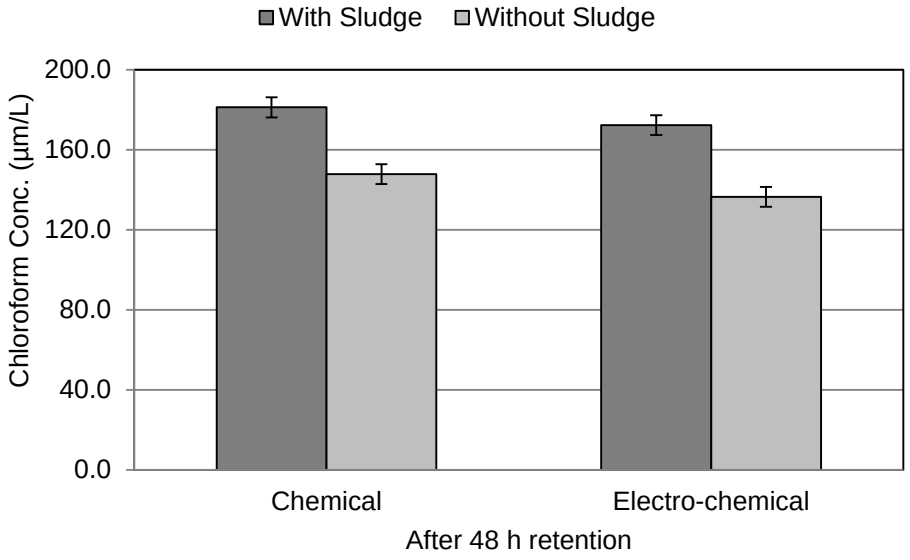

Figure 4.19 – The formation of chloroform in groundwater- post chemical and electrochemical treatment, 48 hours retention with and without the sludge.

4.6 Conclusions

- Groundwater naturally contaminated with iron and manganese, that also contains high concentrations of silica (typically 30 mg/L) and/or TOC (typically 100 mg/L) tend to be problem iron waters because the iron and

manganese form stable suspensions when oxidised by conventional slow air oxidation.

- However when oxidised rapidly using a strong oxidising agent such as chlorine derived from, for example hypochlorite, rapid aggregation and clarification can be achieved.
- It has been shown that the 240 micron gap PEFT cell produced sufficient chlorine from chloride levels as low as 250 mg/L to allow treatment to drinking water standards after four passes through the cell and power consumption was 18.4 kWh/m^3.
- While both chemical oxidation using calcium hypochlorite and electrochemical oxidation result in similar levels of THMs, these were well below the New Zealand drinking water guidelines.

Chapter 5: The PEFT cell as chlorine generator

5.1 Introduction

Applications of electrochemical techniques in water and wastewater treatment processes rely on mediated or indirect oxidation process. During the oxidation of metal ions in groundwater (Chapter 4) it was evident that chlorine based oxidants were the principal agents involved. Thus it was of interest to optimise chlorine production using the 240 micron gap PEFT cell.

5.1.1 Characterization of cell performance

Cell performance was characterized by calculating chlorine current efficiency and energy efficiency. The chlorine current efficiency was calculated using (Pletcher, 1984b):

$$CE = \frac{Q_P}{\Sigma Q} \times 100\% \qquad \textit{(Eq. 5.1)}$$

where CE = current efficiency,

Q_P = charge used forming the product,

Q_{total} = total charge consumed = I t, (where I is current and t is time)

The charge used forming the product was calculated using Faraday Equation (Bard & Faulkner, 2001):

$$Q = N\, n\, F \qquad \textit{(Eq. 5.2)}$$

where N = number of product moles formed in time t,

n = number of electrons transferred per mole,

F = Faraday constant.

Energy efficiency or energy consumption (EC) for chlorine production (specific electrical energy consumption) is the electrical energy in kilowatt hours (kWh) required to produce one kilogram of chlorine (Ghosh, Solanki, & Purkait, 2008) and was calculated using the equation:

$$PC = \frac{E\ I}{q\ c_{Cl_2} M_{Cl_2}} \qquad \textit{(Eq.5.3)}$$

where E = voltage

q = volumetric flow rate

c_{Cl_2} = concentration of chlorine produced

M_{Cl_2} = molecular weight of Cl_2

5.2 Experimental conditions for chlorine production using PEFT cell

The PEFT cell assembled with a stainless steel mesh cathode, perforated graphite anode and 240 µm nylon mesh inter-electrode gap was employed in this work (Figure 3.2 in Chapter 3). Details of the cell assembly and the materials are given in Section 2.1 in Chapter 2. The experimental arrangement is shown in Figure 2.2 in Chapter 2. The sodium chloride solution preparations and residual chlorine determination is given at Section 2.3.1 in Chapter 2.

The effects of electrolyte concentration, current density, flow rate and repeated cycling through the cell were investigated to determine optimum operating conditions and assess electrochemical efficiency of chlorine production in the PEFT relative to other chlorine generators. The range of chloride concentrations was extended to those present in natural waters in order to determine whether sufficient amounts of chlorine could be produced to allow the cell to function as an inline *in-situ* chlorinator without the addition of NaCl.

Volumetric flow rates up to 804 mL/min (effective flow velocity of 16 cm/min) were achieved using the peristaltic pump. Recycling the electrolyzed solution was used to increase effective chlorine concentrations at NaCl concentrations of 0.5 mol/L and 250 mg/L (optimum for chlorine generation and representative of environmental levels respectively).

5.3 Results and discussion

5.3.1 Effect of electrolyte concentration

The effect of electrolyte concentration on chlorine production, current efficiency and energy consumption at constant current is shown in Figure 5.1. The cell performed well as a chlorine generator. At a sodium chloride concentration of 0.5 mol/L (approximating the concentration used in commercial chlorine generators (Chlor Generators Ltd, 2004; Cumberland Electrochemical Limited, 2004) a current efficiency greater than the 60% considered effective in an industrial process (Pletcher, 1984b) and comparable to that achieved in purpose designed cells with anodes of titanium coated with precious metals (Khelifa, et al., 2004), was obtained.

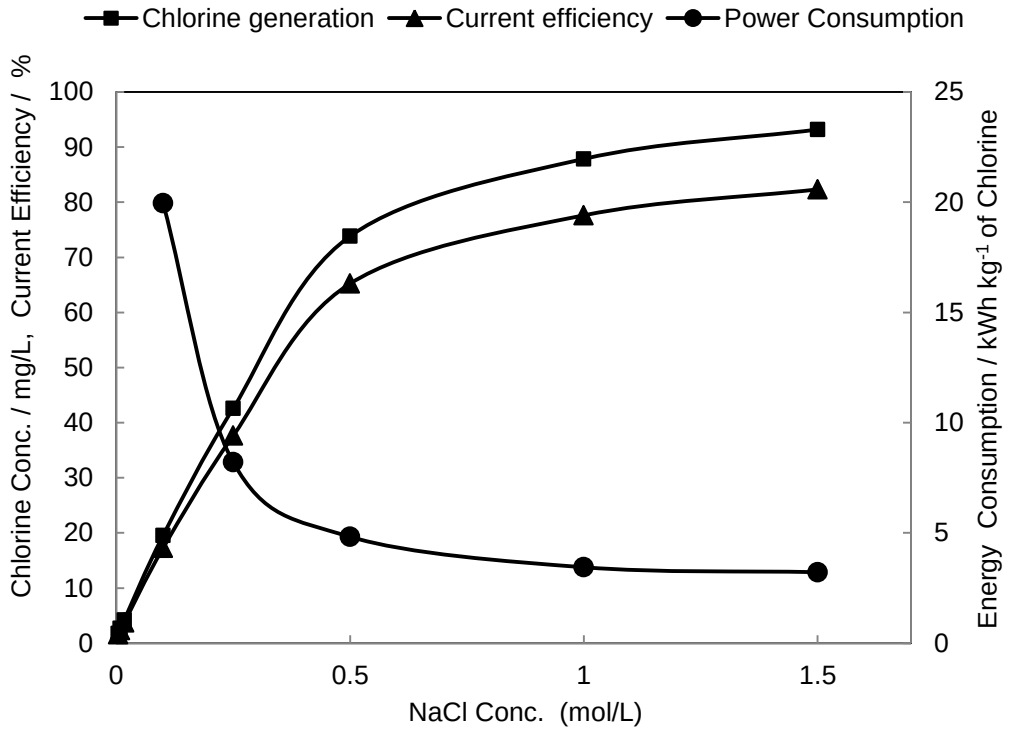

Figure 5.1 - Effect of NaCl concentration on chlorine production, current efficiency and energy consumption at a current density of 20 mA/cm^2 and a flow rate was 195 mL/ min in a single pass experiment.

The chlorine generation and current efficiency responses are linear at low concentration but flatten off at concentrations above, about 0.5 mol/L. This

behaviour is consistent with transport control at the lower concentrations and electrode kinetic control at the higher concentrations. While I did not investigate their presence, oxides of chlorine higher than hypochlorite, may also have been formed.

An advantage of the PEFT cell is that it allows operation with flow from cathode to anode reducing the possibility of cathodic reduction of hypochlorite according to equation 5-4 (Onofrio, et al., 2009).

$$OCl^- + H_2O + 2e^- \leftrightarrow Cl^- + 2HO^- \qquad \textit{(Eq. 5.4)}$$

Figure 5.1 also gives the energy consumption curve as a function of concentration. At the optimum concentration for chlorine production in the vicinity of 0.5 mol/L, bulk producers of active chlorine consume 4.8–5.5 kWh/kg of chlorine (Chlor Generators Ltd, 2004; Cumberland Electrochemical Limited, 2004). The energy consumption results obtained at 0.5 mol/L NaCl in the present work was 4.83 kWh/kg, indicating that the PEFT cell if scaled up is capable of cost effective commercial production of active chlorine.

5.3.2 Operation at low electrolyte concentrations

The initial linear response with NaCl concentration and the slopes of the current efficiency and chlorine production curves at concentrations below 0.5 mol/L indicate that useful chlorine production might be achieved at concentrations typical of drinking waters. The range of NaCl concentrations was thus extended down to 250 mg/L. Data for the concentration range from 0.5 to 0.004 mol/L (29 g/L to 250 mg/L) are included on Figure 5.2. Linearity is maintained down to the lowest concentration and the data appear to extrapolate through the origin. Even at the very lowest chloride concentrations used, finite chlorine production was observed. Furthermore the chlorine concentration increased linearly with voltage from approximately 2 mg/L at 11 V to 4 mg/L at 22 V.

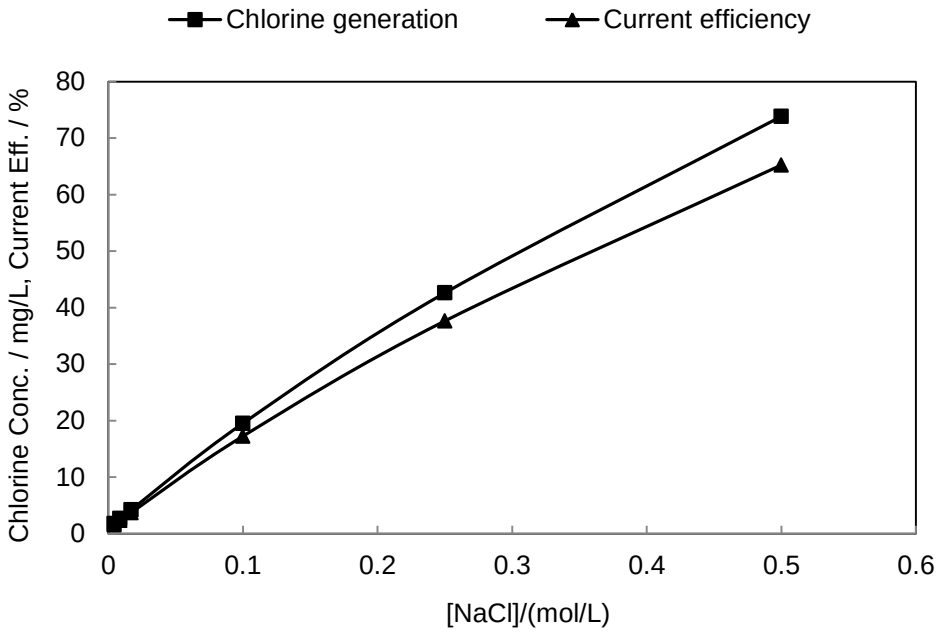

Figure 5.2 - Effect of low NaCl concentration on chlorine production and current efficiency at a current density of 20 mA/cm^2 and a flow rate was 195 mL/ min in a single pass experiment.

5.3.3 Effect of current density

Data for the effect of current density on production of chlorine at a flow rate of 195 mL/min and NaCl concentrations of 0.1 mol/L, 0.5 mol/L and 1.0 mol/L are summarized in Figure 5.3.

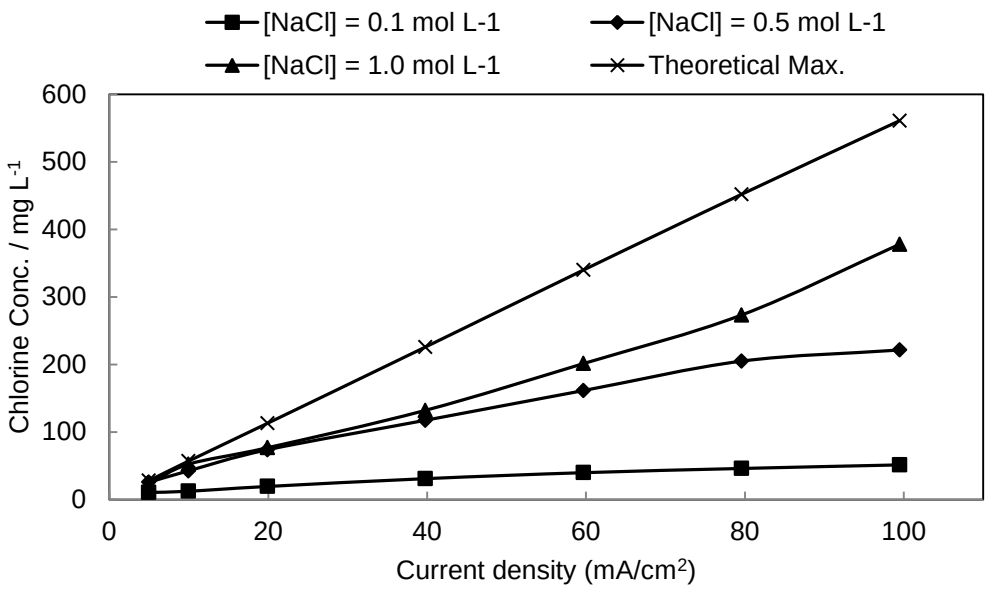

Figure 5.3 - Effect of current density and NaCl concentration on electro-generation of active chlorine at a flow rate 195 mL/min in a single pass experiment.

The curves for chlorine production indicate that, for current densities below 40 mA/cm^2, increasing NaCl concentration above 0.5 mol/L NaCl had little effect on chlorine production. However above 60 mA/cm^2, the chlorine production curves at 0.5 mol/L and 1.0 mol/L diverged, possibly indicating transport limitation at the lower concentration.

The change in energy consumption with current density at different concentrations is plotted in Figure 5.4. As expected energy consumption approached the theoretical minimum at the higher NaCl concentrations where cell resistance is low and hence energy loss through resistive heating was less. The data show that a satisfactory energy consumption of 5.5 kWh/kg of chlorine can be achieved at current densities of up to 20 and 35 mA/cm^2 for 0.5 and 1.0 mol/L respectively.

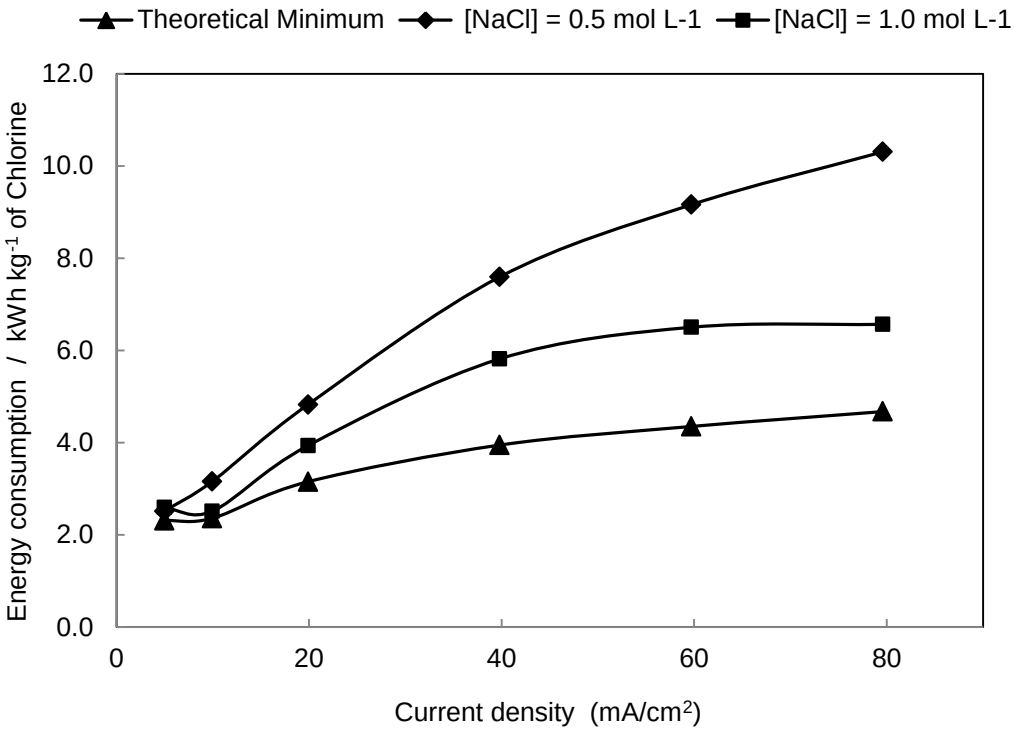

Figure 5.4 - The effect of current density on energy consumption at 0.5 and 1.0 mol/ L and a flow rate of 195 mL/ min in a single pass experiment.

5.3.4 Effect of flow rate

The effect of flow rate on chlorine generation is shown in Figure 5.5. The current density was maintained at 20 mA/cm^2 and the electrolyte concentration was 0.5 mol/L NaCl. As expected, active chlorine concentration decreases with increased flow rate due to dilution. Improvement in current efficiency could be due to the improved flushing of gas bubbles from the inter-electrode space at the higher flow rates or the thinning of the diffusion layer at the anode surface.

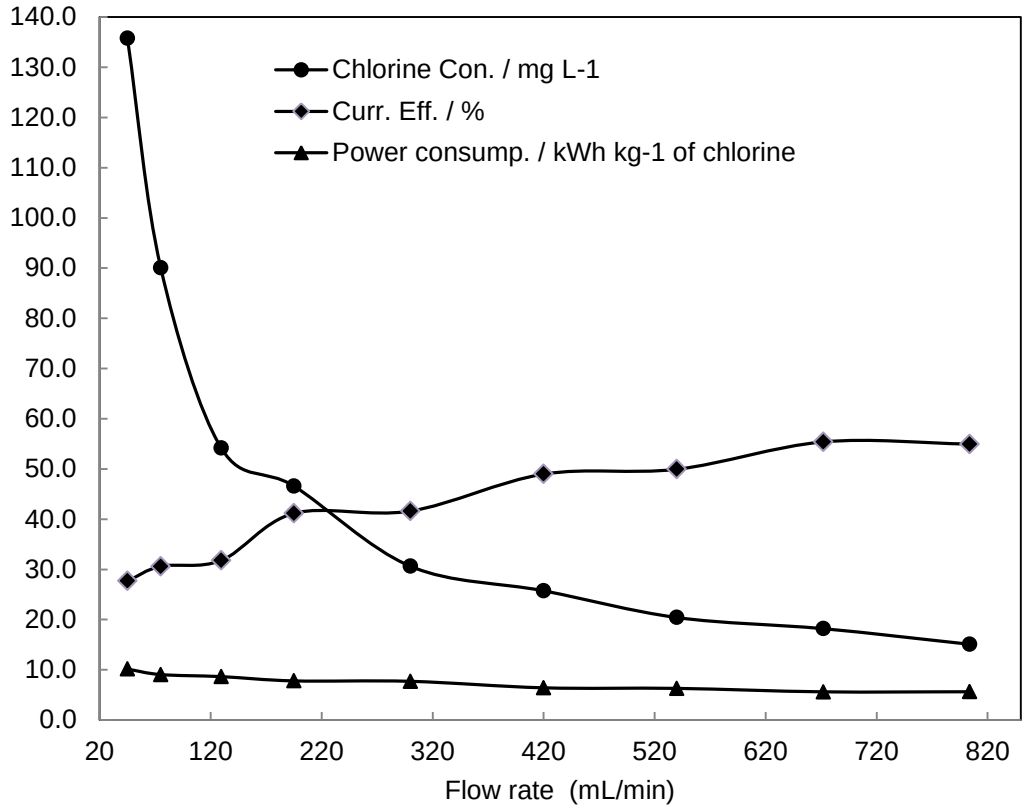

Figure 5.5 - The effect of flow rate on active chlorine generation at a current density of 20 mA/cm^2; an electrolyte concentration of 0.5 mol/L NaCl and with a single pass experiment.

5.3. 5 Effect of recycling the electrolyzed solution

Data for experiments in which the electrolyte was recycled through the cell a number of times are summarized in Figure 5.6 and indicate that the active chlorine concentration increases linearly with cycle number. For the 29.2 g/L (0.5 mol/L) NaCl solution, a constant increment in chlorine concentration was observed whereas for the 250 mg/L the increment for successive recycles was approximately half the chlorine concentration produced by the initial pass through the cell. This reduced chlorine increment was probably due to chlorine loss during the time taken to recycle the solution. The energy consumption for the 29.2 g/L concentration remained below 5.5 kWh/kg of chlorine but increased slightly with cycle number possibly resulting from gas build up at the electrodes.

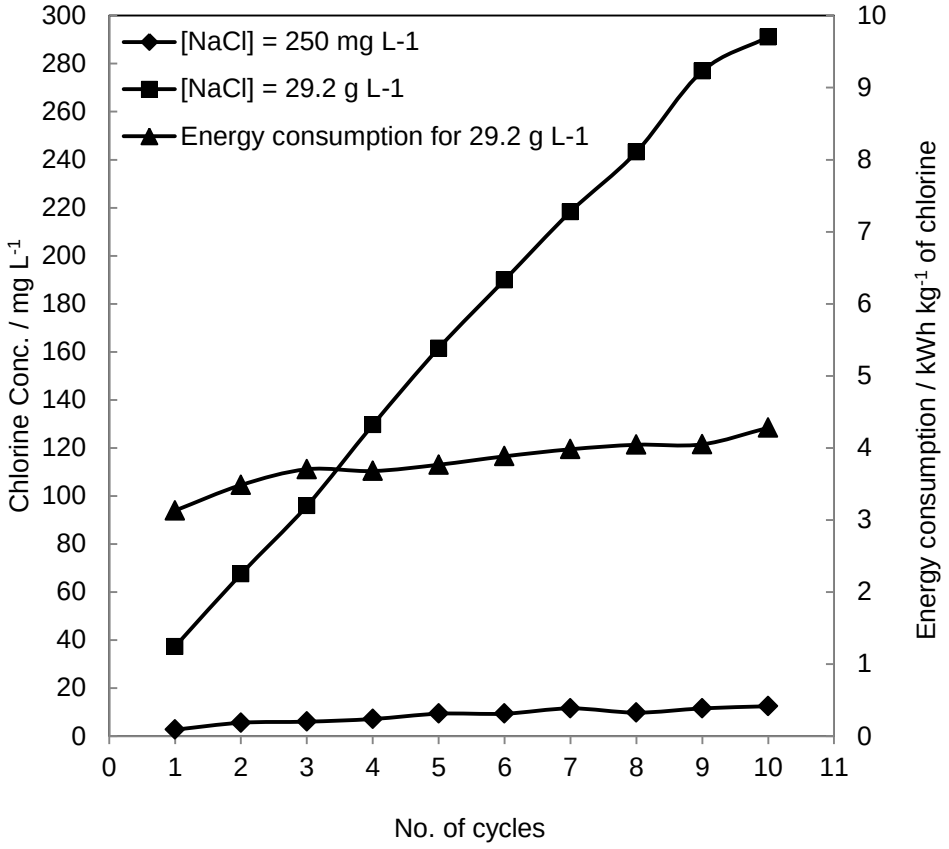

Figure 5.6 - The effect of electrolyte recycling on chlorine production at 29.2 g/L and 250 mg/ L NaCl, current density 10 mA/cm^2 and a flow rate 195 mL/ min.

5.3.6 Applications of the PEFT cell for electro-chlorination

One useful application of the PEFT cell could be the electro-chlorination of drinking water, particularly if developed as a portable device for water disinfection in times of emergency. A recent study of sodium hypochlorite (NaOCl) dosages required for disinfecting household water and for disaster response water treatment revealed that 1.875 mg/L NaOCl was 86.6% effective for samples with turbidity < 10 NTU and 3.75 mg/L NaOCl was 91.7% effective for unimproved sources with turbidity of 10–100 NTU. The free chlorine residual criteria of < 2.0 mg/L 1 hour after NaOCl addition and > 0.2 mg/L after 24 hours of storage have been recommended (Daniele, 2008). The active chlorine produced by the PEFT cell at a chloride concentration of 250 mg/L and a current density of

20 mA/cm^2 after one cycle was 4.88 mg/L, significantly higher than results reported for other electro-chlorinators at similar current densities (Kerwick, et al., 2005; Khelifa, et al., 2004; Martinez-Huitle & Brillas, 2008) and sufficient to provide effective disinfection. Furthermore, control of current density provides a means of ensuring that drinking water standards are not exceeded (USEPA 1980, recommend a chloride limit of 250 mg/L and WHO drinking water standards specify a maximum permissible limit of 600 mg/L (Roscoe, 1990). Sufficient chlorine concentrations to effect disinfection of natural waters containing chloride concentrations 250 mg/L and above can be achieved using the PEFT cell electro-chlorinator, without addition of salt, by a single pass of the water through the cell operating at 11 volts. The possibility of a portable device operated by a 12 volt battery is indicated.

5.3.7 Application of the PEFT cell for electro-generation of chlorine

It is possible that the PEFT cell could be applied to the commercial production of hypochlorite solutions. Energy efficiencies obtained at the bench scale demonstrate that this would be economically feasible. Issues relating to the durability, scaling and clogging of the perforated electrodes under prolonged operating conditions would need to be investigated. Acid cleaning may necessitate the use of more durable materials such as DSAs, currently used commercially. Such electrodes are not incompatible with the PEFT system and could offer the advantage of even further improved efficiencies.

5.4 Conclusions

- The optimum conditions for chlorine production using the PEFT cell were NaCl concentration above 0.5 mol/L, current densities below 20 mA/cm^2 and high flow rates consistent with producing adequate concentration for the intended application.

- Adequate current efficiencies for chlorine production have been demonstrated at sodium chloride concentrations lower than previously possible using graphite and stainless steel electrodes.
- When operated with 0.5 mol/L NaCl, commercially viable current efficiencies for chlorine production were achieved. When operated using water with 250 mg/L chloride (in natural water range), sufficient chlorine to effect disinfection was achieved at less than 12 volts.
- The active chlorine concentration generated by the cell can be increased by increasing current density with only modest decrease in current efficiency.
- Current efficiency increased with flow rates.
- The chlorine concentrations produced can be raised by recycling.

Chapter 6: Electrochemical degradation of textile dyes

6.1 Introduction

The efficient production of chlorine by the PEFT cell (Chapter 5) offered the possibility of more efficient chlorine mediated electro-oxidative decolourisation and degradation of organic dyes in textile effluents. The literature gives enough evidence that aqueous dyestuff solutions can be completely removed by indirect electro-oxidation with strong oxidants generated during electrolysis. Electrochemically produced active chlorine and other short lived oxidizing species break down the chromophores of the organic dye molecules and further oxidise them to complete mineralisation. The major drawback of electrochemical treatment of textile effluents has been the higher energy consumption. The fact that the PEFT cell can produce chlorine at much reduced energy consumption makes the commercial possibility of electro decolourisation more achievable. In this chapter experiments to determine the colour and TOC removal performance of the PEFT cell under realistic conditions of electrolyte (NaCl and other) concentration and pH likely to be found in dye effluents from the cotton industry will be described.

The PEFT cell provides the indirect electro-oxidation as the main decolourisation mechanism some electro-reduction (at the cathode) and direct oxidation may also be involved. The strongly oxidizing active chlorine species are generated at the anode by the initial oxidation of chloride ions. During indirect electro-oxidation process the concentration of the electro-generated oxidizing species would be depending on the type of electrolyte and its concentration in solution. Earlier work by Cameselle et al. 2005 and Dogan and Turkdemir 2005, confirms that electrolyte NaCl had been highly effective in decolourisation of indigo dye from effluents. The graphite anode used in the PEFT cell is not known to be efficient in causing direct oxidation of organic compounds (Martınez-Huitle & Brillas, 2009). Therefore the colour and TOC removal will be largely dependent on the active chlorine species generated by the oxidation of chloride ions in water

6.1.1 Textile dyestuffs

The global production of dyestuffs is over 7 million tons per annum (Martınez-Huitle & Brillas, 2009) and a large fraction of this is used in the textile industry. There are different types of dyes such as Vat dyes, reactive dye, disperse dye, sulphur dye etc. used in textile processing according to the type of fabric and finish required. Dye molecules have a chromophore group which gives the colour and a reactive group which binds it to the fabric. Dyes are generally classified by the chromophore group (Martınez-Huitle & Brillas, 2009). The two common textile dyestuffs, indigo carmine (IC) and reactive blue 2 (RB2) will be used in this work to investigate the electrochemical oxidation capabilities of the PEFT cell.

Indigo Carmine (IC) Dye is one of the initial forms of naturally derived organic dyestuff (Vat dye). It is used in dyeing cotton fabrics, especially in the denim (blue jeans) production; generally know as the denim dye. As global denim production has increased, synthetic indigo dye production has also increased and is now estimated to be 22,000 tons per annum (Dogan & Turkdemir, 2005). The solubility of the indigo dye is relatively low < 2 mg/L; therefore it is reacted with sulphuric acid to form the readily soluble indigo carmine dye, see Figure 6.1.

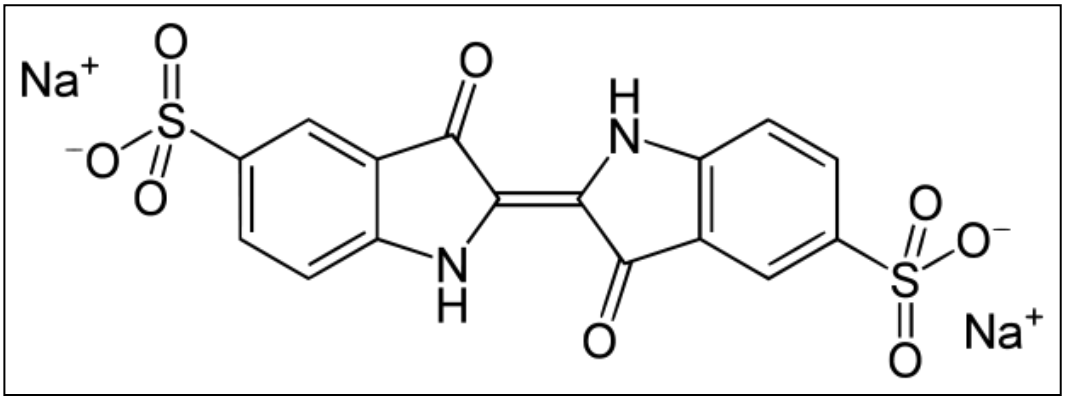

Figure 6.1- Chemical structure of Indigo Carmine dye.

Reactive blue 2 (RB2) dye is an anthraquinone based reactive dye (see Figure 6.2) mostly used with cellulosic fabrics. A nucleophilic displacement of the halide group at the hydroxyl group on cellulose forms a covalent bond which fixes the

dye molecule to the fibre (Carneiro, Fugivara, Nogueira, Boralle, & Zanoni, 2003). During alkaline textile processing, hydrolysis of the dye molecules takes place as a side reaction leading to dye inactivation. After the dyeing cycle the fabric is washed a number of times to remove the unfixed dye and hydrolysed dyes which enter the effluent stream. The reactive dye concentrations in wastewaters are relatively high due its low fixation, especially to cotton and viscose fibres. In addition textile dyeing processes use very large amounts of salts, specifically chlorides and sulphates, since dyeing of cotton fabric with reactive dyes requires 5-80 g/L of salts in dye solutions (FaridaYunus, Zheng, Nanayakkara, & Chen, 2009). Reactive dyes account for approximately 12% of the global dye production (Riera-Torres & Gutiérrez, 2010). Reactive blue 2, one of the commonly used dyes in cotton textile processing, will be used in studies of the electrochemical degradation of reactive dyes by the PEFT cell

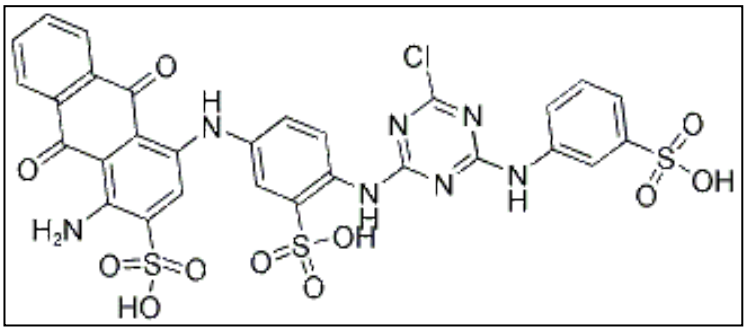

Figure 6.2 - Chemical structure of Reactive Blue 2 dye.

6.2 Materials and methods

6.2.1 Chemicals and electrode material

The two dyestuffs indigo carmine (disodium salt) and Reactive blue 2 were obtained from May & Baker Ltd, Dagenham, England and Sigma Aldrich Chemicals respectively. Sodium chloride (BDH analar grade), sodium sulphate (BDH analar grade), sodium bicarbonate (BDH analar grade), sodium hydroxide (BDH analar grade) and diluted sulphuric acid (Merck) were used in synthetic effluent preparation with deionized water (conductivity < 2.0 µS/cm) from Millipore Milli-Q system. The perforated (1.0 mm holes with 6 holes/cm^2 hole

density hexagonally arranged, staggered hole configuration) stainless steel cathode and a graphite anode was used in the PEFT cell with a 50 µm inter-electrode gap using cello tape material 3M Scotch^{TM} tape 375, USA (see Figure 3.3 in Section 3.1.4). The electrolytic cell components, assembly of components and experimental set up was the same as explained in Section 2.2.

6.2.2 Details of dye solution preparation and cell operation

The synthetic dye samples were prepared by dissolving 100 mg/L of dyestuff (except when higher concentrations tested) in the water and salts were added according to the experimental conditions and finally pH was adjusted to 7 using sodium bicarbonate (0.1mol/L) solution. During the pH variation experiment, pH 10 and 3 were maintained by 0.1 mol/L NaOH solution and a diluted sulphuric acid solution respectively. Current densities were gradually reduced by dropping the current through the cell to determine the optimum current density for the treatment. Sodium sulphate was used as the alternative electrolyte to compare the dye degradation efficiency without sodium chloride. Effect of flow rate was studied by keeping all the other physiochemical parameters constant and varying the flow rate by adjustment of the peristaltic pump. The possibility of treating higher dye concentrations was tested by dissolving 50, 100, 200, 300 mg/L of dyestuff in to the water sample. A 250 mL of the synthetic dye effluent was passed one or more times through the PEFT cell. After each cycle a small aliquot of the treated effluent was drawn out to 10 mL falcon tubes for colour and TOC analysis (see Section 2.3.10 and 2.3.11). Flow rate was maintained at 190 mL/min and the flow direction through the cell was from cathode to anode at all times.

6.2.3 Analysis of colour and TOC

The experimental details of colour and TOC analysis are given in Section 2.3.10 and 2.3.11and the spectrums of the dyes and calibration curves are given in Appendix D.

6.3 Results

6.3.1 The effect of NaCl concentration on colour and TOC removal

The effects of increasing NaCl concentration on the Indigo carmine dye colour removal and TOC removal with the number of cycles through the PEFT cell are summarised in Figures 6.3 and 6.4.

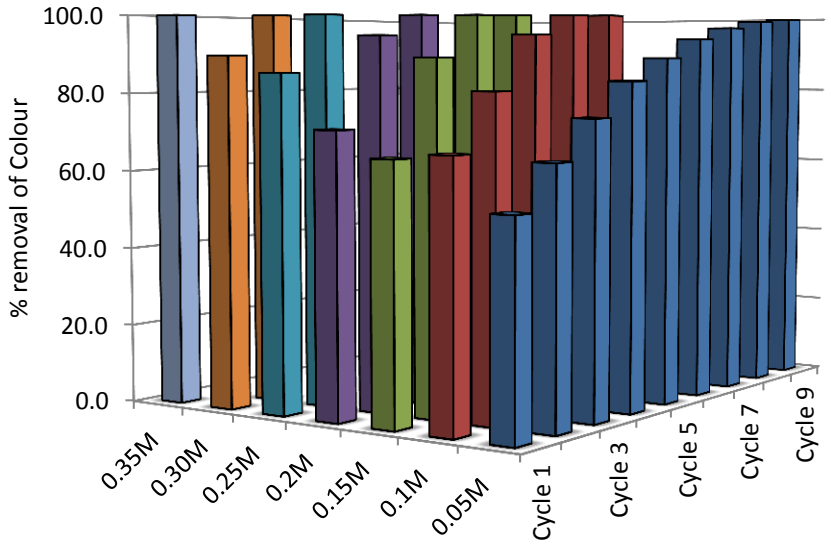

Figure 6.3 - The effect of increasing NaCl concentrations on IC dye colour removal with number of cycles through the PEFT cell (flow rate 190 mL/min, pH 7, current density 80 mA/cm^2, temperature 20°C and IC dye concentration 100 mg/L).

Maximum removal of both dye and TOC was achieved under the conditions favouring maximum chlorine production (i.e. maximum chloride ion concentration at the current density used). Removal of colour was 100% after a single cycle through the cell at 0.35 mol/L of NaCl simultaneously removing 85% of the TOC in the synthetic dye solution.

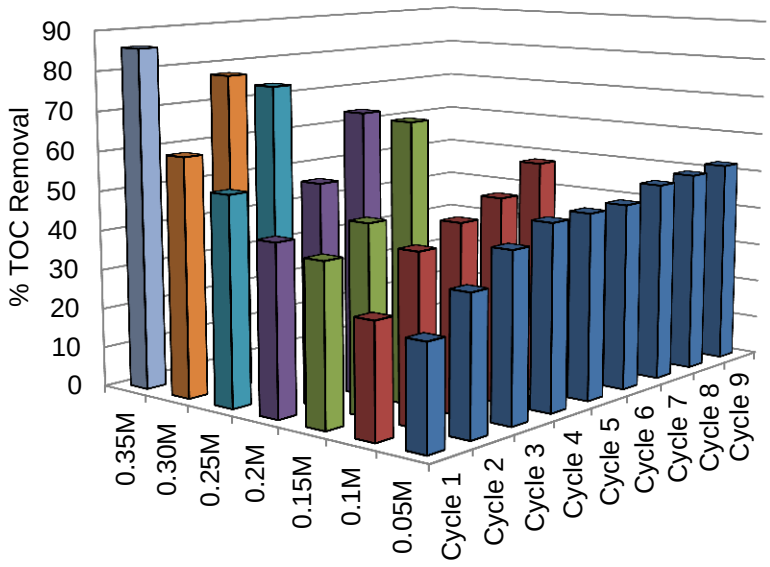

Figure 6.4 - The effect of increasing NaCl concentrations on the TOC removal with number of cycles through the PEFT cell (flow rate 190 mL/min, pH 7, current density 80 mA/cm^2, temperature 20°C and IC dye concentration 100 mg/L).

The energy consumption at each NaCl concentration used is given in Figure 6.5. Energy consumption shows an approximate inverse relationship with the NaCl concentration consistent with resistance reduction.

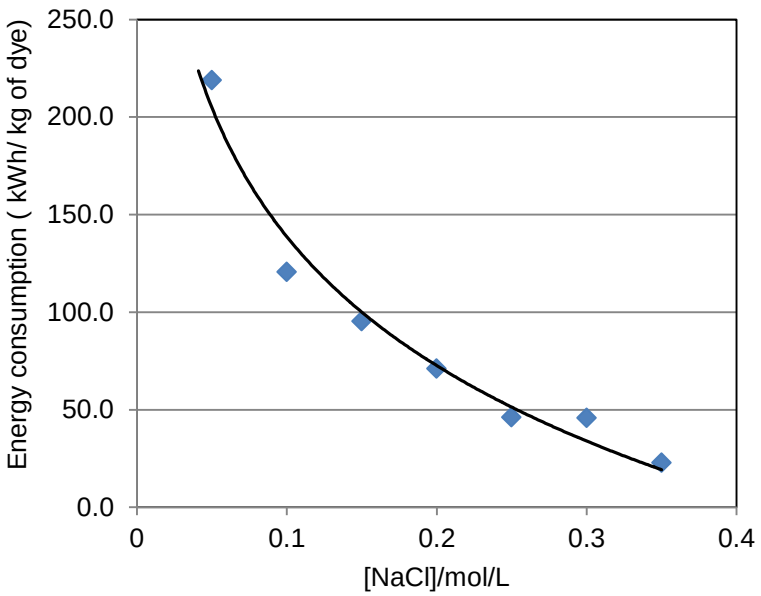

Figure 6.5 - The effect of increasing NaCl concentrations on energy consumption (flow rate 190 mL/min, pH 7, current density 80 mA/cm^2, temperature 20°C and IC dye concentration 100 mg/L).

The effect of the increasing NaCl concentration on colour and TOC removal of the reactive blue 2 (RB2) dye stuff was studied up to NaCl concentrations of 0.1mol/L. At NaCl concentrations higher than 0.1mol/L, in the absence of dispersing agents, the dye stuff aggregates. The results of percentage colour removal are given in Figure 6.5. The colour removal efficiencies with the RB2 dye stuff achieved almost 98% at 0.1mol/L NaCl concentration with 3 cycles through the cell.

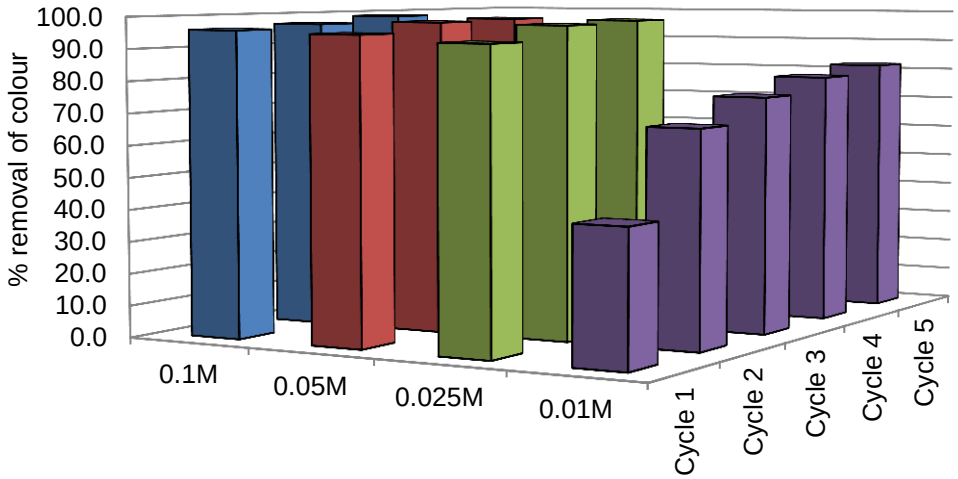

Figure 6.6 - The effect of increasing NaCl concentrations on the colour removal with number of cycles through the PEFT cell (flow rate 190 mL/min, pH 7.0, current density 80 mA/cm^2, temperature 20°C and RB2 dye concentration 100 mg/L).

In Figure 6.7 the percentage removal of TOC after three cycles through the cell with increasing electrolyte concentrations are plotted for the RB2 dye. Best results are again at the highest (0.1 mol/L) NaCl concentration, where approximately 60% of TOC removal with three cycles through the cell was achieved.

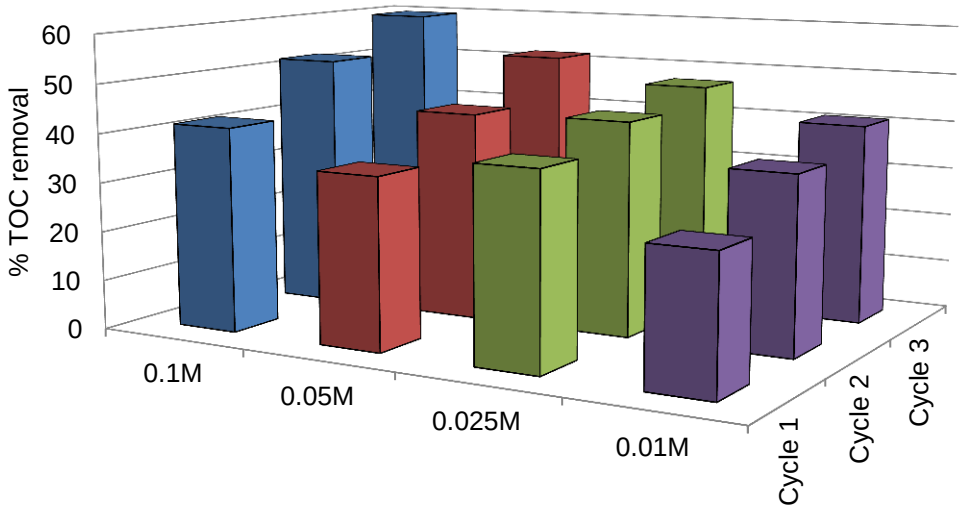

Figure 6.7 - The effect of increasing NaCl concentrations on the TOC removal with number of cycles through the PEFT cell (flow rate 190 mL/min, pH 7.0, current density 80 mA/cm^2, temperature 20°C and RB2 dye conc. 100 mg/L)

6.3.2 Effect of pH on colour and TOC removal

The efficiency of colour removal of IC dye from water was studied at three different pH values 3.0, 7.0 and 10.0 and the results are summarised in Figure 6.8. The colour removal was very effective at the lowest pH 3, 100% being achieved after two cycles at an energy consumption of 46.5 kWh/kg of dye. At pH 7, four cycles were required and the energy consumption increased to 96.5 kWh/kg of dye.

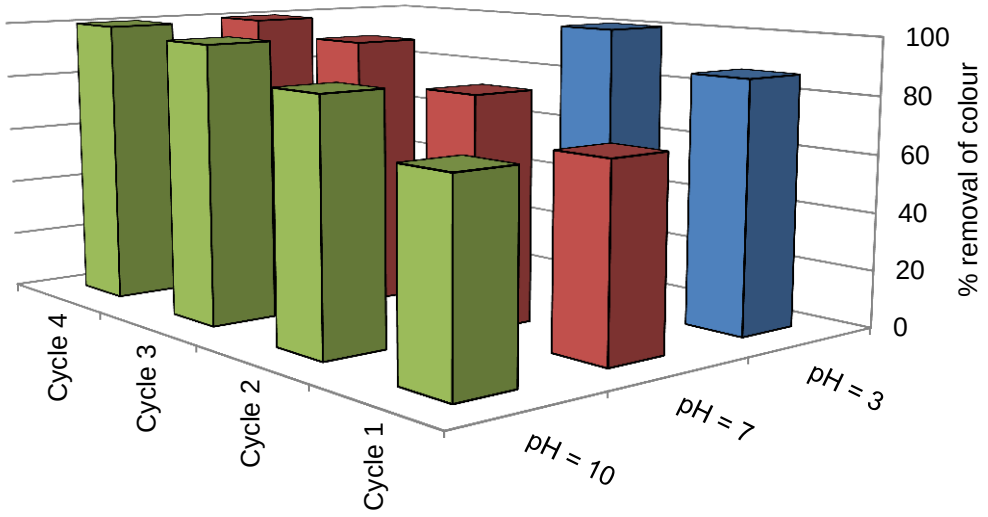

Figure 6.8 - The effect of pH on the IC dye colour removal with number of cycles through the PEFT cell (flow rate 190 mL/min, current density 80 mA/cm^2, temperature 20°C, NaCl concentration 0.1mol/L and IC dye concentration 100 mg/L)

The TOC removal from the IC dye wastewater follows the same pattern as colour removal at the three pH values and results given in Figure 6.9. At the lower pH 3, the TOC removal was significantly above 70% after two cycles through the cell.

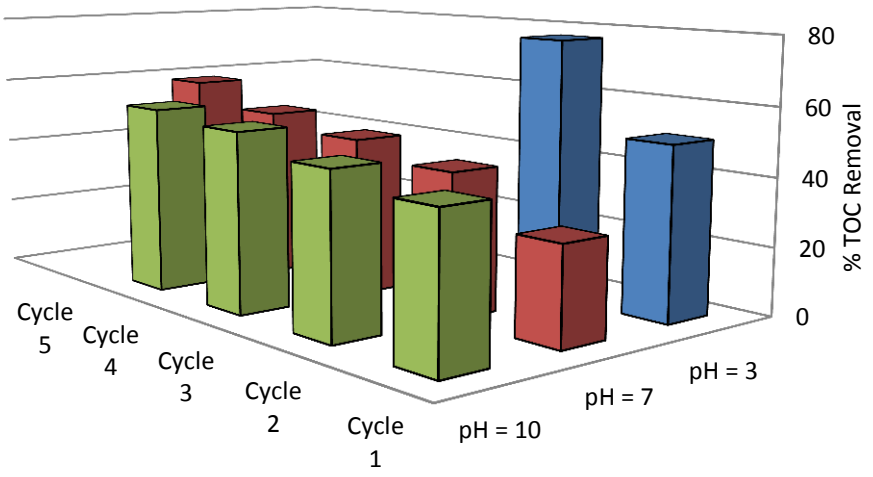

Figure 6.9 - The effect of pH on the TOC removal with number of cycles through the PEFT cell (flow rate 190 mL/min, current density 80 mA/cm^2, temperature 20°C, NaCl concentration 0.1mol/L and IC dye concentration 100 mg/L).

The colour removal efficiencies for RB2 dye at pH values 3, 7 and 10 are given in Figure 6.10. The response to pH variation by the RB2 was similar to IC, better removal efficiencies being achieved at lower pH values.

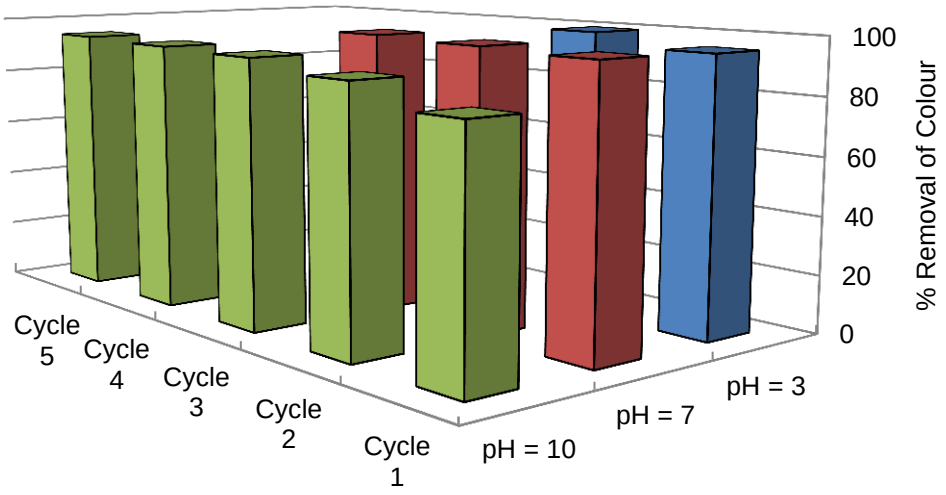

Figure 6.10 - The effect of pH on the colour removal with number of cycles through the PEFT cell (flow rate 190 mL/min, current density 80 mA/cm^2, temperature 20°C, NaCl concentration 0.1 mol/L and RB 2 dye concentration 100 mg/L)

The TOC removal of RB 2 dye at pH values 3, 7 and 10are given in Figure 6.11. The TOC removal follows the colour removal pattern.

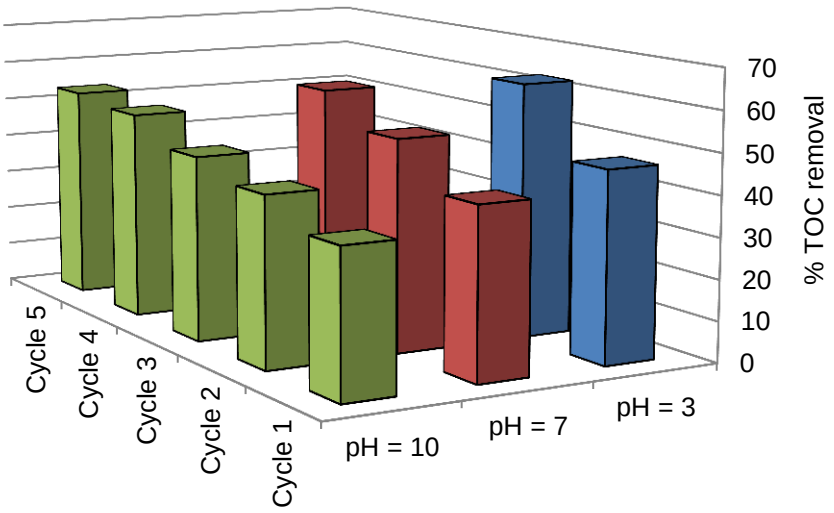

Figure 6.11 - The effect of pH on the TOC removal with number of cycles through the PEFT cell (flow rate 190 mL/min, current density 80 mA/cm^2, temperature 20°C, NaCl concentration 0.1 mol/L and RB2 dye concentration 100 mg/L)

6.3.3 The effect of current density on colour and TOC removal

In order to determine the optimum current density for minimum energy consumption, colour removal was studied as a function of current density. Results are given in Figure 6.12. The results indicate that 100% colour and 55% TOC was removed at 30 mA/cm^2 current density consuming 0.8 kWh/m^3 (8.29 kWh/kg of dye). Above 40% TOC removal, the TOC removal efficiency decreased but continued approximately linearly with current density up to 80% at the maximum current density 80 mA/cm^2 used in the experiment.

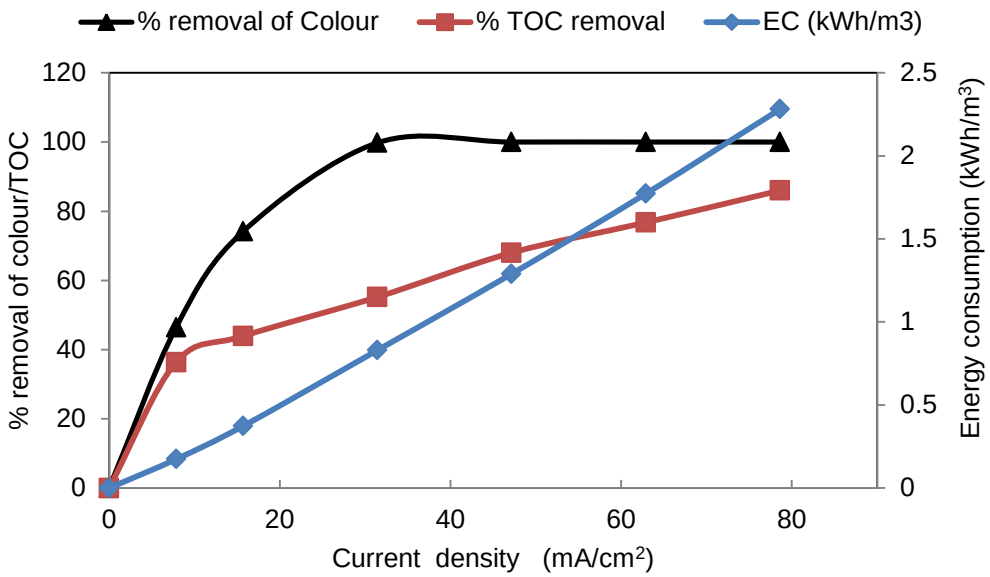

Figure 6.12 - The effect of current density on the colour and TOC removal and energy consumption with a single pass through the PEFT cell (flow rate 190 mL/min, pH 6.0, temperature 20°C, NaCl concentration 0.35 mol/L and IC dye concentration 100 mg/L)

Looking at the electrochemical reactions taking place to remove the colour from the effluents, it is the number of electrons required per volume or the number of coulombs of charge required per litre. The Figure 6.13 is showing the number of coulombs per litre required to remove the colour from the IC dye effluent. The optimum value was 631.7 C/L, at 30 mA/cm^2, where 100% colour removal was achieved.

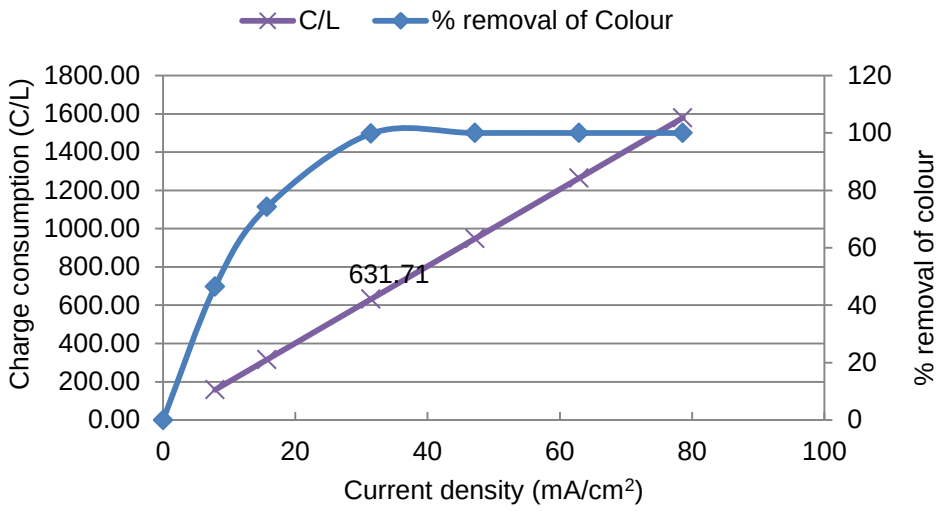

Figure 6.13 - The effect of current density on the colour removal and charge consumption with a single pass through the PEFT cell (flow rate 190 mL/min, pH 6.0, temperature 20°C, NaCl Concentration 0.35 mol/L and IC dye concentration 100 mg/L)

Colour removal and energy consumption for the RB2 dye are given in Figure 6.14. Results show that only 90% colour removal was achieved at an energy consumption of 1.25 kWh/m^3 which is consistent with industrial experience and literature reports (Martınez-Huitle & Brillas, 2009) that note reactive dye colour removal is more difficult and complicated than indigo dye.

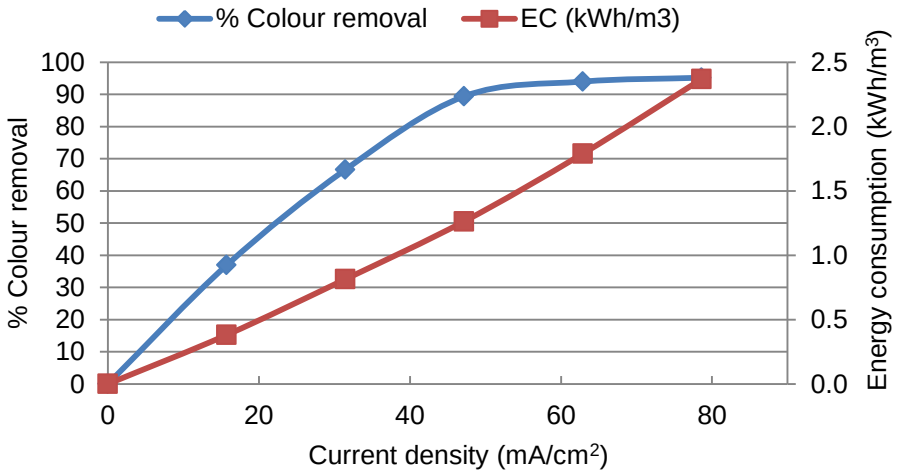

Figure 6.14 - The effect of current density on the colour removal and energy consumption with a single pass through the PEFT cell (flow rate 190 mL/min, pH 6.0, temperature 20°C, NaCl concentration 0.1 mol/L and RB2 dye concentration 100 mg/L).

6.3.4 Effect of electrolyte anion on colour and TOC removal

In indirect electro-oxidation processes, the oxidants generated depend on the dominant anions present. In the results reported to date the dominant electrolyte has been NaCl and the indirect oxidation species were active chlorine species. To investigate the possibility of non chlorine oxidation, a chloride free solution of $Na_2SO_4$was used. The results comparing colour and TOC removal from the chloride and sulphate containing solutions at similar concentration in IC dye wastewater are shown in Figure 6.15. The colour and TOC removal in the presence of chloride were greater than in the presence of sulphate. In the case of chloride the colour removal was greater than TOC removal whereas in the sulphate system TOC removal was greater than colour removal. This result is consistent with the greater tendency of chlorine to add across double bonds thus disrupting the conjugated systems of the chromophores.

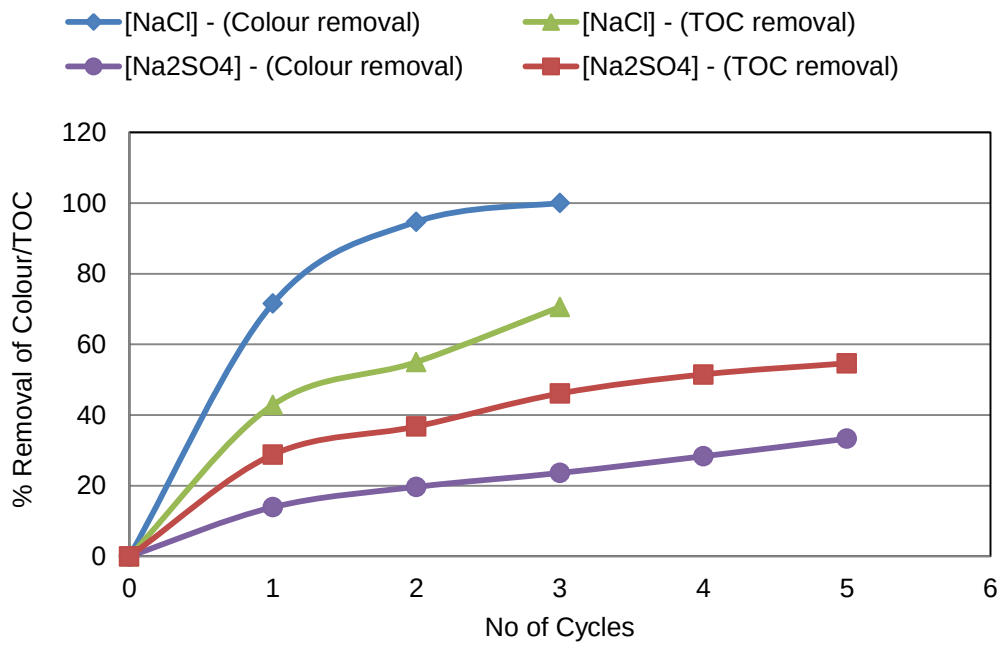

Figure 6.15 - The effect of electrolyte on the colour and TOC removal (flow rate 190 mL/min, current density 80 mA/cm^2, pH 6.0, temperature 20°C, NaCl and Na_2SO_4 concentration 0.20 mol/L and IC dye concentration 100 mg/L).

A similar experiment was carried out for RB2 dye at electrolyte concentration of 0.1 mol/L NaCl and Na_2SO_4. The results obtained were similar to the results for the IC dye and are given in Figure 6.16. Again, better colour and TOC removals were obtained for the chloride system.

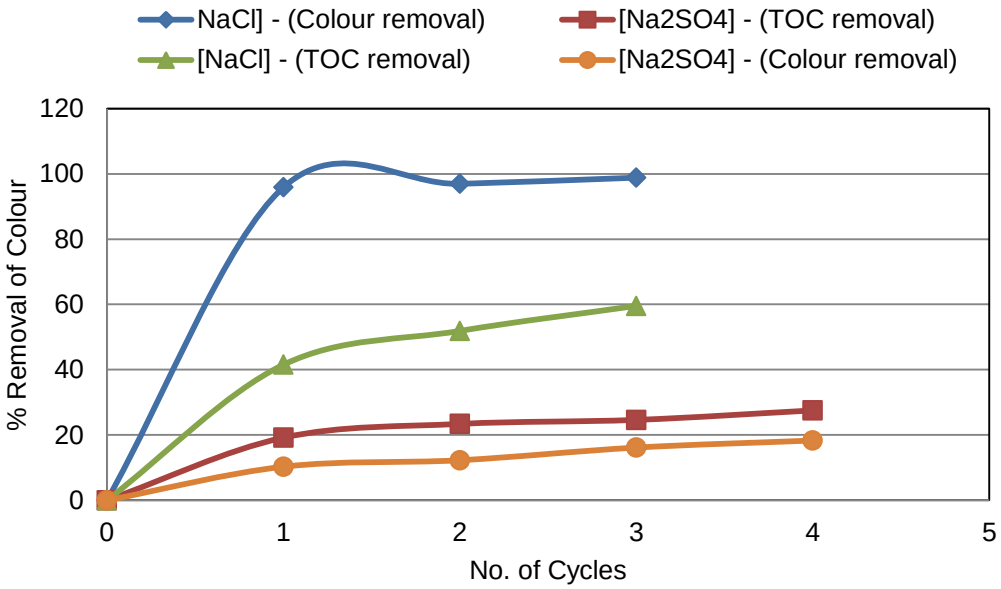

Figure 6.16 - The effect of electrolyte on the colour and TOC removal (flow rate 190 mL/min, current density 80 mA/cm^2, pH 6.0, temperature 20°C, NaCl and Na_2SO_4 concentration 0.20 mol/L and RB2 dye concentration 100 mg/L)

6.3.5 Effect of flow rate on colour and TOC removal

Varying current at constant flow rate is equivalent to varying flow rate at constant current in terms of determining the minimum amount of charge per unit volume required for colour and TOC removal. It was of interest to confirm that if the current density was fixed and less than optimum colour removal was observed, optimum colour removal could be achieved by reducing the flow.

The effect of flow rate for the colour and TOC removal for IC dye is given in Figure 6.17. For colour removal at high flow rates less than 100% removal was achieved. As the flow was decreased colour removal increased and approached 100% removal at a flow rate of 17L/h. At this flow rate the charge consumption per unit volume was 620 C/L which is very similar to the charge consumption

calculated for the experiment described in Section 6.3.3 in which current density was varied at constant flow rate (631.7 C/L). A similar trend was observed for the TOC data except that percentage removals were about 15% less at each flow rate and even at four litres per hour TOC removal was incomplete.

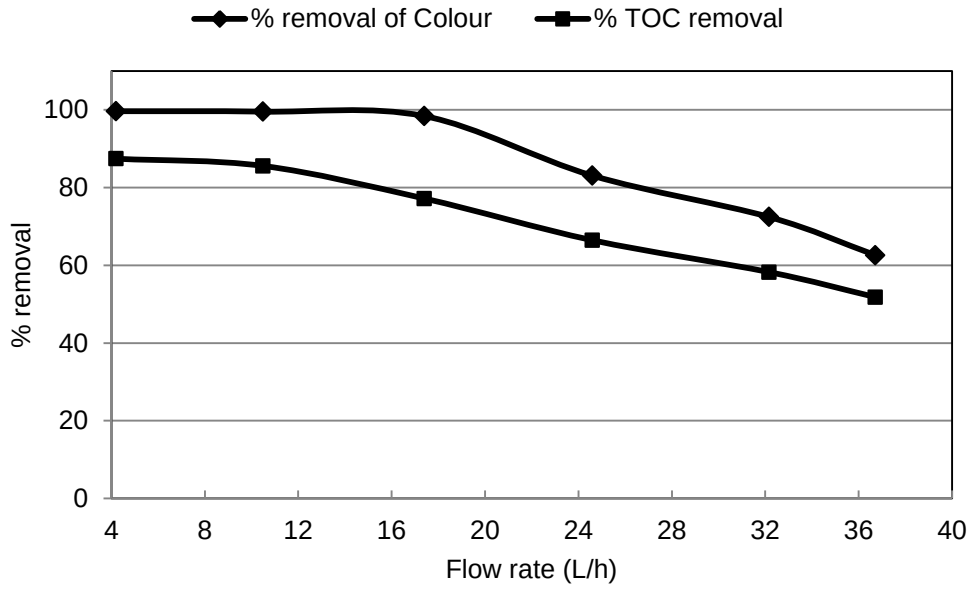

Figure 6.17 - The effect of flow rate on the colour and TOC removal (single pass, pH 6.0, current density 47 mA/cm^2, temperature 20°C, NaCl concentration 0.35 mol/L and IC dye concentration 100 mg/L)

The specific charge consumption, coulombs of charge required to remove a unit mass of contaminant (dye or TOC) with the increasing flow rates are given in Figure 6.18. The optimum specific charge consumption 6800 C/g of IC dye removal (98%) was achieved at 17L/h flow rate and had 15000 C/g of TOC removed (77%) at the same flow rate.

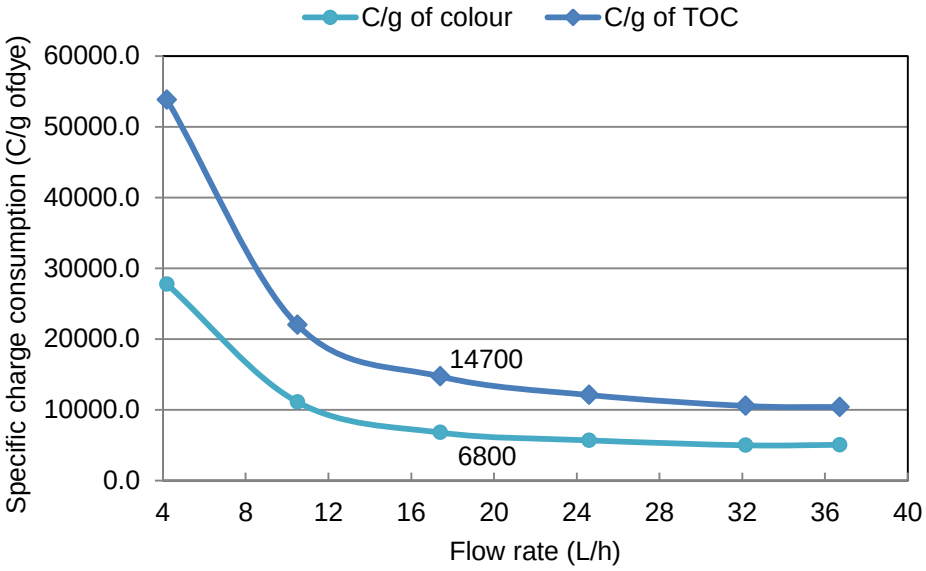

Figure 6.18 – Specific charge consumption with increasing flow rate (single pass, pH 6.0, current density 47 mA/cm^2, temperature 20°C, NaCl concentration 0.35 mol/L and IC dye concentration 100 mg/L)

The effect of flow rate on colour and TOC removal for the RB2 dye is given in Figure 6.19, which shows 100% colour removal for flow rates less than 17 L/h at current density of 80 mA/cm^2 corresponding to a charge consumption of 1030 C/L and a specific charge consumption of 1.05×10^4 C/g of RB2 dye. Again TOC removal was less efficient and required 5.8×10^4 C/g of TOC at the same flow rate.

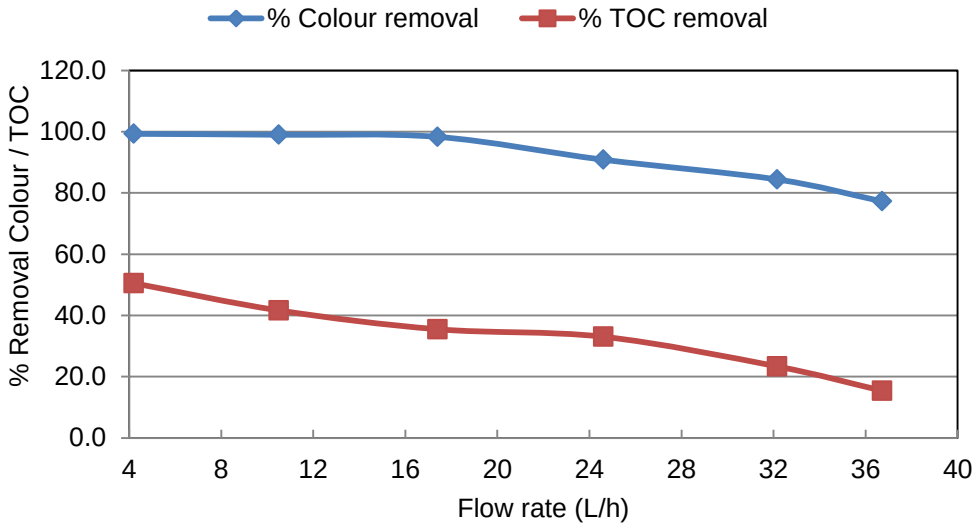

Figure 6.19 - The effect of flow rate on the colour and TOC removal (single pass, pH 7.0, current density 80 mA/cm^2, temperature 20°C, NaCl concentration 0.1 mol/L and RB2 dye concentration 100 mg/L)

6.3.6 Colour removal at varying dye concentrations

Data for colour removal at varying dye concentrations are given in the Figure 6.20. As anticipated, higher concentration of dye required higher treatment times which were provided by successive cycling through the cell. Calculations indicate that the specific charge consumption for colour removal increased as the concentration decreased. This is shown in Figure 6.21, where coulomb efficiency for successive cycles at lower initial dye concentrations decreases dramatically. This is in accord with the observation by Ammar, Abdelhedi, Flox, Arias, & Brillas, 2006.

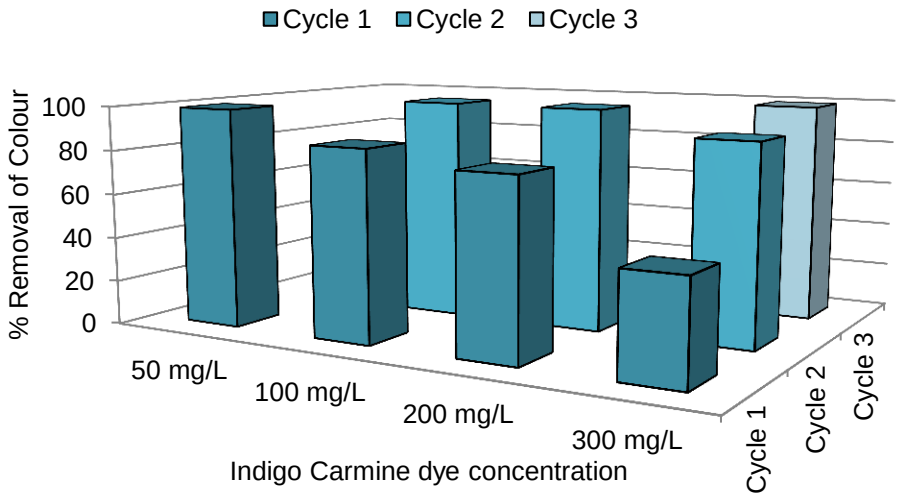

Figure 6.20 - The effect of dye concentration on the colour removal (flow rate 190 mL/min, pH 6.0, current density 80 mA/cm^2, temperature 20°C, NaCl concentration 0.25 mol/L)

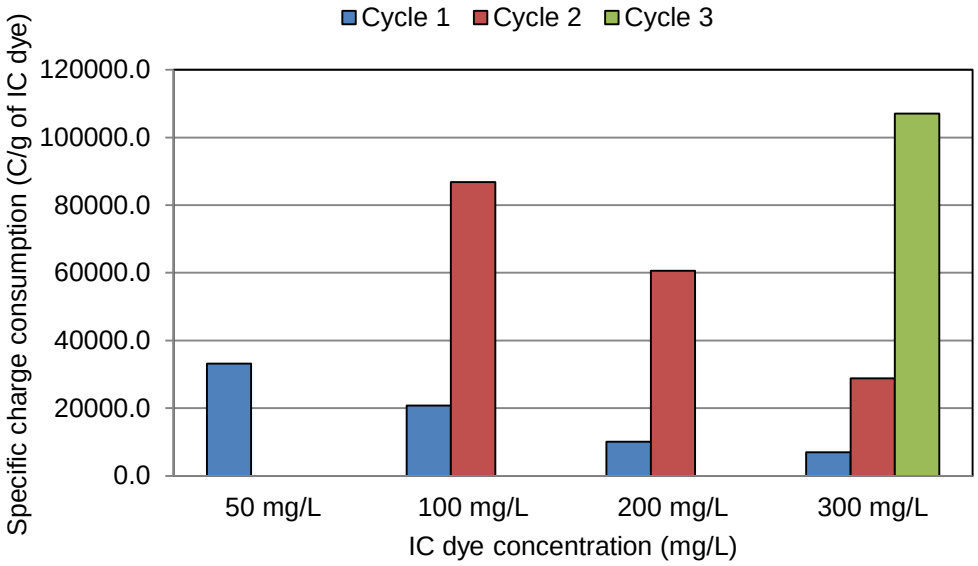

Figure 6.21 – The specific charge consumption per cycle with increasing dye concentrations (flow rate 190 mL/min, pH 6.0, current density 80 mA/cm^2, temperature 20°C, NaCl concentration 0.25 mol/L).

6.3.7 The effect of post electrolysis stand time on colour removal

It was commonly observed that dye solutions continued to fade with prolonged standing times. This effect was studied by allowing a solution of treated RB2 dye to stand for a period of 35 minutes after electrolytic treatment. Results are plotted in Figure 6.22. Approximately 90% of the colour was removed by a single pass through the cell. On standing a further 8% of colour removal was observed. The colour removal rate on standing diminished after 20 minutes. A precipitate formed in the treated dye solutions after a period of several days and total colour removal was observed. It could be that the slow colour removal observed in the present experiment was a result of a slow aggregation processes.

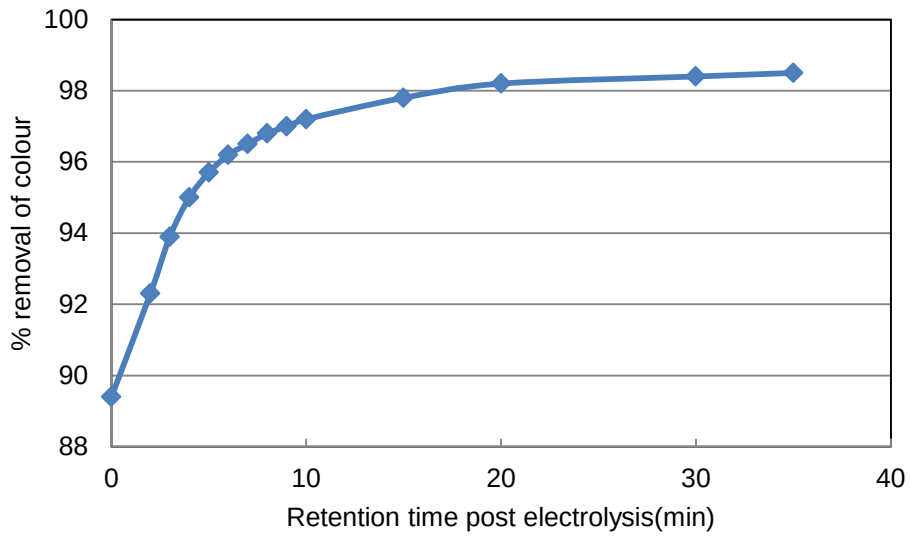

Figure 6.22 - The effect of retention time (post electrolysis) on the colour removal (single pass, flow rate 190 mL/min, pH 7.5, current density 47 mA/cm^2, temperature 20°C, NaCl concentration 0.05 mol/L and RB2 dye concentration 100 mg/L)

A possible application of this result could be providing adequate retention time for the slower processes to go to completion allowing an energy saving due a lower chlorine requirements and/or better quality final discharge.

6.4 Discussion

In this chapter experiments were performed to determine the colour and TOC removal performance of the PEFT cell under realistic conditions of electrolyte (NaCl and other) concentration and pH likely to be found in dye effluents from the cotton textile industry. It has been shown that the PEFT cell provides an efficient means of decolourising the textile dyes indigo carmine and reactive blue 2. For indigo carmine complete decolourisation was achieved at a specific charge consumption of 7.0 × 10^3 C/g of IC dye and energy consumption of 8.29 kWh/kg of IC dye (0.8 kWh/m^3) for a concentration of 100 mg/L. This result is an order of magnitude improvement in energy consumption compared to an electrolytic treatment of IC dye with a graphite anode at a similar NaCl concentration, consuming approximately 11 kWh/m^3 and it had taken 33 minutes of electrolysis

time in a static system and achieving only 90% colour removal (Cameselle, Pazos, & Sanroman, 2005).In this work the energy consumption 0.8 kWh/m^3(8.29 kWh/ kg of dye) is comparable to most reported electrochemical colour removal research work carried out using metal oxide coated DSAs (Martınez-Huitle & Brillas, 2009). The results confirm the fact that the PEFT cell can produce chlorine at a reduced energy consumption making electro-decolourisation a commercially viable option in treating textile effluents. The reduced inter-electrode gap, low cost materials, graphite anode and stainless steel cathode reduced the energy consumption and capital cost respectively. The capability of continuous operation makes the PEFT cell design stand out from other available electrochemical cell designs.

The chloride ion concentration is vital in the indirect electro-oxidation method to oxidize the dye stuffs in water. Even at low NaCl concentrations (0.05 mol/L), 100% colour and 50% TOC removal was achieved for IC dye after nine cycles through the cell. The elevated NaCl concentration in dye effluent reduced the number of cycles to achieve 100% colour removal and at the same time increased the mineralisation of the organic matter reducing the TOC content in the effluent. Increased chloride ion concentrations have the effect of raising the conductivity of the electrolyte and improving the chlorine current efficiency leading to reduced energy consumption. Compared with static systems it is well known that mineralisation of organic matter in flow through systems is poor. The PEFT cell however performed well achieving 85% TOC removal.

Reactive dyes are known to be persistent in water and harder to decontaminate. In achieving 100% colour removal in a single pass at 0.35 mol/L NaCl concentration and at a flow rate of 190 mL/min, the PEFT cell has performed well compared with other electrochemical colour removal techniques such as electro-coagulation, direct anodic oxidation, electro-Fenton and photoelectro-Fenton (Ammar, Abdelhedi, Flox, Arias, & Brillas, 2006; Can, Bayramoglu, & Kobya, 2003; Flox, et al., 2006; Martınez-Huitle & Brillas, 2009).

The indirect electro-oxidation process employed in the PEFT cell strongly depends on the electro-generated chlorine to oxidize the dye chromophore in the

effluents. Depending upon pH, active chlorine exists in solution in different forms such as $Cl_{2(aq)}$, HOCl, and ClO^- (Martınez-Huitle & Brillas, 2009). Aqueous chlorine is the predominant species in the pH range 0 to 3, HOCl in the pH range 3-8 and ClO^- ions above pH 8. The standard oxidation potentials of these species differ largely :($E^0_{Cl^-/Cl_2}$=1.36 V, E^0_{HOCl/Cl^-}= 1.49 V,$E^0_{ClO^-/Cl^-}$= 0.89 V). At neutral pH, active chlorine is more strongly oxidising and might be expected to be more efficient in colour and TOC removal than in acid or basic solutions.

However there was a significant improvement in colour and TOC removal for the IC dye at pH 3 compared with pH 7 and 10. This result points to the greater importance of the actual chemical species present than their oxidizing tendency. At lower pH there will be high concentration molecular chlorine and associated chlorine radical species. The short lived radicals are believed to be highly effective in attacking and destroying conjugated chromophores (Chatzisymeon, et al., 2006; Martınez-Huitle & Brillas, 2009). Above pH 8, pH has little effect because the concentration of molecular chlorine is vanishingly small. TOC removal at low pH was also greater than at higher pH. The TOC removal for IC dye at pH 3 was approximately 40% higher and for RB2 dye it was 60% higher than at pH 7. Carneiro et al. (2003) achieved 56% TOC removal for reactive blue 4 (RB4) dye at pH 2.2 using a metal oxide coated DSA anode. The 60% TOC removal of RB2 in the present work with a graphite anode attests to the efficiency of the PEFT cell. The 50% reduction in power consumption at pH 3 relative to pH 7 for the IC dye is further evidence in favour of low pH dye decolourisation.

It was of interest to assess the effectiveness of the reactive chlorine species relative to other oxidizing species formed in the absence of chlorides. Results of the sulphate systems summarised in Section 6.3.4 indicated that the ROSs formed with chlorides rigorously excluded were much less effective than reactive chlorine species. Interestingly these ROSs were relatively more efficient at TOC removal than colour removal but still less efficient than reactive chlorine species. The reversed removal efficiency for TOC relative to colour indicated that the sulphate system ROSs were better at degrading organic molecules than chromophores.

In the flow rate experiments the colour and TOC removal decreased with the increase in flow rates due to dilution of the active chlorine species. The TOC removal for IC dye was consistently 10% lower than colour removal whereas for the RB2 dye it was 50% lower. This result is consistent with relatively simultaneous decolourisation and decomposition of the IC dye and stepwise decolourisation followed by oxidative decomposition in the case of the RB2 dyes.

Further evidence of stepwise degradation of RB2 dye was provided by RB2 degradation at low electrolyte concentration (0.01 mol/L NaCl, see Appendix D for image). The progressive colour changes from blue to brown before complete decolourisation indicated progressive disruption of the conjugated chromophore as with additional chlorine attack. This experiment also illustrated the greater activity of the chlorine species formed electrolytically. When the equivalent amount of hypochlorite was added at the same pH progressive colour change stopped at yellow. In the case of electrochemical decolourisation some of the dye is destroyed by ROSs produced in addition to chlorine production thus there are more oxidizing species in the system to complete the decolourisation. In other words more decolourisation per mole of chlorine is achieved when chlorine is produced electrochemically than when it is added chemically. A similar result with indigo carmine dye was reported by Dogan and Turkdemir, 2005.

6.5 Conclusions

- Complete electrochemical decolourisation of indigo carmine dye effluent containing 0.35 mol/L NaCl was achieved using the PEFT cell employing a graphite anode with a single pass consuming only 0.8 kWh/m^3 or 8.3 kWh/kg of dye. This is an order of magnitude improvement in the energy consumption compared with existing colour removal data for graphite anodes.
- The energy consumption for decolourisation of IC dye is comparable or better than most colour removal work carried out using metal oxide coated DSAs and BDD anodes.

- The reduction in pH from 7 to 3 reduced the energy consumption for decolourisation of IC dye by 50% in and also increased the TOC removal by 20%.
- Instantaneous colour removal of reactive blue 2 dyes could not be achieved by a single pass through the cell. At energy consumption of 1.25 kWh/m^3 at 100 mg/L dye concentration, 90% instantaneous removal was achieved after single pass. Total removal occurred after on standing for 20 minutes.
- When chloride was rigorously excluded from the electrolytic systems (Na_2SO_4 was used as the electrolyte) colour removal was 80% less effective for both IC and RB2 dyes.
- The PEFT cell allows effective decolourisation at variable flow rates providing higher current densities are used to compensate higher volumetric flow rates.
- Post electrolysis retention time can be used to improve colour removal or reduce energy consumption.

Chapter 7: Electro-disinfection of drinking water

7.1 Introduction

The efficient production of chlorine by the 240 μm PEFT cell (Chapter 5) at chloride levels naturally available in water offered the possibility of applying the cell as an inline *in-situ* electro-disinfection device. The improved 50 μm PEFT cell was employed in this work. The experiments were designed to determine whether the chlorine produced electrochemically at such low chloride concentrations was adequate to achieve disinfection. Also, because the PEFT cell allows good control over experimental conditions and contact times, it allows the possibility of resolving the issue of whether electrochemically produced chlorine is a more effective disinfectant than chemically produced chlorine and determining the role of reactive oxygen species (ROS).

7.2 Materials and methods used in electro-disinfection

7.2.1 PEFT cell assembly and instruments

The 50 μm inter-electrode gap PEFT cell (1.0 mm holes with 6 holes/cm^2 hole density hexagonally arranged, staggered hole configuration) stainless steel cathode and a graphite anode was used (see Figure 3.3 in Section 3.1.4). The electrolytic cell components, assembly of components and experimental set up was the same as explained in Section 2.2.

7.2.2 Chemicals, microorganism and microbiological analysis

The low concentrations of chloride solutions (0 – 500 mg/L) to represent chloride levels in natural waters were prepared using de-ionised double distilled water and

NaCl (BDH analar). The Na_2SO_4 electrolyte was BDH analar grade dissolved in de-ionised water and calcium hypochlorite used was a BDH laboratory grade. The detailed description of materials and preparation of microorganisms and microbiological analysis is given in Chapter 2, Section 2.4.13.

7.2.3 The electro-disinfection experiment

The *E. coli* spiked dilute electrolyte solution was passed once through the electrolytic cell at a constant flow rate and the treated samples were collected from the anodic end into a sterilized sample bottle. After 30 minutes 1.0 mL of 0.1 mol/L $Na_2S_2O_3$ was added to impede action of the oxidation species and microbial analyses carried out. The initial microbial count was maintained at 4×10^6 CFU/mL in all experiments, pH at 6.0 and temperature at 20°C. The flow rate through the cell was maintained at 190 mL/min in all experiments except when it was the variable. The disinfection capabilities of electrolyte concentrations, current densities, flow rates, different electrolytes and effect of electric fields were studied.

The experiment comparing electrochemical disinfection and chemical disinfection used two current densities 16 mA/cm^2 and 31 mA/cm^2 with a water sample containing 100 mg/L of NaCl. The electrolysed sample at the two current densities produced 0.20 mg/L and 0.40 mg/L of available chlorine respectively. A stock solution of chlorine was prepared by diluting freshly prepared calcium hypochlorite. The available chlorine was determined by an iodometric titration (Vogel, 1997). A calculated volume of the diluted chlorine solution was added to the *E. coli* spiked water samples, giving available chlorine concentrations of 0.20 and 0.40 mg/L, stirred and allowed to stand for 30 minutes before they were analysed for residual microbial activity.

For the comparison of the disinfection capabilities of other oxidative species, the chloride free water sample was inoculated with an *E. coli* sample prepared in a special, chloride-free, SK culture medium (Section 2.4.13).

7.3 Results and discussion

7.3.1 Electro-disinfection at drinking water chloride concentrations

Results for electrochemical disinfection at drinking water concentrations of chloride ions after single pass through the cell are given in Figure 7.1. Total inactivation (6.6 log inactivation) of microbes at a current density of 80 mA/cm^2 was achieved at a chloride ion concentrations of 100 mg/L which represents the lower end of chloride concentration found in natural waters. Even in the distilled water system a 1.5 log inactivation was achieved. This result underlines the sensitivity of the experiment to the very low concentrations of chloride (10 mg/L) introduced with the *E. coli* culture medium.

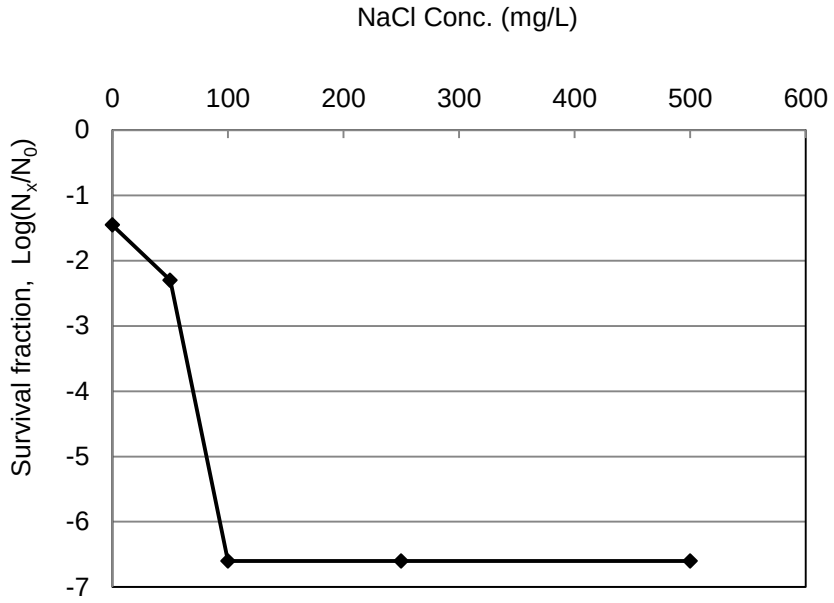

Figure 7.1 - Microbial inactivation with increasing chloride ion concentration (flow rate 190 mL/ min, current density 80 mA/cm^2, single pass through the cell, initial E. coli concentration $N_0 = 4 \times 10^6$, pH 6.0 and Temperature 20°C).

Because the amount of chlorine generated depends on current density (Section 5.3.3) the minimum amount of chlorine generation required for 6 log inactivation, was determined by studying the effect of current density on disinfection at 100 mg/L chloride.

7.3.2 Effect of current density on microbial inactivation

Results for the effect of current density on inactivation and consumption at 100 mg/L chloride concentration are shown in Figure 7.2. The lowest current density required to achieve complete inactivation was 16 mA/cm^2 and the corresponding energy consumption was 0.5 kWh/m^3 of water treated. This energy consumption is lower than literature data for static systems which range from 1 kWh/m^3 to 10 kWh/m^3(Drees, et al., 2003; Jeong, et al., 2009; Martinez-Huitle & Brillas, 2008) and also for the flow through Zappi cell reported by Kervick et al. (2005).

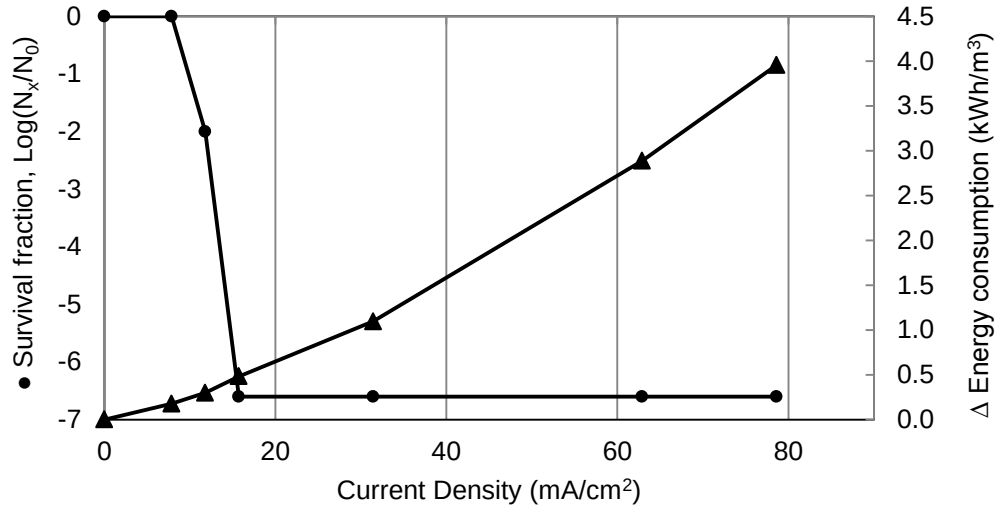

Figure 7.2- Microbial inactivation and energy consumption with current density ([NaCl]/100 mg/L, flow rate 190 mL/ min, single pass through the cell, initial E. coli concentration $N_0 = 4 \times 10^6$, pH 6.0 and temperature 20°C).

7.3.3 Effect of flow rate on microbial inactivation

In order to confirm that active chlorine concentrations at increased flow rates can be maintained by increased current densities, the effect of flow rate on disinfection efficiency was studied at two current densities 16 mA/cm^2 and 8mA/cm^2. Results are given in Figure 7.3. The survival fraction increased almost linearly with flow rate over at least four order of magnitude of $\log(N_x/N_0)$ consistent with active chlorine dilution at the higher flow rates and the Chick-Watson relationship (Ray, 1995) for the constant 30 minute contact times

employed in the experiments. The effect of reduced disinfection at increased flow rates was approximately compensated by increasing current density in direct proportion to flow rate. This is consistent with previous work that has shown a linear relationship between chlorine production and current density in the 240 μm gap PEFT cell (Nath, et al., 2011).

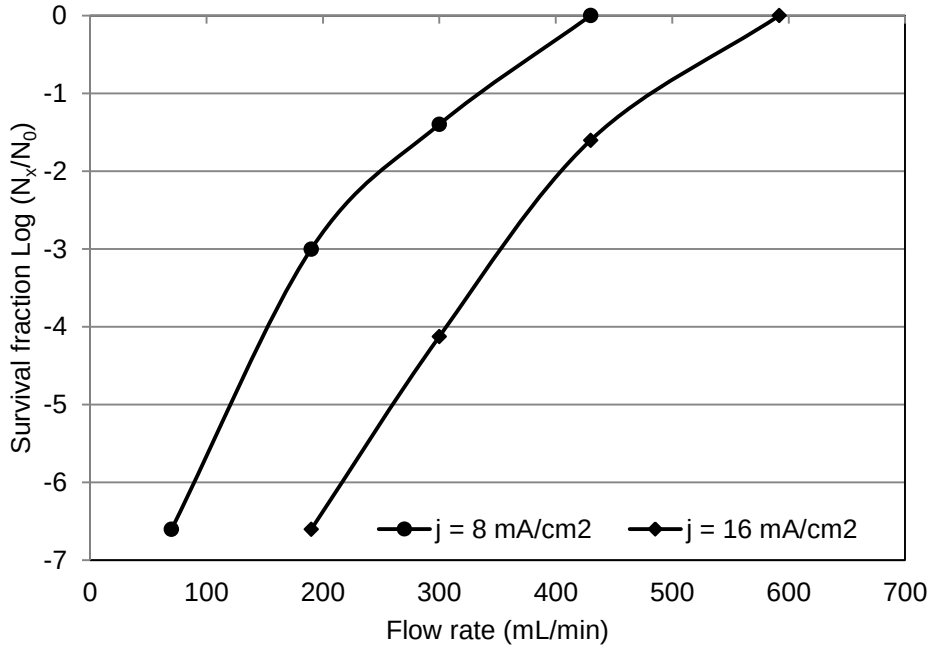

Figure 7.3- Microbial inactivation with increasing flow rates (current density 16 mA/cm^2, [NaCl]/100 mg/L, single pass through the cell, initial E. coli concentration $N_0 = 4 \times 10^6$, pH 6.0 and temperature 20°C).

7.3.4 Comparison of the effectiveness of electrochemically produced chlorine with chemical chlorine

An experiment was designed to compare electrochemical disinfection with chemical disinfection. Two current densities, 16 and 31 mA/cm^2 (see Section 7.3.2, Figure 7.2) where complete inactivation was achieved were selected. The chlorine concentrations generated under these conditions were found to be 0.20 and 0.40 mg/L respectively. The same amount of chlorine was added as calcium hypochlorite to a fresh bacterial suspension while maintaining a constant pH of 6.0 by addition of dilute sulphuric acid. Results given in Figure 7.4 show that

while the chlorine produced electrochemically achieved at least 6 log inactivation, the chlorine added as hypochlorite achieved less than 1 log inactivation at 0.2 mg/L of chlorine and approximately 2 log inactivation at 0.4 mg/L of chlorine consistent. The greater effectiveness of electrochemical chlorine relative to chemical chlorine in chlorine disinfection in these experiments is much higher than results previously reported in the literature (Diao, et al., 2004 ; Helme, et al., 2010). The higher inactivation obtained by electrochemically produced chlorine has been attributed to simultaneous formation of ROSs during the electrochemical process (Jeong, et al., 2006; Kerwick, et al., 2005; H. Li, et al., 2010).

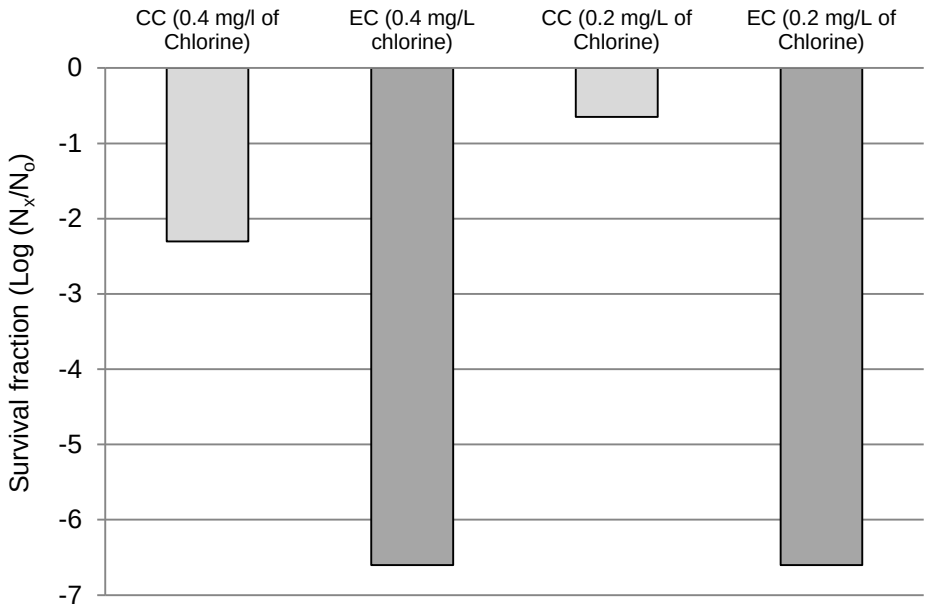

Figure 7.4 - A comparison of disinfection effectiveness of electrochemical chlorine (EC) and chemical chlorine (CC) at the same chlorine concentration.

7.3.5 Examination of the role of reactive oxygen species (ROS)

In order to test for the role of ROS species under conditions where chloride ions and the formation of chlorine was rigorously exclude from the system (see Section 7.2.3) an experiment was performed where the ionic strength was controlled by sodium sulphate. Results are presented in Table 7.1.

Table 7.1 – Effectiveness of electrochemical disinfection in the presence and absence of chloride (Current density 63 mA/cm^2, single pass through the cell, initial E. coli concentration $N_0 = 4\times10^6$, pH 6.0 and temperature 20°C).

Sample	**[NaCl]**/mg/L	**[Na_2SO_4]**/mg/L	**E'Field**/V/cm	**Log(N_x/N_0)**
A	100	0	1646	-6.6
B	10	0	1840	-1.5
C	10	100	1800	0.0
D	0	100	1778	0.0

The results show that inactivation in the presence of chloride is much more effective than in the presence of sulphate with no chloride present. There is no evidence that sulphate derived oxidation products contribute to disinfection under the conditions of the experiment. While Patermarakis & Fountoukidid, (1990) and Li, et al., (2010) have reported that ROSs do contribute to electrochemical disinfection, the results reported above are consistent with the work of Li et al., (2004) who reported no effect from ROSs. Furthermore the results for sample C demonstrate that the presence of sulphate has an inhibitory effect on disinfection even when chloride is present. This can be explained by competition between chloride and the higher concentration of sulphate ions in the anodic oxidation processes. While these results do not prove that ROS species formed in the absence of chloride have no role in electro-disinfection, they do indicate that such a role was insignificant under the conditions of the experiments. Most of the reported work on chloride free electro-disinfection with Na_2SO_4 as the electrolyte used prolonged exposures (several minutes) at the anode surface in static systems (Li, et al., 2010; Polcaro, et al., 2007) or prolonged recycling through flow systems (Kerwick, et al., 2005) in order to allow sufficient exposure of bacteria to ROS species to achieve an effect. Such treatment times are incompatible with practical disinfection requiring large flow rates. The effectiveness at short exposure times and the possibility of residual protection are major advantages of electro-chlorine disinfection.

While the effectiveness of ROSs produced from sulphate do not appear to contribute to disinfection under the conditions of the experiments, the increased

effectiveness of electro-chlorination relative to chemical chlorination has not been resolved. One possibility could be electric field effects resulting from the narrowness of the inter-electrode gap. For example, electric fields generated in the investigation of ROSs are given in Table 7.1. These fields, while being less than those required for irreversible electroporation, are still much higher than other reported studies of electro-disinfection.

7.3.6 Synergistic electric field effects

An experiment was designed to test the effect of increasing the electric field on microbial inactivation. A nutrient broth culture of *E. coli*. containing 10 mg/L of chloride was used. Increasing electric field strengths were generated by varying the applied voltages at a constant current density by adjusting the conductivity of the electrolyte using Na_2SO_4, which does not contribute to microbial inactivation.

Results of inactivation versus field strength are plotted in Figure 7.5. The data shows a dramatic increase in inactivation above a field strength of 1.3 kV/cm, much below the 10.0 kV/cm field strength reported to cause irreversible electroporation (Huang & Wang, 2009; Zhang, et al., 1995). Total inactivation was achieved at a field of 2.5 kV/cm providing evidence of enhanced disinfection by the field. The constant current density used in these experiments ensured that the concentration of electrochemically generated disinfectant species remained constant. The energy consumption was 5.7×10^{-3} kWh/L which at worst would cause an instantaneous temperature rise of 4.9°C.

The effect of the field can be explained by considering the inactivation mechanism by chlorine species. Inactivation of microbes occurs when chlorine species diffuse through the cell wall causing impairment of the internal enzyme system (Li, et al., 2004; White, 2010). Studies on electroporation have confirmed that long pulses of electric fields above 1.0 kV/cm typically cause reversible cell damage (Fox et al., 2006; Wang, et al., 2006). In the current work, field pulses of 0.1 second duration were produced hydrodynamically by flow through the cell. The synergy between electric field and electrochemically produced active chlorine

species, suggested by Abderrahmane, Himour, & Ponsonnet, (2008); Feng, Suzuki, Zhao, et al., (2004), has been demonstrated. The specific lethality of the chlorine in a field of 2.5 kV/cm is at least 50 L/mg min, i.e. at least two orders of magnitude higher than in the absence of the field.

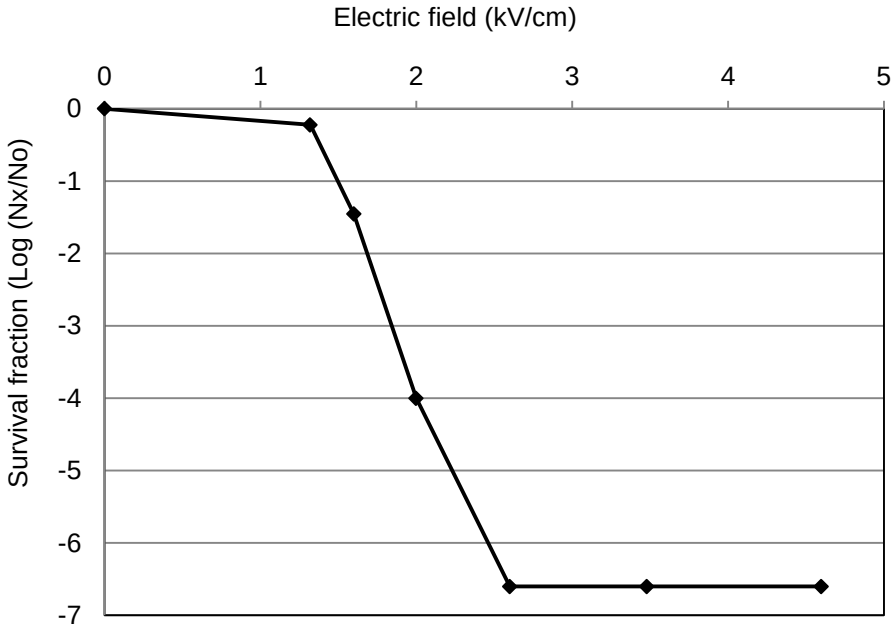

Figure 7.5 - The effect of electric field on electrochemical disinfection at very low NaCl concentration ([NaCl]= 10 mg/L, current density 80 mA/cm^2, flow rate 190 mL/min, initial E. coli concentration $N_0 = 4\times10^6$, pH 6.0 and temperature 20°C)

7.3.7 Advantages of the 50μ PEFT cell for disinfection

The reduction of the inter-electrode gap to 50 μm in the PEFT cell has allowed a water treatment cell to achieve effective electro-disinfection at very low chloride concentrations and relatively low energy consumption. In addition the direction of flow and hydrodynamics offer advantages in the disinfection process. Flow direction from cathode to anode in the PEFT cell minimises the possibility of cathodic reduction of the electrochemically produced oxidation products that are effective in the disinfection. The short residence time in the cell gives little opportunity for the further oxidation of active chlorine species to higher oxidation states such as chlorite, chlorate and perchlorate ions. These ions are considered to

be detrimental disinfection by-products (Polcaro, Vacca, Mascia, Palmas, &Ruiz, 2009). Forcing the water through the micro-gap between electrodes results in high flow velocities, high Reynold's numbers, high turbulence and hence rapid and complete mixing of the disinfectant species. A simplified treatment of the PEFT cell hydrodynamics is given in Appendix B.6.

In the context of practical applications, the flow through configuration allows for easy coupling to inline treatment processes. Monitoring instruments could be connected through a programmable circuit to control the electrical variables of the treatment process to optimise the disinfection efficiency. The micro gap PEFT cells can be assembled as modules to scale up or down according to the requirements. The stainless steel and graphite electrode materials are relatively inexpensive and operating applied voltages of less than 12 Volts allowing battery or a solar panel operation. The graphite anode is compatible with drinking water systems but the longevity of the anode needs to be investigated. Dimensionally stable anodes (DSAs) are commonly used in commercial hypochlorite generation processes (Jeong, et al., 2009; Khelifa, et al., 2004) in undivided electrochemical cells due to it high efficiency and compatibility with water treatment. The use of a perforated DSA could increase the durability and offer the possibility of further improvement of the energy consumption.

7.4 Conclusions

- The 50 µm inter-electrode gap PEFT cell has achieved single pass 6 log inactivation of *E. coli* suspended in NaCl concentrations typical of natural water at a applied voltage of 5.5 volts and an energy consumption of 0.5 kWh/m^3. This performance is significantly better in terms of energy consumption, reduced salt concentration and reduced contact time than other electro-disinfection devices reported in the literature.
- In addition, the 50 µm inter-electrode gap of the PEFT cell allowed high fields (>1 kV/cm) to be generated by low applied voltages. These fields are capable of causing electroporation of the cell membranes. The results show that the synergistic effect of these field effects in the presence of very low salt

concentrations (10 mg/L) contribute to a 6 log inactivation at fields above 2.5 kV/cm. Electro-disinfection is thus possible using much reduced chlorine concentrations and thus reduced possibility of disinfection by-product (DBP) formation.

- In the experiments, with a single short exposure of the treated solution to electrolysis and where chloride ions were rigorously excluded, there was no evidence for any significant contribution of reactive oxygen species (ROS) to disinfection.

Chapter 8: Electro-catalytic effect

8.1 Introduction

During the studies of field induced electro-disinfection, experiments were performed with insulated anodes in an attempt to study inactivation in the absence of chlorine. Imperfect insulation of the anode surface led to the abandonment of this work, but not before surprisingly high current efficiencies for chlorine production was observed. The purpose of the work described in this Chapter was to investigate this effect. Improved current efficiencies for chlorine production, particularly at low chloride ion concentrations, could have significant practical advantages in electrochemical treatment of aqueous systems.

8.2 Insulated electrode in a PEFT cell

8.2.1 Preparation of insulated electrodes

A 50 μm gap PEFT cell with the graphite anode replaced by a stainless steel anode was used in this work. The anode surface facing the cathode was modified according to the details given in Section 2.1.1. The cathode was stainless steel with the same hole size (1mm perforations) and hole density (6 holes/cm^2). The electrodes were arranged so that a staggered configuration of holes with symmetrical flow paths between cathode and anode was obtained (Figure 8.1). Stainless steel was used for the anode in the current work because it provided a more satisfactory surface for the application of the polyurethane film than the graphite previously used in the PEFT cell. In preliminary work, the imperfect insulation achieved by polyurethane coating the electrode surface was attributed to the polyurethane not penetrating and covering the walls of perforations. For the present work, in order to ensure that the perforation walls were completely free of polyurethane, they were re-drilled after the application of the polyurethane film.

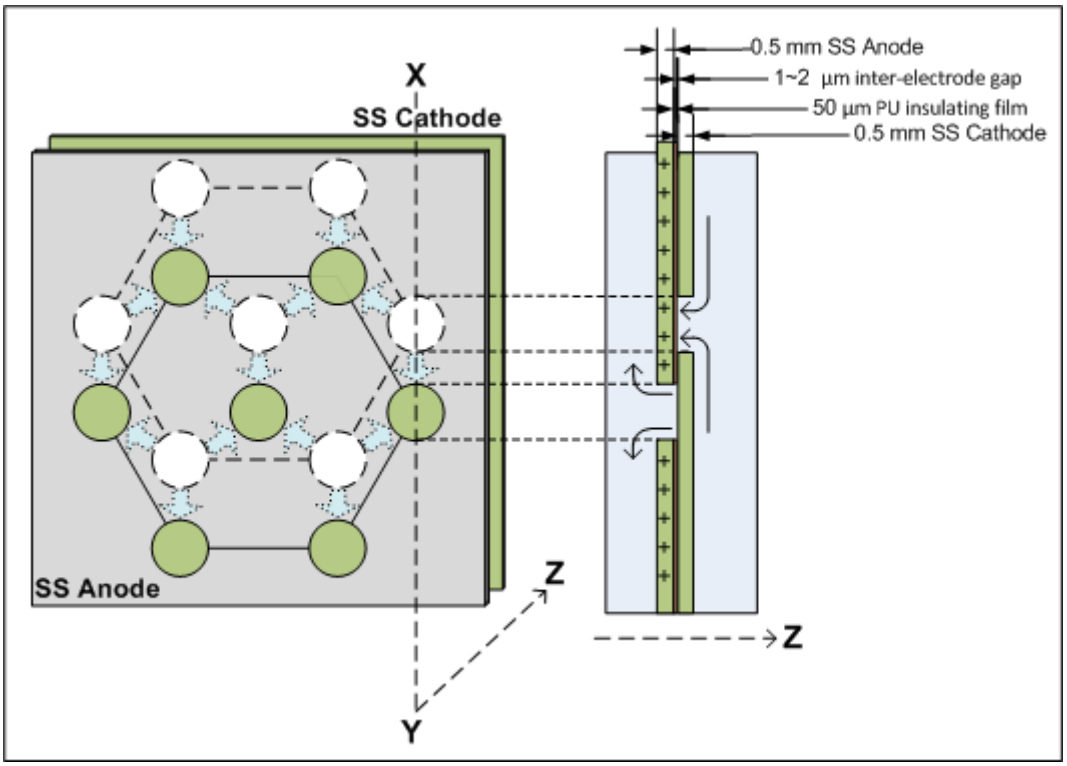

Figure 8.1 - Schematic showing staggered hexagonal pattern of electrode perforations, the insulating layer and the flow pattern between cathode and anode

The two stainless steel electrodes were clamped together and the solution to be electrolysed was forced through flow gap (~ 2 µm) between the exposed cathode and the insulated anode as shown in Figure 8.1. Electrical contact was made between the bare cathode surface and the exposed metal surfaces of the walls of the perforations in the coated anode. In experiments where a non insulated anode was used, the inter-electrode gap was maintained by 50 µm spacers.

8.2.2 Preparation of dilute chloride ion solutions and chlorine analysis

The electro-active species of interest in the present work were the chloride ions of a series of dilute NaCl solutions (0.85 mmol/L – 17 mmol/L). All the sodium chloride solutions were prepared by dissolving NaCl (BDH analar reagent) in de-ionized water (conductivity < 2 µS/cm). Chlorine was determined by an iodometric titration given in Section 2.4.1. The chlorine current efficiency (CE) and energy consumption (EC) were calculated according to procedure described in Section 5.1.1.

8.3 Enhanced chlorine production at a partially insulated anode

An experiment was performed to compare the current efficiency of chlorine production using the partially insulated system with chlorine production under identical conditions but without the insulation. Figure 8.2 presents data showing the improved current efficiency and reduced energy consumption that was obtained with the partially insulated system. At a concentration of 0.85 mmol/L NaCl and a current density of 2 mA/cm^2, current efficiency was more than tripled and energy consumption was reduced by a factor of two.

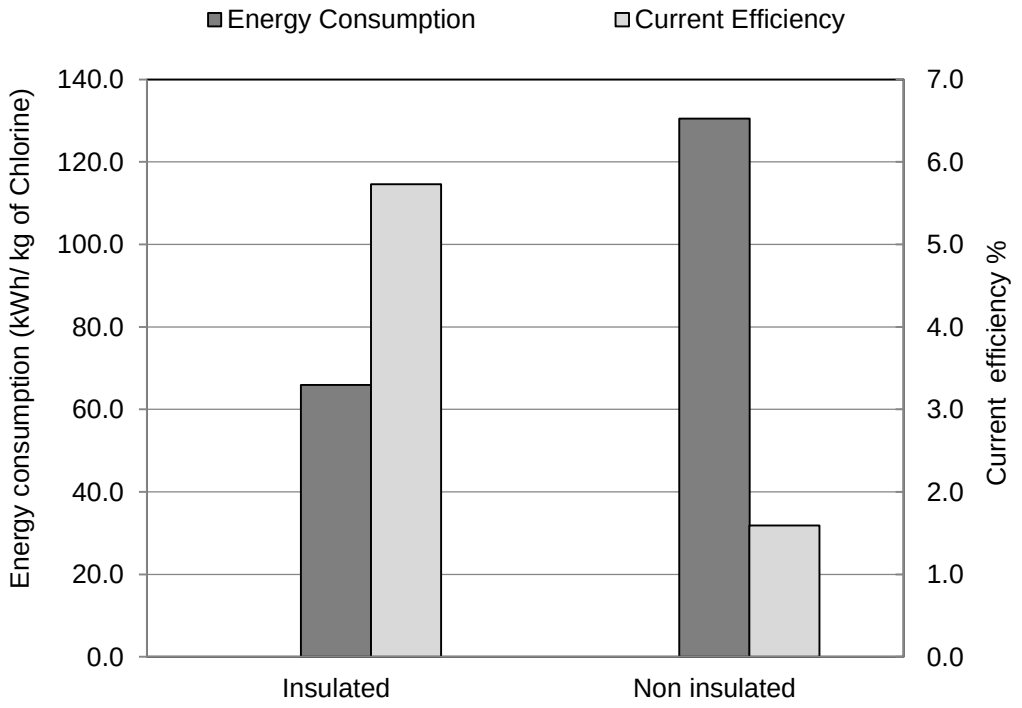

Figure 8.2 - Current efficiency and energy consumption at an insulated and non insulated anode surface, electrolysing 0.85 mmol/L, NaCl solution, 2 mA/cm^2 current density, 190 mL/min, effective electrode area 61.3 cm^2.

A ten-fold increase in the resistance of the cell was caused by the insulation but this was much less than the reduction in active electrode surface area.

In an attempt to further understand the enhanced current efficiency, experiments were performed to test the effects of flow direction, flow path, electrolyte concentration, current density and hole density.

8.3.1 Effect of flow direction

Direction of flow through the PEFT cell is likely to be important for electrochemical processes where gases are produced and where electrolytic products may undergo secondary electrode reactions.

Figure 8.3 (a) gives performance data for an insulated anode where flow direction is from cathode to anode and Figure 8.3 (b) gives the data where the flow direction is from anode to cathode. The cathode to anode flow resulted in reduced resistance, a 50% increase in the current efficiency and a corresponding reduction in energy consumption compared to anode to cathode flow.

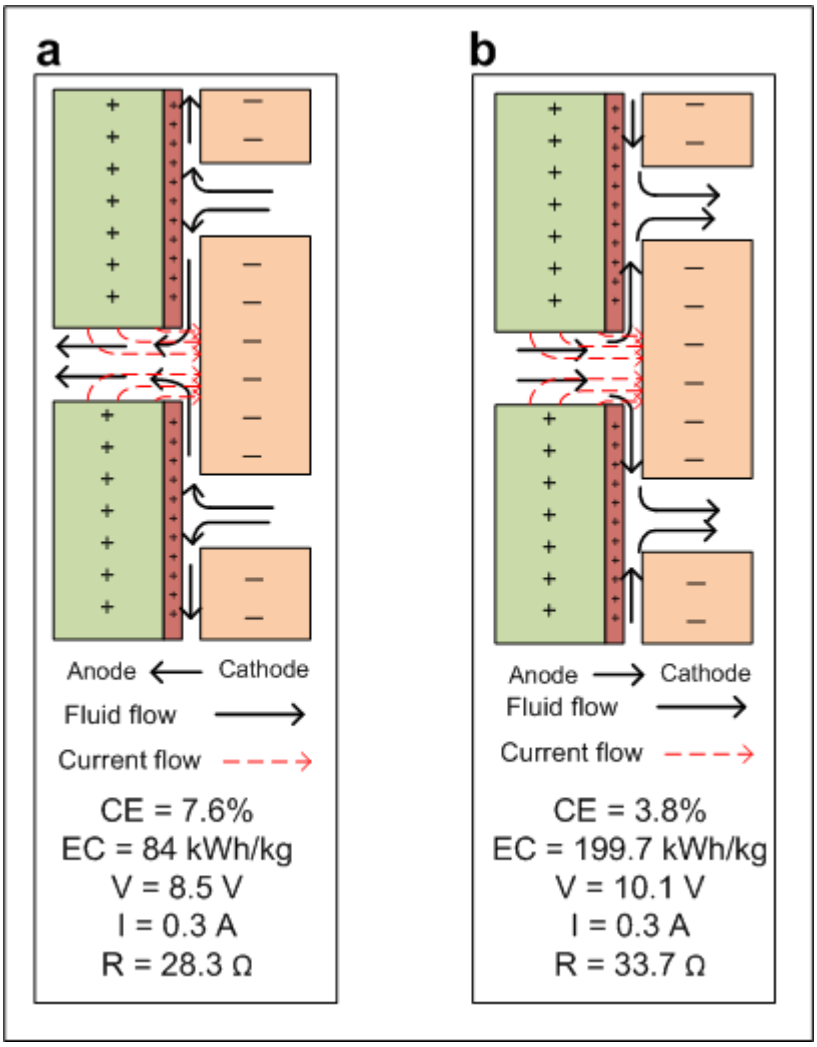

Figure 8.3 – The effect of flow direction when anode surface was insulated on the PEFT cell performance (NaCl concentration 0.85 mmol/L, constant flow rate 190 mL/min, constant current density 5 mA/cm^2, electrode staggered configuration)

Figure 8.4 present performance data where the partially insulated electrode was used as the cathode and the flow direction was from cathode to anode (Figure 8.4 a) and anode to cathode (Figure 8.4b). The cathode to anode flow resulted in increased resistance and a large reduction in current efficiency relative to anode to cathode flow.

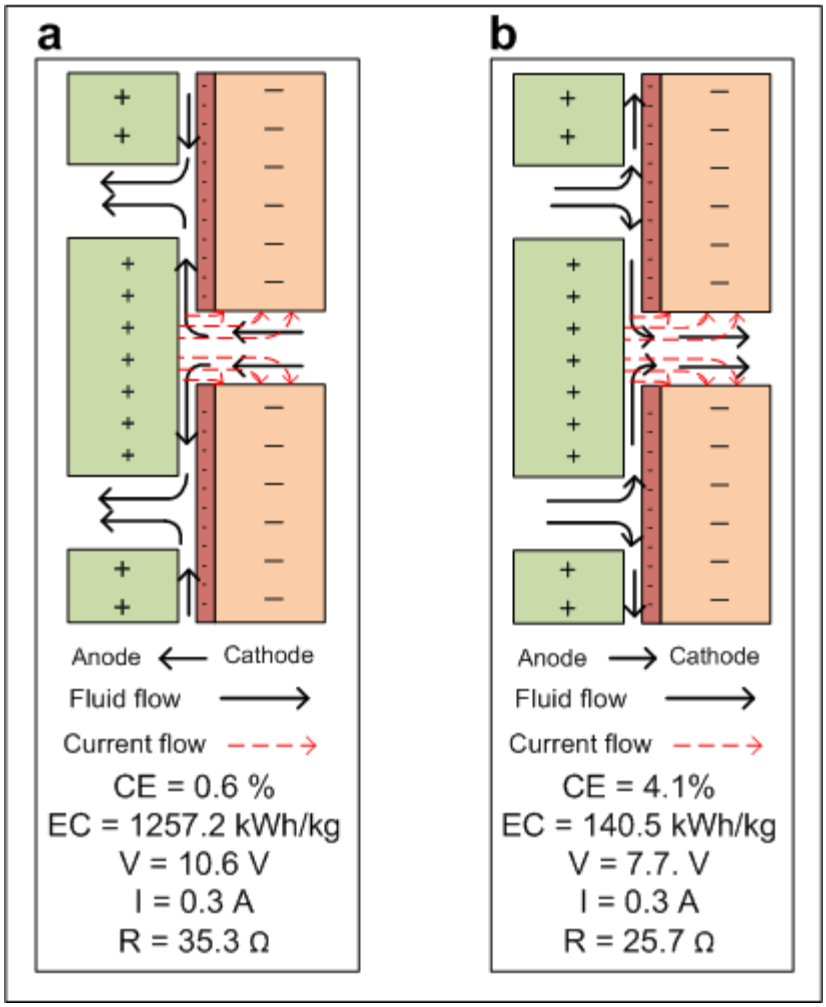

Figure 8.4 - The effect of flow direction when cathode surface was insulated on the PEFT cell performance (NaCl concentration 0.85 mmol/L, constant flow rate 190 mL/min, constant current density 5 mA/cm^2, electrodes staggered configuration)

8.3.2 Effect of electrolyte concentration

Figure 8.5 shows that as sodium chloride concentration was increased, the CE of both the insulated and non insulated electrodes increased but the difference between them decreased at concentrations above 3.4 mmol/L. This result, suggests the possibility that improved CEs observed for the insulated electrode systems were in some way due to enhanced concentrations associated with the insulating film.

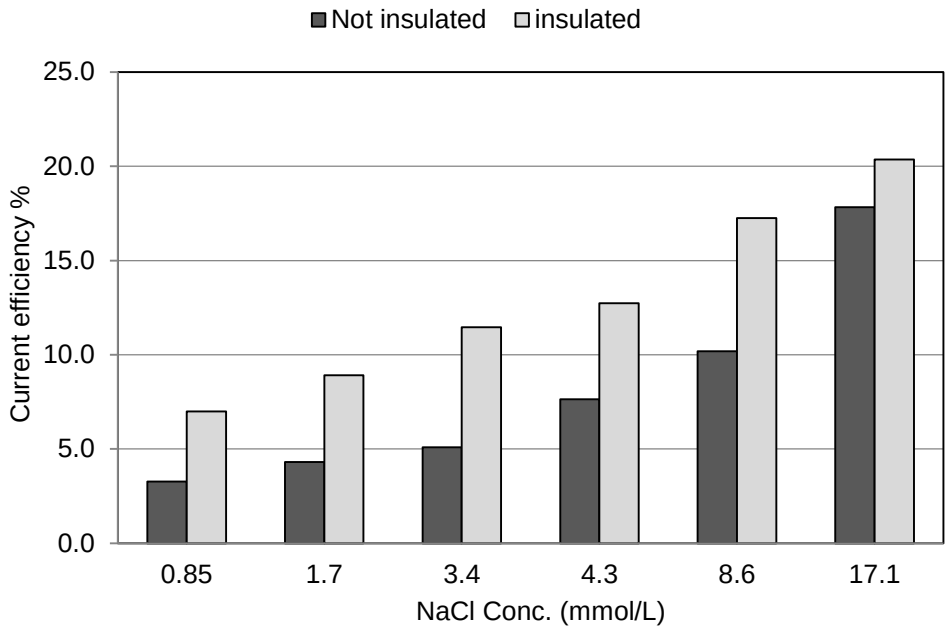

Figure 8.5 - Chlorine current efficiency with increasing electrolyte concentrations at constant current density 5 mA/cm^2 and a flow rate of 190 mL/min, holes staggered configuration, flow direction – cathode to anode.

8.3.3 Effect of hole configuration: aligned and staggered

The effect of aligned and staggered hole configuration was studied by setting up the PEFT cell as illustrated in Figure 8.6. Results for CE, given in Figure 8.7, indicate that the staggered hole configuration achieved higher current efficiencies, particularly at low electrolyte concentration.

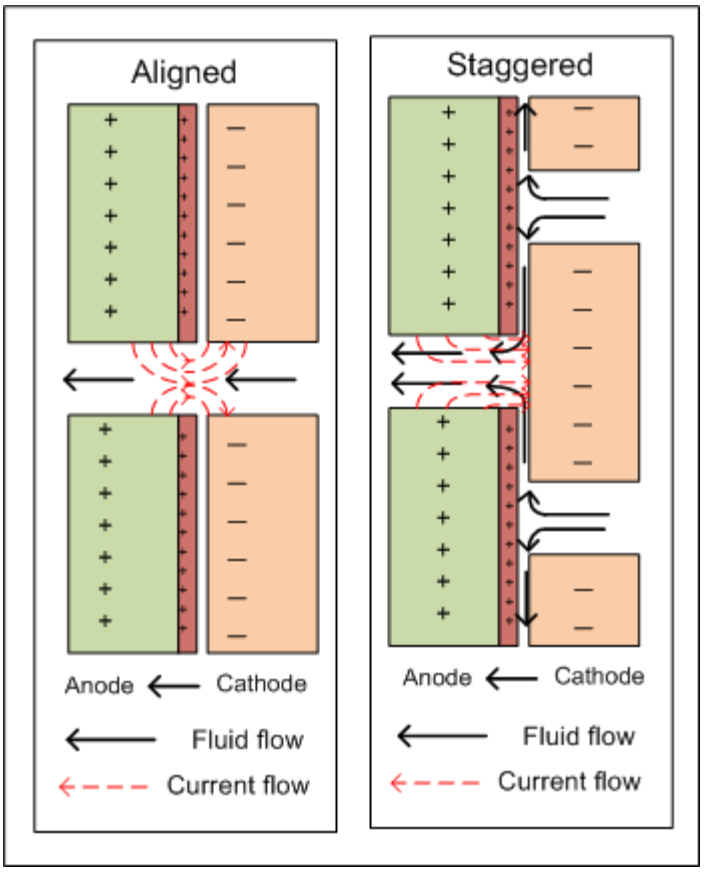

Figure 8.6 - Holes aligned and staggered configuration when the anode surface insulated facing the cathode and flow direction from cathode to anode.

The higher current efficiency with the staggered hole configuration provides further evidence of the likelihood that pre-concentration of chloride ions at the insulated film contributes to the effects observed. Figure 8.6 represents the two experimental systems. If chloride ions are pre-concentrated on the insulating film, in the staggered configuration they will be swept with the electrolyte flow towards the exposed anode rim where they will be discharged. However in the aligned configuration, while pre-concentration will also occur, transport to the anode rim will be solely by surface diffusion. Furthermore, once the electrolyte in the inter-electrode gap has been depleted it can only be replenished by slow bulk diffusion.

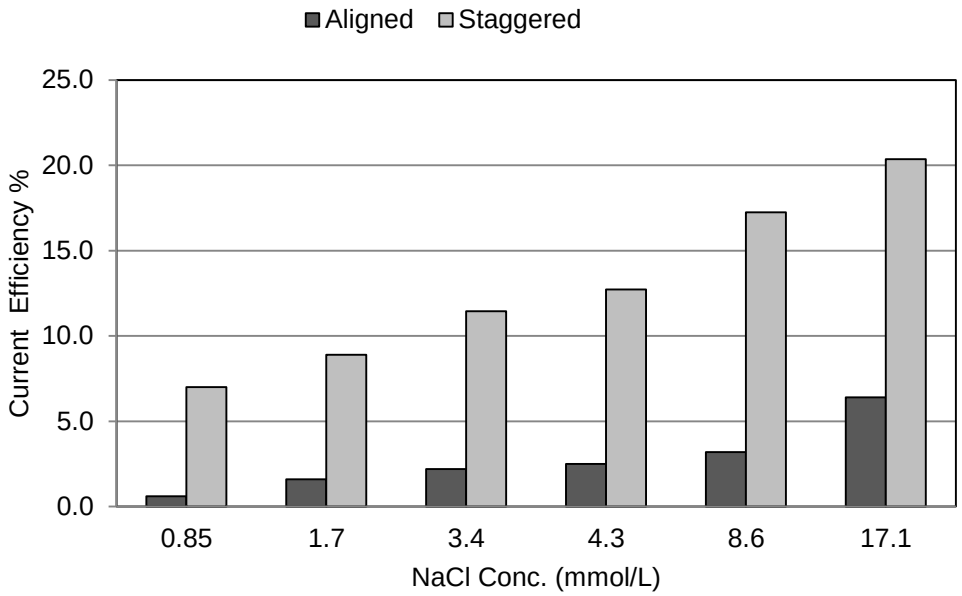

Figure 8.7 - Chlorine current efficiency with increasing electrolyte concentrations when holes aligned and staggered configuration (constant current density 5 mA/cm^2, flow rate of 190 mL/min, flow direction – cathode to anode)

8.3.4 Effect of current density

The effect of increased current density on CE and chlorine generation at the sodium chloride concentration of 1.7 mmol/L for the insulated and non insulated electrodes is shown in Figure 8.8. The improved current efficiency for the partially insulated electrode relative to the non insulated electrode is evidence for higher chloride ion concentrations at the active anode surface, further supporting the pre-concentration by the insulation film.

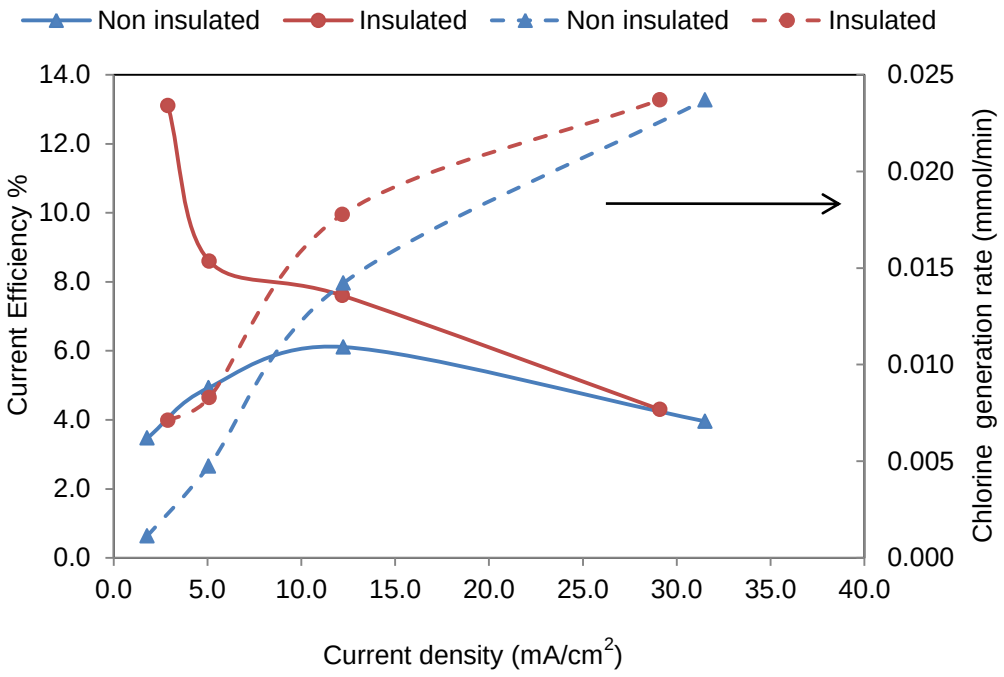

Figure 8.8 - Chlorine current efficiency and chlorine generation with increasing current density at 1.7 mmol/L NaCl concentration and a flow rate of 190 mL/min, holes staggered configuration, flow direction – cathode to anode.

8.3.5 Effect of hole density

The initial experiments were performed using a partially insulated anode with 6 holes/cm^2. The effect of hole density was investigated by reducing this to 3 holes/cm^2. Figure 8.9 shows that at the two current densities used, the chlorine generation at 6 holes/cm^2 was approximately twice than at 3 holes/cm^2. In addition, when the hole density was halved, the voltage required reduced approximately by 50% for a given current density. This is evidence that each hole has an associated conducting path, such that increasing hole density is equivalent to adding conductors in parallel.

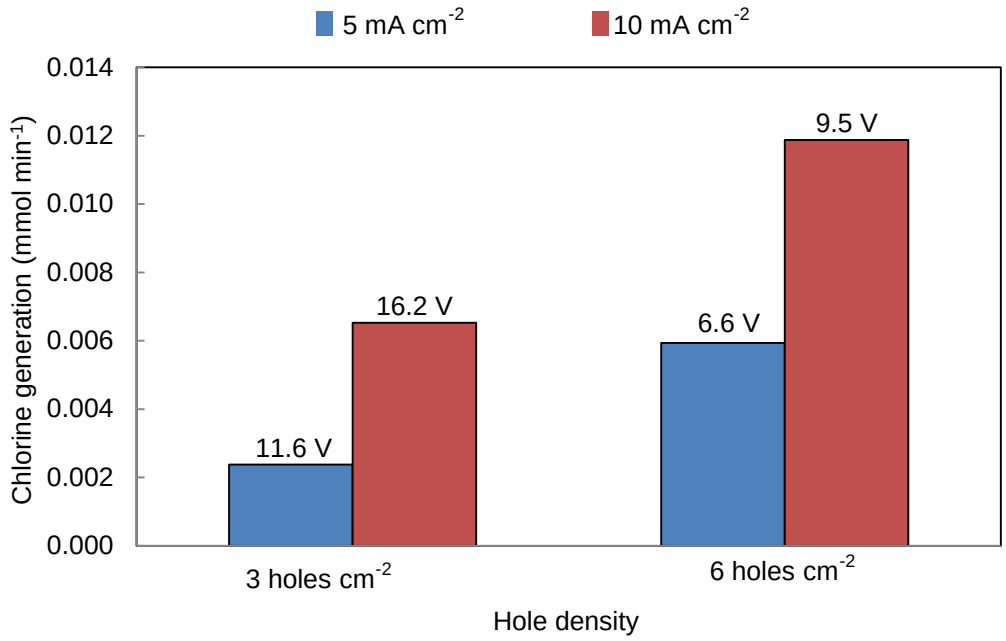

Figure 8.9 - Chlorine generation with increasing number of holes on the anode surface at 1.7 mmol/L NaCl concentration and a flow rate of 190 mL/min.

8.4 Discussion

It is clear from the data that has been presented that the presence of the insulating film, for certain flow conditions, has had a catalytic effect on the chloride electrolysis at low concentrations, increasing the current efficiency and lowering the energy consumption. Any agent that increases current efficiency at constant current density is an effect increasing the rate of the desired electrochemical reaction. That agent with thus be acting as a catalyst. Two factors could be contributing to the electro-catalytic effect. The presence of the field will result in an induced charge of the same sign as the electrode on the insulated surface in contact with the electrolyte solution (Calculations of free and bound charge densities on conducting and insulating surfaces is given in Appendix B.7). In the case of the anode this will be positive and will result in the formation of a double layer containing an excess on anions. The effect could be the result of the pre-concentration of the chloride ions by this mechanism. Alternatively or in addition to the higher electric flux associated with sharp rim edge could facilitate the electron transfer process resulting in oxidation at improved current efficiencies.

The electro-catalytic effect was observed only when the anode was insulated and flow was from cathode to anode. When the cathode was insulated or when flow was from anode to cathode, reduced current efficiencies and higher resistances were observed. Two factors could be contributing this result. Firstly, the cathodic reaction produces hydrogen gas. When the flow direction was such that the gas has to pass through the 1-2 μm gap between the insulating film and the exposed electrode, it is likely that some bubbles will become lodged around the perimeter of the perforation. Here they will obstruct the conductivity of the electrolyte, resulting in an increase in the cell resistance. Secondly, when flow is from anode to cathode, cathodic reduction of chlorine could occur. The absence of enhanced current efficiencies when flow is from anode to insulated cathode (pre-concentration of cations on the insulated surface should occur) can be attributed to the fact that sodium ions are not involved in the cathodic reaction. The cathodic reaction involves electrolysis of water.

Hydrodynamic considerations (Reynold's number) indicate that an adequate supply of chloride ions cannot be generated by bulk phase diffusion (Fick's first law) across the boundary layers of the capillary holes (Pletcher, 1984b). Pre-concentration of the chloride ions is required. This pre-concentration can be achieved by the formation of a double layer at the insulated surface due to the field induced surface charge. As the gap between the insulated anode surface and the exposed cathode is of the order of 1-2 microns and much less than the thickness of a double layer at the concentration used, the plane of shear will necessarily have to be within the double layer and close to the phase boundary. Ions pre-concentrated in the double layer will be swept towards the exposed rim of the anode and be further concentrated as flow is forced down the restricted volume of the perforation. The rim of the anode consists of a sharp edge where the electric flux will be much higher than that of a planar surface. Enhanced electron transfer can be expected in this region of high flux.

Figure 8.10 illustrates the essential features of pre-concentration mechanism. Chloride anions are pictured as being adsorbed (in a double layer) at the insulating film and then swept towards the anode perforation where they become concentrated and discharged at the sharp rim edge. The increased concentration of

the chloride anions will have the effect of reducing the concentration overpotential. It will also provide a more conducting path down the 50 micron deep perforation in the insulating film, thus reducing resistance overpotential. Increased flux at the sharp perimeter edge will reduce the electron transfer overpotential.

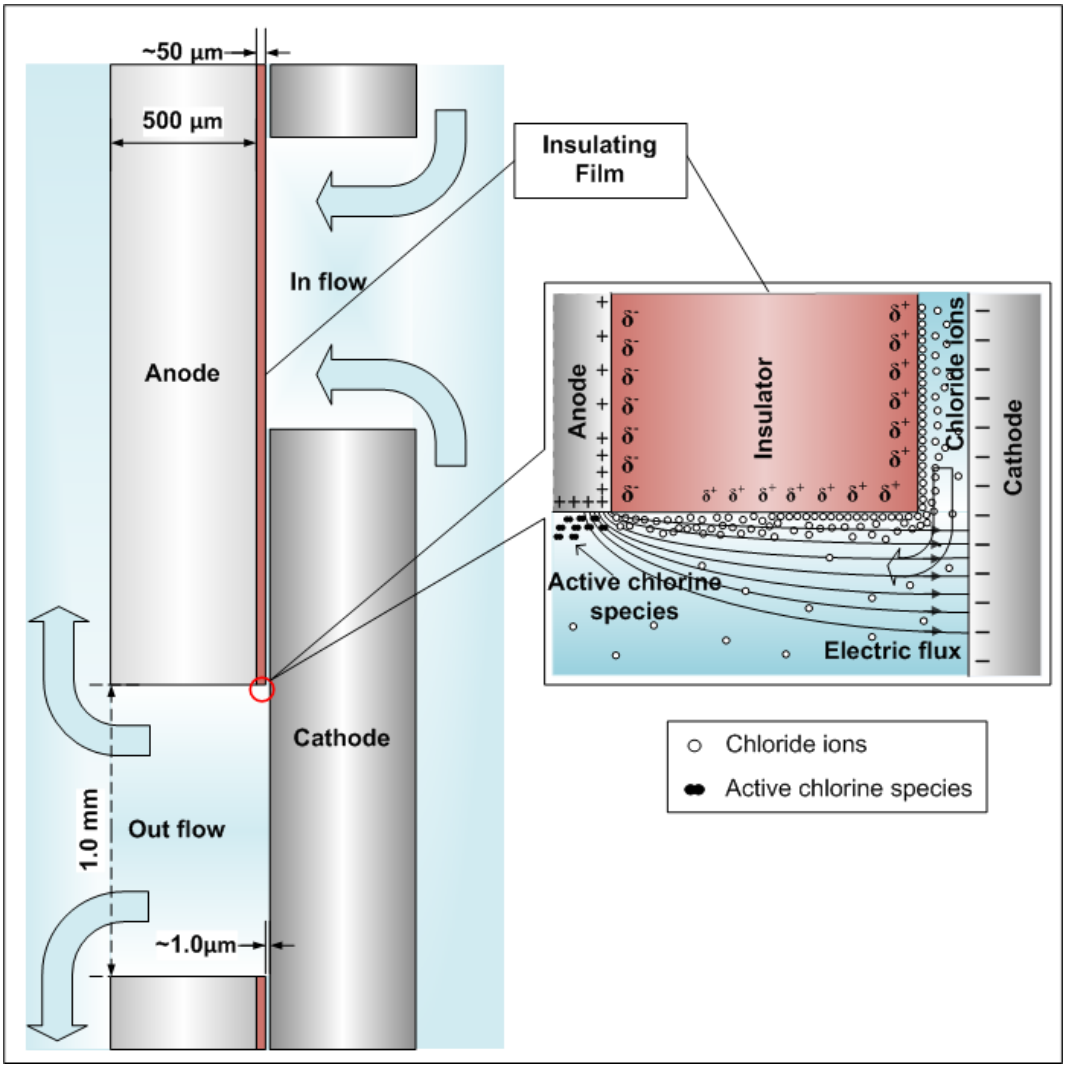

Figure 8.10 - Schematic showing details of field and transport effects at the insulated anode (not to scale).

A practical illustration of the usefulness of the effect is provided by data for electro chlorine generation for disinfection. Chlorine generation rate in the PEFT cell with non insulated electrodes and the same 50 µm inter-electrode gap (6

holes/cm^2, 5 volts, 1.7 mmol/L NaCl, flow rate of 190 mL/min) was 0.02 mmol/min at 95 kWh/kg of chlorine. A similar chlorine production rate under these conditions but using the insulated electrode system should be achievable at 47 kWh/kg of chlorine using 12 holes/cm^2.

In the experiments using stainless steel anodes some evidence of corrosion at the perforation perimeters was observed. Stainless steel is not the optimum anode metal. In practical applications dimensionally stabilised titanium anodes would be preferable.

8.5 Conclusion

- Application of an insulating film to the anode of a PEFT cell has achieved markedly, improved current efficiencies and reduced energy consumption at low electrolyte concentrations.
- This electro-catalytic effect could find application in the electrolysis of dilute electrolyte solutions such as inline electrochemical disinfection of drinking water.

Chapter 9: Non thermal electro-pasteurisation

9.1 Introduction

It was identified in Chapter 7 that the 50 micron inter-electrode gap PEFT cell should be capable of generating quite high electric fields (<10 kV) even at the low applied voltage used. Such fields can cause reversible electroporation. To achieve irreversible electroporation or to facilitate complete inactivation of microbes, the high fields required could be achieved by applied voltages of less than 100 V.

To achieve electroporation, the suspending medium must be conducting and in electrical contact with, ideally, inert electrodes. However, when high potentials are applied to highly conducting fluids (such as liquid foods), high currents flow and high ohmic heating will result. In the absence of cooling, microbial inactivation is then likely to be dominated by thermal effects. In the literature on pulsed electric field (PEF) treatment systems, external cooling is needed and a large amount of energy is wasted. The energy lost and the cooling required further add to the processing cost. The high voltages required also pose safety issues (Lung, Masanet, & McKane, 2006; Machado, et al., 2010; Zhang, et al., 1995). Uchida et al. demonstrated that to a large extent these problems can be overcome by minimising the inter-electrode gap to 100 μm and reducing electrode area to approximately 100 mm^2 so that the required field strength could be achieved at lower applied voltages, with lower currents, greater safety and less expensive electronic equipment (Uchida, Houjo, & Tochikubo, 2008).

Following from this work of Uchida, it seemed possible that repeated exposures of limited duration to a DC field could be made as effective as a pulsed field. The use of DC field would allow further simplicity and cost reduction. The flow through configuration of a PEFT cell allows both continuous operation and repetitive doses of limited duration by successive cycling of the suspended organism through the field between the electrodes, achieving a pulse effect, although with very much increased pulse widths and reduced pulse frequencies.

To determine if microbe inactivation could be achieved using an electrode system of much reduced active area, at realistic ionic strengths, without excessive current flow and the associated problems of high energy consumption and ohmic heating.

9.2 Materials and methods used for electro-pasteurisation

9.2.1 Modification of the PEFT cell assembly

The 50 micron inter-electrode gap PEFT cell was customized to reduce the active electrode area and to allow higher voltages with small currents at high conducting fluids. In initial experiments, the new cell consisted of stainless steel electrodes with 1 mm holes drilled in a hexagonal array and where a film of Duraseal containing 100 µm diameter holes was applied to the anode.

In later work a titanium anode was used and the insulating material was a self organised TiO_2 nano film generated in-situ by anodizing in 1 mol/L $(NH_4)H_2PO_4$ (fluoride free) as described in detail in Chapter 2, Section 2.1.1. The inter-electrode gap was maintained at 40 µm using Duraseal spacers. Fortuitously the accelerated growth of the film in the higher field associated with perforation rims resulted in a less coherent TiO_2 deposit which was easily removed upon gentle abrasion exposing a narrow conducting surface a few microns wide. This avoided the need to re-drill the perforations and left them with a well defined conducting edge. The electrodes were arranged so that a staggered configuration of symmetrically placed holes was obtained and flow paths between cathode and anode holes were minimised and uniform (3.5 mm). The hole pattern and layout of the cell is illustrated in Figure 9.1.

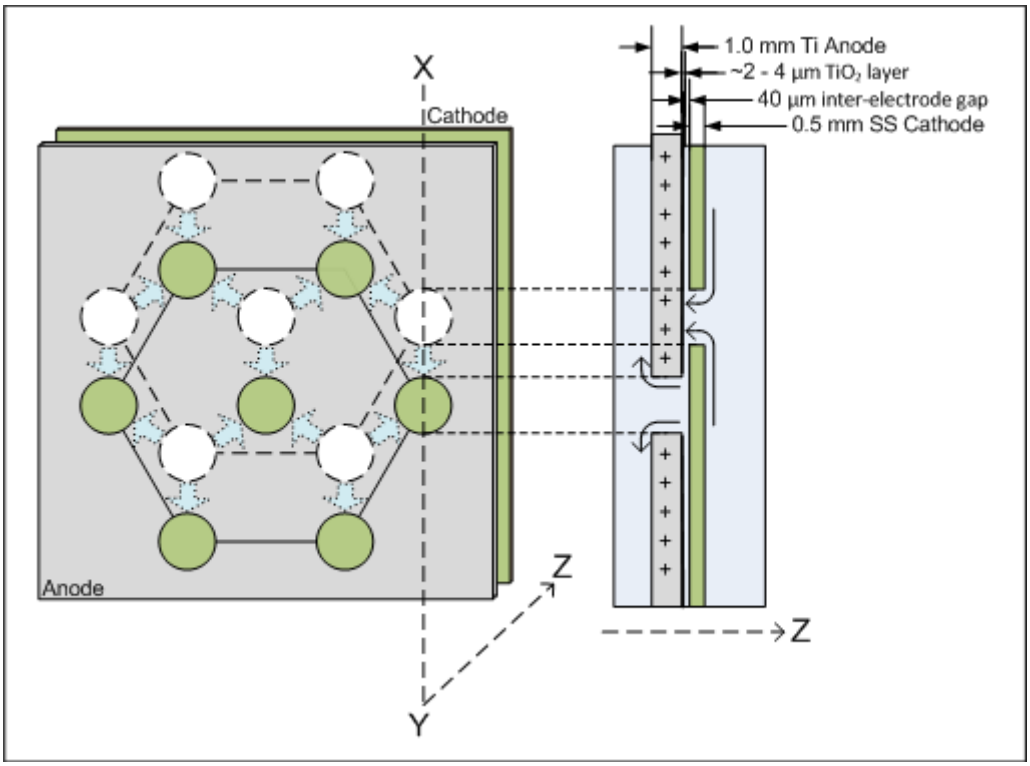

Figure 9.1- Schematic showing a section of the staggered hexagonal pattern of electrode perforations, the insulating layer and the flow pattern between cathode and anode (not to scale).

Scanning electron micrographs of a perforated titanium electrode is given in Figure 9.2, image (a) shows a perforation on the titanium electrode before the anodizing carried out and image (b) shows an edge of the same perforation anodized to form titanium oxide coating. The occurrence of globular oxide growth is not to be seen at the edge of the rim where excessive growth formed large globules which had fallen off making a conducting rim edge.

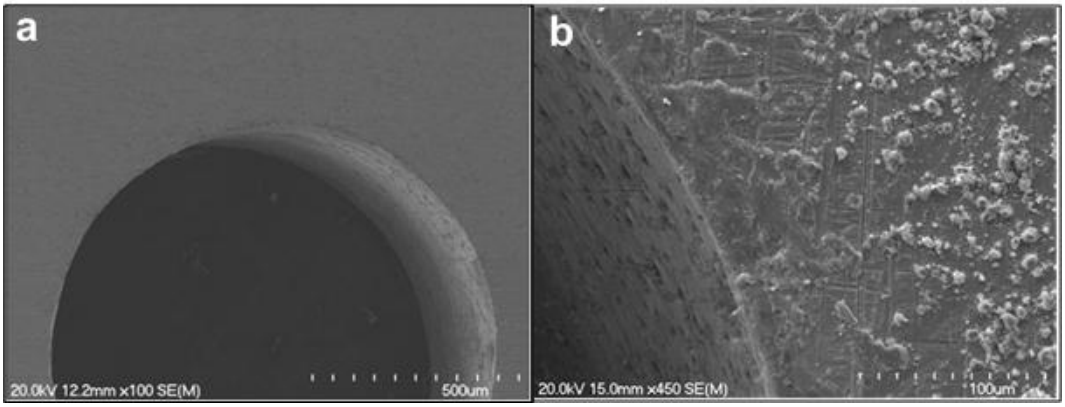

Figure 9.2 – SEM images of a perforation on the titanium electrode: (a) without anodizing and (b) an edge of a perforation after anodizing.

9.2.1 Electrical power supply and instruments

The PEFT cell was powered by two direct current sources connected in series applying voltages (1. Dick-Smith Electronics, 0 – 30 V, 5 A, 2. Topward 6303A, 0 – 60V, 3 A both having regulated DC power with variable current limit, input 230 – 240 V AC 50 Hz) through an ammeter (Fluke 73 III Multimeter) and a voltmeter (Fluke 77 Series II Multimeter) to measure the current and voltage. A variable flow peristaltic pump (Watson Marlow 504S, with regulated DC power supply) fed water to the cell, and the out flow was collected aseptically in a beaker and re-circulated. The temperature was monitored using a mercury bulb thermometer (-10 to 110^{o}C) and a stopwatch was used to record the run time. The pH and conductivity was measured and maintained accordingly.

9.2.3 Treatment media and microorganism

A high conducting treatment media (4.2 mS/cm and pH 5.7 at 19°C) was prepared to mimic a fruit juice using doubled distilled water and Na_2SO_4 (BDH Analar) salt. The detail description of materials and preparation of microorganisms and microbiological analysis is given in Section 2.4.13, Chapter 2.

9.2.4 Experimental procedure

A known volume (150 mL) of the treatment medium spiked with *E. coli* initial concentration of 4×10^6 CFU/mL was taken to a sterilized beaker and allowed to pump through the electrolytic cell at a constant flow rate (190 mL/min) where a constant high DC electric field was applied. DC voltages were applied from 50 to 90 at 10 V increments generating electric field strengths of 12.5 to 22.5 kV/cm (inter-electrode gap 40 µm). Each increment was a separate experiment. The current through the cell was recorded. The samples were recycled through the cell 20 times to achieve adequate microbial inactivation levels. After 20 cycles a portion of the sample was collected to a sterile bottle and within 2 hours microbiological tests were carried out to determine the survival fraction of *E. coli.*

9.3 Microbial inactivation by electroporation

9.3.1 Preliminary results

The possibility of inactivating microbes by limited exposure to a high DC field was indicated by an experiment in which a chloride free *E. coli* suspension was passed through the 50 µm gap between a stainless steel cathode and a graphite anode of a PEFT cell similar to that described in Figure 3 in Section 3.1.4. A 2 log inactivation was achieved at 40 V applied DC voltage (8 kV/cm field strength) after an estimated exposure time of 0.26 s which resulted after a single cycle in 16^{o}C ohmic heating. To overcome the heating effect current flow was limited by covering the anode surface with an insulating film leaving the capillary rims of the perforations exposed. Best results were obtained with a stainless steel anode and Duraseal to provide the insulation. Experiments with this system where the spiked solution was passed 5 times through the cell gave a 2 log microbial inactivation at the maximum field of 12 kV/cm^2 with ohmic heating of less than 4.5^{o}C after the 7 min duration of the experiment. However reproducibility between runs was poor and subsequent deterioration of the insulating film in the vicinity of the perforation rim subsequently allowed increasing currents and excessive ohmic heating to occur. The results were sufficiently promising to warrant the development of the more robust TiO_2/Ti electrode system described in Section 9.2.1.

9.3.2 Microbiological inactivation using the Ti/TiO_2 anode

Results for an experiment in which the spiked solution was passed 20 times through the cell at a flow rate 190 mL/min with the Ti/TiO_2 anode at increasing voltages and field strengths are given in Figure 9.3a. The results indicate a kill of more than 6 log at 22.5 kV/cm field strength. Inactivation of *E. coli* starts at approximately 10kV/cm. The recorded maximum temperature was 42^{o}C at 22.5 kV/cm field strength after 20 cycles indicating that cooling was not required. The performance of the cell remained stable and reproducible over several hours of use.

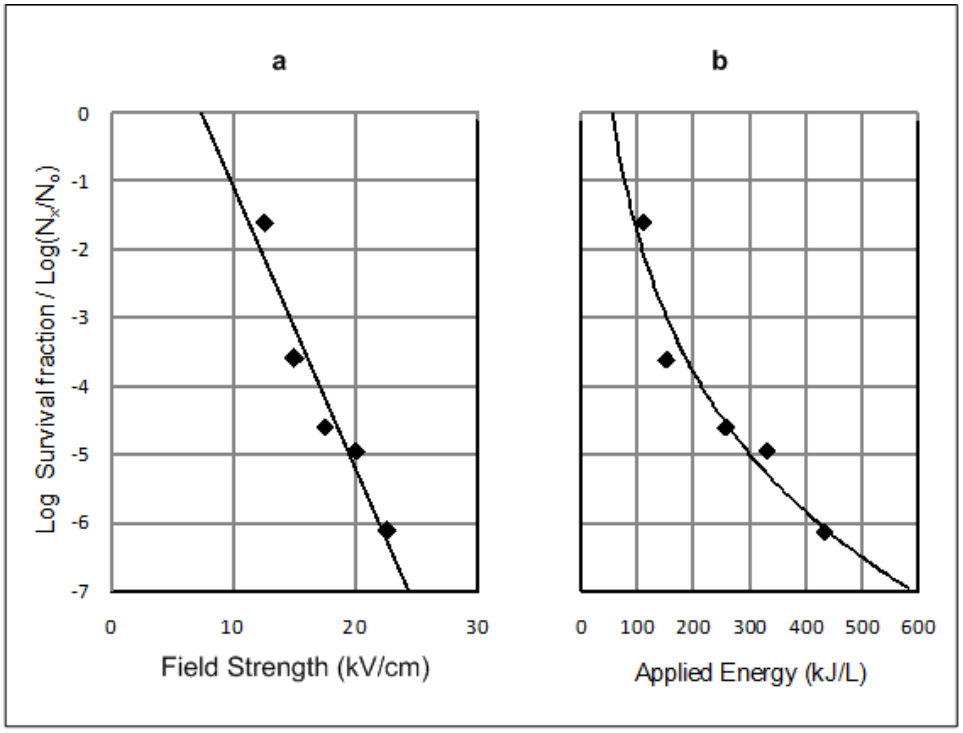

Figure 9.3 - a. Log survival fraction of E. coli with increasing electric field; b. Total energy applied to achieve log cycles of E. coli inactivation (190 mL/min flow rate after 20 cycles through the reactor, initial E. coli count [N_o] was 4 × 10^6 CFU/mL).

The plot of *E. coli* inactivation against energy consumed is given in Figure 9.3b. The total energy required to achieve a 6 log inactivation of *E. coli* was 430 kJ/L (0.12 kWh/L). This result is approximately three orders of magnitude less than earlier work in the field, comparable to more recent work and thermal pasteurisation (Gonzalez, 2010; Wan, Coventry, Swiergon, Sanguansri, & Versteeg, 2009; Zhang, et al., 1995).

The amount of energy consumed at increasing electric field strengths is given in Figure 9.4. The applied voltage between the electrodes is also given in the Figure at the corresponding datum point.

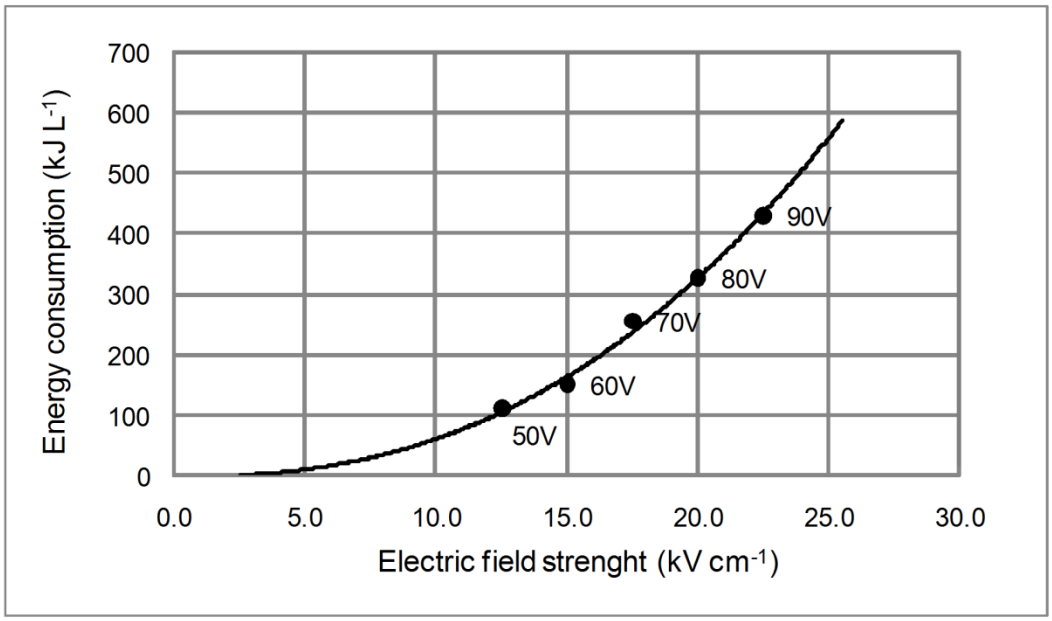

Figure 9.4 – Energy consumption and corresponding voltages for treatment at increasing electric field strengths.

9.4 Discussion

9.4.1 Inactivation at low applied DC voltages

The results confirm that bacterial inactivation can be achieved at relatively low applied DC voltages with modest power consumption and without the need for electronic pulsing characteristic of PEF systems. An effect equivalent to electronic pulsing is achieved by forcing flow through a highly defined localised field formed between the stainless steel cathode and the conducting rim of a TiO_2 coated anode (see Figure 9.5). After 20 such hydrodynamically controlled pulses a microbial inactivation above 6 log was achieved. According to Uchida et al., log kill data can be used to determine the fraction of killed bacteria per one pulse using the equation:

$$\gamma = 1 - \eta^{1/n} \ ,$$

where η = survival fraction after *n* cycles. Using the data from Figure 9.3 where the value of γ after 20 cycles at 22.5 kV/cm under the flow conditions described in Section 9.3.2, a value for the fraction of bacteria killed per pulse (cycle) of 0.5

was determined. This compares favourably with values derived from Uchida's work which ranged from 0.002 to 0.03. The increased per pulse kill fraction in the present work is consistent with the much greater pulse width employed and the upward trend in this quantity with pulse width, reported by Uchida et al. The 6 log kill observed might have been achieved with fewer passes through the cell. The flow rate and cell dimensions are such that for each pass through the cell the circulating fluid experiences the field for 77 ms and the average delay between exposures was 0.8 minutes. It can be concluded that broad, widely separated hydrodynamically generated pulses are at least if not more effective as the high frequency narrow electronically generated pulses that have been used in previous PEF work. Fields of the required strength (12.5 to 22.5 kV/cm) were achieved at low applied voltages (40 to 90 V) by forcing the flow through a reduced gap of 40 μm made possible by the insulating TiO_2 film on the anode. The insulating layer also reduced electrode area minimising current flow and hence ohmic heating. The large area to volume ratio of the cell, (250 cm^{-1}) allowed such heating that did occur to be dissipated during the passage of the fluid through the cell. From the energy dissipation per cycle under conditions of perfect thermal insulation, an ohmic heating of 6^oC could be anticipated. The observed temperature rise between inlet and outlet of the cell was 1.1^oC indicating that thermal effects were not involved in microbial inactivation and that heat loss during passage through the cell was adequate, without further cooling, to maintain the temperature below 42^oC after 20 cycles through the cell.

The nature of the TiO_2 film is of interest for two reasons. The first is that it is the instability of the coating formed at the capillary rims that allows the exposure to the underlying metal and hence the fabrication of ring electrodes of micron dimensions. Assuming the field extends vertically from the ring electrode, the width of this field will be of the order of a few microns. Thus the exposure time of fluid flowing with an average flow velocity of 1.06 cm s^{-1} will be of the order of milliseconds. The nature of the TiO_2 film is also of interest because while TiO_2 is of very low conductivity, its method of deposition on the Ti metal surface was such that even when the surface was evenly coated, some current still passed. This is due to micron size defects (Figure 9.6) in the oxide coating (Ghicov, et al.,

2005). During operation of the cell, the field created at these micro pores probably added to the field induced inactivation.

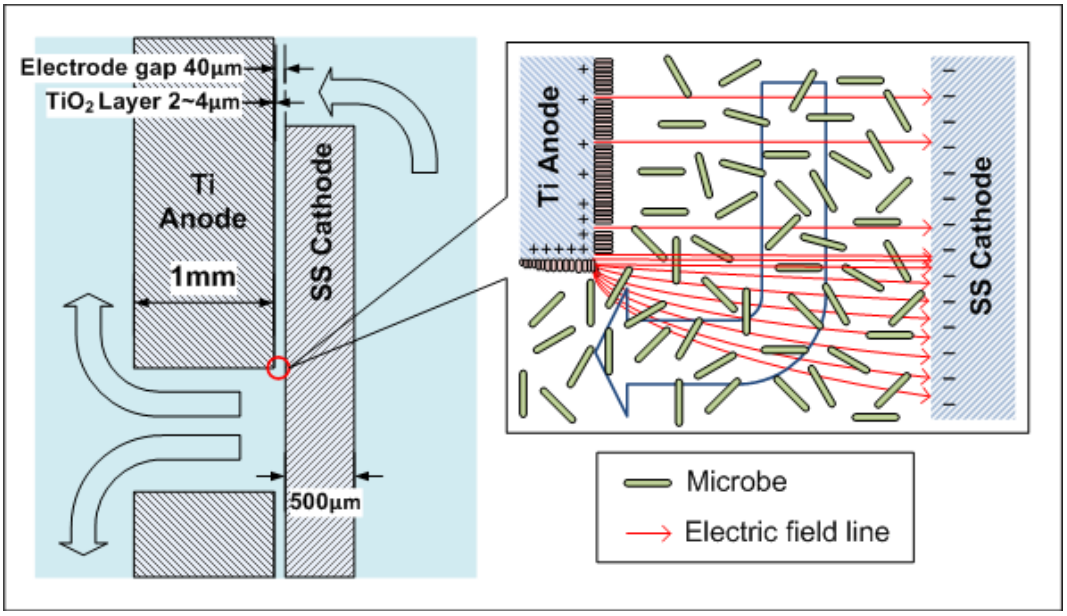

Figure 9.5 - A schematic diagram of the microbial inactivation process in the electrolytic reactor (not to scale) showing the postulated field from the perforation rim edge and the microelectrodes formed by the micro pores in the titanium oxide coating.

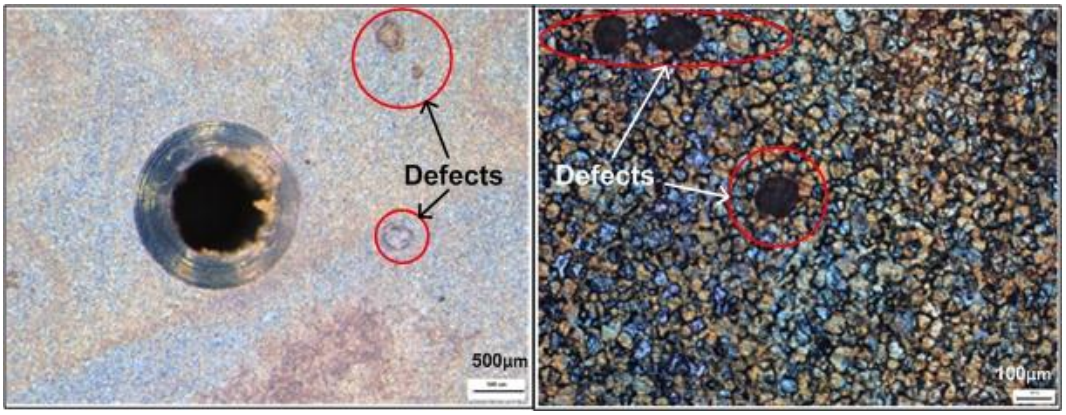

Figure 9.6 – Micrographs (optical) of the TiO_2 layer on the titanium electrode pointing out the defects on the oxide layer.

9.4.2 Possible applications

While in its present form, the system described is not suitable for application as a practical treatment process, never-the-less the effects observed suggest that an

alternative approach to the more widely studied PEF systems for non thermal electro-pasteurisation might be possible. Most PEF devices developed have ohmic heating problems and employ external cooling systems to maintain temperatures (Alkhafaji & Farid, 2007; Heinz, Alvarez, Angersbach, & Knorr, 2002). According to the present results a longer pulse width at a much lower pulse frequency can achieve a high level of microbial inactivation without external cooling. A system with the optimum number of appropriately spaced flow through electrodes in series should suffice to achieve continuous inactivation with a single pass through the device, eliminating the requirement of electronic pulse generators. Operating at relatively low voltages and without external cooling would make the device simple, safe and affordable. A remaining problem associated with any DC system, pulsed or continuous, is electrolysis and the effects of electrolysis products. In the present work chloride free suspensions were used to eliminate the possibility of microbe inactivation by chlorine species. For this reason bipolar pulses produced by periodic field reversal will be desirable in any practical system where chlorinated products have to be avoided. A simple polarity reversing switch (with or without pauses between switching) should suffice. An advantage of incorporating pauses between the DC signals would be reduced energy consumption and a further lowering of ohmic heating.

A further application of a more fundamental nature and of interest to gene technology might be the use of the PEFT (TiO_2/Ti anode) at lower voltages as a continuous flow device in the expanding field of electroporation. (Fox, et al., 2006; Geng et al., 2010).

9.5 Conclusions

- The development of a micro-gap perforated electrode flow through cell has allowed 6 log inactivation of *Escherichia coli* at applied electric fields of 22.5 kV/cm generated by 90 V DC supply at an energy consumption of 430 J/mL while recording a highest temperature at 42^{o}C without external cooling.

- The hydrodynamically generated pulses avoid the need for electronic pulsing and the increased pulse widths have achieved much higher per pulse kill fractions than previously reported.
- The reduced applied voltages, the elimination of the need for pulsed electric fields, avoidance of external cooling and the simplicity of the experiment bring commercial electro-pasteurisation one step closer.

Chapter 10: General discussion

10.1 Introduction

The design, development and application trials of the perforated electrode flow through (PEFT) cell system has made contributions to electrochemical cell design by devising cells with very small inter-electrode gaps. It has been demonstrated that the PEFT system offers potential solutions to water pollution problems and also provides novel ways for water disinfection. This chapter is an overview of the nature of these contributions and their possible extensions and applications.

10.2 Advantages of the PEFT cell design

The electrochemical cell designs used in different applications of electrochemistry look quite different, for example the rectangular open tanks used in electroplating, the parallel plates in the chlor-alkali industry and the complex designs in organic electro-synthesis. This is because in different applications, the relative importance of the figures of merit varies. Thus in electroplating, the quality of product is given priority over energy consumption because the charge used in plating is small. Conversely for power intensive processes like the chlor-alkali and aluminium production processes, current efficiency and energy consumption are important figures (Pletcher, 1984b). In spite of these differences there are general rules in cell design that need to be observed. The PEFT cell meets most of these design requirements.

10.2.1 Design features of the PEFT cell

Inter-electrode gap: The anode–cathode gap should be small. The PEFT cell designed for water purification with its 50 µm inter-electrode gap has achieved an inter-electrode gap smaller than any cell previously reported for such applications. The gap was further reduced by 10 µm to 40 µm in the electro-pasteurisation cell. The controlled use of spacers of precise thicknesses eliminated the need for

insulating mesh spacers and allowed a staggered hole configuration without compromising hydraulic flow. The narrowness of the gap minimises the active cell volume and hence maximises the ***space time yield***.

Current and potential distribution: The PEFT cell, in contrast to cells with porous or porous bed electrodes, has perforations drilled in solid plate electrodes. This allows flow through while maintaining uniform current and potential distribution across the electrodes. The staggered arrangement of the symmetrically drilled hexagonal hole pattern both allows the highest potential hole density and facilitates electrolyte flow through short and symmetrical flow paths. Therefore the design does not require any counter-electrodes of complex shapes, auxiliary electrodes or non conducting shields to direct the current path.

Electrolyte transport regime: The transport of electrolyte species to the electrode is vital in electro-chemical reactions. Electrolyte flow and/or stirring is used to promote mass transport to the electrodes. The micron dimension inter-electrode gap in the PEFT cell generates highly turbulent flow paths (Reynold's number $Re > 10000$) creating excellent mixing at the active electrode areas. No stirring or additional mixing by baffles, beds of particles or other turbulence promoters is required.

Compatible material: The materials used in the construction of the PEFT cell can be chosen to be compatible with the intended applications. For example in the water treatment applications, the anode was graphite and the cathode was stainless steel to be compatible with potable water. Graphite as an anode is not ideal for chlorine generation because of overpotential and stability problems. This drawback can easily be addressed by the use of metal oxide coated DSA for the anode in future water treatment applications. Similarly, the Ti/TiO_2 anode used in the electro-pasteurisation cell was chosen to be compatible with food processing.

Simple and cost effective: A cell design should aim to achieve process requirements in a simple and cost effective manner. The electrode assembly is housed in a simple PVC casing making the PEFT cell a completely sealed pressurisable unit. When the electrodes are made out of graphite and stainless

steel the cost of the PEFT cell for a domestic supply capacity (3 m^3/day) would be approximately 150.00 $NZ (without the DC power source). With Ti or DSAs the cost would be no more than double this amount.

10.2.2 The flow through configuration and reduced gap

Most flow through cells are based on a parallel plate electrode configurations, where the electrodes are arranged horizontally or vertically. Parallel plate electrodes have good properties of current and voltage distribution but the inter-electrode gaps have been in the range of centimetres which makes them not energy efficient due the high resistance, the attempts to improve by reducing the gap did achieve good electrical efficiencies but required high pressure pumping to allow the electrolyte to flow by the electrodes. The PEFT cell uses parallel plate electrodes, but perforating the cathode and anode plates and staggering the perforations allows the electrolyte to sweep the electrode surfaces for a short distance between the perforations. The distances between the holes are determined by the whole density and are a few millimetres at most; hence there is relatively small hydraulic resistance. This feature means that the only limitation on electrode spacing is the need to avoid short circuiting. Reducing the inter-electrode gap to micron dimensions also reduced the effective volume in the reactor and the *electrolyte volume* to *electrode area* ratio improved which was beneficial for mass transfer processes. The micron dimension inter-electrode gap made the flow between electrodes turbulent which brought about good mixing without turbulence promoters.

10.2.3 Special effects from a micro gap PEFT cell

Reducing the inter-electrode gap to 50 µm in the PEFT cell produced electric field strengths of 1 kV/cm at low applied voltages. These were sufficient to cause reversible electroporation in microbes and enhanced the toxicity of chlorine produced electrochemically. The synergistic effect of electric field and electro-chlorination achieved 6 log inactivation of *E.coli* with a single pass at 10 mg/L of chloride ions in water. This result is superior to the limited work reported on the

synergistic effect of electric fields during electro-chlorination disinfection (Abderrahmane, Himour, & Ponsonnet, 2008; Drees, et al., 2003; Feng et al., 2004). Increasing the voltage to 50 V in the 50 µm gap PEFT cell, produced 10 kV/cm fields, sufficient to cause irreversible electroporation. This capability was used in the non thermal electro-pasteurisation experiments and found to be effective. The results obtained were much better than most pulse electric field (PEF) technology work reported (Alkhafaji, 2006; Barsotti, et al., 1999; Heinz, et al., 2002 ; Lung, et al., 2006; Toepfl, Heinz, & Knorr, 2007; Zhang, et al., 1995). Reducing the gap between the electrodes reduces the reactor volume relative to the surface area of the electrodes where the heat generated can dissipate effectively. In addition the low cell volume and flow through design means that all the sample is exposed to the field uniformly.

10.3 Chlorine mediated electro-oxidation

The PEFT cell has proven effective in generating chlorine from low conducting and low chloride containing electrolytes. Chlorine mediated indirect oxidation is the most common and effective mechanism employed in effluent treatment applications. Results from Chapters 4 and 6 have lent further support to the observation that electro-generated chlorine is more effective than chemical chlorine.

The chlorine generation efficiency was improved with the discovery of electro-catalytic effect reported in Chapter 8. Improved efficiencies of chlorine production will allow the PEFT cell to completely oxidize the naturally occurring iron and manganese of Waikato bore water after a single pass provided the chloride ion concentration is at least 250 mg/L of chloride ions in water. For those bore waters where chloride ion concentration is less than 250 mg/L, single pass and instant oxidation can be achieved by appropriate reduction of the flow rate to ensure the critical chlorine concentration is achieved. Alternatively an electrode stack could be used.

Figure 10.1 illustrates a proposed cell design incorporating an electrode stack along with an electro-floatation mechanism to separate the metal sludge. The separator makes use of the gas bubbles formed during electrolysis. The number of cells in series can be powered according to the level of contamination. The gap between the electrode pairs of the stack can be adjusted to provide optimum retention time to maximise chlorine utilisation. The first up flow column is connected to a gas vent to release large gas bubbles which might otherwise prevent the formation of a scum flotation layer. The oxidized effluent and remaining micro bubbles pass into a floatation column where coagulation and floatation occur. If the floatation velocity is greater than the over flow velocity then good separation should be achievable. Water draw off and sludge removal can be controlled by valves.

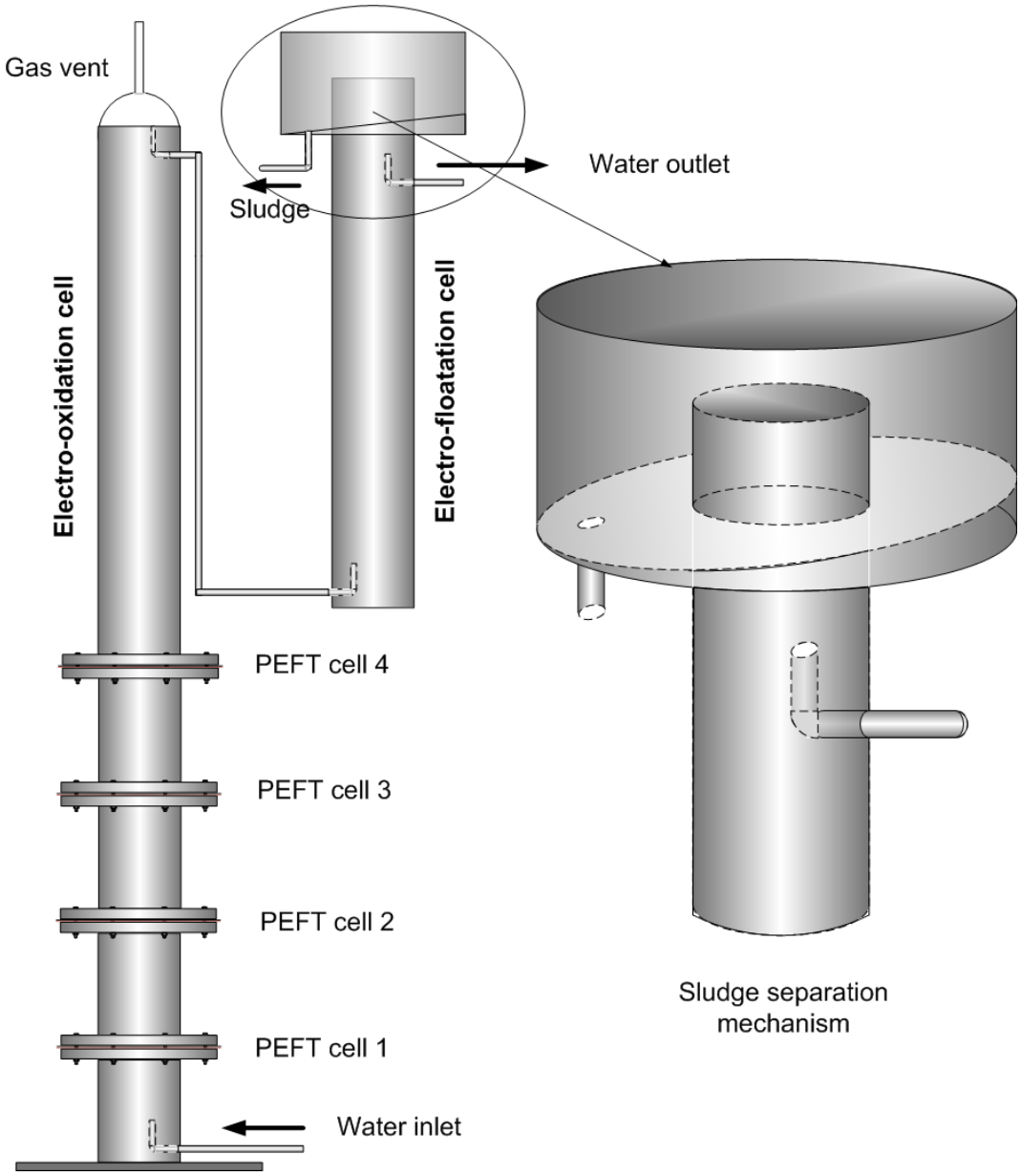

Figure 10.1 - Electrode stack electro-oxidation system coupled with an electro-floatation device for sludge removal

10.3.1 Scale up PEFT system for practical applications

Scaling up of electrochemical cells cannot be done by simple extrapolation of cell dimensions to accommodate high volumetric flow requirements. The mechanical constraints of maintaining precise control over the electrode gap will limit the scale up of the electrode area of a single unit. Desired increase in flow rates can best be achieved, at no increased energy cost, by operating optimum modules in parallel. For example, with the 90 mm diameter laboratory unit, a flow of 3

m^3/day was achieved at pressure of 33 kPa. A flow 30 m^3/day could be achieved by installing 10 units in parallel. A module based upon the laboratory system for applications of this sort is shown in Figure 10.2.

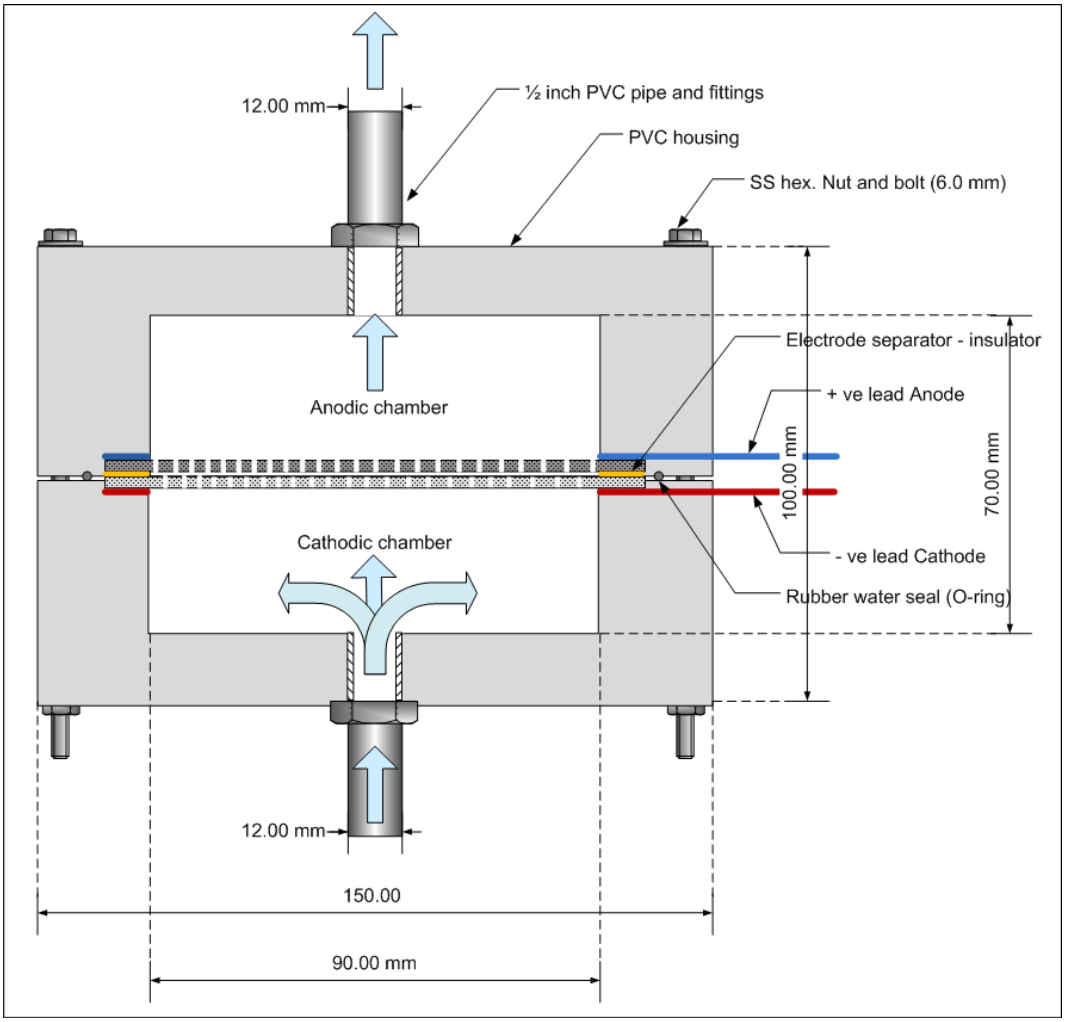

Figure 10.2 – A cross sectional diagram of the module of the PEFT cell having a capacity of 3 m^3/day.

A diagram of what the assembled cell might look like is given in Figure 10.3.

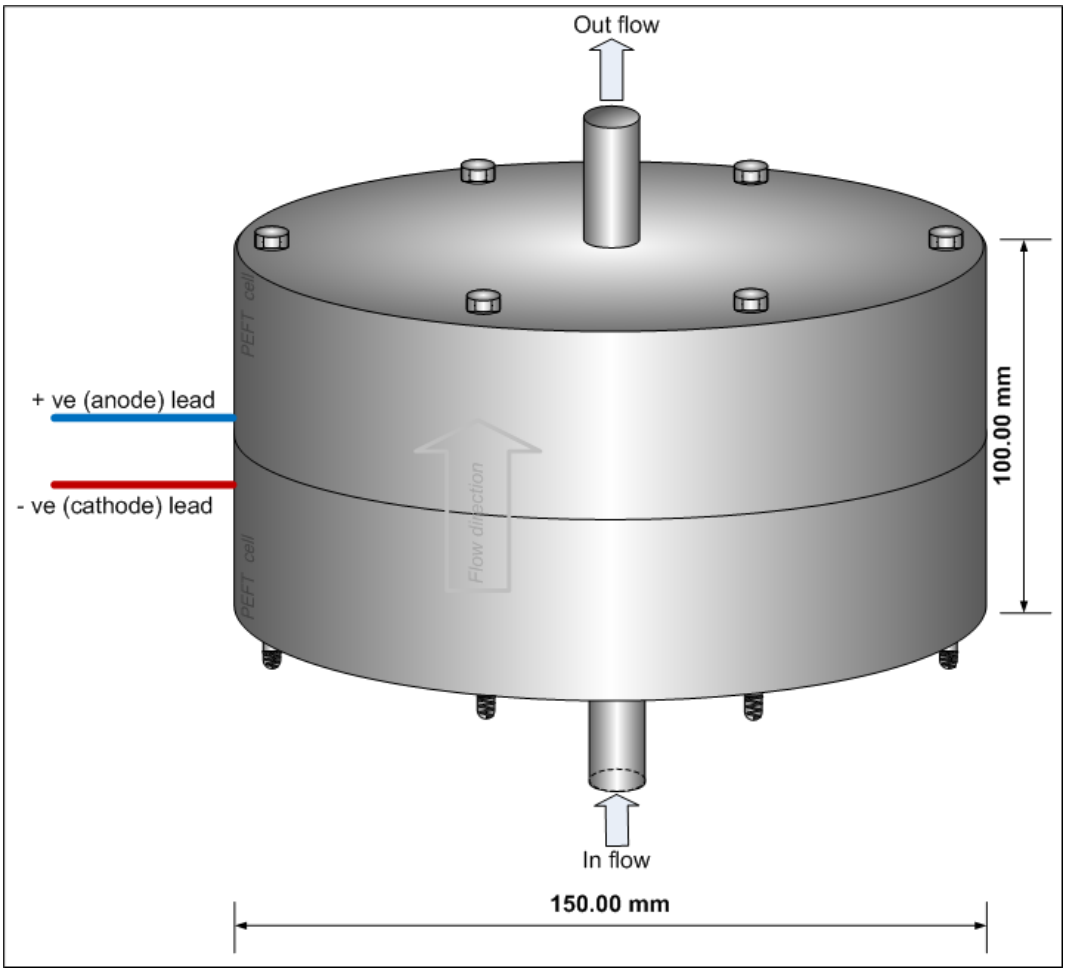

Figure 10.3 – A diagram of the assembled commercial PEFT cell

The representation of the assembled commercial PEFT cell given in Figure 10.3 and 10.4 illustrates an improved electrode contact system where the spiral wire system (see Section 2.1) is replaced by rim washers that offer more reliable contact.

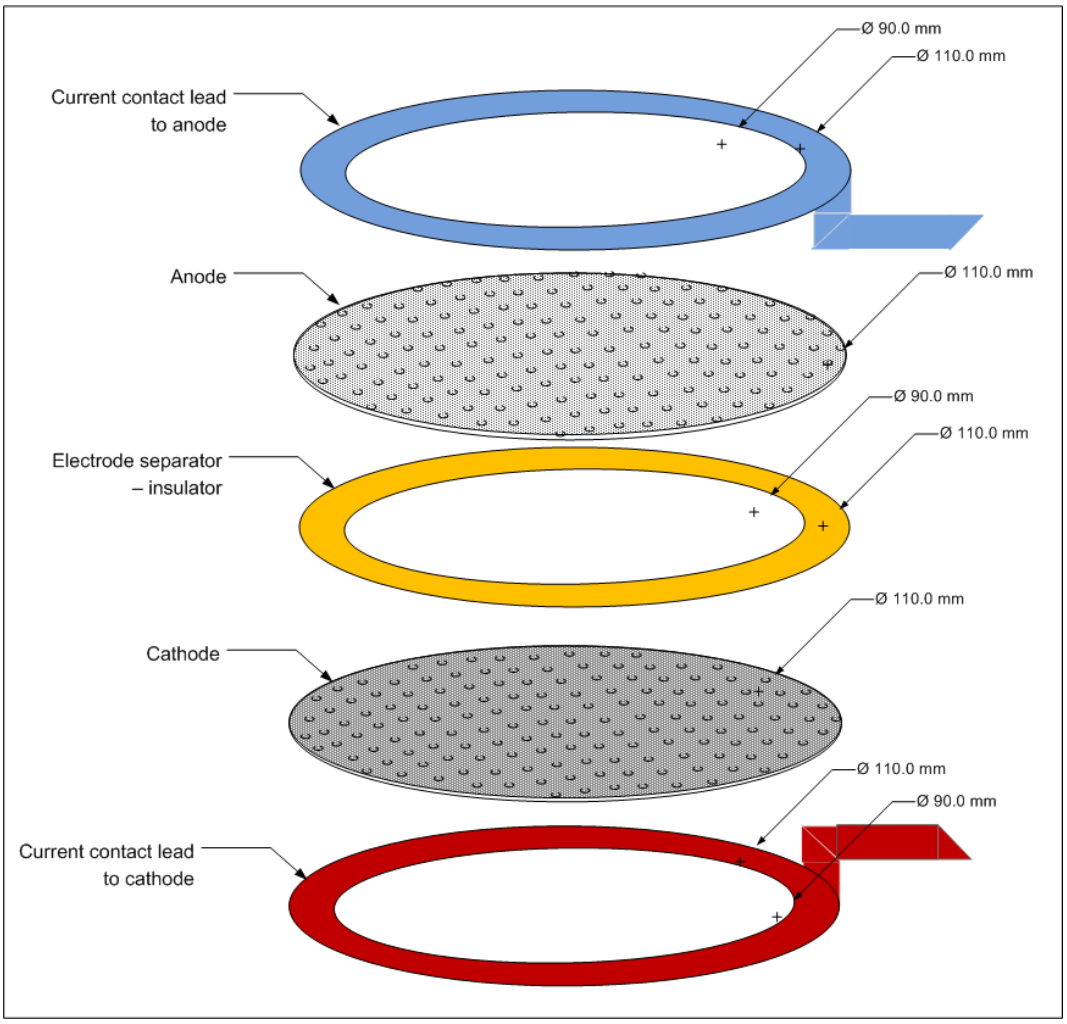

Figure 10.4 – The electrode assembly of a proposed practical PEFT cell design

10.3.2 Integration of the PEFT cell into water treatment systems

The usefulness of the PEFT cell for treating iron and manganese contaminated bore water and dye contaminated effluents has been demonstrated. It can also be used for chlorine generation and disinfection. It could also find application in other operating systems such as an oxidation step post biological treatment as a polishing step to remove the residual organics and colour, and also for the pre-treatment removal of iron and manganese that can cause fouling in membrane filtration technologies such as in reverse osmosis (RO) and ultra filtration (UF).

Diagrammatic representation of integration of the PEFT cell with other treatment processes is given in Figure 10.5.

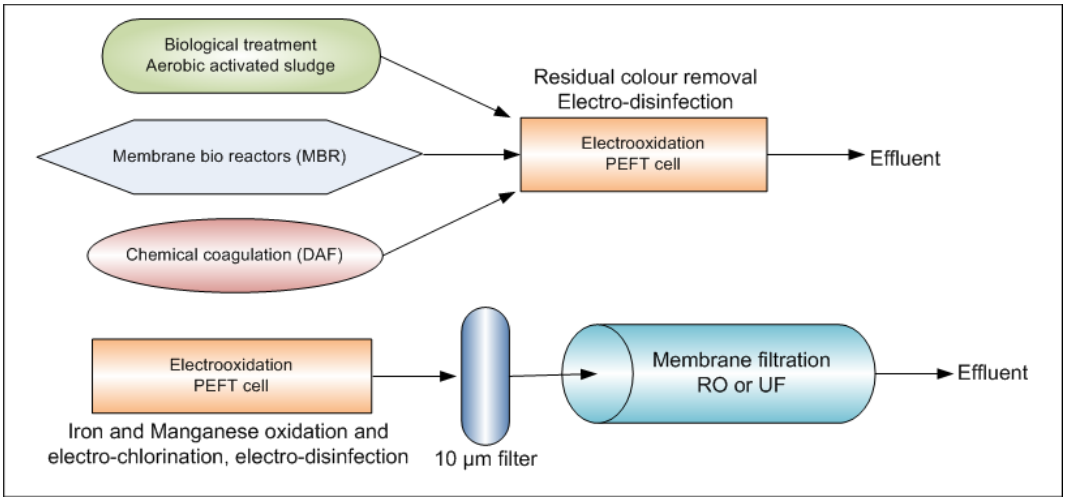

Figure 10.5 - PEFT cell as an electrooxidation device operating as post treatment (polishing step) and pre-treatment system.

Another application could be to provide a treatment system for small scale rural water supplies particularly those affected by iron and manganese contamination and generally to provide disinfection protection against microbial contamination. It has been demonstrated that the commercial prototype of the laboratory cell can deliver the 3 m^3/day necessary to meet domestic requirements. A schematic diagram of a system to remove iron and provide residual disinfection for water sources containing less than 20 mg/L of iron is given in Figure 10.6.

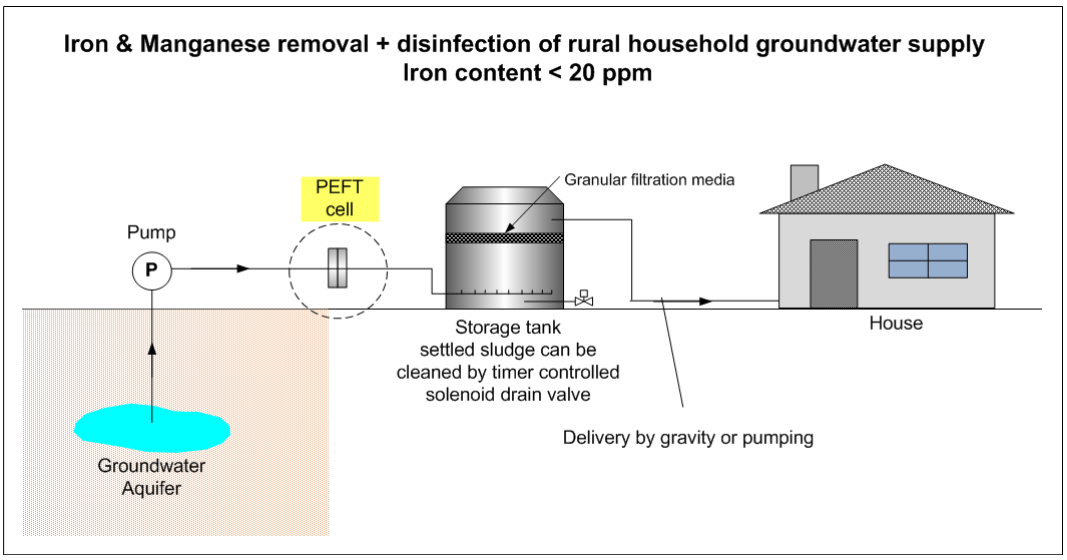

Figure 10.6 – The PEFT cell operated to oxidize iron and manganese from groundwater and to provide disinfection for a domestic water supply (iron content < 20 mg/L).

For iron contents higher than 20 mg/L, cost of treatment can be reduced by conventional air oxidation and the PEFT cell used for removing the residual iron and manganese that is often troublesome in the treatment of very high iron contamination. A schematic diagram is given in Figure 10.7 where most of the iron removal is achieved by accelerated air oxidation using a venturi mechanism coupled with a filter system (DEFERUM). The PEFT cell is integrated as a post oxidation device to remove residual metal ions and to provide the disinfection.

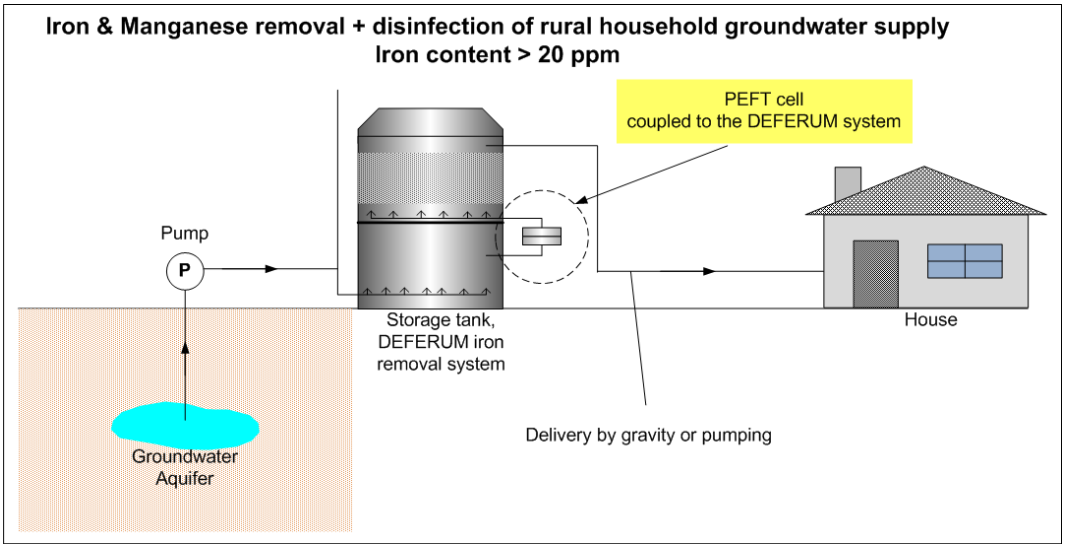

Figure 10.7 - The PEFT cell operated as post oxidation device to oxidize residual iron and manganese from groundwater and to provide disinfection for a domestic water supply.

10.4 Electrochemical disinfection

The single pass 6 log inactivation qualifies the PEFT cell as an inline *in-situ* disinfection device. It could be retrofitted to existing water supplies to provide safer water. A schematic diagram of integrating the PEFT cell as a disinfection device to a rural domestic water supply is given in figure 10.8.

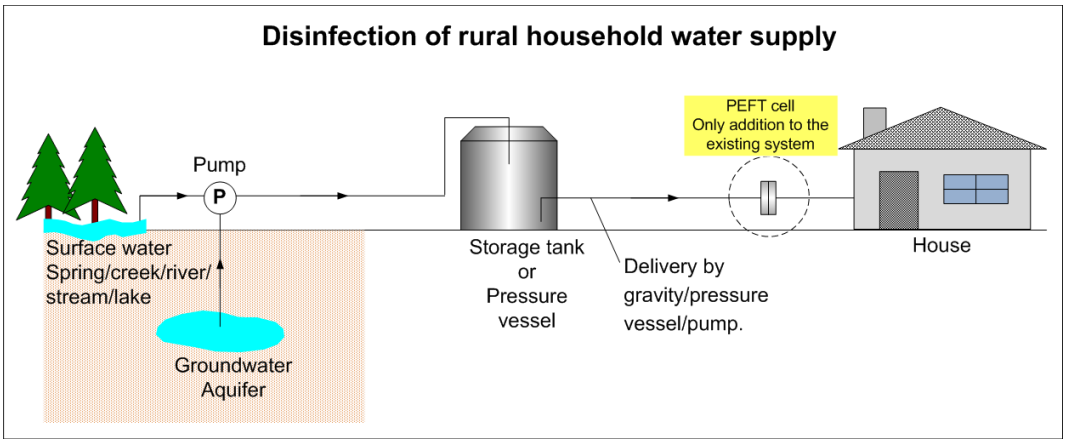

Figure 10.8 – The PEFT cell integrated to a rural domestic water supply as a disinfection device.

The special features of PEFT cell is that it offers disinfection at two levels of chlorine treatment: low chlorine by the synergistic field effect and conventional electro-chlorination. The advantage of the low chlorine treatment is that residual protection can be achieved with low risk of DBPs. Most other techniques developed for disinfection such as UV and Ozone treatment do not have this capability. Table 10.1 summarises the essential features of chemical, UV and PEFT disinfection and highlights the advantages of the PEFT system.

Generally chlorine is overdosed when the water has to be reticulated to considerable distances to maintain residual chlorine levels. The PEFT cell can provide a solution to this problem by operating as a booster in the reticulation systems avoiding excessive chlorine concentration.

Table 10.1- Comparing the PEFT cell with chemical and UV disinfection

	Chemical	**UV**	**PEFT Cell**
Capable of	Primary and residual disinfection	Primary disinfection only	Primary and residual disinfection
Disinfection effectiveness	Very high	Very high	Very high (against E'coli to be tested against other species)
CT factor	High	N/A	Low
Process of disinfection	Purely chemical	Purely physical	Physio-chemical
Residual effects	High (DBP's formation e.g.THM's)	Nil	Very low
Operation/application	Generate, handle, transport, or store toxic/hazardous or corrosive chemicals	User-friendly operation	User-friendly operation
Contact time	Minimum 30 mins.	Approx. 30 seconds	Approx. 2-3 mins. (To be confirmed, may be less)
Space required	High (storage, dosage)	Low (compact device)	Low (compact device)
Possibility of reactivation	Nil	Sometimes repair & reverse (dark repair)	Nil
Supply water quality	Able to treat turbid & TSS containing water	Need high quality w.r.t. turbidity and TSS (<30 mg/L)	Able to treat turbid & TSS containing water
Cost of treatment Depends on the quality of water	10-20 cents/m^3	Approximately 1.0 \$/m^3 (this value differ product to product)	Approx. 7 – 10 cents/m^3 ($3m^3$/day cell)

CT = concentration x time, DBPs – disinfection by-products, THMs - Trihalomethanes

10.5 Other applications

Another novel application is a possibility that further development of the power supply to provide a bipolar pulsed electric field will allow chlorine free disinfection of water and non thermal electro-pasteurisation of fluid foods. The results of Chapter 9 have demonstrated that 6 log inactivation can be achieved by 20 hydrodynamically generated pulses of a DC field for systems where chlorine was rigorously excluded. For chloride containing systems a bipolar square wave pulse with a moderate frequency (100 Hz) and pulse widths of milliseconds should achieve the same effect in a single pass without electrolytic production of chlorine. The residence time in the cell is sufficient to provide at least 20 pulses with such a system. The use of a delay between pulses will reduce energy consumption and ohmic heating effects.

Electroporation is a research area that is receiving wide spread interest. The PEFT cell provides a continuous flow electroporation device for gene transfection and similar applications. Its considerable advantages in such an application are likely to be that, unlike existing micro systems (Fox, et al., 2006; Geng, et al., 2010; H. Wang, et al., 2006), it is a continuous flow device capable of high flows and all sample is uniformly treated.

Chapter 11: Summary and Conclusions

11.1 General conclusions

This thesis describes the development and applications of a novel micro-gap perforated electrode flow through (PEFT) electrochemical cell. It is an undivided cell with an inter-electrode spacing reduced to micron dimensions. The reduced inter-electrode gap reduces cell resistance, improves electrical efficiency and allows economic electrochemical processing of low conducting electrolytes such as natural water and industrial effluents.

11.1.1 Cell design

The staggered configuration of the electrode perforations provides a flow path through the cell of a few mm. The short flow path means that the inter-electrode gap can be reduced to 50 μm and less while maintaining adequate flow rates at modest pressures. The reduced resistance of the cell has made possible economic electrochemical treatment of solutions of low ionic strength such as natural water and industrial effluents.

11.1.2 Treatment of Waikato problem iron waters

Chlorine electrochemically produced by the PEFT cell was found to provide a rapid, effective and efficient oxidiser of the iron and manganese contaminants in Waikato's problem bore waters. Electrochemically produced chlorine was found to be superior to chlorine added as calcium hypochlorite. Rapid electrochemical oxidation prevents the formation of stable colloids protected by the naturally occurring silica and organic content of the water. While THMs were formed during the electro oxidation, the levels were similar to those formed with calcium hypochlorite oxidation and were well within New Zealand drinking water guidelines.

11.1.3 Chlorine production

Even with low cost and less than optimum graphite anodes, the PEFT cell was an efficient electro chlorine generator. A 240 μm gap PEFT cell produced chlorine from a solution of 0.5 mol/L NaCl at commercially viable current efficiencies and energy consumption. When operated using water with 250 mg/L chloride (in the natural water range), sufficient chlorine to effect disinfection was achieved at less than 12 volts. The partial insulation of the PEFT cell anode had the effect of markedly improving current efficiency and reducing energy consumption at low electrolyte concentrations.The PEFT cell with a partially insulated anode produced sufficient chlorine to disinfect water where chloride levels were as low as 50 mg/L. This electro-catalytic effect could find application in the electrolytic treatment of dilute electrolyte solutions such as are found in inline *in-situ* electrochemical disinfection of drinking water. Further improvement of efficiency of the system can be anticipated by the use of metal oxide coated DSAs for the exposed part of the anode.

11.1.4 Treatment of industrial effluents

The usefulness of the PEFT cell for the treatment of industrial effluents was demonstrated by degradation of textile dyes. Complete single pass electrochemical decolourisation of indigo carmine (IC) dye containing 0.35 mol/L NaCl was achieved using the PEFT cell employing a graphite anode. Energy consumption was a competitive 0.8 kWh/m^3 or 8.3 kWh/kg of dye. This is an order of magnitude less than the energy consumption reported for previous work with graphite anodes. It is comparable or better than most colour removal work carried out using metal oxide coated DSAs and BDD anodes.

11.1.5 Electric field effects

The reduction in the inter-electrode gap to 50 μm and below has allowed the production of electric field strengths of greater than 10 kV/cm from applied voltages of less than a 100V. Field strengths between 1 and 10 kV/cm are known

to cause reversible electroporation whereas irreversible electroporation occurs above 10 kV/cm. The application of DC electric fields between 1 and 10 kV/cm have a synergistic effect on chlorine disinfection increasing the specific lethality of chlorine by two orders of magnitude. Fields of greater than 10 kV/cm achieved disinfection in the absence of chloride. Treatment with 20 hydrodynamically generated pulses of a DC field of 22.5 kV/cm achieved disinfection in the absence of chloride. These effects have been attributed to electroporation and could find application in non thermal electro-pasteurisation.

11.2 Recommendations for future work

11.2.1 Design and development of the PEFT cell

A more optimum hole pattern consisting of two complementary hexagonal hole densities, allowing totally symmetric flow through the cell when staggered, has been proposed (Figure 3.5 b). This configuration, which will allow maximum hole density and optimum flow distribution across the electrode surfaces, needs to be tested.

Hole density has been identified as an important parameter affecting cell performance. Preliminary investigations have indicated that cell performance improved with increased hole density. Maximum hole density is determined by hole size. Studies to determine optimum hole sizes and densities are suggested.

Dimensionally stable anodes (DSAs) with specialised catalytic coatings could improve the efficiency of chlorine production and need to be investigated.

Theoretical studies of the physics of field effects and the hydrodynamics of flow through the PEFT cell would be useful.

The role of the anode insulation film in the electrocatalytic effect needs to be studied. The possibility exists that further improvement can be achieved by application of ion specific coatings.

11.2.2 Applications

Metal ion removal from groundwater using the proposed multi electrode stack PEFT cell (Figure 10.1) should be investigated.

The scaled up version (3 m^3/day, see section 10.3) designed for practical application needs to be tested by field studies of electro-disinfection and electro-oxidation.

Confirmation that electroporation takes place at various applied electric fields generated in the PEFT cell can be obtained by appropriate microbiological studies. Control of electroporation in a PEFT cell could provide macro scale continuous flow electroporation for gene transfection.

Appendices

Appendix A

A.1 Monitoring the Ti electrode anodizing process

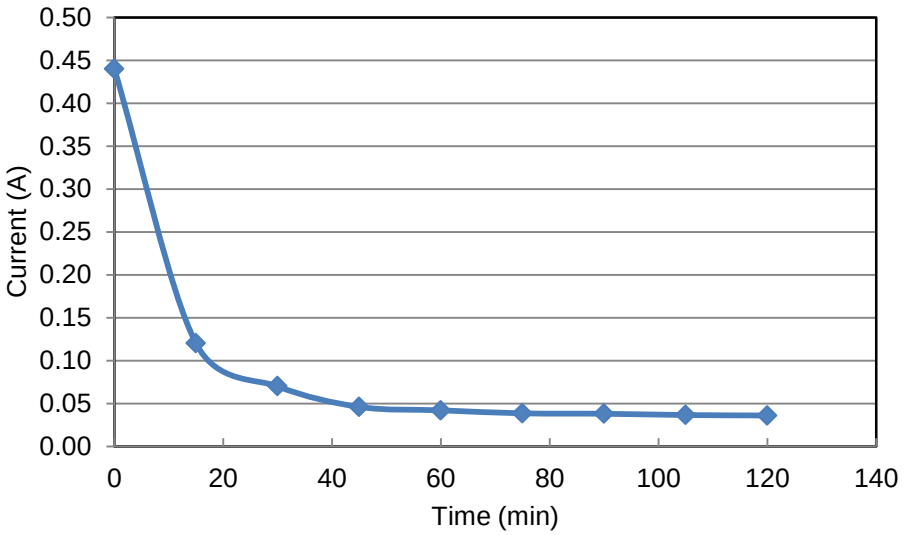

Figure A. 1- Reduction in the current flow with time during the anodizing of the titanium electrode at constant voltage (20V DC, conductivity of 1mol/L $(NH_4)H_2PO_4$solution 42.6 mS/cm)

A.2 SEM EDAX elemental mapping data on the anodized TiO_2 surface of the titanium electrode

The elemental mapping data given in Figure A.2 shows that oxygen, nitrogen and phosphorous coming from the anodizing process was uniformly distributed on the surface of the electrode.

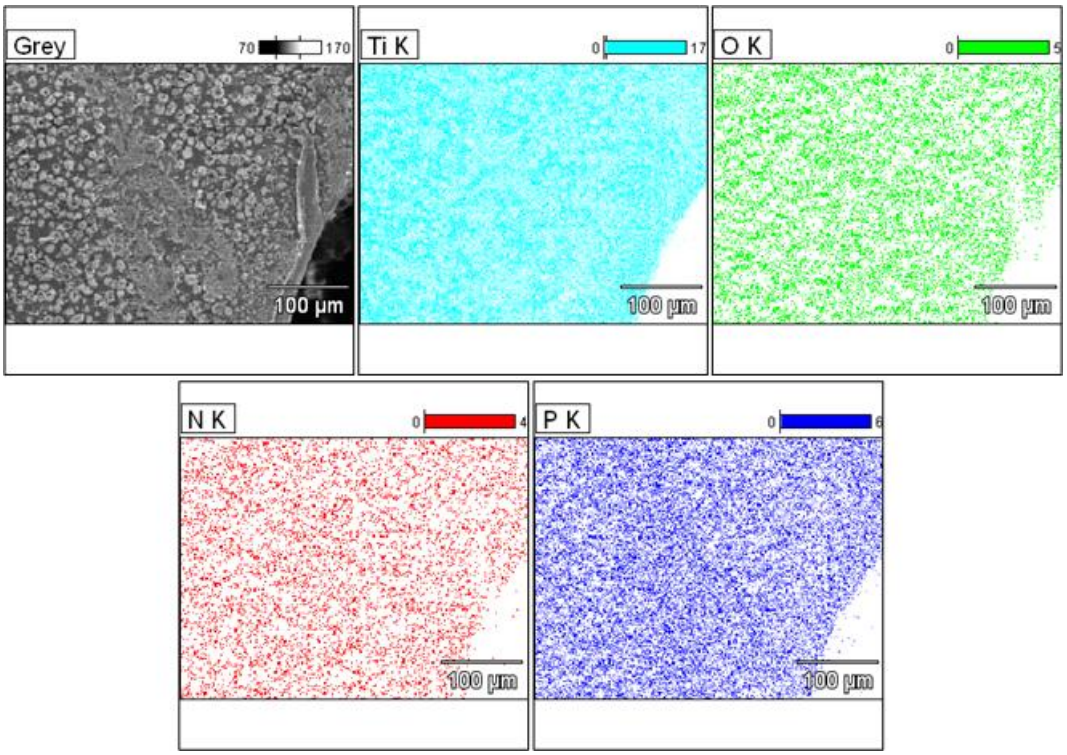

Figure A.2 - The uniform distribution of oxygen, nitrogen and phosphorous elements on the anodized surface of the Ti electrode

Taking a closer look at the globular growth points and carrying out an elemental mapping reveals that the globules are growths of oxides formed on the surface, see figure A.2.

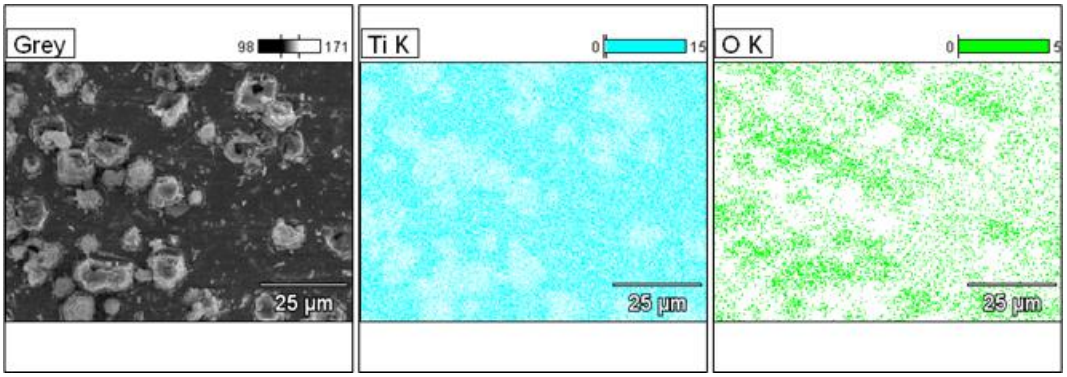

Figure A.3 – Elemental mapping of the globular growth on the anodized surface

A.3 Location of the bore well A

Figure A.4 – A map of New Zealand locating the bore well (A) used to extract water for groundwater treatment studies.

A.4 Analysis of ferrous ion concentration in water using 1, 10 Phenanthrolein spectrophotometric method

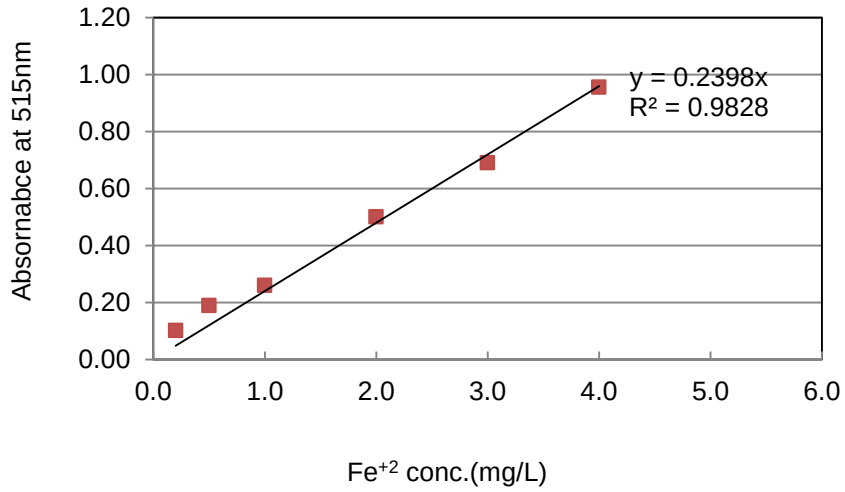

Figure A.5- Calibration curve of ferrous ion concentration versus absorbance at 515 nm.

A.5 Calibration plot for the analysis of chloride ions concentration in water using Mercury (II) thiocyanate spectrophotometric method

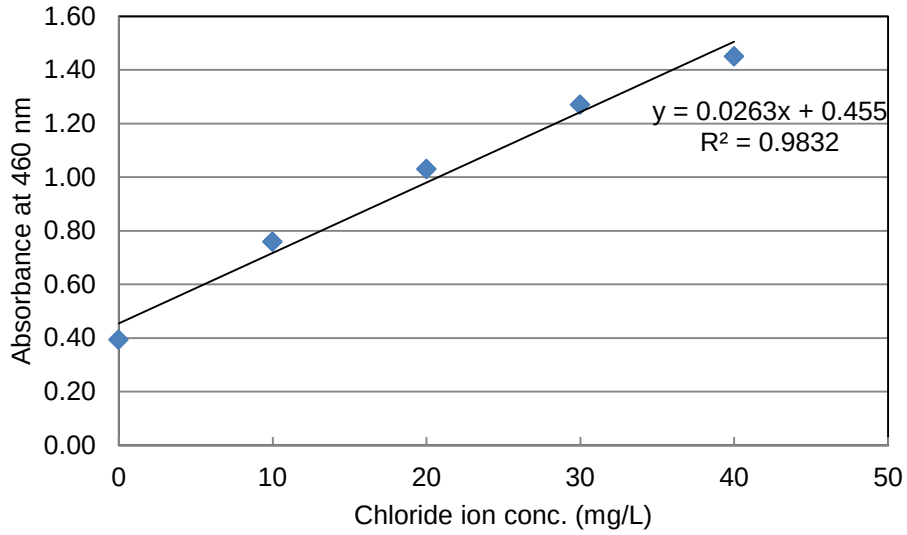

Figure A. 6- Calibration curve of chloride ion concentration versus absorbance at 460nm.

Table A.1- Commonly used chloride ion concentrations and unit conversions

NaCl concentration			
mmol/L	mg/L	mol/L	g/L
0.85	50	0.1	5.85
1.70	100	0.25	14.63
3.40	200	0.5	29.30
4.30	250	1.0	58.50
8.60	500	1.5	87.85
17.10	1000	2.0	117.00

A.6 Analysis of THMs in groundwater samples using HS SPME GC MS technique

A number of analytical techniques have been reported for the determination of THMs and other volatile compounds in water such as direct aqueous injection, liquid-liquid extraction, static headspace technique, dynamic headspace technique (purge and trap) and headspace solid phase microextraction technique (Choa, et al., 2003). The headspace solid phase microextraction (HS-SPME) is a simple solvent free alternative for the extraction of organic compounds (Pawliszyn, 1998). The HS-SPME integrates sampling, extraction, concentration and sample introduction into a single solvent free step. The principle behind SPME is the partitioning of analytes between the sample matrix and the extraction medium with subsequent sorption of analytes onto a liquid polymeric coating on a fused silica fibre. The analytes are subsequently desorbed in the injection port of a gas chromatograph (GC) (Stack, et al., 2000). Volatile organics in the sample are directly extracted and concentrated to the microextraction fibre. This technique has been successfully applied to the analysis of the THMs, BTEX, organochlorine pesticides, PAHs, PCBs and volatile organic compounds in water samples. It is fast, sensitive, inexpensive, portable and solvent free. No special sample preparation was required and sampling times were very short typically 2-5 minutes.

Figure A.7- A: SPME manual injection fibre assembly; B: Fibre assembly mounted on vial with fibre suspended in the headspace.

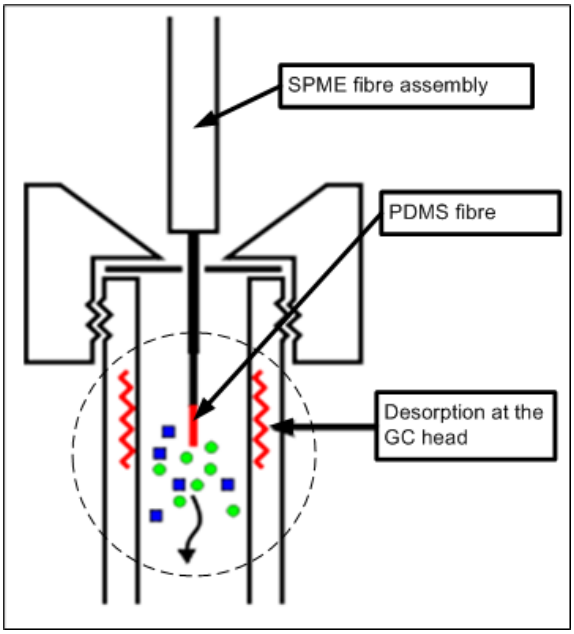

Figure A.8- Desorption of the THMs into the GC column

A.7 Calibration curve for the analysis of chloroform

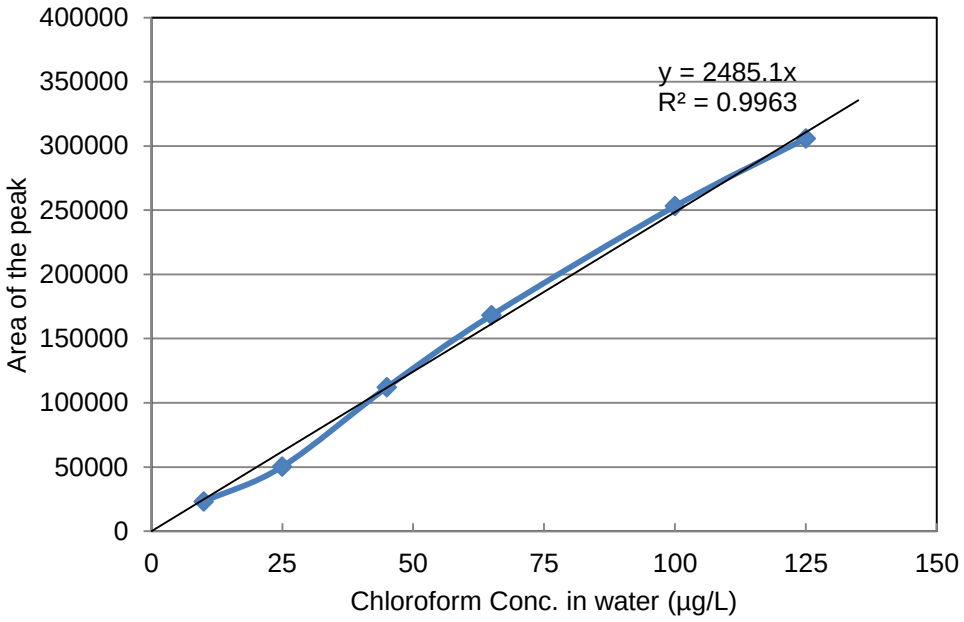

Figure A.9- Calibration plot for chloroform in water

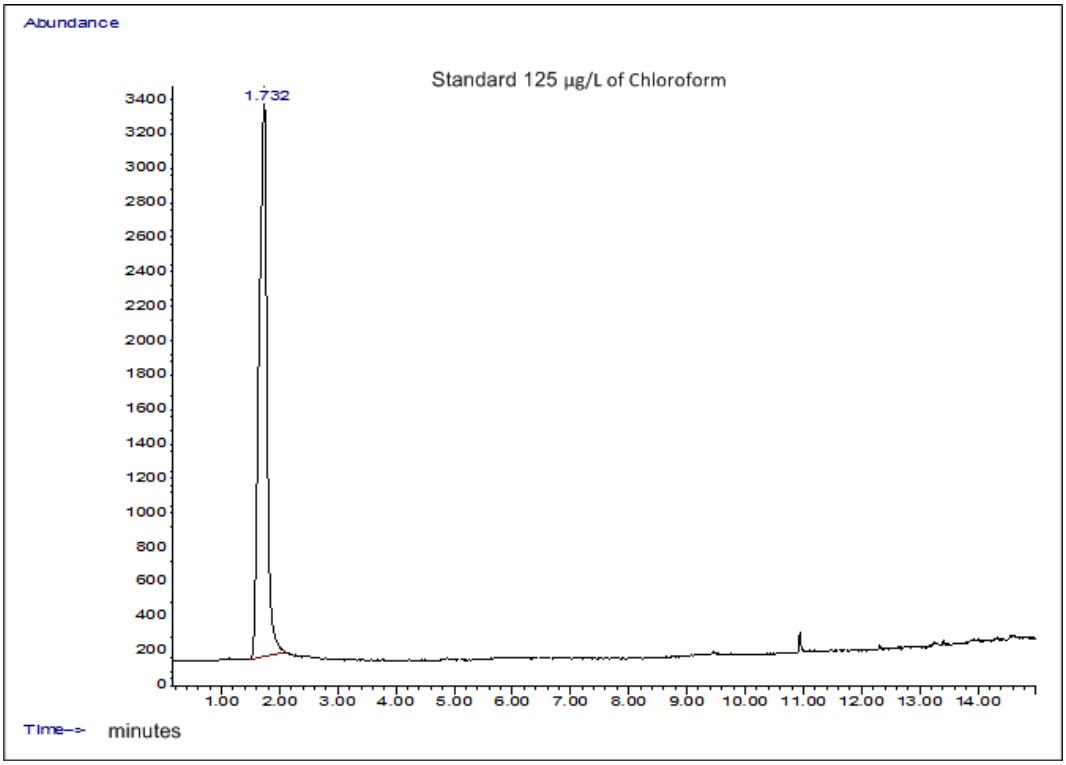

Figure A.10- A typical chromatogram of chloroform (obtained for 125 µg/L chloroform standard, GCMS in SIM mode, ions used were m/z 83, 85 and 87 with dwell time of 100 ms)

Appendix B

B.1 Cylindrical cell design

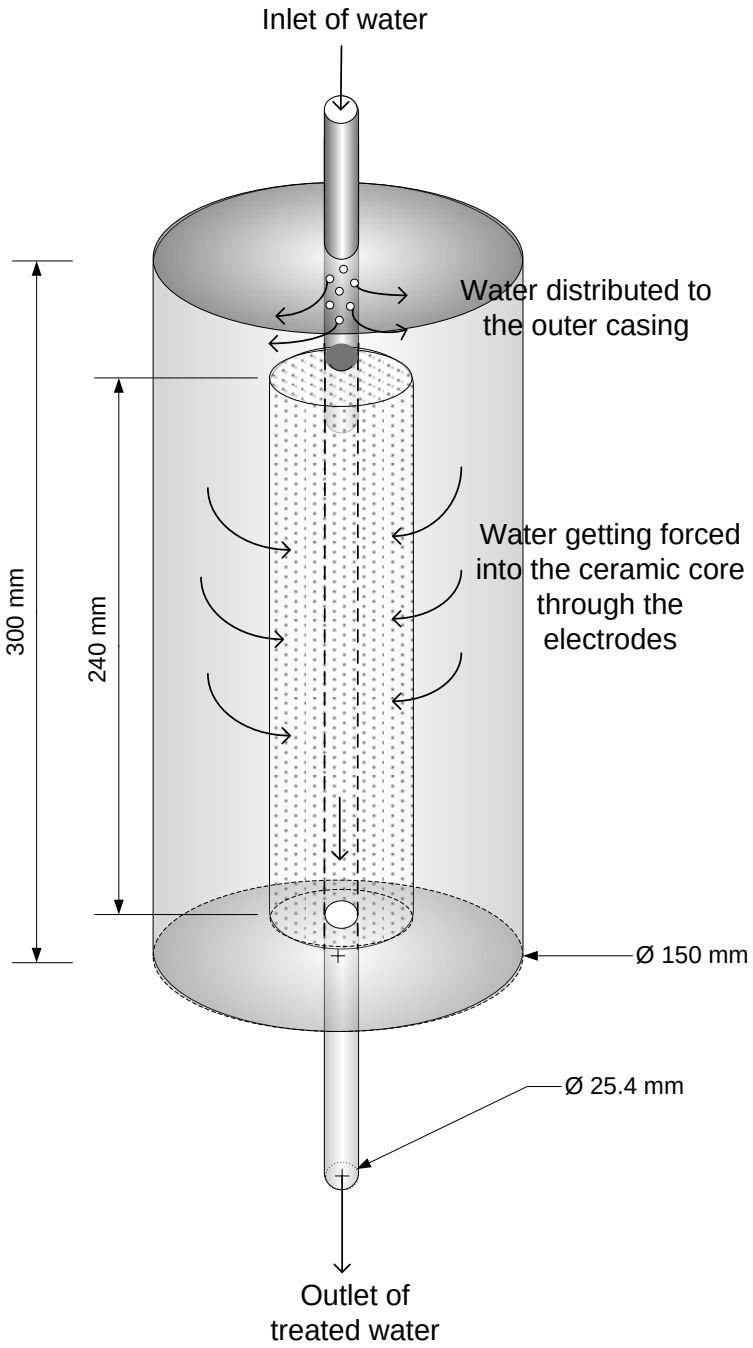

Figure B.1- Piping and flow direction of the cylindrical cell configuration

Figure B.2 - Image of the cylindrical cell configuration

B.2 New Thinking – PEFT cell

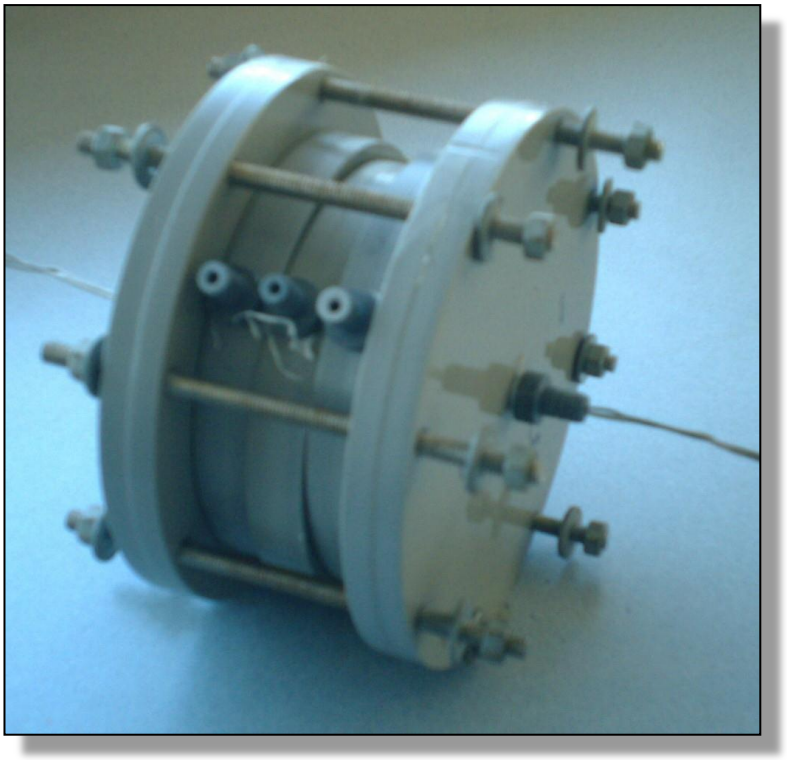

Figure B.3 – Three compartment divided electrochemical cell (X. Wang, 2005)

B.3 Hole density – 3holes/cm^2

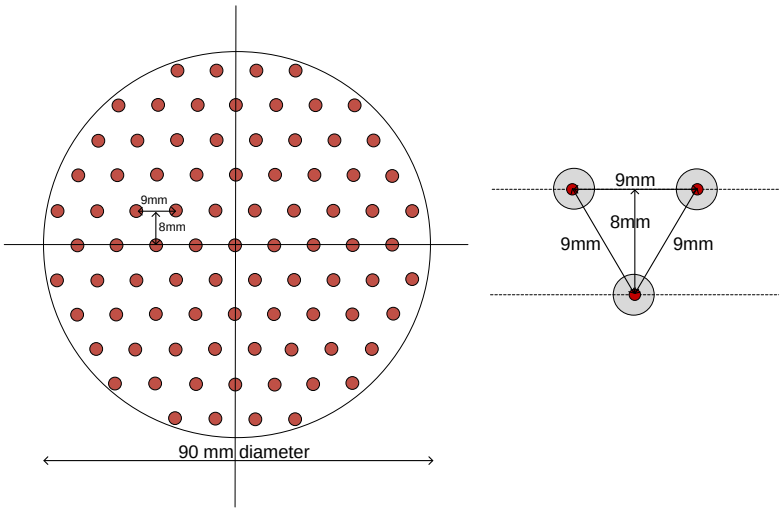

Figure B.4 – Hexagonally arranged hole (1mm diameter) drilling pattern: 3 holes/cm^2

B.4 Hole density – 6 holes/cm^2

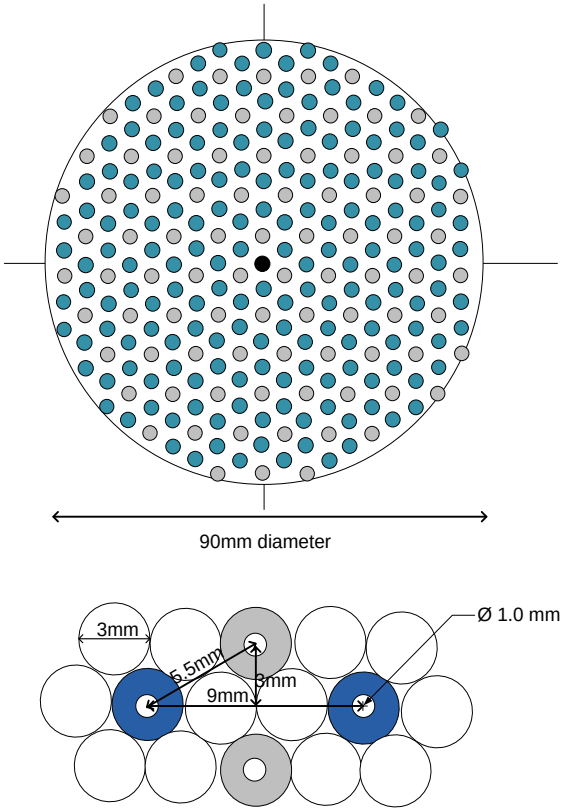

Figure B.5 - Hexagonally arranged hole (1mm diameter) drilling pattern: 6 holes/cm^2.

B.5 The effect of hole size and hole density on the total active electrode area

The effective area is obtained by reducing the hole area and adding the area gained by the wall area of the perforations to the available electrode area.

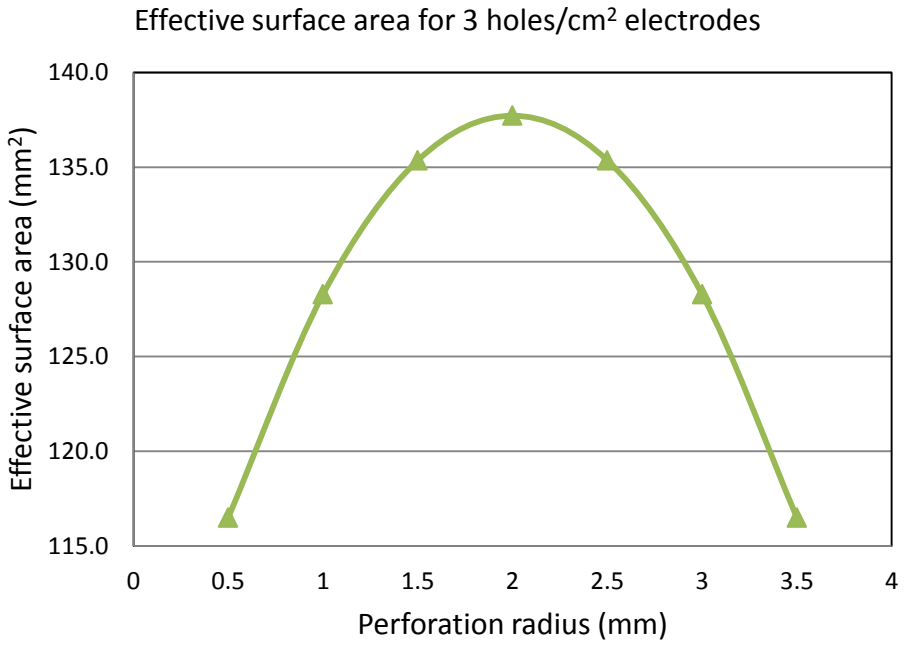

Figure B.6 – Effect of perforation radius on the effective electrode surface area for a hole density of 3 holes/cm²

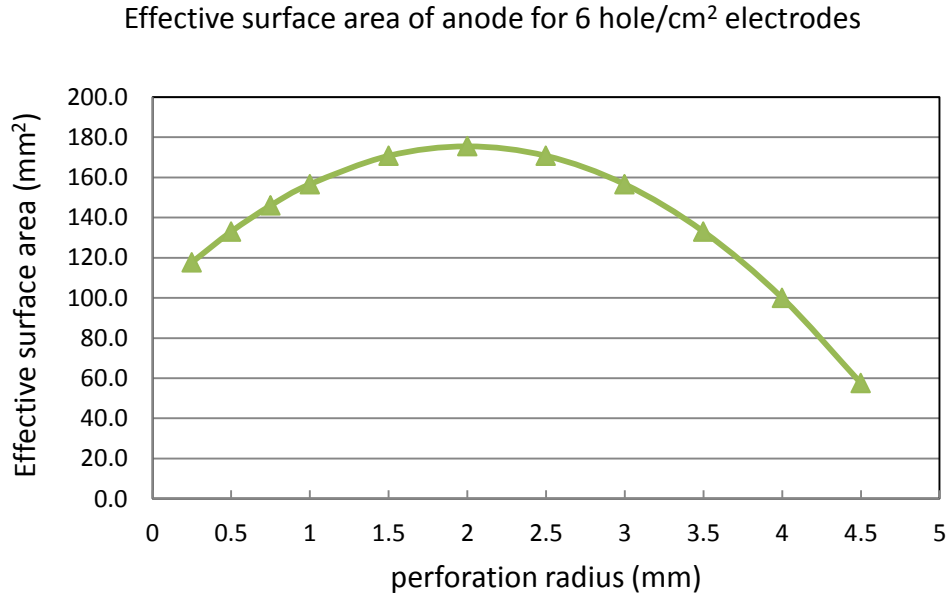

Figure B.7 - Effect of perforation radius on the effective electrode surface area for a hole density of 6 holes/cm².

B.6 Calculation of Reynolds's number in the PEFT cell design

The hydrodynamics of the PEFT cell are complicated by the flow patterns set up when fluid flows through the entrance perforation of the first electrode, impinges upon the second electrode, flows in the inter-electrode gap perpendicular to the perforations and exits through perforations of the second electrode. In order to gain an initial understanding of the flow characteristics, the flow has been approximated to flow between parallel plate electrodes and Reynolds numbers and boundary layer thicknesses has been estimated.

The Reynolds number (Re) provides a criteria for laminar or turbulent flow and it is calculated using the following equation (Pletcher, 1984);

$$Re = \rho l \bar{u} / \mu \qquad \textit{(Eq. B.1)}$$

where ρ is density of the solution = *1000* kg/m^3

l is characteristic length (avg. length between electrodes) = 5×10^{-3}m

$\bar{u}$ is mean flow velocity = 70.3 m/s (at a volumetric flow rate of 3.16 mL/s)

μ is viscosity = 0.001 kg/ms

Substituting the values in Eq. B.1

$$Re = 351500$$

When $Re > 3000$ the flow is considered to be turbulent (Pletcher, 1984).

Boundary layer thickness (δ) for turbulent flow is given by the following equation (Bishop, Gibbs and Cunningham, 1997)

$$\delta = 4.64\,(x/Re)^{0.5} \qquad \textit{(Eq. B.2)}$$

where δ is the thickness of the boundary layer

x is the distance between the plates.

Re is Reynolds number

In the case where

volumetric flow rate (Q) at 3.16 mL/s through the PEFT cell

Re is the Reynolds number = 351500

x is the distance between the plates = 1 µm (electrocatalytic effect cell)

Substituting the values in *Eq. B.2* gives

$$\delta = 8\ nm$$

Under the same flow conditions when $x = 40$ µm (Electro-pasteurisation cell)

The Reynolds number Re_{40} = 8800

Hydrodynamic boundary layer thickness from *Eq. B.2*

δ = 0.3 µm or 300 nm

Under the same flow conditions when $x = 50\ \mu m$ (other applications)

The Reynolds number Re_{50} = 7030

Hydrodynamic boundary layer thickness from *Eq. B.2*

δ = 0.4 µm or 400 nm

B.7 Free and bound charge densities on conducting and insulating surfaces

Free charge density

The Gauss's law gives

$$\sigma_f = \epsilon_0 \times E_n \qquad \textit{(Eq. B.3)}$$

where σ_f is the free charge density

ϵ_0 is the permittivity of free space = 8.85×10^{-12} C^2/Nm^2

E_n is the Electric field = 10^5 *N/C* (considering 5 V applied across 50 µm inter-electrode gap)

Substituting the values in Equation B.3

σ_f = 8.85×10^{-7} C/m^2

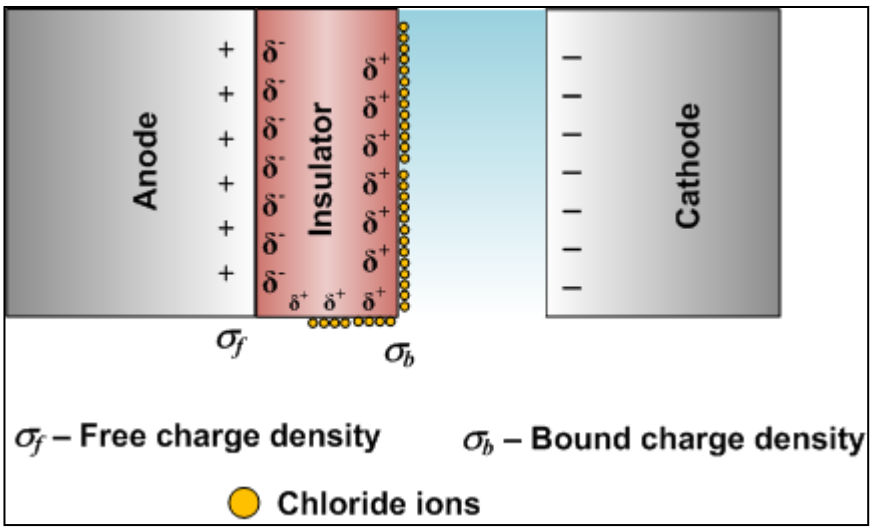

Figure B.8 – Free and bound charge density on a surface of the electrode and the on the surface of an insulator

Bound charge density

The bound charge density on an insulator surface is given by the following equation (Tipler, 1990);

$$\sigma_b = (\kappa - 1)/\kappa \times \sigma_f \qquad \textit{(Eq. B.4)}$$

where σ_b is the bound charge density

σ_f is free charge density

κ is the dielectric constant of the insulator

κ for the Polyurethane varnish is ~ 6.5

Substituting the values in equation *B.4*

$$\sigma_b = 7.48\times10^{-7}\ \mathrm{C/m^2}$$

Appendix C

C.1 Chemical oxidation of problem groundwater

Calcium hypochlorite as the oxidizing agent

Iron removal by calcium hypochlorite oxidation

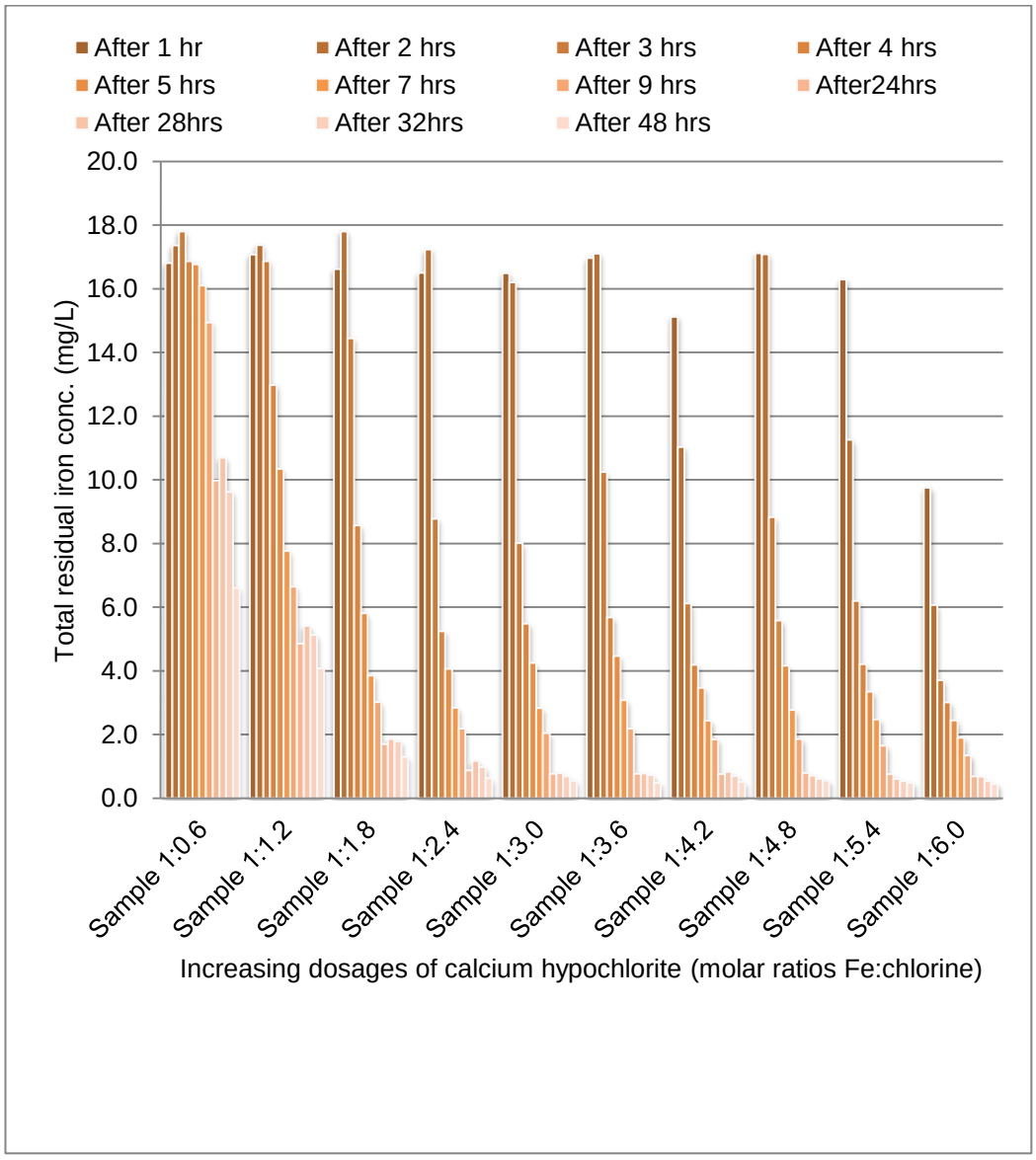

Figure C.1 - Removal of iron from problem groundwater post calcium hypochlorite oxidation.

Manganese removal by calcium hypochlorite oxidation

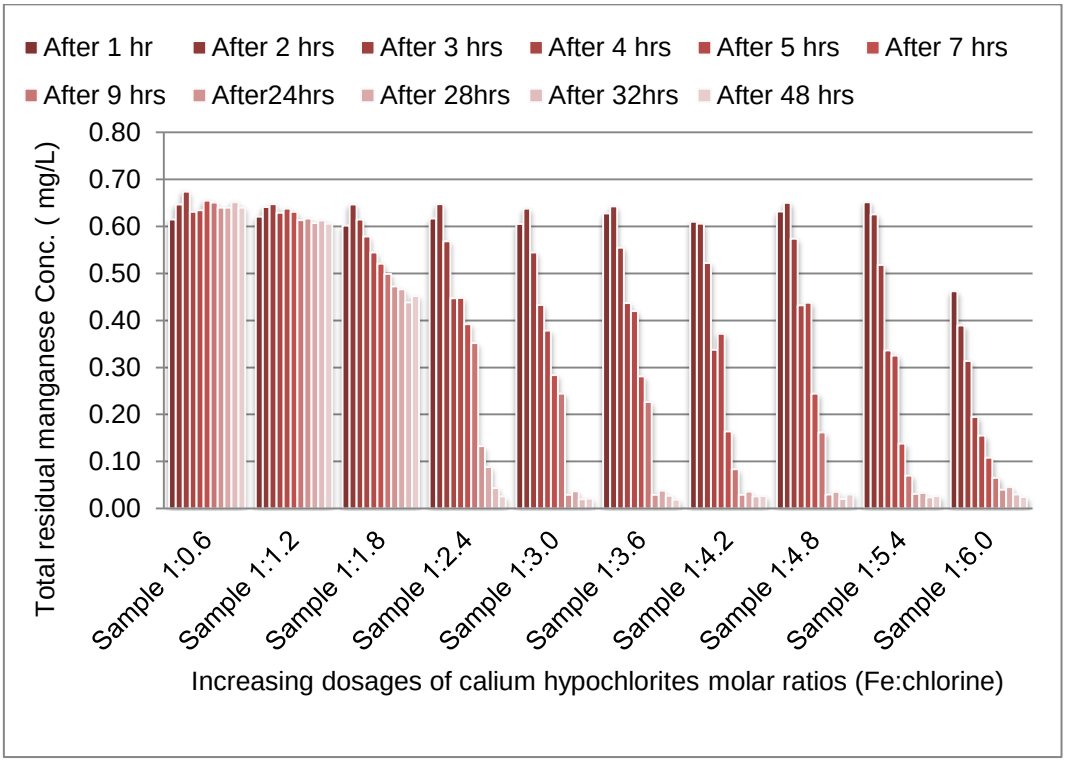

Figure C.2 - Removal of manganese from problem groundwater post calcium hypochlorite oxidation.

Turbidity removal by calcium hypochlorite oxidation

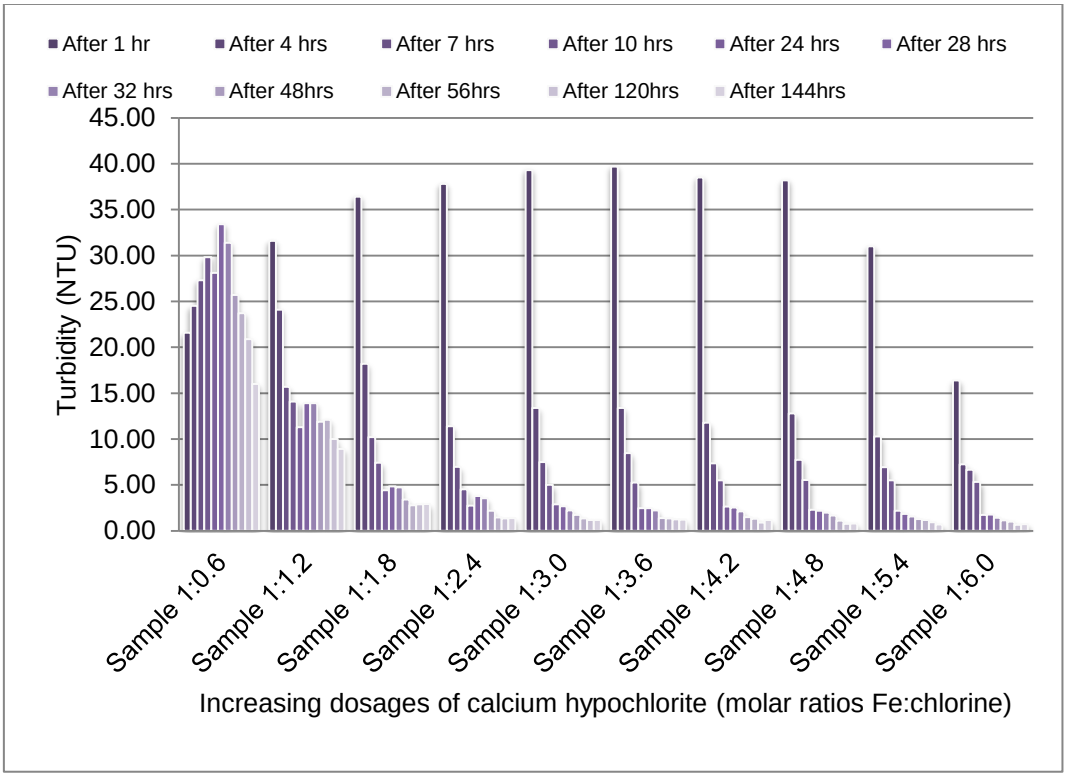

Figure C.3 – Turbidity removal from problem groundwater post calcium hypochlorite oxidation.

Sodium hypochlorite as the oxidizing agent

Iron removal by sodium hypochlorite compared with calcium hypochlorite

The residual iron content in groundwater after 5, 24, and 48 hours post sodium hypochlorite oxidation is given in a light colour (see figure C.4) adjacent to calcium hypochlorite data for the same.

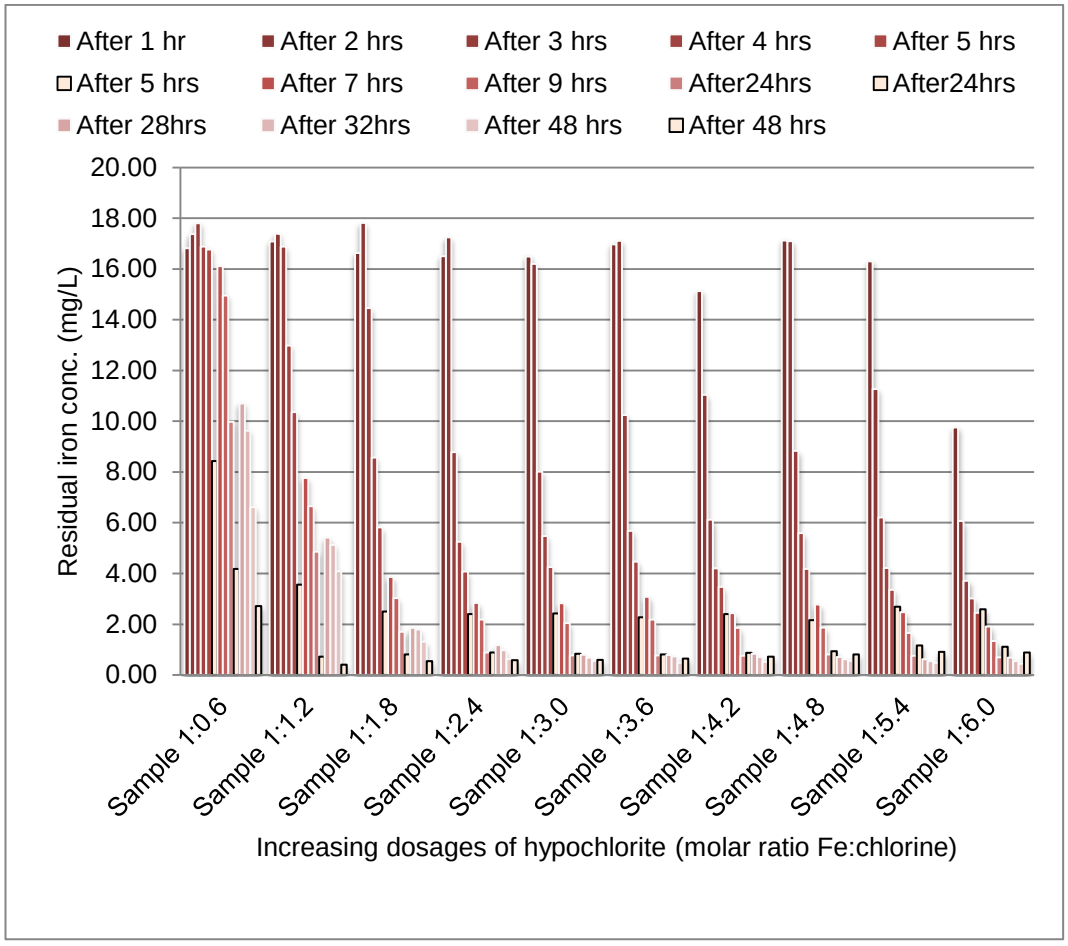

Figure C.4 - Removal of iron from problem groundwater post sodium hypochlorite oxidation is compared with calcium hypochlorite oxidation

Manganese removal by sodium hypochlorite compared with calcium hypochlorite

The residual manganese content in groundwater after 5, 24, and 48 hours post sodium hypochlorite oxidation is given in a light colour (see figure C.5) adjacent to calcium hypochlorite data for the same.

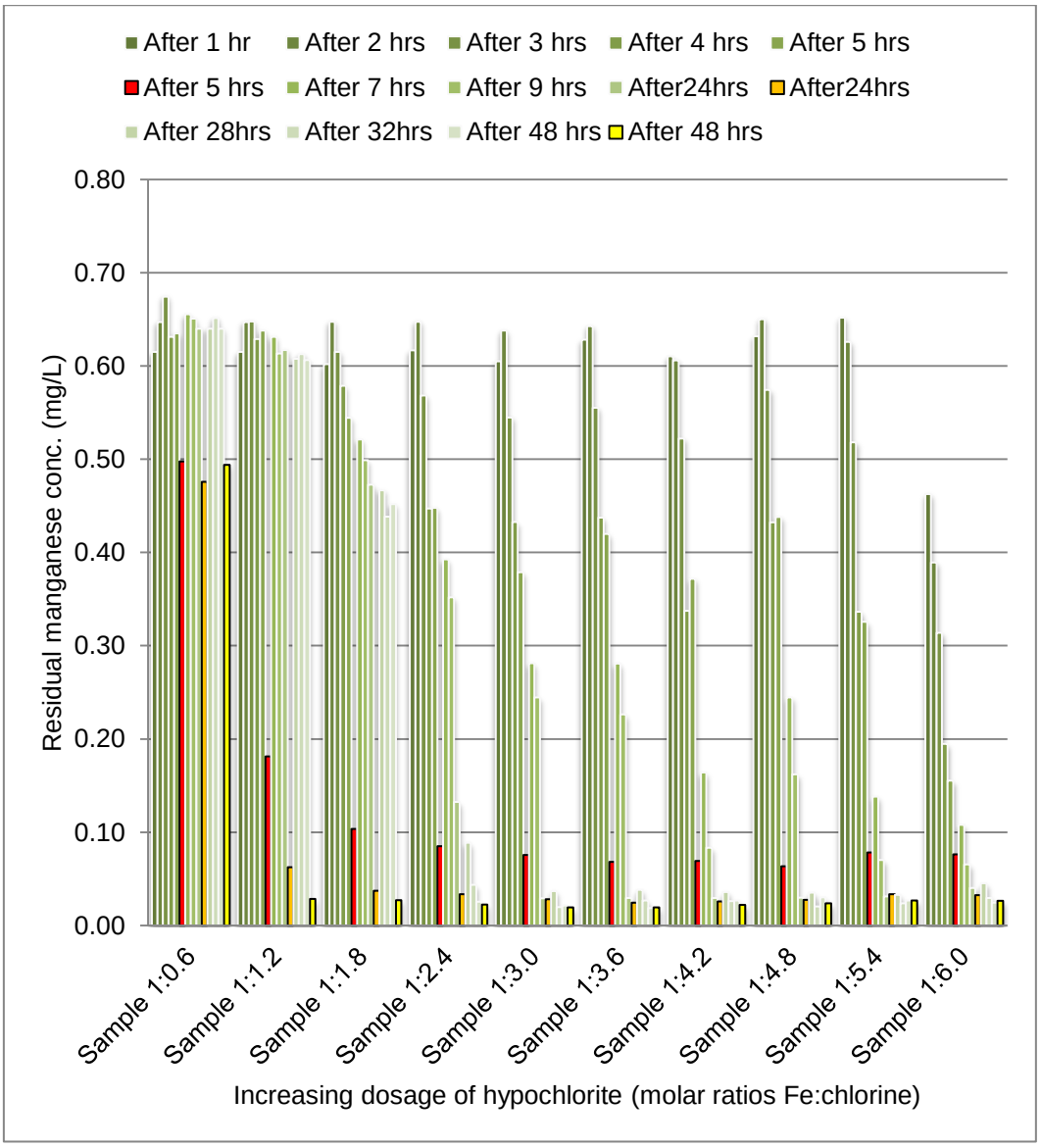

Figure C.5 - Removal of manganese from problem groundwater post sodium hypochlorite oxidation is compared with calcium hypochlorite oxidation

Turbidity removal by sodium hypochlorite oxidation

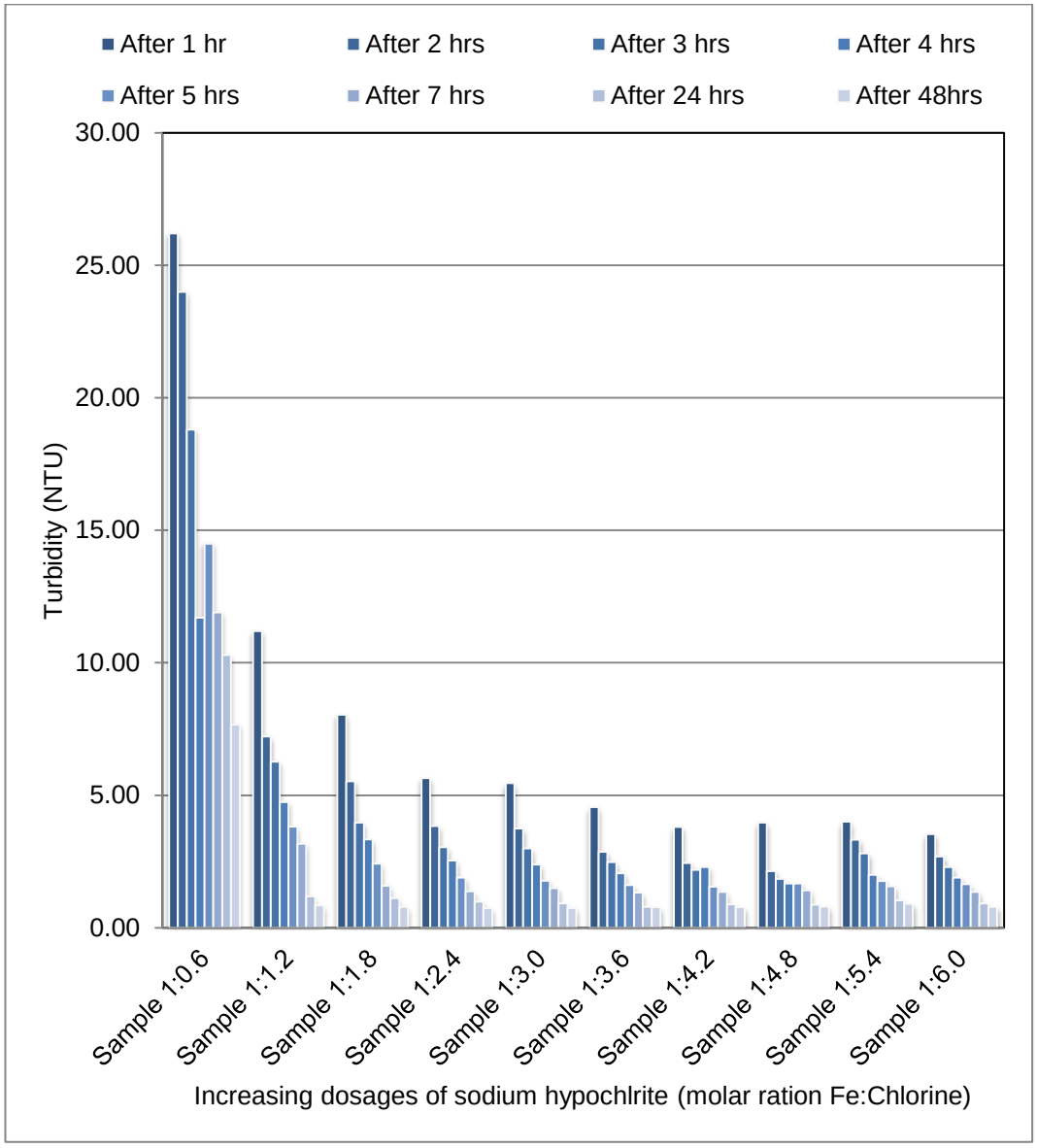

Figure C.6 - Turbidity removal from problem groundwater post sodium hypochlorite oxidation.

Potassium persulphate as the oxidizing agent

Potassium persulphate is known to be a strong oxidizing agent and hence it was tried in oxidizing the problem groundwater.

Iron removal by potassium persulphate oxidation

As expected the iron removal with potassium persulphate was not as efficient as it was with the hypochlorite systems.

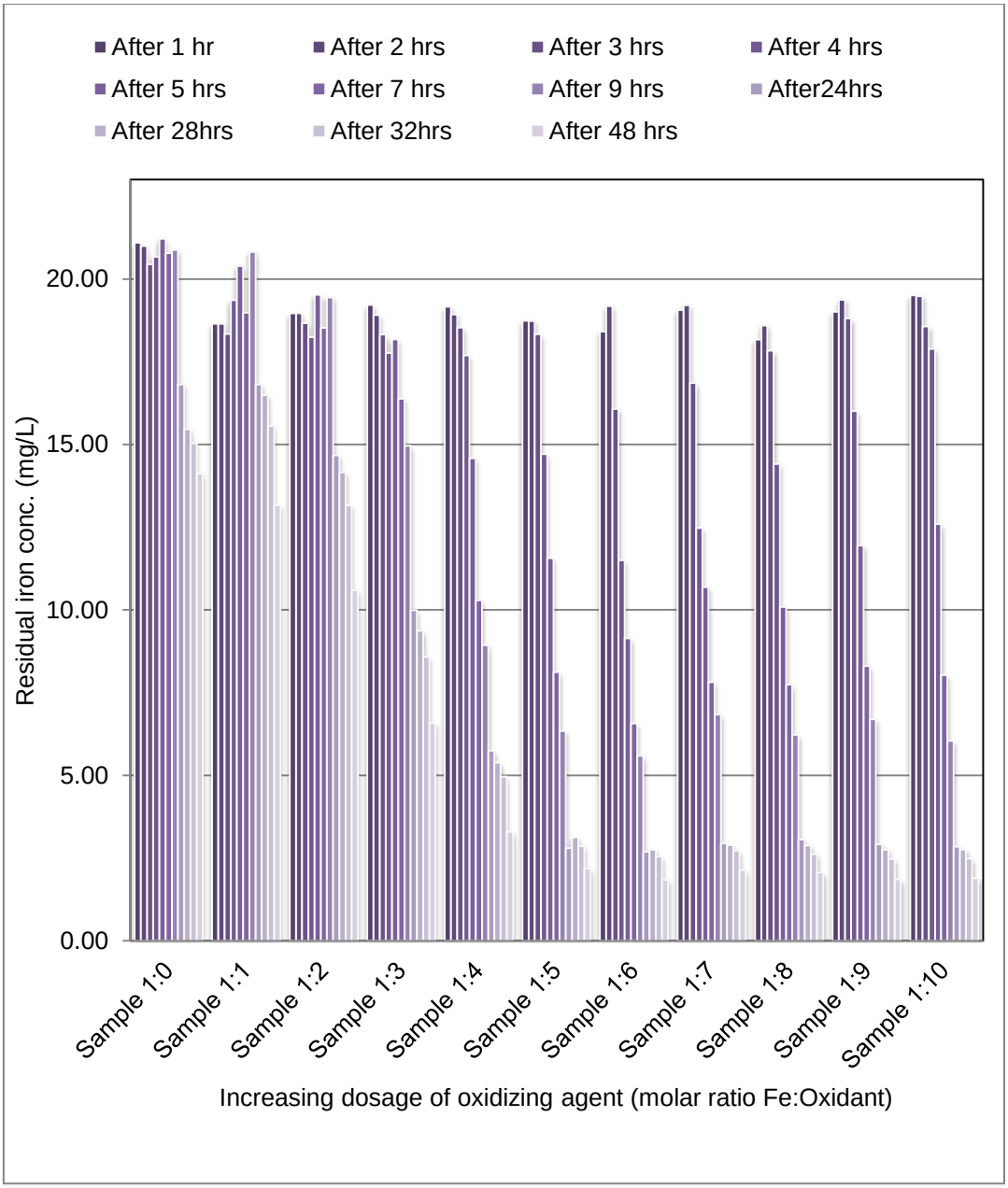

Figure C.7 - Removal of iron from problem groundwater post potassium persulphate oxidation.

Manganese removal by potassium persulphate

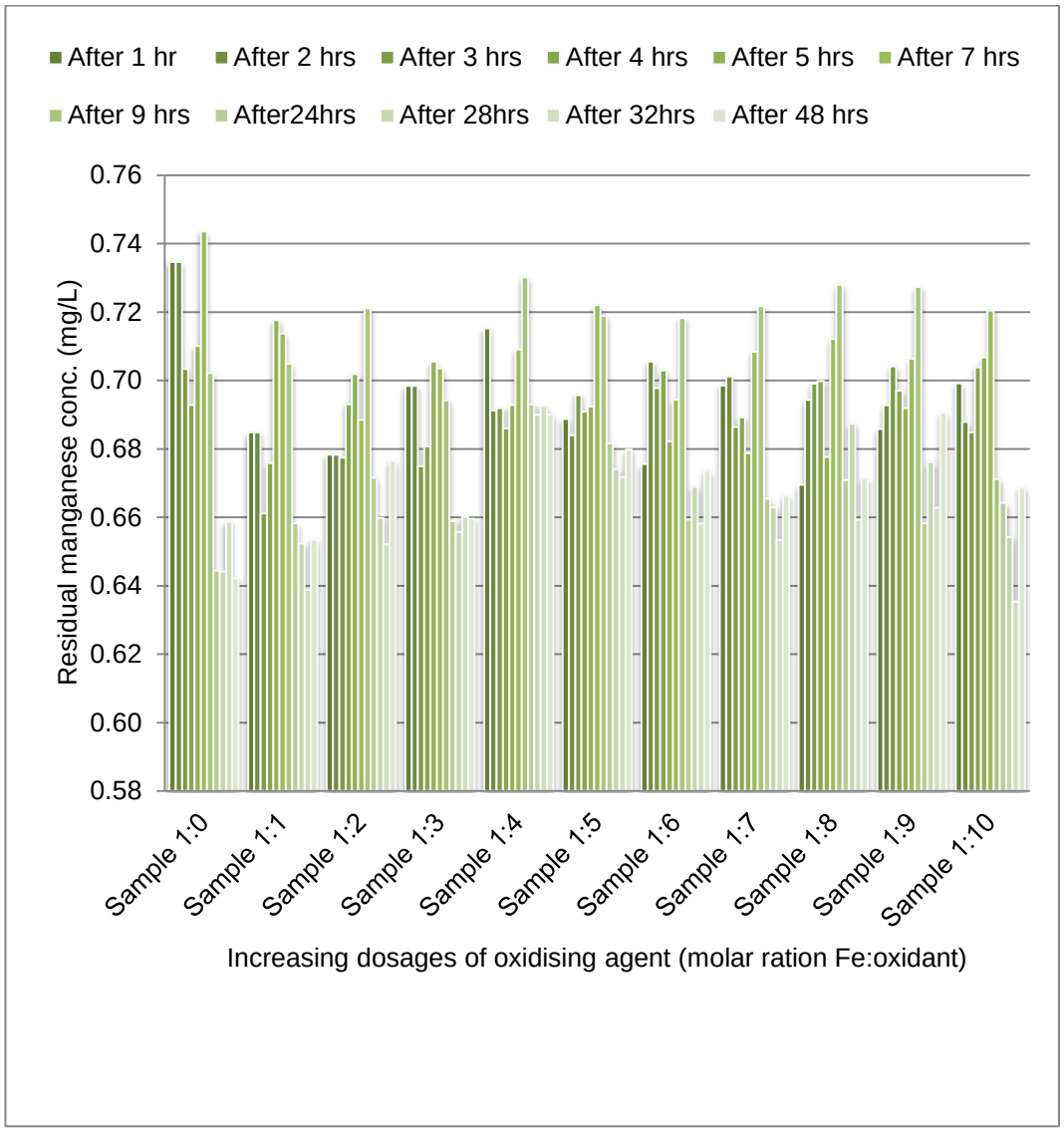

Figure C.8 - Removal of manganese from problem groundwater post potassium persulphate oxidation

Turbidity removal by potassium persulphate oxidation

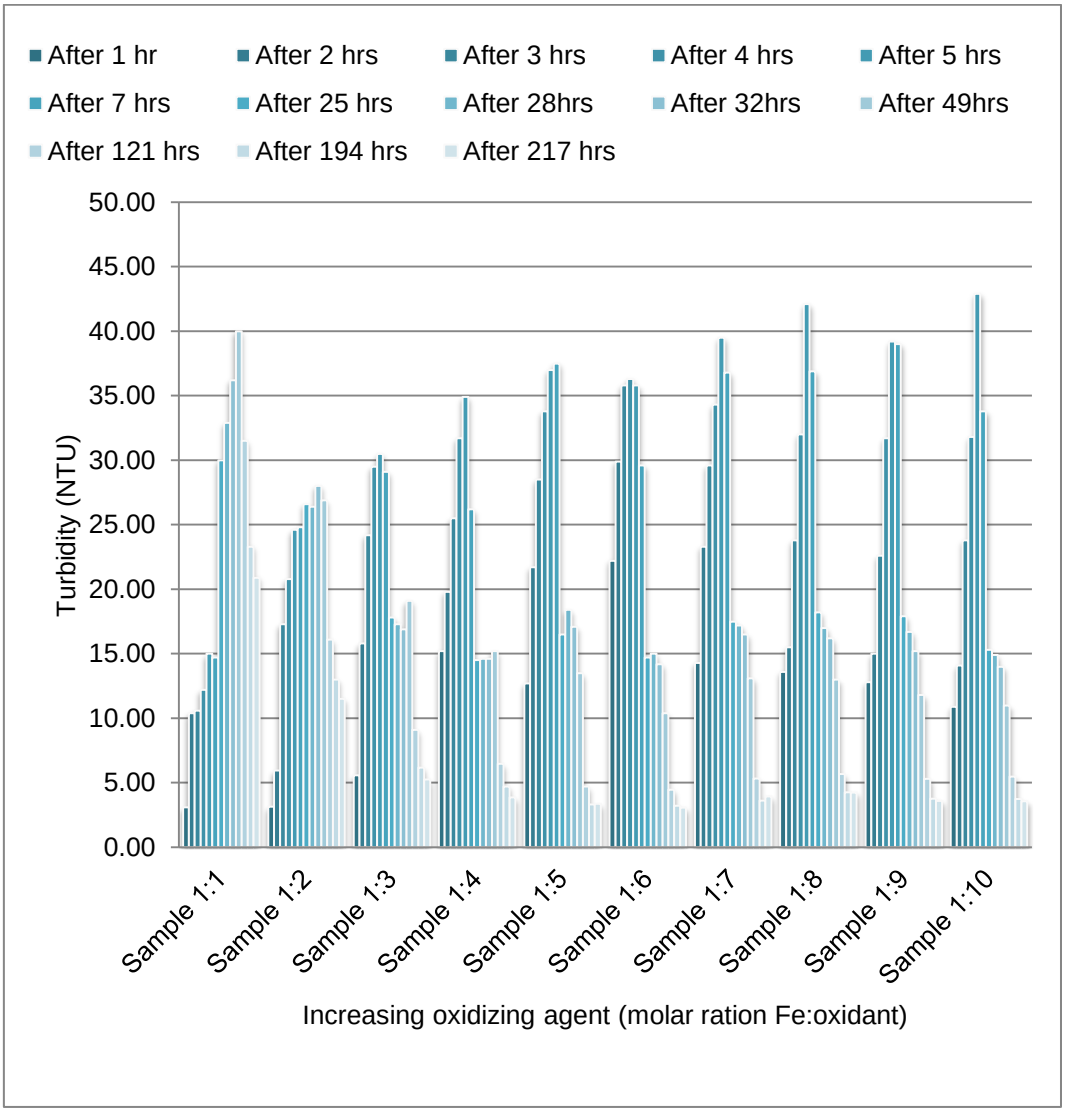

Figure C.9 - Turbidity removal from problem groundwater, post potassium persulphate oxidation.

C.2 The interaction of iron and silica in natural groundwater

The interaction of iron and silica during the stable colloidal suspension formation in natural groundwater is compared with the preparation of silica coated iron nano composite preparation. The figure C.1 shows TEM images taken by Yuan et al. 2010, during the preparation of Fe/SiO_2 core/shell nanocomposites.

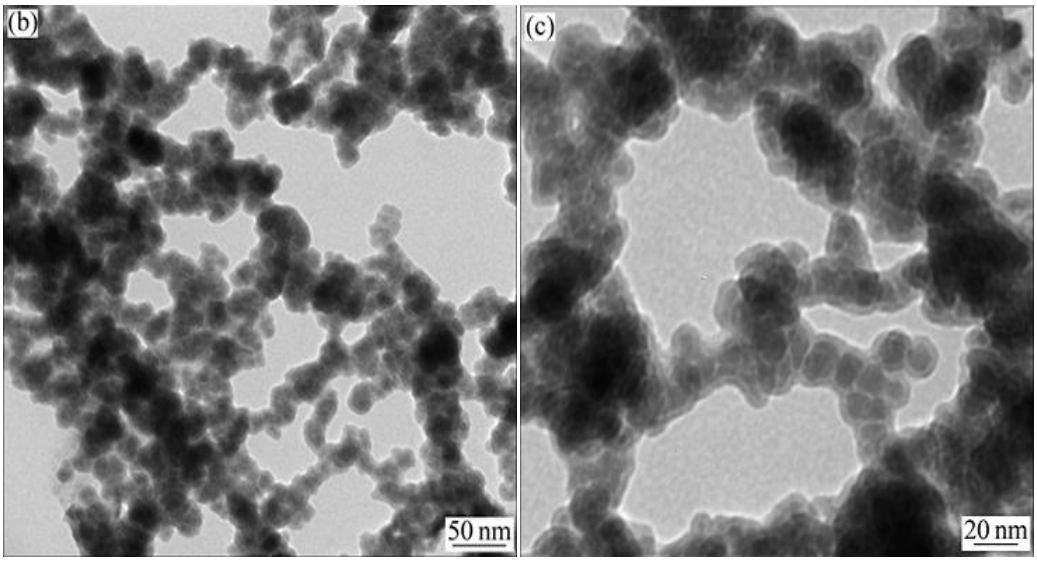

Figure C.10- TEM images taken during the synthesis of Fe/SiO_2 core/shell nano composites(Yuan, et al., 2010).

The dark spots are the iron core and the chain-like particles growth is the silica in the TEM images given in figure C.1. The magneto-static behaviour of iron is responsible for the chain-like growth pattern of the silica particles. A similar result was reported by Mohammadreza et al. 2007, in preparation of nano composites of silica coated iron. The figure C.2 shows two TEM images (20 and 100 nm scale) taken during problem (Waikato) groundwater undergoing natural air oxidation compares well with the nano composite preparation images in C.1, where similarities such as the iron core/dark spots in the middle and the chain-like growth of silica particles around it.

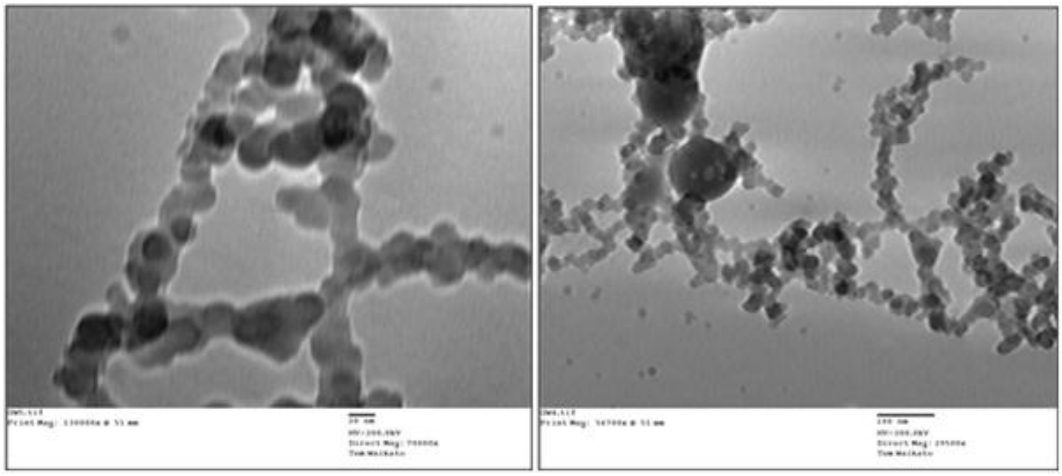

Figure C.11 - TEM images taken during problem Waikato groundwater undergoing natural (slow) oxidation process.

Appendix D

D.1 UV-VIS spectrums and calibration curve for Indigo Carmine dye

The UV-VIS spectrums were obtained by CARY 100 Scan UV-VISIBLE spectrophotometer (Varian) made in Australia.

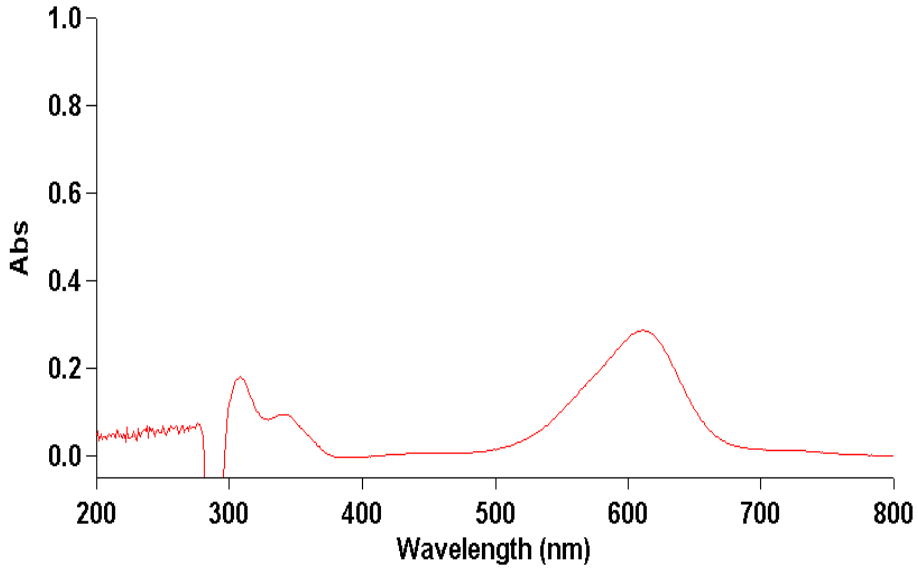

Figure D.1- Indigo Carmine dye: UV-VIS spectrum

Peak Table
Peak Style Peaks
Peak Threshold 0.0100
Range 800.00nm to 200.00nm

Wavelength (nm)	Abs	Wavelength (nm)	Abs
611.00	0.287	238.00	0.070
341.00	0.095	231.00	0.063
308.00	0.180	228.00	0.055
276.00	0.075	223.00	0.066
264.00	0.070	220.00	0.050
256.00	0.070	215.00	0.058
250.00	0.070	212.00	0.050
240.00	0.065	203.00	0.049

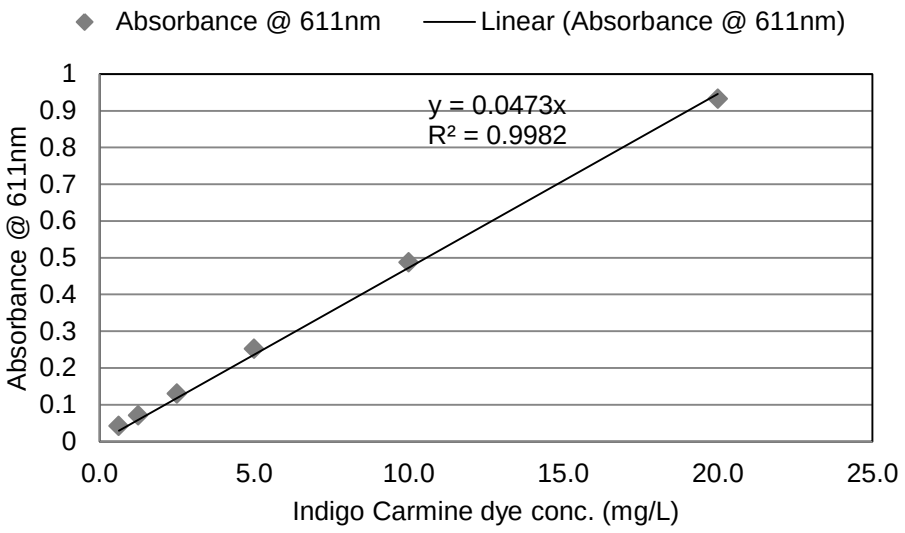

Figure D.2- Indigo Carmine dye -calibration curve

D.2 UV-VIS spectrum and calibration curve for Reactive blue 2 dye

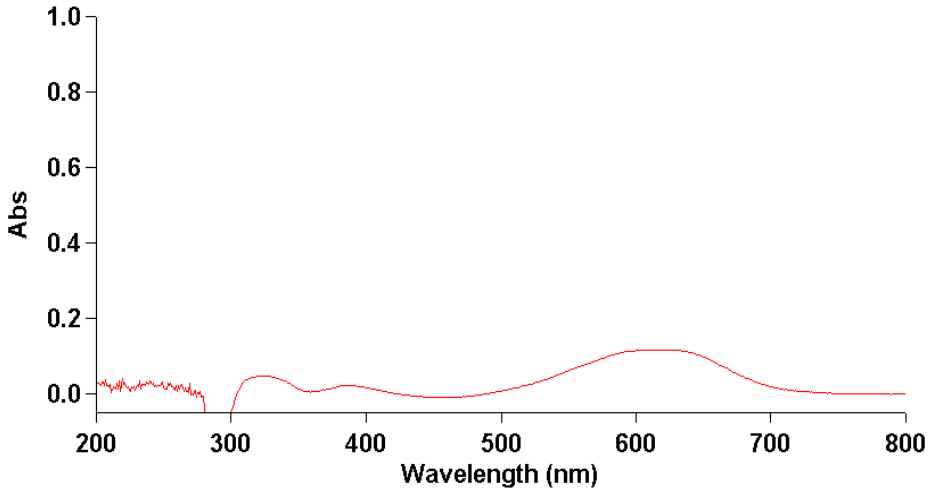

Figure D.3 - Reactive Blue 2 dye UV-VIS spectrum

Peak Table
Peak Style Peaks
Peak Threshold 0.0100
Range 800.00nm to 200.00nm

Wavelength (nm)	Abs	Wavelength (nm)	Abs
617.00	0.117	255.00	0.029
385.00	0.022	249.00	0.031
323.00	0.048	240.00	0.034
277.00	0.008	232.00	0.033
273.00	0.010	219.00	0.041
269.00	0.029	217.00	0.034
263.00	0.026	215.00	0.029
259.00	0.023	207.00	0.039

Calibration curve

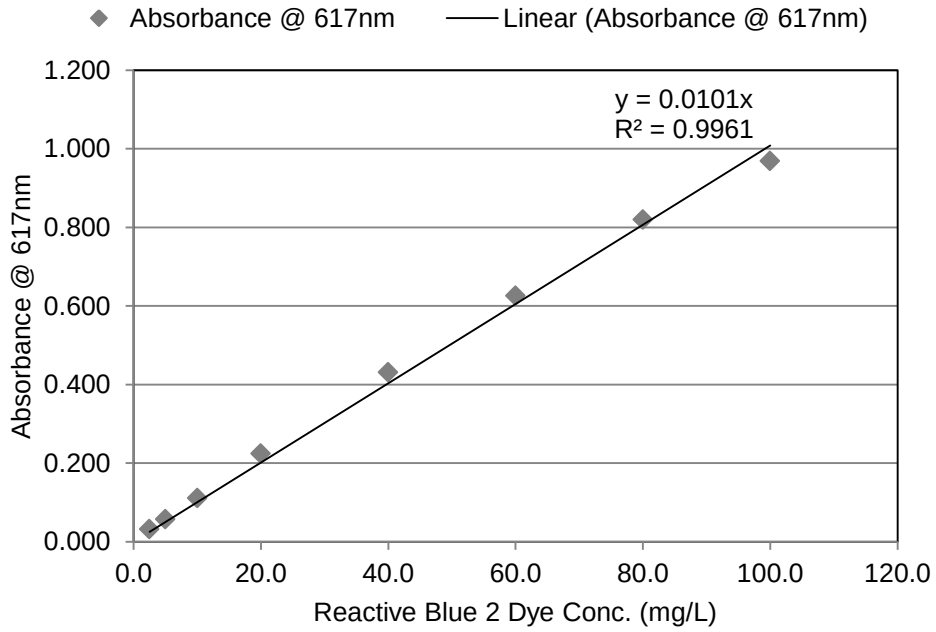

Figure D.4 - Reactive Blue 2 dye calibration curve

D.3 The colour change for reactive blue 2 dye

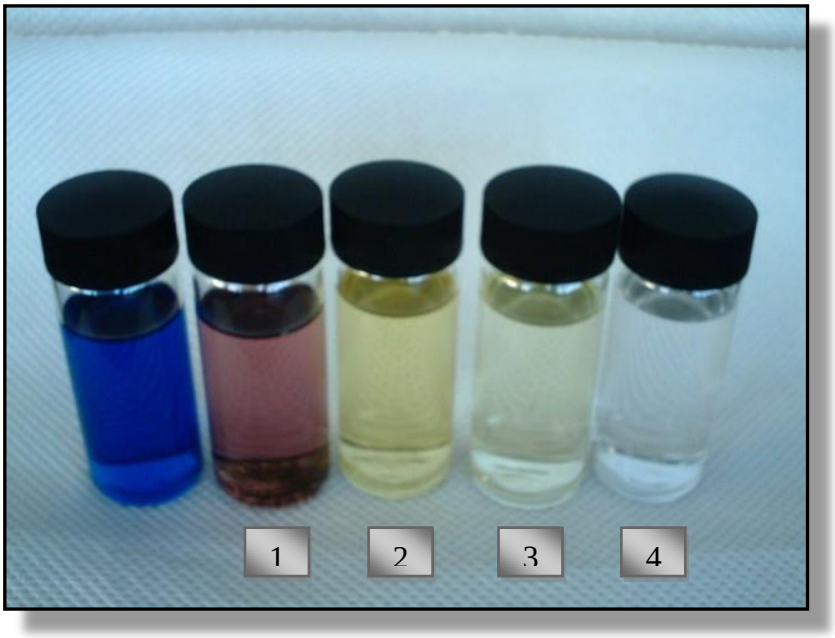

Figure D.5 - The colour changes for 4 cycles through the PEFT cell, 0.01mol/L NaCl Conc.

D.4 The colour changes for indigo carmine dye

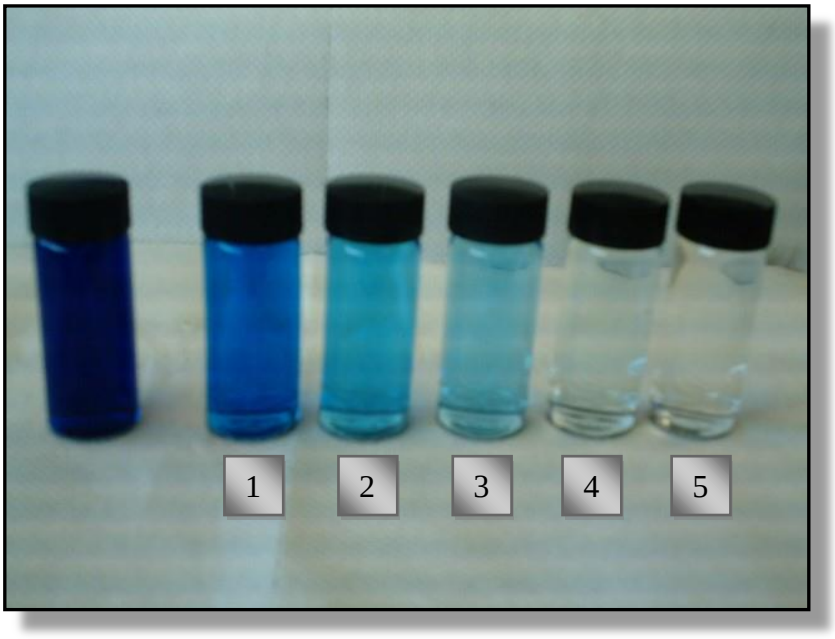

Figure D.6 - The colour changes for 5 cycles through the PEFT cell at 0.1 mol/L NaCl, pH 7.0, current density 80 mA/cm^2, 100mg/L IC dye conc.

References

Abderrahmane, S., Himour, A., & Ponsonnet, L. (2008). Inactivation of E. coli and Pseudomonas aeruginosa by electrochloration under bipolar pulsed polarization. *Materials Science and Engineering C, 28* 901–905.

Alkhafaji, S. (2006). *An Investigation on the Non Thermal Pasteurisation Using Pulsed Electric Fields.* University of Auckland, Auckland.

Alkhafaji, S. R., & Farid, M. (2007). An investigation on pulsed electric fields technology using new treatment chamber design. *Innovative Food Science and Emerging Technologies 8*, 205–212.

Ammar, S., Abdelhedi, R., Flox, C., Arias, C., & Brillas, E. (2006). Electrochemical degradation of the dye indigo carmine at boron-doped diamond anode for wastewaters remediation. *Environ Chem Lett. , 4*, 229–233.

Anglada, A., Urtiaga, A., & Ortiz, I. (2009). Contributions of electrochemical oxidation to waste-water treatment: fundamentals and review of applications. [Review]. *J Chem Technol Biotechnol, 85*, 1747-1755.

Ateya, B. G., Al-Kharafi, F. M., Abdallah, R. M., & Al-Azab, A. S. (2005). Electrochemical removal of hydrogen sulfide from polluted brines using porous flow through electrodes. *Journal of Applied Electrochemistry 35*, 297–303.

Ateya, B. G., Arafat, E. A. S., & Kafafi, S. A. (1977). Hydrodynamic effects on the efficiency of porous flow- through electrodes. *Journal of Applied Electrochemistry, 7*, 107-112.

Bae, C., Chakrabarti, H., & Roberts, E. (2008). A membrane free electrochemical cell using porous flow-through graphite felt electrodes. *Journal of Applied Electrochemistry 38*, 637–644.

Bard, A. J., & Faulkner, L. R. (2001). *Electrochemical methods: fundamentals and applications* (2 ed.). NewYork: Wiley.

Barsotti, L., Merle, P., & Cheftel, J. C. (1999). Food processing by pulsed electric fields. I. Physical aspects. *Food Reviews International, 15*(2), 163 — 180.

Bergmann, M. E., & Rollin, J. (2007). Product and by-product formation in laboratory studies on disinfection electrolysis of water using boron-doped diamond anodes. *Catalysis Today, 124*, 198–203.

Bergmann, M. E. H., Rollin, J., & Lourtchouk, T. (2009). The occurrence of perchlorate during drinking water electrolysis using BDD anodes. *Electrochimica Acta, 54*, 2102–2107.

Bishop, P. L., Gibbs, J. T., & Cunningham, B. E. (1997). Relationship between concentration and hydrodynamic boundary layers over biofilms. *Environmental Technology, 18*(4), 375 — 385.

Buckow, R., Schroeder, S., Berres, P., Baumann, P., & Knoerzer, K. (2010). Simulation and evaluation of pilot-scale pulsed electric field (PEF) processing. *Journal of Food Engineering 101*, 67–77.

Bull, R. J., Birnbaum, L. S., Cantor, K. P., Rose, J. B., Butterworth, B. E., Pegram, R., et al. (1995). Water chlorination: Essential process or cancer hazard. *Fundamentals of Applied Toxicology, 28*(2), 155-166.

Cameron, A. J., & Liss, P. S. (1984). The stabilization of "dissolved" iron in freashwater *Water Research, 18*, 179-185.

Cameselle, C., Pazos, M., & Sanroma´n, M. A. (2005). Selection of an electrolyte to enhance the electrochemical decolourisation of indigo. Optimisation and scale-up. *Chemosphere 60*, 1080–1086.

Can, O. T., Bayramoglu, M., & Kobya, M. (2003). Decolorization of reactive dye solutions by electrocoagulation using aluminum electrodes. *Ind. Eng. Chem. Res., 42*(14), 3391-3396.

Carlson, L., & Schwertmann, U. (1987). Iron and manganese oxides in Finnish ground water treatment plants. *Water Research, 21*(2), 165-170.

Carneiro, P. A., Fugivara, C. S., Nogueira, R. F. P., Boralle, N., & Zanoni, M. V. B. (2003). A comparative study on chemical and electrochemical degradation of reactive blue 4 dye. *Portugaliae Electrochimica Acta, 21* 49-67.

Chang, E. E., Chao, S. H., Chiang, P. C., & Lee, J. F. (1996). Effects of chlorination on THMs formation in raw water. . *Toxicol. Environ. Chem., 56*, 211-225.

Chatzisymeon, E., Xekoukoulotakis, N. P., Coz, A., Kalogerakis, N., & Mantzavinos, D. (2006). Electrochemical treatment of textile dyes and dyehouse effluents. *Journal of Hazardous Materials B137*, 998–1007.

Chiangi, L. C., Changi, J., & Wen, T. (1995). Indirect oxidation effect in electrochemical oxidation treatment of landfill leachate. *Water Research, 29*(2), 671-678.

Chlor Generators Ltd. (2004). Electrochlorination. 2008, from http://www.chlorgenerators.com

Choa, D., Kongb, S., & Ohb, S. (2003). Analysis of trihalomethanes in drinking water using headspace-SPME technique with gas chromatography. *Water Research, 37* 402–408.

Cumberland Electrochemical Limited. (2004). Cumberland's PANCLOR™ Technology. from http://www.Cumberlandec.com/panclor.htm

Daniele, S. L. (2008). Sodium hypochlorite dosage for household and emergency water treatment. *e-Journal AWWA, 100*(8).

Deng, Y., & Englehardt, J. D. (2007). Electrochemical oxidation for landfill leachate treatment. *Waste Management 27*, 380–388.

Diao, H. F., Li, X. Y., Guc, J. D., Shi, H. C., & Xie, Z. M. (2004). Electron microscopic investigation of the bactericidal action of electrochemical disinfection in comparison with chlorination, ozonation and Fenton reaction. *Process Biochemistry 39*, 1421–1426.

Dogan, D., & Turkdemir, H. (2005). Electrochemical oxidation of textile dye indigo. *Journal of Chemical Technology and Biotechnology, 80,* 916–923.

Drees, K. P., Abbaszadegan, M., & Maiera, R. M. (2003). Comparative electrochemical inactivation of bacteria and bacteriophage. *Water Research 37*, 2291–2300.

El-Dib, M. A., & Ali, R. K. (1995). THMs Formation during cglorination of raw Nile river water. *Water Research 29*(1), 375-378.

FaridaYunus, R., Zheng, Y., Nanayakkara, K. G. N., & Chen, J. P. (2009). Electrochemical Removal of Rhodamine 6G by Using RuO2 Coated Ti DSA. *Ind. Eng. Chem. Res. , 48,* 7466–7473.

Feng, C., Suzuki, K., S., Z., Sugiura, N., Shimada, S., & Maekawa, T. (2004). Water disinfection by electrochemical treatment. *Bioresource Technology, 94* 21–25.

Fiessinger, F., Richard, Y., Hontiel, A., & Husquere, P. (1981). Advantages and disadvantages of chemical oxidation and disinfection by ozone and chlorine dioxide. *The Science of the Total Environment, 18* 245-261.

Flox, C., Ammar, S., Arias, C., Brillas, E., Vargas-Zavala, A. V., & Abdelhedi, R. (2006). Electro-Fenton and photoelectro-Fenton degradation of indigo carmine in acidic aqueous medium. *Applied Catalysis B: Environmental 67*, 93–104.

Fox, M. B., Esveld, D. C., Valero, A., Luttge, R., Mastwijk, H. C., Bartels, P. V., et al. (2006). Electroporation of cells in microfluidic devices: a review. *Anal Bioanal Chem 385*, 474–485.

Geng, T., Zhan, Y., Wang, H., Witting, S. R., Cornetta, K. G., & Lu, C. (2010). Flow-through electroporation based on constant voltage for large-volume transfection of cells. *Journal of Controlled Release 144*, 91–100.

Ghicov, A., Tsuchiya, H., Macak, J. M., & Schmuki, P. (2005). Titanium oxide nanotubes prepared in phosphate electrolytes. [Short Communication]. *Electrochemistry Communications, 7*, 505–509.

Ghosh, D., Solanki, H., & Purkait, M. K. (2008). Removal of Fe(II) from tap water by electrocoagulation technique. *Journal of Hazardous Materials, 155*, 135–143.

Gonzalez, R. O. (2010). *Hurdle Technologies : Microbial Inactivation by pulsed electric fields during milk processing.* The University of Guelph, Ontario.

Gregory, J. (2006). *Particles in water, properties and processes*. UK: CRC Press

Guerrini, E., & Trasatti, S. (2006). Recent Developments in Understanding Factors of Electrocatalysis. *Russian Journal of Electrochemistry, 42*(10), 1017–1025.

Guohua, C. (2004). Electrochemical technologies in wastewater treatment. [Review]. *Separation and Purification Technology 38*, 11–41.

Hadfield, J. (2001). Waikato. In M. R. Rosen & P. A. White (Eds.), *Groundwaters of New Zealand* (pp. 315-326). Wellington: New Zealand Hydrogeological Society.

Heinz, V., Alvarez, I., Angersbach, A., & Knorr, D. (2002). Preservation of liquid foods by high intensity pulsed electric fields—basic concepts for process design. *Trends in Food Science & Technology 12*, 103–111.

Helme, A. J., Ismail, M. N., Scarano, F. J., & Yang, C. L. (2010). Bactericidal efficacy of electrochemically activated solutions and of commercially available hypochlorite. *British Journal of Biomedical Science, 67*(3), 105-108.

Hsu, C. H., Jeng, W. L., Chang, R. M., Chien, L. C., & Han, B. C. (2000). Estimation of Potential Lifetime Cancer Risks for Trihalomethanes from Consuming Chlorinated Drinking Water in Taiwan. [Paper]. *Environmental Research 85*, 77-82.

Huang, K., & Wang, J. (2009). Designs of pulsed electric fields treatment chambers for liquid foods pasteurization process: A review. *Journal of Food Engineering, 95*, 227–239.

Ivancev-Tumbas, I., Bozo, D., Tamas, Z., & Karlovic, E. (1999). The effect of differenct drinking water treatment processes on the rate of chloroform formation in the reaction of natural organic matter with hypochlorite. *Water Research, 33*(18), 3715-3722.

Jeong, J., Kim, C., & Yoon, J. (2009). The effect of electrode material on the generation of oxidants and microbial inactivation in the electrochemical disinfection processes. *Water Research, 43*, 895-901.

Jeong, J., Kim, J. Y., & Yoon, J. (2006). The role of reactive oxygen species in the electrochemical inactivation of microorganisms. *Environ. Sci. Technol., 40*, 6117-6122.

Juttner, K. (2007). Technical scale of electrochemistry. In A. J. Bard & M. Stratmann (Eds.), *Encyclopedia of Electrochemistry* (5 ed., Vol. 5, pp. 3-19). Weinheim: Wiley.

Kerwick, M. I., Reddy, S. M., Chamberlain, A. H. L., & Holt, D. M. (2005). Electrochemical disinfection, an environmentally acceptable method of drinking water disinfection? *Electrochimica Acta 50*, 5270–5277.

Khamtorn, P., Shin, I., Jeong , W., & Chung, D. (2009). Kinetic modeling of active chlorine generation by low-amperage pulsating direct current in a circulating brine solution. *Journal of Food Engineering, 92* 461-466.

Khelifa, A., Moulay, S., Hannane, F., Benslimene, S., & Hecini, M. (2004). Application of an experimental design method to study the performance of electrochlorination cells. [Research Paper]. *Desalination 160*, 9 l-98.

Kim, J. G., & Rajkumar, D. (2006). Oxidation of various reactive dyes with in situ electro-generated active chlorine for textile dyeing industry wastewater-treatment. *Journal of Hazardous Material B, 136*, 203–212.

Kohn, T., & Roberts, A. L. (2006). The effect of silica on the degradation of organohalides in granular iron columns. *Journal of Contaminant Hydrology, 83*, 70– 88.

Kool, H. J., & Van, K. C. F. (1984). Formation & removal of mutagenic activity during drinking water preparation. *Water Research, 18*, 1011-1016.

Körbahtia, B. K., & Tanyolac, A. (2009). Continuous electrochemical treatment of simulated industrial textile wastewater from industrial components in a tubular reactor. *Journal of Hazardous Materials 170*, 771–778.

Lapicque, F. (2004). Electrochemical engineering: An overview of its contributions and promising features. *Chemical Engineering Research and Design, 82*(A12), 1571–1574.

Li, H., Zhu, X., & Ni, J. (2010). Inactivation of Escherichia coli in Na2SO4 electrolyte using boron-doped diamond anode. *Electrochimica Acta 56*, 448–453.

Li, X. Y., Diao, H. F., Fan, F. X. J., Gu, J. D., Ding, F., & Tong, A. S. F. (2004). Electrochemical wastewater disinfection: Identification of its principal germicidal actions. *Journal of Environmental Engineering, 130*(10), 1217–1221.

Lung, R. B., Masanet, E., & McKane, A. (2006). *The Role of Emerging Technologies in Improving Energy Efficiency: Examples from the Food Processing Industry.* Paper presented at the Twenty-Eighth Industrial Energy Technology Conference, New Orleans.

Machado, L. F., Pereira, R. N., Martins, R. C., Teixeira, J. A., & Vicente, A. A. (2010). Moderate electric fields can inactivate Escherichia coli at room temperature. *Journal of Food Engineering 96*, 520–527.

Mahmoud, M. S. (1999). Mathematical modeling of gas evolving flow-through porous electrodes. *Electrochimica Acta () 45* 959–967.

Marcos, R. G., Santos, M. O. F. G., Josealdo, T., & Carmem, L. P. S. Z. (2006). The application of electrochemical technology to the remediation of oily wastewater. *Chemosphere 64* 393–399.

Martınez-Huitle, C. A., & Brillas, E. (2009). Decontamination of wastewaters containing synthetic organic dyes by electrochemical methods: A general review. *Applied Catalysis B: Environmental, 87*, 105–145.

Martinez-Huitle, C. A., & Brillas, E. (2008). Electrochemical alternatives for drinking water disinfection. *Angew. Chem. Int. Ed., 47*, 1998-2005.

Martınez-Huitle, C. A., & Brillas, E. (2009). Decontamination of wastewaters containing synthetic organic dyes by electrochemical methods: A general review. *Applied Catalyst B: Environment, 87*, 105-145.

Mathieson, G., Langdon, A., & Jamieson, G. (2004). *Production of Hydrogen by Electrolytic Purification of Water*. Paper presented at the Hydrogen technologies and opportunities for Australia.

Mathieson, G. A. (2006). *Electrolytic purification of water.* University of Waikato, Hamilton.

Mayer, T. D., & Jarrell, W. M. (1996). Formation and stability of iron(II) oxidation products under natural concentrations of dissolved silica [Research paper]. *Water Research, 30*(5), 1208-1214.

Meneses, N., Jaeger, H., Moritz, J., & Knorr, D. (2010). Impact of insulator shape, flow rate and electrical parameters on inactivation of E. coli using a continuous co-linear PEF system. *Innovative Food Science and Emerging Technologies*, In Press.

Menini, R., Henuset, Y. M., & Fournier, J. (2005). Electrochemical oxidation of phenolic compounds using a flow-through electrolyser with porous solid electrodes. *Journal of Applied Electrochemistry 35*, 625–631.

Ministry of Health. (2005). *Drinking water standards for New Zealand*.

Mohan, N., Balasubramanian, N., & Ahmed Basha, C. (2007). Electrochemical oxidation of textile wastewater and its reuse. *Journal of Hazardous Materials, 147* 644–651.

Morales-de la Pen, M., Salvia-Trujillo, L., Rojas-Grau¨, M. A., & Martı´n-Belloso, O. (2010). Impact of high intensity pulsed electric field on antioxidant properties and quality parameters of a fruit juice–soymilk beverage in chilled storage. *LWT - Food Science and Technology 43* 872–881.

Munter, R., Ojaste, H., & Sutt, J. (2005). Complexed Iron Removal from Groundwater. *Journal of Environmental Engineering, 131*(7), 1014-1020.

Murphy, O. J., Hitchens, G. D., Kaba, L., & Verostko, C. E. (1992). Direct electrochemical oxidation of organics for wastewater treatment. *Water Research, 26*(4), 443-451.

Nath, H., & Langdon, A. (2010a). *Electrochemical decontamination of iron and manganese from groundwater*. Paper presented at the Groundwater 2010, Canberra, Australia.

Nath, H., & Langdon, A. (2010b). *Electrochemical oxidation of iron and manganese.* Paper presented at the Water New Zealand annual conference 2010, Christchurch.

Nath, H., & Langdon, A. (2010). New Zealand Patent No. NZ 590016.

Nath, H., & Langdon, A. (2011). New Zealand Patent No. NZ 593920.

Nath, H., Wang, X., Torrens, R., & Langdon, A. (2011). A novel perforated electrode flow through cell design for chlorine generation. *Journal of Applied Electrochemistry, 41*, 389–395.

Nava, J. L., Oropeza, M. T., Ponce de León, C., González-García, J., & Frías-Ferrer, A. J. (2008). Determination of the effective thickness of a porous electrode in a flow-through reactor; effect of the specific surface area of stainless steel fibres, used as a porous cathode, during the deposition of Ag(I) ions. *Hydrometallurgy, 91*, 98–103.

Nazaroff, W. W., & Alvarez-Cohen, L. (2001). *Environmental Engineering Science* (1 ed.). New York: Wiley.

Newman, J., & Tobias, C. W. (1962). Theoretical analysis of current distribution in porous electrodes. *Journal of Electrochemical Society, 109*, 1183–1191.

Onofrio, S., Serena, R., Alessandro, G., & Giuseppe, S. (2009). Electrochemical oxidation of organics in water: Role of operative parameters in the absence and in the presence of NaCl. *Water Research, 43* 2260 –2272

Palmas, P., Polcaro, A. M., Vacca, A., Mascia, M., & Ferrara, F. (2007). Influence of the operating conditions on the electrochemical disinfection process of natural waters at BDD electrodes. *Journal of Applied Electrochemistry, 37*, 1357–1365.

Panizza, M., & Cerisola, G. (2005). Application of diamond electrodes to electrochemical processes. [Critical review]. *Electrochimica Acta, 51* 191–199.

Panizza, M., & Cerisola, G. (2009). Direct And Mediated Anodic Oxidation of Organic Pollutants. *Chemical Reviews, 109*(12), 6541–6569.

Pawliszyn, J. (1998). *Solid Phase Microextraction: Theory and Practice*. New York: Wiley-VCH.

Picart, L., Dumay, E., & Cheftel, J. C. (2002). Inactivation of Listeria innocua in dairy fluids by pulsed electric fields: influence of electric parameters and food composition. *Innovative Food Science and Emerging Technologies, 3*, 357–369.

Pletcher, D. (1984a). Electrocatalysis: present and future. [Review]. *Journal of Applied Electrochemistry, 14*(9), 403-415.

Pletcher, D. (1984b). *Industrial Electrochemistry* (1 ed. Vol. 1). London: Chapman and Hall.

Polcaro, A. M., Vacca, A., Mascia, M., & Ferrara, F. (2008). Product and by-product formation in electrolysis of dilute chloride solutions. *Journal of Applied Electrochemistry, 38*, 979-984.

Polcaro, A. M., Vacca, A., Mascia, M., Palmas, S., Pompei, R., & Laconi, S. (2007). Characterization of a stirred tank electrochemical cell for water disinfection processes. *Electrochimica Acta 52*, 2595–2602.

Putri, I. R., Syamsiana, I. N., & Hawa, L. C. (2010). Design of high voltage pulse generator for pasteurization by pulse electric field (PEF). *International Journal of Computer and Electrical Engineering, 2*(5), 916 - 923.

Raghu, S., & Ahmed Basha, C. (2007). Electrochemical treatment of Procion Black 5B using cylindrical flow reactor—a pilot plant study. *Journal of Hazardous Material B, 139*, 381– 390.

Rajeshwar, K., & Ibanez, J. G. (1997). *Environmental Electrochemistry: Fundamentals and Applications in Pollution Abatement*. New York: Academic Press.

Rajeshwar, K., Ibanez, J. G., & Swain, J. G. M. (1994). *Journal of Applied Electrochemistry 24*, 1077.

Rajkumar, D., & Kim, G. J. (2006). Oxidation of various reactive dyes with in situ electro-generated active chlorine for textile dyeing industry wastewater treatment. *Journal of Hazardous Material B, 136*, 203–212.

Rajkumar, D., & Palanivelu, K. (2004). Electrochemical treatment of industrial wastewater. *Journal of Hazardous Material B, 113*, 123–129.

Ray, B. T. (1995). *Environmental Engineering*. Boston: PWS.

Riera-Torres, M., & Gutiérrez, M. C. (2010). Colour removal of three reactive dyes by UV light exposure after electrochemical treatment. *Chemical Engineering Journal 156* 114 –120.

Robert Soliva-Fortunya, Ana Balasab, Dietrich Knorrb, & Olga Martı´n-Belloso. (2009). Effects of pulsed electric fields on bioactive compounds in foods: a review. *Trends in Food Science & Technology 20*, 544 - 556.

Roscoe, M. (1990). *Handbook of ground water development* (1 ed.): Wiley.

Rosen, M. R. (2001). Hydrochemistry of New Zealand's aquifers *Groundwaters of New Zealand* (pp. 77-110). Wellington: New Zealand Hydrological Society.

Saleh, M. M. (2004). On the effectiveness factor of flow-through porous electrode. *Journal Physical Chemistry B, 108*, 13419–13426.

Scott, K. (1992). Industrial Electrochemical Synthesis Processes. *Developments in Chemical Engineering and Mineral Processing, 1*(2/3), 71-117.

Stack, M. A., Fitzgerald, G., O'Connell, S., & James, K. J. (2000). Measurement of trihalomethanes in potable and recreational waters using solid phase micro extraction with gas chromatography-mass spectrometry. *Chemosphere, 41*, 1821-1826.

Stainer, R. Y., Ingraham, J. L., Wheelis, M. L., & Painter, P. R. (1986). *General Microbiology*. USA: Macmillan Education.

Stumm, W., & Morgan, J. J. (1981). *Aquatic Chemistry: An introduction emphasizing chemical equilibria in natural waters* (2 ed.). New York: Wiley.

Toepfl, S., Heinz, V., & Knorr, D. (2007). High intensity pulsed electric fields applied for food preservation. *Chemical Engineering and Processing 46*, 537–546.

Trasatti, S. (1995). Electrochemistry and the environment: the role of electrocatalysis. *International Journal of Hydrogen Energy, 20*, 835.

Tipler, P. A. (1990). *Physics for Scientist and Engineers* (3 ed. Vol. 2). New york: Worth Publisher.

Uchida, S., Houjo, M., & Tochikubo, F. (2008). Efficient sterilization of bacteria by pulse electric field in micro-gap. *Journal of Electrostatics, 66*, 427–431.

Una, U. T., Altay, U., Koparal, A. S., & Ogutveren, U. B. (2008). Complete treatment of olive mill wastewaters by electrooxidation. *Chemical Engineering Journal, 139* 445–452.

United Nations Environmental Program. (2003). *Groundwater and its susceptibility to degradation*. Nairobi: United Nations Environmental Program.

Vogel, A. I. (1997). *Textbook of Quantitative Chemical Analysis* (5 ed.). London: Longman.

W.H.O. (2004). *Guidlines for drinking water quality*. Geneva: World Health Organisation.

W.H.O. (2006). *Meeting the MDG drinking water and sanitation: the urban and rural challenge of the decade*. Geneva: World Health Organization.

Wan, J., Coventry, J., Swiergon, P., Sanguansri, P., & Versteeg, C. (2009). Advances in innovative processing technologies for microbial inactivation and enhancement of food safety - pulsed electric field and low-temperature plasma. *Trends in Food Science & Technology 20*, 414 - 424.

Wang, H., Bhunia, A. K., & Lua, C. (2006). A microfluidic flow-through device for high throughput electrical lysis of bacterial cells based on continuous dc voltage. *Biosensors and Bioelectronics*, *22*, 582–588.

Wang, X. (2005). *The development of electrochemical cell for the production of chlorine in dilute aqueous solutions.* University of Waikato, Hamilton.

Wesierska, E., & Trziszka, T. (2007). Evaluation of the use of pulsed electrical field as a factor with antimicrobial activity. *Journal of Food Engineering 78*, 1320–1325.

White, G. C. (2010). *Handbook of chlorination and alternative disinfectants* (5 ed.). New Jersey: Wiley.

Yang, C. Y. (2004). Drinking water chlorination and adverse birth outcomes in Taiwan. *Toxicology 198* 249–254.

Yang, D., & James, D. E. (2007). Electrochemical oxidation for landfill leachate treatment. *Waste Management 27*, 380–388.

You, D., Zhang, H., & Chen, J. (2009). Theoretical analysis of the effects of operational and designed parameters on the performance of a flow-through porous electrode. *Journal of Electroanalytical Chemistry, 625*, 165–171.

Yuan, M., TAO, J., Yan, G., Tan, M., & Qiu, G. (2010). Preparation and characterization of Fe/SiO2 core/shell nanocomposites. *Transactions of nonferrous met. Soc. China, 20*, 632-636.

Zappi, G. D., & Weinberg, N. L. (2001). USA Patent No. 6,315,886. U. S. Patent.

Zhang, Q., Barbosa-Canovas, G. V., & Swansonb, B. G. (1995). Engineering Aspects of Pulsed Electric Field Pasteurization. *Joumal of Food Engineering 25*, 261-281.

Zimmermann, Pilwat, G., & Riemann, F. (1974). Dielectric Breakdown ofCell Membranes. *Biophysical Journal, 14*, 881- 899.